COMPARISON OF FATIGUE ANALYSIS APPROACHES FOR PREDICTING FATIGUE LIVES OF HOT-MIX ASPHALT CONCRETE (HMAC) MIXTURES

A Dissertation

by

LUBINDA F. WALUBITA

Submitted to the Office of Graduate Studies of
Texas A&M University
in partial fulfillment of the requirements for the degree of

DOCTOR OF PHILOSOPHY

May 2006

Major Subject: Civil Engineering

COMPARISON OF FATIGUE ANALYSIS APPROACHES FOR PREDICTING FATIGUE LIVES OF HOT-MIX ASPHALT CONCRETE (HMAC) MIXTURES

A Dissertation

by

LUBINDA F. WALUBITA

Submitted to the Office of Graduate Studies of
Texas A&M University
in partial fulfillment of the requirements for the degree of

DOCTOR OF PHILOSOPHY

Approved by:

Chair of Committee,	Amy Epps Martin
Committee Members,	Robert L. Lytton
	Dallas N. Little
	Michael Speed
Head of Department,	David Rosowsky

May 2006

Major Subject: Civil Engineering

ABSTRACT

Comparison of Fatigue Analysis Approaches for Predicting Fatigue Lives
of Hot-Mix Asphalt Concrete (HMAC) Mixtures. (May 2006)
Lubinda F. Walubita, B.Eng., University of Zambia;
M.S., University of Stellenbosch
Chair of Advisory Committee: Dr. Amy Epps Martin

Hot-mix asphalt concrete (HMAC) mixture fatigue characterization constitutes a fundamental component of HMAC pavement structural design and analysis to ensure adequate field fatigue performance. HMAC is a heterogeneous complex composite material of air, binder, and aggregate that behaves in a non-linear elasto-viscoplastic manner, exhibits anisotropic behavior, ages with time, and heals during traffic loading rest periods and changing environmental conditions. Comprehensive HMAC mixture fatigue analysis approaches that take into account this complex nature of HMAC are thus needed to ensure adequate field fatigue performance. In this study, four fatigue analysis approaches; the mechanistic empirical (ME), the calibrated mechanistic with (CMSE) and without (CM) surface energy measurements, and the proposed NCHRP 1-37A 2002 Pavement Design Guide (MEPDG) were comparatively evaluated and utilized to characterize the fatigue resistance of two Texas HMAC mixtures in the laboratory, including investigating the effects of binder oxidative aging.

Although the results were comparable, the CMSE/CM approaches exhibited greater flexibility and potential to discretely account for most of the fundamental material properties (including fracture, aging, healing, visco-elasticity, and anisotropy) that affect HMAC pavement fatigue performance. Compared to the other approaches, which are mechanistic-empirically based, the CMSE/CM approaches are based on the fundamental concepts of continuum micromechanics and energy theory.

The CMSE/CM approaches utilize the visco-elastic correspondence principle, Paris' Law of fracture mechanics, and Schapery's work potential theory to monitor cumulative fracture damage in HMAC mixtures under laboratory repeated uniaxial tensile tests. Additionally, the CMSE/CM results exhibited relatively lower statistical variability.

For the materials and test conditions considered, laboratory aging reduced HMAC mixture fatigue resistance and its ability to heal. This finding signifies the importance of discretely incorporating aging effects in HMAC mixture fatigue characterization, and the CMSE/CM aging shift factors developed in this study produced promising results. In terms of HMAC mixture comparison, the results showed that HMAC mixture fatigue resistance is a complex function of mix-design parameters, material properties, traffic, pavement structure, and environment, and that these factors need to be taken into account when modeling HMAC mixture fatigue resistance. However, more research is recommended to further validate the CMSE/CM approaches and quantify the effects of aging.

DEDICATION

I dedicate this dissertation to my mother, Ms. Grace M. Muyunda. Thanks, Mum, for all the hardships you have endured to bring me where I am today. I will always cherish your love.

ACKNOWLEDGMENTS

I hereby acknowledge my sincere appreciation and due gratitude to my advisor and study leader, Dr. Amy Epps Martin (E.B. Snead II Associate Professor), for the academic guidance, mentorship, and technical advice rendered during the course of this study. This study would not have been completed without her exemplary motivation and encouragement. Special thanks also go to Dr. Robert L. Lytton (Benson Chair Professor), who was also on my study committee, for his continued and unparalleled technical support which inevitably made this research study a success. Special thanks are also owed to my committee members Professor Dallas N. Little and Professor Michael Speed for their valuable input and time spent serving on my study committee. A special word of appreciation is also due to Professor F. Hugo (University of Stellenbosch in South Africa) for his dedicated professional mentorship and moral support. Through his encouragement and motivation, I was able steer ahead and remain afloat in the pursuit of my Ph.D. degree at Texas A&M University. The valuable technical contribution and extensive binder testing including subsequent data analysis provided by Dr. Charles J. Glover and Sung Hoon Jung are gratefully acknowledged.

This study was conducted as part of Texas Department of Transportation (TxDOT) Research Project 0-4468 entitled "Evaluate the Fatigue Resistance of Rut Resistance Mixes." I thank TxDOT and the Federal Highway Administration (FHWA) for their support in funding this research study and all Texas Transportation Institute (TTI) and Texas Engineering Experimentation Station (TEES) personnel for their help in the course of this research work. In particular, special thanks are due to Rick Canatella, Lee Gustavus, Gerry Harrison, Cathy Brian, Pam Kopf, and Jeffrey Perry.

The success of my Ph.D. program would not have been possible without the financial, academic, technical, and moral support of my family and personal friends. In this regard, I wish to mention some friends by name: Jenny Liu, Navin N. Natarajan, Jeong-Ho Oh, Dr. A. Smit, Pieter Poolman, Scott Hubley, Aparna Kanungo, Edward O. Abebresse, and Manjula Bhatina. Lastly, but not the least, all the various persons and entities that rendered help towards the success of this study are gratefully thanked.

TABLE OF CONTENTS

Page

TABLE OF CONTENTS (continued)

CHAPTER Page

TABLE OF CONTENTS (continued)

TABLE OF CONTENTS (continued)

TABLE OF CONTENTS (continued)

TABLE OF CONTENTS (continued)

TABLE OF CONTENTS (continued)

Page

LIST OF FIGURES

LIST OF FIGURES (continued)

FIGURE Page

LIST OF FIGURES (continued)

LIST OF FIGURES (continued)

FIGURE Page

LIST OF TABLES

LIST OF TABLES (Continued)

LIST OF TABLES (Continued)

CHAPTER I
INTRODUCTION

Hot-mix asphalt concrete (HMAC) is a heterogeneous complex composite material of air, binder, and aggregates used in pavement construction. Approximately 500 million tons of HMAC (valued at about $11.5 billion) are used in pavement construction yearly in the United States (Si 2001). Despite, this widespread usage, the fatigue characterization of HMAC mixtures to ensure adequate field fatigue performance is not very well established, and fundamental fatigue predictive models still remain to be developed.

Under traffic loading and changing environmental conditions, HMAC exhibits non-linear visco-elastic and anisotropic behavior. Its mechanical properties and performance are dependent on loading rate, temperature, and direction of loading (Lytton et al. 1993, Lytton 2000, Kim et al. 1997a, Lee 1996, Tashman et al. 2003, Arramon et al. 2000). With time, HMAC also ages but has the potential to heal (closure of fracture surfaces) during traffic loading rest periods (Kim et al. 1997b, Si 2001, Cheng 2002). Inevitably, this complex nature of HMAC response behavior under changing traffic loading and environmental conditions makes it difficult to adequately model HMAC mixture properties, particularly with respect to fatigue cracking.

Complicating the prediction of HMAC mixture resistance to fatigue are the effects of binder oxidative aging (as a function of time) that increase both the binder viscosity and elastic moduli, thus reducing the HMAC mixture ductility and increasing its susceptibility to fatigue cracking (Glover et al. 2005). However, little is understood nor documented about the effects of binder oxidative aging on both HMAC mixture properties and fatigue resistance.

This dissertation follows the style of the *Journal of Engineering Mechanics*.

Comprehensive HMAC mixture fatigue analysis approaches that take into account the complex nature of HMAC are thus desired to ensure adequate field fatigue performance. Analysis models associated with such approaches should have the potential to utilize fundamental mixture properties that are critical to HMAC pavement fatigue performance when predicting mixture fatigue resistance and pavement fatigue life (N_f). Such analysis models should be based on data input obtained from simple routine laboratory tests that measure fundamental material properties instead of time-consuming fatigue tests. Their failure criteria should also be based on a simulation of direct relationship between crack development and fatigue damage accumulation in the field. Various fatigue analysis approaches have been developed and some are in use today, but many are inadequate in producing fatigue resistant HMAC mixtures or pavement structures that are structurally adequate in fatigue throughout the pavement's design life. Consequently, fatigue cracking continues to be prevalent in today's HMAC pavements. Additionally, mixture resistance to fatigue cracking is directly tied to its mechanical response under repeated traffic loading that depends on the entire pavement structure, i.e., the fatigue response behavior of the top HMAC layer under traffic loading is also dependent on the material properties and structural capacity of the underlying layers. This unique characteristic inevitably calls for fatigue analysis approaches that adequately interface both HMAC mixture fatigue characterization and pavement structural design.

PROBLEM STATEMENT

HMAC mixtures are designed to resist aging and distresses induced by traffic loading and changing environmental conditions. Common HMAC distresses include rutting, stripping (moisture damage), and fatigue. Over the past decade, research efforts were focused on improving mixture design to preclude rutting in the early life of HMAC pavements, which also offers increased resistance to moisture damage. However, a concern arises that these HMAC mixtures may be susceptible to fatigue cracking, particularly if the binder stiffens excessively due to aging.

RESEARCH OBJECTIVES

The primary objectives of this research study were threefold:

1) to evaluate and recommend a fatigue HMAC mixture design and analysis system to ensure adequate mixture fatigue performance in a particular pavement structure under specific environmental and traffic loading conditions that utilizes fundamental material properties,
2) to investigate the effects of binder oxidative aging on HMAC mixture properties and fatigue resistance, and
3) to evaluate and compare the fatigue resistance of selected common TxDOT HMAC mixtures.

To accomplish these goals, four fatigue analysis approaches listed below were comparatively utilized to predict the fatigue lives of selected TxDOT HMAC mixtures:

- the mechanistic empirical (ME) approach developed during the Strategic Highway Research Program (SHRP) using the bending beam fatigue test (Tayebali et al. 1992, Deacon et al. 1994, AASHTO 1996a),
- the new proposed NCHRP 1-37A 2002 Pavement Design Guide (MEPDG) using the dynamic modulus test (Witczak 2001, AASHTO 2004),
- a calibrated mechanistic (CM) approach developed at Texas A&M University that requires strength and repeated loading tests in uniaxial tension and relaxation tests in uniaxial tension and compression for material characterization and monitoring dissipated pseudo strain energy (Lytton et al. 1993, Kim et al. 1997a), and,
- an updated calibrated mechanistic (CMSE) approach developed at Texas A&M University that also requires measuring surface energies of component materials in addition to the material characterization tests from the original CM approach (Lytton et al. 1993, Kim et al. 1997a, b).

WORK PLAN AND SCOPE OF STUDY

The work plan entailed utilization of the four fatigue analysis approaches (mechanistic empirical and calibrated mechanistic) to predict the fatigue lives of common TxDOT HMAC mixtures and other TxDOT HMAC mixtures frequently used for rutting resistance under representative environmental conditions and typical traffic loading conditions in standard HMAC pavement structures. Thereafter, the best approach for fatigue design and analysis was recommended based on a value engineering assessment criteria including the ability to incorporate the important effects of aging, fracture, healing, and anisotropy; variability; required resources; implementation issues; and practicality. The general scope of the study was limited to:

- two HMAC mixtures that represent common basic and rut-resistant HMAC mixtures often used in the Texas environment,
- four fatigue analysis approaches described above that include mechanistic empirical and calibrated mechanistic approaches,
- three laboratory aging exposure conditions that simulate Texas HMAC field aging conditions,
- five hypothetical field HMAC pavement structures under representative traffic loading conditions,
- two Texas environmental conditions that are critical to fatigue cracking, and
- one typical reliability level (95%) for statistical analysis.

RESEARCH METHODOLOGY

The research methodology for this study involved the following major tasks: information search, experimental design and materials selection, laboratory testing, laboratory test data analysis, material characterization, stress-strain analysis, prediction of HMAC mixture fatigue lives, comparison and evaluation of the fatigue analysis approaches, conclusions and recommendations, and documentation. These tasks are briefly discussed in the subsequent text.

Task 1: Information Search

An information search was conducted to gather data on current fatigue design and analysis approaches; related laboratory tests, materials, pavement structures, and designs; corresponding standards or references; and resources or methodologies used to obtain fatigue-resistant HMAC mixtures. As well as aiding in the selection of the fatigue analysis approaches for a comparative evaluation and HMAC mixture N_f prediction, these data from the information search also served as the basis for formulating the experimental design program which included materials selection.

Task 2: Experimental Design and Materials Selection

Two HMAC mixture types representing a common basic TxDOT Type C mixture and a rut-resistant 12.5 mm Superpave Type D mixture frequently used for rutting resistance were utilized. Three laboratory aging exposure conditions (0, 3, and 6 months) at 60 °C that simulate approximately up to 12 years of Texas field HMAC aging at the critical pavement service temperature were selected to investigate the effects of aging on binder and HMAC mixture properties and N_f (Glover et al. 2005). For field conditions, five hypothetical field HMAC pavement structures under representative traffic loading conditions and two Texas environmental conditions (wet-warm and dry-cold) that are critical to fatigue cracking were considered (TxDOT 2003a). A typical 95% reliability level was used in the study.

Task 3: Laboratory Testing and Data Analysis

In line with the study's experimental design, a series of laboratory tests at various aging exposure conditions were accomplished for each fatigue analysis approach. Output data from these laboratory tests served as input data for both characterizing the HMAC mixture properties and predicting mixture N_f using the four fatigue analysis approaches under consideration. Because HMAC fatigue damage is generally more prevalent at intermediate pavement service temperatures, most of the laboratory tests were conducted at 20 °C; otherwise the test data were normalized to 20 °C during the analysis phase.

Task 4: Stress-Strain Analysis

Elastic strains (tensile and shear) within the HMAC layer at certain critical locations in a representative HMAC pavement structure are required as input parameters for fatigue analysis (Tayebali et al. 1992, Lytton et al. 1993). An elastic multi-layer software, ELSYM5, was utilized for the stress-strain analysis, but the response was adjusted based on finite element (FEM) simulations to account for more realistic HMAC behavior in terms of visco-elasticity and plasticity (Ahlborn 1969, Park 2004).

Task 5: HMAC Mixture Property Characterization and Prediction of N_f

This task involved HMAC mixture property characterization and prediction of mixture N_f consistent with each fatigue analysis approach for each mixture type and aging condition. Under this task, HMAC mixture properties and fatigue resistance were also comparatively evaluated, including development of an aging shift factor due to binder oxidative aging for the CMSE and CM fatigue analysis approaches.

Task 6: Comparison and Evaluation of Fatigue Analysis Approaches

Under this task, the four fatigue analysis approaches (ME, CMSE, CM, and MEPDG) were comparatively evaluated in terms of the fundamental concepts, laboratory testing, equipment requirements, input data, data analysis, failure criteria, results and variability, and associated costs. Thereafter, a value engineering assessment criterion utilizing the following assessment parameters in their descending order of significance was conducted to select the appropriate fatigue analysis approach:

- results (N_f variability and tie to field performance);
- costs,
- input data variability;
- analysis (simplicity, failure criteria, and versatility of input data);
- laboratory testing; and
- incorporation of material properties (mixture volumetrics, modulus/stiffness, fracture, tensile strength, healing, aging, and anisotropy).

Task 7: Conclusions and Recommendations

Upon completion of data analysis and comparison of the fatigue analysis approaches, the results were synthesized to draw conclusions and recommendations. The conclusions include the significant findings of the study as well as the selected and recommended fatigue analysis approach. The recommendations in turn highlight the general applicability and validity aspects of the selected fatigue analysis approach and its limitations. This final task involved documentation of all the fatigue analysis approaches including the literature review, laboratory test procedures, analysis procedures and associated models, results, conclusions, and recommendations.

DISSERTATION LAYOUT

This dissertation consists of eleven chapters including this chapter (Chapter I) that provides the motivation for the research, the overall objectives and work plan, and the scope of this study. The layout is schematically summarized in a flowchart in Fig. 1-1. The subsequent chapters describe the information search (Chapter II) and experimental design (Chapter III), which includes selection of the fatigue analysis approaches, materials, specimen fabrication protocols, laboratory aging exposure conditions, and typical pavement structures.

Next, the four fatigue analysis approaches (ME, CMSE, CM, and the MEPDG) presented in this dissertation are described in detail in Chapters IV through VII. For each fatigue analysis approach, the description includes the fundamental theory, input/output data, laboratory testing, fatigue failure criteria, analysis procedure and associated models, and statistical analysis. Then, the results including HMAC mixture properties, the resulting fatigue lives from all the approaches, the aging evaluation, and the comparison and selection of the recommended fatigue analysis approach are described and discussed in Chapters VIII through X. The dissertation concludes in Chapter XI with a summary of the findings and recommendations. Appendices of detailed laboratory test results and other important data are also included.

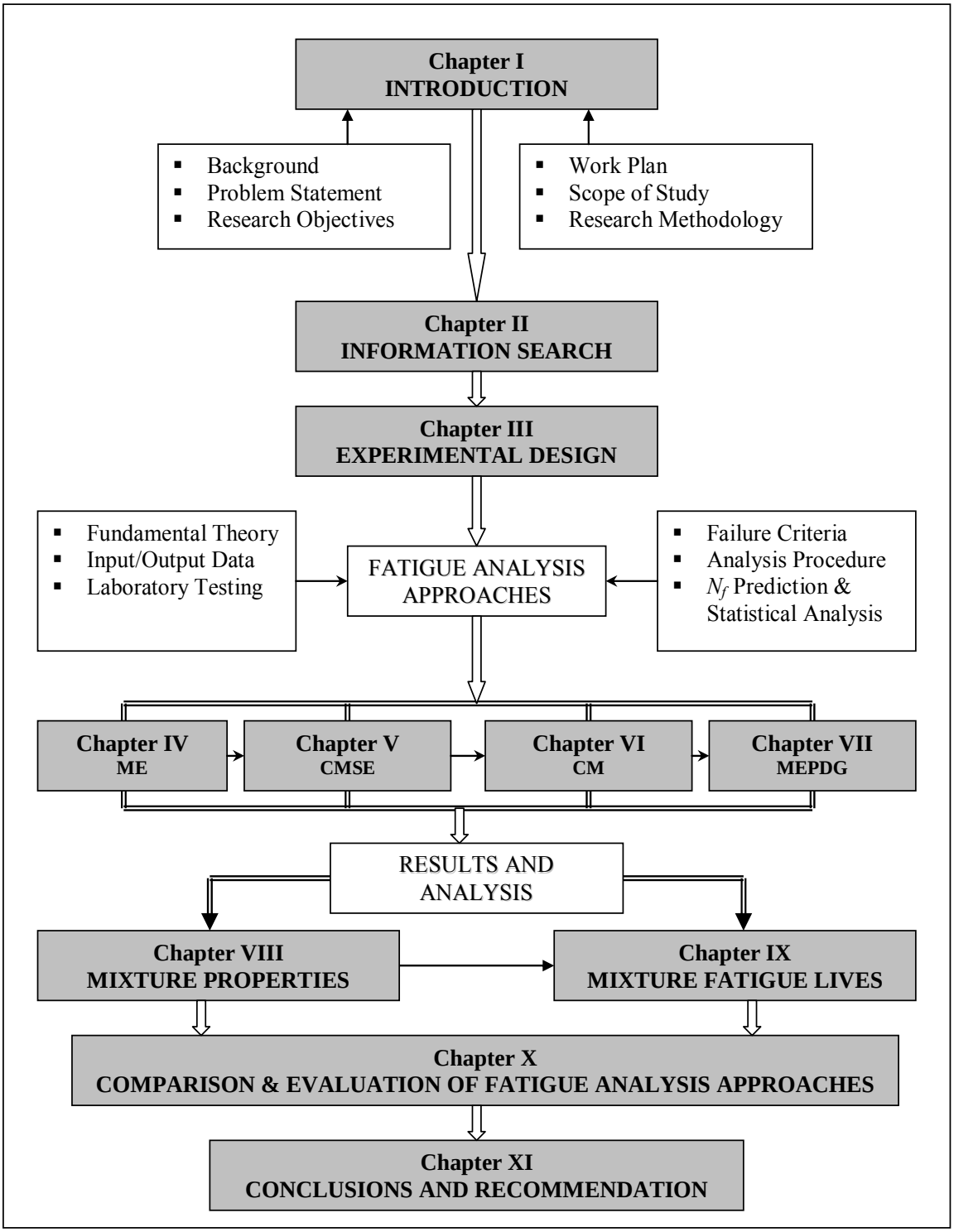

Fig. 1-1. Dissertation Outline

SUMMARY

In this introductory chapter, the background, problem statement, and study objectives were discussed. The work plan, scope of study, and research methodology were then described, followed by the dissertation layout.

CHAPTER II
INFORMATION SEARCH

An information search utilizing a field survey questionnaire, electronic databases, and resulting publications was conducted to gather data on current fatigue design and analysis approaches; related laboratory tests, materials, pavement structures, and design; corresponding standards or references; and resources or methodologies used to obtain fatigue-resistant HMAC mixtures. Effects of aging, healing, and fracture on HMAC mixture fatigue performance were also reviewed, and the literature found was summarized and documented. Commonly used TxDOT HMAC mixtures, material characteristics, and other general input parameters including pavement structures, traffic loading, environmental conditions, mix-designs, aging conditions, and reliability levels were also reviewed and documented.

Data gathered from this information search aided in selecting the appropriate fatigue analysis approaches for a comparative evaluation and subsequent selection of the best fatigue analysis approach. These data also served as the basis for formulating the experimental design program, including materials selection for this study.

FIELD SURVEY QUESTIONNAIRES

A field survey of government agencies and the industry addressed some of the key aspects of fatigue analysis approaches, laboratory tests, material characteristics, pavement structures and design, corresponding standards or references, and resources used for fatigue resistant HMAC mixtures. Appendix A shows an example of the field survey questionnaire with results summarized for six respondents.

Thirty-nine surveys were emailed to a list of familiar contacts in the industry, academia, and relevant personnel at state departments of transportation (DOTs). Approximately half (10) of the 23 responses received do not consider fatigue in their HMAC mixture design and analysis. Some of the responses referred the survey to other contacts, and seven responses, primarily from research agencies, provided valuable references and information that were reviewed and incorporated into the research methodology and experimental design for the study.

Of the positive responses received, a majority of the DOTs and private industry personnel use the Superpave, mechanistic empirical, AASHTO, Asphalt Institute, and visco-elastic continuum-damage analysis either for HMAC mix-design and analysis or just to check for fatigue resistance in the final HMAC pavement structural design (see Appendix A). Laboratory tests used include bending beam, dynamic modulus, indirect tension, uniaxial fatigue, moisture sensitivity, and retained indirect tensile strength. Some of these approaches and associated laboratory tests have been included in the experimental design and are discussed in subsequent chapters.

LITERATURE REVIEW

From a detailed review of the information search, the following information on the prediction of HMAC mixture fatigue resistance and binder aging and its effects on HMAC mixture fatigue resistance were summarized.

Prediction of HMAC Mixture Fatigue Resistance

An approach that predicts HMAC mixture resistance to fatigue requires an understanding and description of material behavior under repeated loads that simulate field conditions (Deacon et al. 1994). This broad description is valid for approaches that are mechanistic empirical to varying degrees. A more empirically based approach requires that the laboratory test simulate field conditions, but a constitutive law for material behavior in a more mechanics-based approach requires only material properties determined from laboratory test(s) measured using a simple stress state if possible.

In a review of flexure, direct uniaxial, diametral or indirect tension, triaxial, fracture mechanics, and wheel-tracking test methods; continued research in the use of dissipated energy and fracture mechanics approaches with flexure or direct or indirect tension testing were recommended (Deacon et al. 1994). This recommendation highlighted the shift from more empirically based approaches to those able to incorporate a more fundamental mechanistic understanding of fatigue crack initiation, crack propagation, and failure.

The shift over the last decade toward the use of more applicable material behavior models and numerical analysis methods to simulate the fatigue mechanism and failure was possible due to the rapid increase in computing power. This section provides a brief review of previous and current approaches that are more empirical in nature, those that provided a bridge toward mechanistic analysis methods, and current mechanistic analysis approaches.

Mechanistic Empirical Approaches

Most previous approaches for predicting fatigue resistance of HMAC involved either controlled stress or controlled strain laboratory testing at a single representative temperature over a series of stress or strain levels, respectively, and determination of fatigue life at a stress or strain level assumed to be critical and caused by a single type of wheel loading. These approaches predict the number of stress or strain cycles to crack initiation in flexure, direct or indirect tension, or semi-circular bending tests (Tayebali et al. 1992, Walubita et al. 2000, 2002). A method to determine a single representative temperature for laboratory testing and a temperature conversion factor to account for the fact that loading occurs over a range of temperatures are required. A composite shift factor is also required to account for other differences between field and laboratory test conditions, including the effects of wander, healing, and crack propagation. A lengthy testing program is required with replicate tests (to account for relatively large variability) at different stress or strain levels to sufficiently define an empirical fatigue relationship for a specific HMAC mixture.

The determination of the critical stress or strain at the critical location within the pavement structure in the HMAC layer constitutes the mechanistic part of this type of approach, and this calculated value varies depending on the assumed model of material behavior (where layered elastic is most commonly used because of simplicity). The location of the critical stress or strain also limits the analysis to either bottom-up or top-down fatigue cracking without simultaneous consideration of both.

Even with the limitations of mechanistic empirical approaches, validation has been illustrated through comparisons with fatigue life measured in the field, particularly at accelerated pavement testing (APT) facilities. The mechanistic empirical approach developed at the University of California at Berkeley during SHRP as part of Project A-003A provides a widely used example with results validated with full-scale heavy vehicle simulator (HVS) tests (Tayebali et al. 1992, Harvey et al. 1998, Epps et al. 1999).

Another mechanistic empirical approach explored at the University of Nottingham in conjunction with the SHRP A-003A project was validated using a laboratory scale APT device. Indirect tensile fatigue testing was also utilized at the University of Nottingham, and this testing method was included in a comprehensive APT project that included scaled testing with the model mobile load simulator (MMLS3). These approaches are described in brief detail in the subsequent text, followed by a subsection on improvements in mechanistic empirical approaches to account for changing environmental and loading conditions.

SHRP A-003A (University of California at Berkeley). The SHRP A-003A approach utilizes the flexural beam fatigue test (third-point loading); incorporates reliability concepts that account for uncertainty in laboratory testing, construction, and traffic prediction; and considers environmental factors, traffic loading, and pavement design (Tayebali et al. 1992). Specimen preparation by rolling wheel compaction is strongly recommended as part of this approach to simulate the engineering properties of extracted HMAC pavement cores.

Conditioning prior to testing to a representative or worst-case aging state is also suggested. This approach was selected for this study as the mechanistic empirical approach discussed in more detail in Chapter IV.

University of Nottingham. Fatigue research at the University of Nottingham provided validation of the SHRP A-003A analysis system through wheel tracking tests and trapezoidal fatigue testing (Tayebali et al. 1992, Rowe and Brown 1997a). Validation of flexural beam fatigue tests for one aggregate type was successful for the thick wheel tracking slabs that approximated a controlled stress mode of loading. HMAC mixture rankings by the laboratory scale APT device were also approximately equivalent to those based on indirect tensile stiffness and fatigue life determined by an indicator of the ability to dissipate energy. Large variability in the wheel tracking results was highlighted.

Fatigue analysis continued at the University of Nottingham with the inclusion of a visco-elastic model for material behavior that utilizes improvements in the conversion of dynamic shear test results to dynamic flexural results, which was first developed as part of the SHRP A-003A system (Tayebali et al. 1992, Rowe and Brown 1997b). A visco-elastic material model was used in a mechanistic empirical fatigue relationship to predict crack initiation based on dissipated energy to account for nonsymmetrical stress/strain response measured under full-scale loads and to remove the effect of mode of loading during laboratory testing. This model provides dissipated energy contour maps where the maximum value can be located throughout the HMAC layer.

Indirect Tension Testing. Indirect tension offers a simple mode for dynamic frequency sweep, fatigue, or strength testing, although a biaxial stress state and the inability to test with stress reversal have been cited as the major disadvantages (Mathews et al. 1993). The University of Nottingham has utilized this testing mode in measuring stiffness and evaluating the fatigue resistance of HMAC mixtures for overlay design (Rowe and Brown 1997b).

More extensive indirect tensile fatigue testing for a range of materials in a complex layered pavement structure was included in a comprehensive evaluation of two rehabilitation strategies by TxDOT (Walubita et al. 2000, 2002). Relative fatigue lives were defined as the ratio of fatigue resistance of untrafficked materials in these structures compared with those of the same materials trafficked with a scaled APT device (MMLS3). These ratios provided an indication of the detrimental effect of moisture damage and the improvement in fatigue resistance due to increased temperatures and subsequent compaction. A series of time-consuming tests with an average duration of 20 hours was completed at a single representative temperature (20 °C) and frequency (10 Hz) with no rest periods in a controlled stress mode at a stress level equal to 20 percent of the indirect tensile strength of the same HMAC material. Tensile strength tests were also conducted in a semi-circular bending (SCB) mode that induces a direct tensile load in the center zone of a semi-circular shaped HMAC specimen to supplement the indirect tensile test results (see Fig. 2-1).

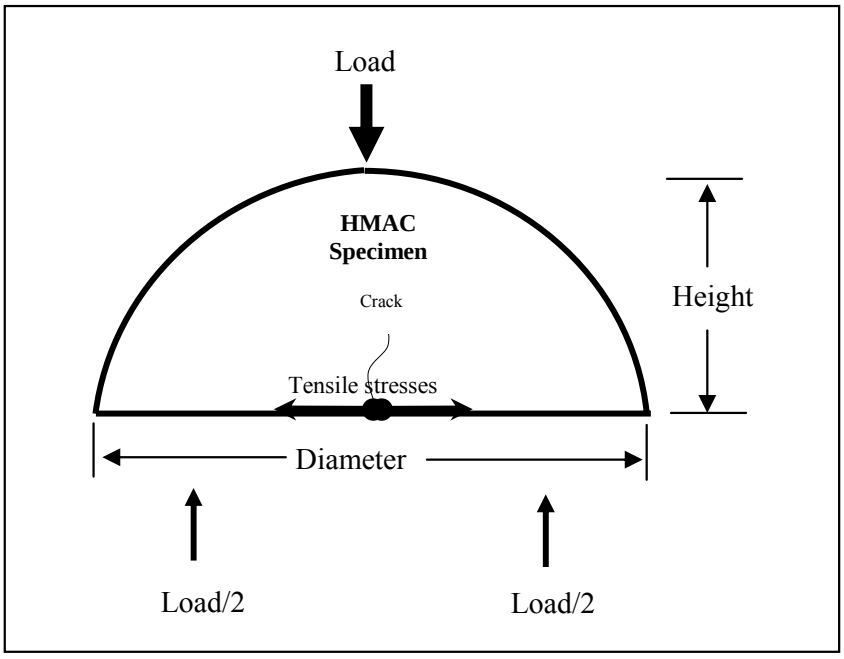

Fig. 2-1. SCB Test-Loading Configuration

The SCB test was considered as a possible candidate for fatigue testing in this study due to reduced load requirements for the same stress level as compared to indirect tensile testing, but it was not selected for evaluation because the associated analysis system is still under development (van de Ven et al. 1997).

Improvements to Mechanistic Empirical Approaches

The approach first developed during SHRP A-003A has been expanded further using the full-scale APT WesTrack project to develop fatigue models and associated pay factors based on construction quality (Monismith et al. 2000, Tsai et al. 2002). The models developed were used to predict fatigue crack initiation in the 26 original WesTrack sections. Hourly changes in both environmental and traffic conditions (wander) were incorporated in this mechanistic empirical analysis that assumed:

- a critical binormal strain distribution beneath dual tires at the base of the HMAC surface layer,
- layered elastic behavior, and
- valid extrapolation of fatigue life for temperatures greater than 30 °C.

No shift factor was applied to the fatigue life relationship that must be defined through laboratory testing for each HMAC mixture type that is different from the Superpave WesTrack HMAC mixtures. Empirical fatigue relationships developed by the Asphalt Institute and Shell have also been improved through the definition of a continuous function of cumulative fatigue damage using Miner's Law to replace prediction of a specific level of fatigue cracking (Miner 1945, Ali et al. 1998). This function assumes bottom-up cracking and utilizes a layered elastic material behavior model but accounts for changing environmental and loading conditions in the accumulation of fatigue damage. Further refinement with an expanded long-term pavement performance (LTPP) dataset that contains pavements exhibiting fatigue failure was recommended. Tsai et al. (2004) have also adopted the Recursive Miner's Law for cumulative fatigue damage analysis of HMAC mixtures (Miner 1945).

This Recursive Miner's Law approach attempts to directly incorporate the significant effects of traffic, environment, material properties, and pavement structure in HMAC mixture fatigue modeling using mechanistic empirical relationships and a Weibull-type fatigue life deterioration function. In their findings, Tsai et al. (2004) observed that mixture properties played the most significant role in the fatigue damage accumulation of HMAC pavement structures under traffic loading. The randomness of vehicle speed and traffic wander had the least effect. Other research to further improve mechanistic empirical fatigue analysis has accounted for the effects of dynamic loads (Castell and Pintado 1999). This approach that considers a moving and fluctuating concentrated load again utilizes Miner's Law (Miner 1945) and assumes bottom-up cracking to predict fatigue crack initiation and cumulative fatigue damage.

The M-E Pavement Design Guide

The new M-E Pavement Design Guide adopts a mechanistic empirical approach for the structural design of HMAC pavements (AASHTO 2004). The basic inputs for pavement design include environmental, materials, and traffic data. There are two major aspects of ME-based material characterization: pavement response properties and major distress/transfer functions (Witczak 2001). Pavement response properties are required to predict states of stress, strain, and displacement within the pavement structure when subjected to external wheel loads. These properties for assumed elastic material behavior are the elastic modulus and Poisson's ratio. The major distress/transfer functions for asphalt pavements are load-related fatigue fracture, permanent deformation, and thermal cracking.

The current version of the M-E Pavement Design Guide (and its software), which is discussed in greater detail in Chapter VII, utilizes the modified Asphalt Institute fatigue damage predictive equation (Bonnaure et al. 1980). Unlike most ME-based approaches, this procedure incorporates two types of fatigue damage criteria. Bottom-up fatigue cracking assumes crack initiation at the bottom of the asphalt layer and propagation through the HMAC layer thickness to the surface.

Top-down fatigue cracking assumes crack initiation at the pavement surface and propagation downward through the HMAC layer. In both failure criteria, tensile strain is the primary mechanistic failure load-response parameter associated with crack growth. The M-E Pavement Design Guide is one of the fatigue analysis approaches utilized in this study.

Toward Mechanistic Analysis

The shift toward mechanistic analysis of fatigue cracking was recognized and encouraged through a review of the use of fracture mechanics in both HMAC and Portland cement concrete (PCC) pavements (Ioannides 1997*)*. This history highlighted early efforts utilizing linear elastic fracture mechanics and a single material property (K_{1c}) providing the driving force for crack propagation characterized by Paris' Law of fracture mechanics (Paris and Erdogan 1963).

Further efforts to consider a process zone ahead of the crack tip were also reviewed, and the concept of similitude to provide a dimensionless parameter equivalent for both field and laboratory conditions was described. A warning considering the HMAC specimen-size effect and its implications for scaling cracking behavior was also issued. The application of fracture mechanics to composite materials to advance the understanding of the mechanism of fatigue cracking was recognized as a slow process but one worth pursuing. This pursuit has continued to address the limitations of previous ME approaches and expand the knowledge base and application of HMAC fatigue analysis approaches.

Lengthy Test Programs. To address the limitation of a lengthy testing program, researchers suggested characterizing the stiffness of HMAC using a master-curve from simple dynamic direct or indirect tensile tests that reflects the HMAC dependence on both time of loading and temperature (Molenaar and Medani 2000).

Parameters from the master-curve were successfully used to predict the coefficients in empirical fatigue relationships. The range of HMAC mixture variables, including modified binders utilized in developing the regression relationships, were also provided.

Linear Visco-elastic Models and Numerical Techniques. To address the limitation of assumed layered elastic material behavior, other researchers produced an integrated HMAC mixture and pavement design approach that allows for more realistic linear visco-elastic behavior (Hopman and Nilsson 2000). This type of material model accounts for asymmetrical stress-strain distributions under moving wheel loads and the effect of time of loading history. In a multi-tiered analysis, the approach separately utilized two conventional empirical fatigue relationships (based on strain and dissipated energy) for crack initiation and Paris' Law for crack propagation as described by Schapery (1984*)*.

Laboratory testing requirements include frequency sweep, creep, and strength testing in direct tension or compression at relevant temperatures. A non-linear finite element simulation of a multi-layer pavement structure that selects an appropriate HMAC stiffness as a function of a more realistic asymmetrical stress state was also utilized in conjunction with mechanistic empirical fatigue relationships (Mamlouk and Khanal 1997). Numerical techniques were also used to model the behavior of three specific materials using elastic-plastic fracture mechanics (Zhang and Raad 2001). Both crack initiation and propagation were modeled, but the viscous behavior of HMAC was not taken into account.

Fracture Mechanics Approach. Further research toward improving the linear elastic fracture mechanics approach with Paris' Law as described by Schapery (1984) related the material fracture coefficients A and n and described the use of uniaxial dynamic and strength tests to determine both parameters from a stiffness master-curve and HMAC mixture correction factors (Jacobs et al. 1996).

Crack propagation using Paris' Law was also incorporated successfully in two- and three-dimensional FEM simulations (Simons and Seaman 2000). This approach spread complex simulation computations over the material lifetime, incorporating damage and resulting stress redistribution. Crack propagation was extrapolated between simulations to determine fatigue life from propagation of an initial crack size assumed related to maximum aggregate size. This approach that assumes elastic material response to a single type of load was validated using flexural beam fatigue tests. Non-linear fracture mechanics were applied to compare crack propagation parameters of different materials at low temperatures and highlight the need to include effects of inelastic dissipated energy in fatigue analysis (Mobasher et al. 1997).

Continuum Mechanics Approach. Research in fatigue analysis over the past decade has expanded to include investigation of both damage due to repeated loading and healing due to repeated rest periods (Kim et al. 1997a, b). Recovery of a loss in stiffness monitored during fatigue testing was noted for short rest periods in direct uniaxial testing in a review of laboratory fatigue tests, and the lack of fatigue cracking in thick HMAC pavements was attributed to a healing effect in an evaluation toward revising design procedures (Mathews et al. 1993, Nishizwa et al. 1997).

A continuum mechanics approach developed through research efforts at North Carolina State University and Texas A&M University successfully accounted for damage growth through crack initiation and propagation and healing for any load history or mode of loading (Kim et al. 1997a, b). This approach utilizes the visco-elastic correspondence principle and work potential theory (WPT) described by Schapery (1984) to remove viscous effects in monitoring changes in pseudo-stiffness in repeated uniaxial tensile tests. Coefficients in the visco-elastic constitutive model describe differences in damage and healing behavior of different materials. This model was validated with both laboratory and field results, and with behavior predicted from the micromechanical approach also developed at Texas A&M University and described in Chapters V and VI of this dissertation (Kim et al. 1997b).

The continuum approach has also led to the development of two simplified fatigue analysis systems (Daniel and Kim 2002, Wen and Kim 2002). One system predicts fatigue behavior for temperatures less than 20 °C from a characteristic damage curve generated based on frequency sweep and strength tests in uniaxial tension at multiple temperatures (Daniel and Kim 2002).

Improvements to this system to consider aging and healing and application to other HMAC mixture types were recommended. The other system utilizes indirect tensile creep and strength testing with a longer gauge length than the standard Superpave mixture test and visco-elastic analysis of material response (AASHTO 2000, Wen and Kim 2002). The use of fracture energy based on tests at 20 °C to predict fatigue cracking was validated using data from the full-scale APT WesTrack project.

With a shift toward more mechanics-based approaches, fatigue analysis is expected to become independent of many factors and variables that limit the application of ME approaches that were the only available analysis tools prior to the rapid increase in computing power. These factors and variables include mode of loading (controlled stress or controlled strain), laboratory test type, time of loading, temperature, type and location of loading, rest periods, and HMAC mixture variables.

Empirical to ME to Calibrated Mechanistic

A major reason for the gradual change of HMAC mixture fatigue analysis from empirical or phenomenological to ME to calibrated mechanistic is the greatly increased capabilities of computers to model material behavior realistically, using mechanics and user-friendly computational packages such as finite element programs. As computers become faster with larger memories in the future, these approaches will most likely be the simplest, most direct, and most practical way to design HMAC mixtures and pavements.

These computational packages can only utilize material properties as input, instead of empirical constants or ME regression coefficients used in previous approaches. This development brings with it an added bonus that laboratory or non-destructive field measurement of material properties is much simpler than determination of these constants and coefficients through extensive laboratory testing.

Calibrated Mechanistic Approaches. The calibrated mechanistic approaches are based on the theory that HMAC is a complex composite material that behaves in a non-linear visco-elastic manner, ages, heals, and requires that energy be stored on fracture surfaces as load-induced damage in the form of fatigue cracking. Energy is also released from fracture surfaces during the healing process. HMAC mixture resistance to fatigue cracking thus consists of two components, resistance to fracture (both crack initiation and propagation) and the ability to heal; processes which both change over time.

Several approaches that predict fatigue life, require material characterization and account for both the fracture and healing processes in HMAC have been developed over the past decade. In the SHRP A-005 project, a complete model of fatigue fracture and healing was developed (Uzan 1996). Other researchers showed the importance of the use of fracture and dissipated energy in measuring the fracture resistance of an HMAC mixture (Lee et al. 1995). This same concept of dissipated energy per load cycle provides the driving force for fatigue crack initiation and propagation, and researchers demonstrated that the fracture energy approach was able to accurately predict the fatigue life of a wide variety of HMAC mixture designs as compared to other approaches (Zhou and Liang 1996, Liang and Zhou 1997). SHRP A-005 results and a finite element computer program have been used to illustrate substantial agreement with these results in predicting the two phases of crack growth, initiation, and propagation (Uzan 1997).

The Texas A&M Calibrated Mechanistic Approach. A micromechanical approach developed at Texas A&M University based on the SHRP A-005 results requires only creep or relaxation, strength, and repeated load tests in uniaxial tension and compression and a catalog of fracture and healing surface energy components of asphalt binders and aggregates measured separately (Lytton et al. 1993, Little et al. 1998, 2000). Surface energy components of various common aggregates and binders have been measured at the Texas Transportation Institute (TTI) in various studies (Little et al. 1998, 2000, Hefer 2004, CastelloBlanco 2004).

These surface energy results have been cataloged (see Appendix B) and are also proving useful in other ongoing TTI studies including moisture sensitivity analysis in HMAC mixtures. In this approach selected for evaluation in this study, HMAC behavior in fatigue is governed by the energy stored on or released from crack faces that drive the fracture and healing processes, respectively, through these two different mechanisms (fracture and healing). Chapter V discusses this approach in greater detail.

Binder Aging and HMAC Mixture Fatigue Resistance

TTI's Center for Asphalt and Materials Chemistry (CMAC) has studied the effect of oxidative aging on asphalt binders over the last 15 years (Glover et al. 2005). During this time, CMAC researchers have conducted a comprehensive study of the oxidation kinetics of binders under varying conditions of temperature and oxygen pressure and of the effect of this oxidation on the physical properties of binders. Both of these issues are crucial to understanding the rate at which asphalt binders age in service in the field and the results of these changes on HMAC pavement fatigue performance.

Fundamentally, the oxidation of binder results in compounds that are more polar and therefore form strong associations with each other. These associations result in both a greater resistance to flow (higher viscosity) and larger elastic modulus. Together, these effects result in higher stresses in HMAC under loading. This greater resistance to flow can be beneficial at high temperatures by reducing permanent deformation and rutting.

A problem emerges, however, when aging is excessive, leading to excessively large stresses that result in binder failure at intermediate and lower temperatures (cracking). This effect of oxidative aging must also contribute to failure by repeated loading (fatigue cracking) through its effect on HMAC stiffness that governs material response to loading. It also explains why producing binders that have higher high-temperature Superpave grades (and thus provide stiffer mixtures at rutting temperatures) may be more prone to premature fatigue cracking, particularly if the binder is very susceptible to oxidative aging under changing environmental and traffic loading conditions.

Effect of Aging on Binder Viscosity

Binder viscosity increases dramatically due to oxidation, in fact, by orders of magnitude over the life of a pavement. The effect is most significant at high temperatures (low frequency) but plays a role in HMAC pavement performance at all practical temperatures. According to Glover et al. (2005), the increase in binder log viscosity (η) with oxidation is linear and has no bound within the practical limits encountered by binder during a normal pavement life. Fig. 2-2 illustrates the η-time relationship based on unaged and rolling thing film oven test (RTFOT) aged binders.

Fig. 2-2 shows the increase in low shear-rate dynamic viscosity (η_0^*) measured at 60 °C versus aging time at 60 °C and atmospheric air pressure for two binders AAB-1 and AAG-1. These data were obtained in thin films, and thus the hardening rates reflected by the slope of these lines are higher than those that actually occur in the field. However, the effect and the ultimate result that is dependent on binder type are nonetheless very clear.

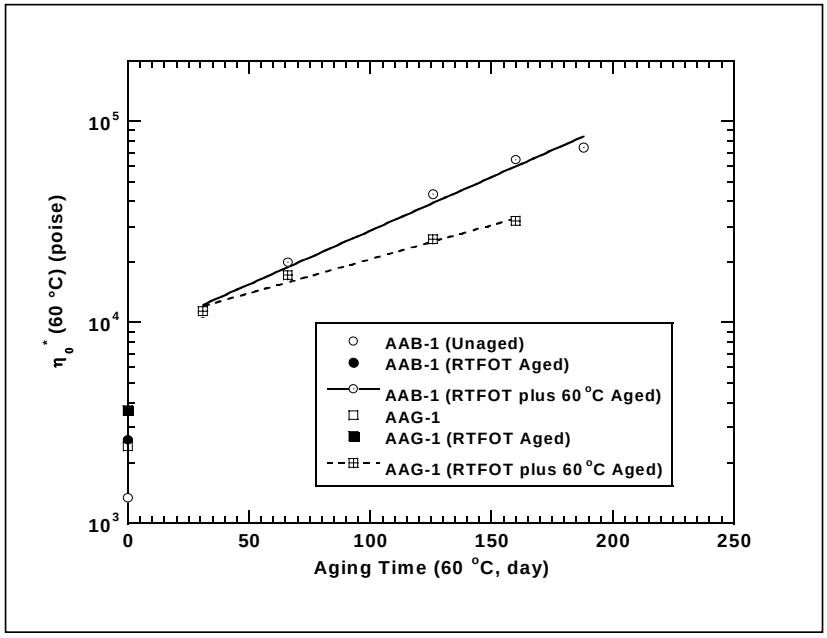

Fig. 2-2. The η_0^*-Aging Relationship (Glover et al. 2005)

Effect of Aging on Low-Temperature Superpave Performance Grade

Viscosity is inversely related to the *m*-value (the slope of the plot of log stiffness versus log time) in the Superpave low-temperature performance grade for binders and elastic modulus is related to binder stiffness. Thus as binders age, *m* decreases and the stiffness increases. This increase in stiffness (and decrease in *m*) results in a deterioration of the low-temperature grade as a binder oxidizes (Knorr et al. 2002). These are essentially the same phenomena that occur due to aging in HMAC pavement field conditions.

Effect of Aging on Ductility and Shear Properties

One of the significant results from the literature is that ductility at 15 °C relates well to HMAC pavement performance (Doyle 1958, Halstead 1984). According to these studies, when the ductility of a binder decreases to a minimum value in the range of about of 3 to 5 cm (at an extension rate of 1 cm/min), the HMAC pavement condition tends to suffer from fatigue cracking.

CMAC researchers have related this ductility to the dynamic shear rheometer (DSR) loss (*G''*) and storage moduli (*G'*) (Glover et al. 2005). As these moduli increase with aging, the binder (and subsequently the HMAC mixture) breaks or rather fails at smaller values of strain (loss of ductility) due to higher values of stress, thus becoming more susceptible to fatigue cracking. Fig. 2-3 illustrates the relationship between binder ductility and the DSR function *(G″/[η″/G″])* for some 20 conventional (unmodified) binders in the low-ductility region thought to be near HMAC pavement failure. In general, the DSR function increases and the ductility decreases with oxidative aging, respectively (Glover et al. 2005). A decrease in ductility is often associated with a loss in fatigue resistance and subsequently poor field fatigue performance for HMAC pavements.

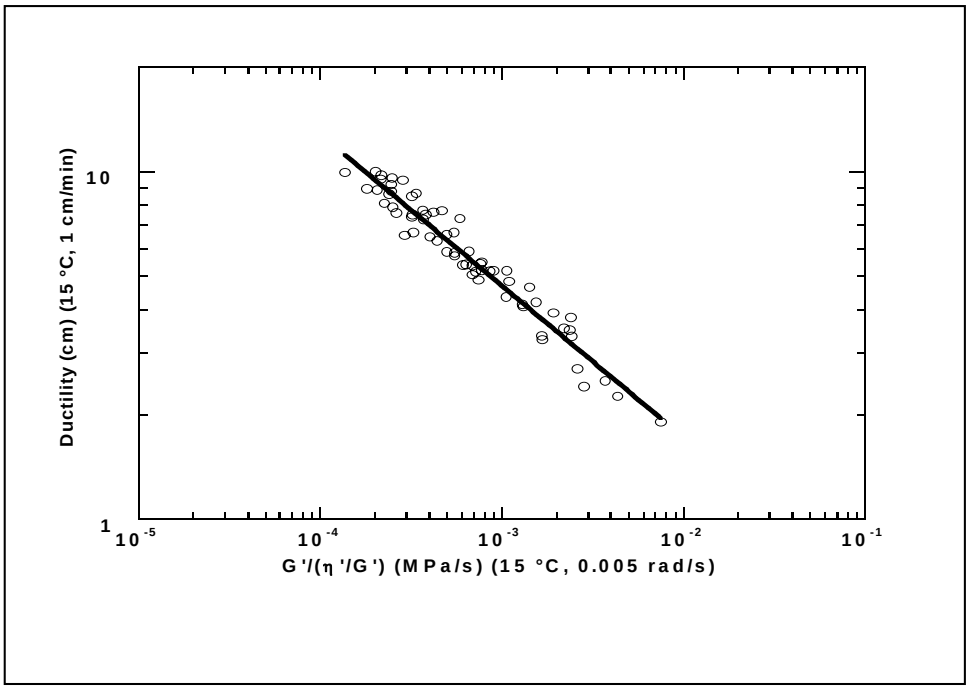

Fig. 2-3. Ductility versus DSR Function (*G''/[η''/G'']*) (Glover et al. 2005)

Based on this discussion, CMAC researchers hypothesized a correlation between binder oxidative aging and HMAC pavement fatigue failure by two mechanisms (Glover et al. 2005):

- increased stresses under loading that result from a decreased ability to flow and an increased elastic stiffness, both leading to cracking due to the HMAC mixture's inability to sufficiently relieve applied stresses, and
- a decreased ability to self-heal that results in a decrease in fatigue resistance.

Consequently, an approach that predicts HMAC mixture fatigue resistance must be sensitive to changes in binder properties that occur due to oxidative aging. These changes vary for binder types that are different chemically and will thus exhibit different physical properties over time depending on the effects of oxidation. Assessment of the impact of aging on HMAC mixture fatigue resistance and the ability of different approaches to incorporate this effect in predicting fatigue life is therefore significant and was investigated in this study.

SELECTED FATIGUE ANALYSIS APPROACHES

Based on this extensive literature review, the following four fatigue analysis approaches, which are discussed in more detail in Chapters IV through to VII, were selected for comparative evaluation in this study:

1) the mechanistic empirical approach with flexural bending beam fatigue testing,
2) the calibrated mechanistic approach with surface energy measurements,
3) the calibrated mechanistic approach without surface energy measurements,
4) the proposed NCHRP 1-37A 2002 Pavement Design Guide approach with dynamic modulus testing.

SUMMARY

The following bullets summarize the key points from the information search:

- Of the positive responses received, the field survey questionnaire indicated that the majority of the DOTs use Superpave, mechanistic empirical, AASHTO, Asphalt Institute, and visco-elastic continuum-damage analysis for their fatigue HMAC mix-design, analysis, and/or structural design check. Laboratory tests include the bending beam, dynamic modulus, indirect tension, uniaxial fatigue, moisture sensitivity, and retained indirect tensile strength.
- A detailed literature review indicated that the major disadvantage of most ME approaches is the lengthy test programs and the fact that these approaches are phenomenologically or empirically based and often assume HMAC linear elastic behavior.
- With advances in computer technology, there has been a drive towards more realistic calibrated mechanistic approaches that utilize continuum micro-mechanics with fracturing and healing as the two primary mechanisms governing HMAC fatigue damage.
- FEM analysis has the potential to model HMAC visco-elastic behavior while calibration constants are utilized to realistically simulate field conditions in calibrated mechanistic approaches.
- Binder oxidative aging has a significant impact on HMAC pavement fatigue performance, primarily in terms of the HMAC mixture's resistance to fracture damage and the ability to heal during traffic loading rest periods and changing environmental conditions. The incorporation of aging effects into the fatigue design and analysis of HMAC mixtures is thus profoundly significant.
- Four fatigue analysis approaches (ME, CMSE, CM, and MEPDG) were selected for comparative evaluation and are discussed in this dissertation.

CHAPTER III
EXPERIMENTAL DESIGN

The research methodology for this study involved an information search discussed in Chapter II and subsequent selection of fatigue analysis approaches, drafting of an experimental design program, laboratory testing, and subsequent data analysis. This chapter discusses the experimental design program, including materials selection and the corresponding HMAC specimen fabrication protocols and aging conditions. Field conditions in terms of the selected pavement structures, traffic, and environmental conditions are also presented. Laboratory testing including the appropriate fatigue analysis approaches are discussed in Chapters IV through VII.

HMAC MIXTURES AND MIX DESIGN

HMAC mixtures commonly used by TxDOT include Type C, coarse matrix high binder (CMHB)-Type C, CMHB-Type F, Type A, Type B, Type D, Type F, Superpave, stone mastic asphalt (SMA), stone filled (SF) mixture, and porous friction course (PFC) (TxDOT 1995). Type C and CMHB-Type C are the most common. More specialized HMAC mixtures include the SMA and SF designs developed to provide superior rutting performance.

Aggregates generally include limestone, igneous, and gravel characterized and blended to typical TxDOT or Superpave standards. Among the performance-graded (PG) binders used by TxDOT, notable ones include PG 58-22, PG 64-22, PG 70-22, and PG 76-22 for Texas environmental conditions.

For this study, two commonly used TxDOT HMAC mixtures were selected for comparative fatigue resistance evaluation. These were basic TxDOT Type C and rut resistant Superpave HMAC mixtures, defined as the Bryan (BRY) and Yoakum (YKM) mixtures, respectively, to represent the districts where the mix-designs were obtained. Note that development of mix-designs was not part of this study.

The Bryan Mixture - Basic TxDOT Type C (PG 64-22 + Limestone)

The Bryan HMAC mixture was designed using standard TxDOT gyratory design protocols from the Bryan District (TxDOT 2002). This HMAC mixture consists of a PG 64-22 binder mixed with limestone aggregates to produce a dense-graded TxDOT Type C mixture. The aggregate gradation curve for this mixture is shown in Fig. 3-1. This mixture was used on highways US 290 and SH 47 in the Bryan District, Texas (TxDOT 2002).

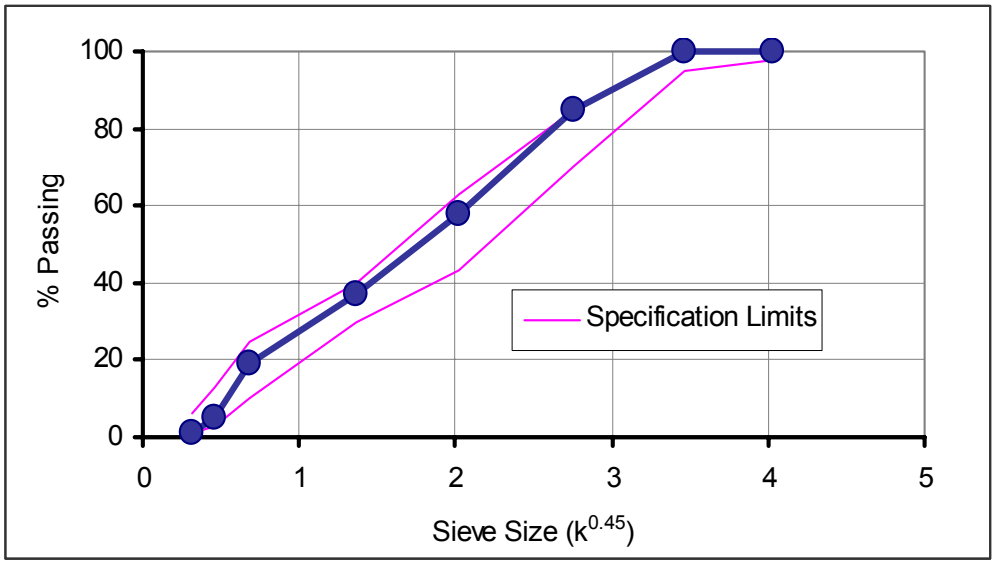

Fig. 3-1. Limestone Aggregate Gradation Curve for TxDOT Type C Mixture

The PG 64-22 binder was supplied by Eagle Asphalt, and the limestone aggregate was supplied by Colorado Materials, Inc., from its Caldwell plant. The mix-design was 4.6% binder content by weight of aggregate (4.4% by weight of total mix) with an HMAC mixture theoretical maximum specific gravity of 2.419 (TxDOT 2002). The target HMAC specimen fabrication air void (AV) content was 7±0.5% to simulate in situ field construction and trafficking when fatigue resistance is considered critical.

The Yoakum Mixture -12.5 mm Superpave (PG 76-22 + Gravel)

The Yoakum HMAC mixture from the Yoakum District was a 12.5 mm Superpave mixture designed with a PG 76-22 binder and crushed river gravel. This mixture was used on US 59 near the city of Victoria in Jackson County, Texas, and is considered a rut-resistant HMAC mixture. This type of HMAC mixture was selected to examine its fatigue properties on the assumption that although rut-resistant HMAC mixtures generally exhibit superior rutting performance in the field, they may often perform poorly in fatigue or other forms of cracking, particularly if the binder stiffens excessively due to aging.

The binder and aggregates were sourced from the Eagle Asphalt (Marlin Asphalt), Inc., and Fordyce Materials plant, respectively. Unlike PG 64-22, PG 76-22 is a modified binder with about 5% styrene-butadiene-styrene (SBS) polymer that improves its high-temperature properties in terms of the shear and viscosity properties. In addition to the crushed river gravel, the Yoakum mixture used 14% limestone screenings and 1% hydrated lime. Fig. 3-2 shows the combined dense gradation of the Yoakum river gravel.

The mix-design was 5.6% binder content by weight of aggregate (5.3% by weight of total mix) with an HMAC mixture theoretical maximum specific gravity of 2.410. Like for the Bryan mixture, the target HMAC specimen fabrication AV content was also 7±0.5%.

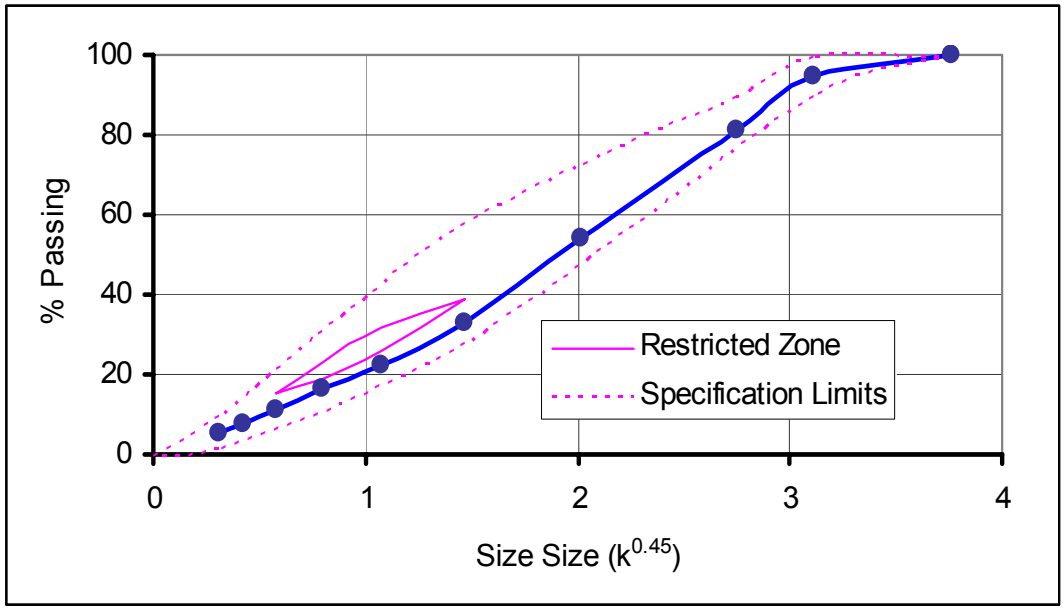

Fig. 3-2. Gravel Aggregate Gradation Curve for the 12.5 mm Superpave Mixture

Material Properties for the Binders

Laboratory characterization of the binder materials based on the AASHTO PP1, PP6, T313, and T315 test protocols produced the results shown in Figs. 3-3 through 3-5 (AASHTO 1996b, 1998). These results represent mean values of at least two binder test samples. In Fig. 3-3, "delta" represents the phase angle "δ" measured in degrees (°).

These verification results shown in Figs. 3-3 through 3-5 indicate that the binders meet the PG specification consistent with the material properties for PG 64-22 and PG 76-22 binders (AASHTO 1996b, 1998).

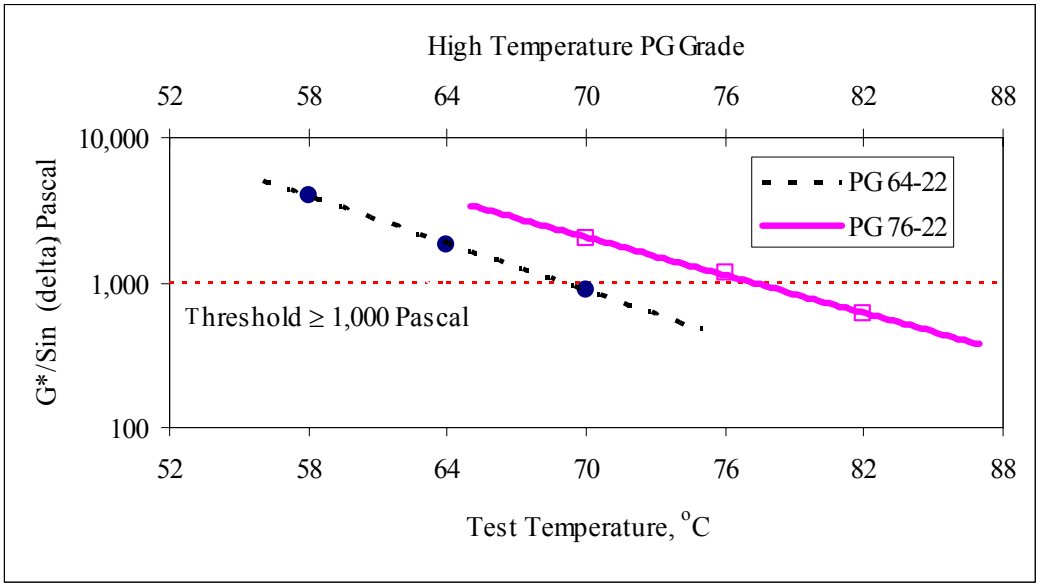

Fig. 3-3. Binder High-Temperature Properties -G*/Sin (delta) (Pascal)

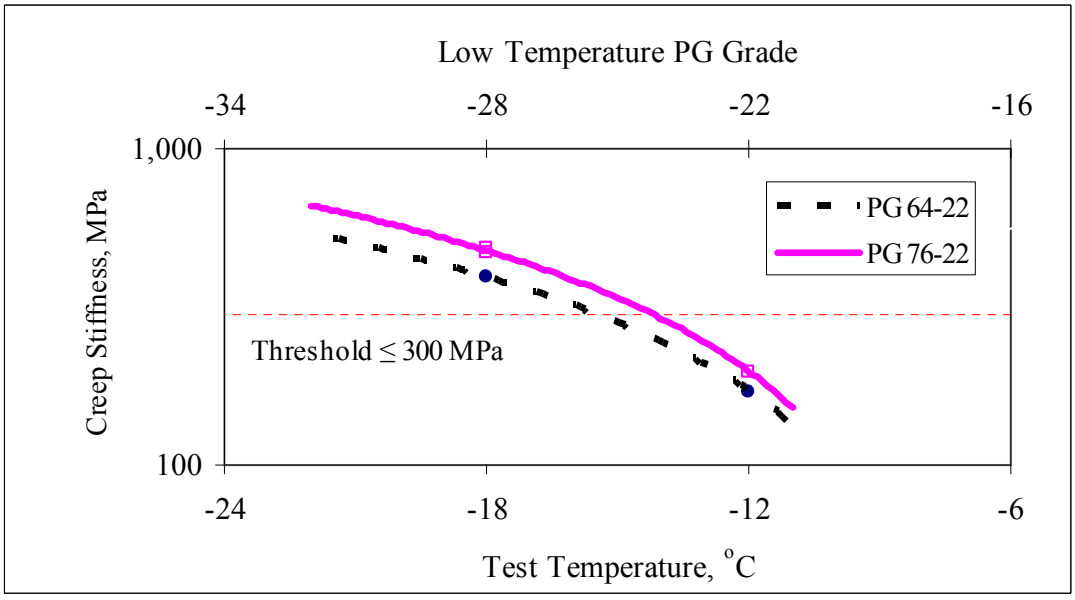

Fig. 3-4. Binder Low -Temperature Properties - Flexural Creep Stiffness (MPa)

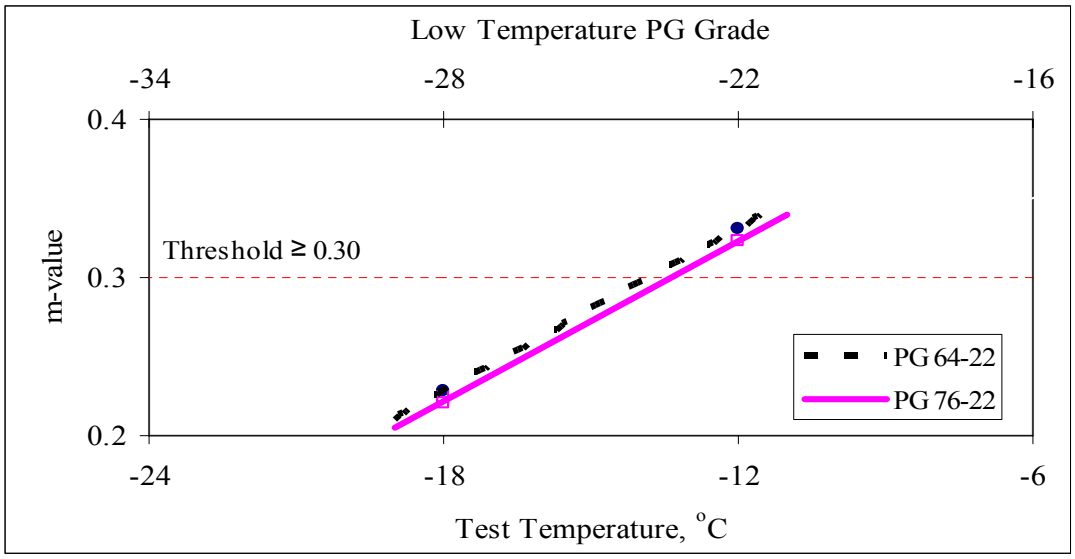

Fig. 3-5. Binder Low-Temperature Properties (m-value)

Table 3-1 shows the measured intermediate temperature properties of the binders at 25 °C in terms of the complex shear modulus (G^*) and the phase angle (δ). The results represent average values of three tests on three different binder samples per binder type. These properties quantify the binders' resistance to fatigue associated cracking based on the PG grading system. As shown in Table 3-1, both the PG 64-22 and PG 76-22 met the required maximum specified threshold value of a $G^* \times Sin\ \delta$ of 5000 kPa (AASHTO 1996b, 1998).

Table 3-1. Intermediate Temperature Properties of the Binders at 25 °C

Binder	**Average Value**		**Standard Deviation of G*Sin δ (kPa)**	**COV (G*Sin δ) (%)**	**PG Specification (kPa)**
	δ (°)	**G*Sin δ (kPa)**			
PG 64-22	65	600	10.91	1.82	≤ 5,000
PG 76-22	62	1,019	70.03	6.90	≤ 5,000

Note that these measured binder properties also constitute input parameters for the proposed M-E Design Guide Level 1 analysis discussed in Chapter VII. These material property results also indicate that, as expected, the complex shear modulus and flexural stiffness of the modified PG 76-22 binder at any test temperature was relatively higher than that of PG 64-22.

Material Properties for the Aggregates

Material properties for the aggregates listed in Table 3-2 indicate that the aggregate meets the specification consistent with the respective test methods shown in Table 3-2 (TxDOT 2003a). The bulk specific gravity for the combined aggregates was 2.591 and 2.603 for limestone and gravel, respectively.

Table 3-2. Aggregate Properties

Test Parameter	Limestone	Gravel	Specification	Test Method
Soundness	18%	20%	≤ 30%	Tex-411-A
Crushed faces count	100%	100%	≥ 85%	Tex-460-A
Los Angeles abrasion	28%	25%	≤ 40%	Tex-410-A
Sand equivalent	74%	77%	≥ 45%	Tex-203-F

HMAC SPECIMEN FABRICATION

The basic HMAC specimen fabrication procedure involved the following steps: aggregate batching, binder-aggregate mixing, short-term oven aging (STOA), compaction, sawing and coring, and finally volumetric analysis to determine the AV. These steps are briefly discussed in this section. Note that the acronym AASHTO PP2 is also used synonymously with the acronym STOA in this dissertation.

Aggregate Batching

Aggregates were batched consistent with the gradations shown in Tables 3-3 and 3-4, which correspond to those shown in Figs. 3-1 and 3-2, respectively.

Table 3-3. Limestone Aggregate Gradation for TxDOT Type C Mixture

Sieve Size		TxDOT Specification (TxDOT 1995)		% Passing
	mm	Upper Limit (%)	Lower Limit (%)	
5/8″	15.9	100	98	100.0
1/2″	12.5	100	95	100.0
3/8″	9.5	85	70	84.8
#4	4.75	63	43	57.9
#10	2.0	40	30	36.9
#40	0.425	25	10	19.0
#80	0.175	13	3	5.0
#200	0.075	6	1	1.0

Table 3-4. Gravel Aggregate Gradation for 12.5 mm Superpave Mixture

Sieve Size		TxDOT Specification (TxDOT 1995)		% Passing
	mm	Upper Limit (%)	Lower Limit (%)	
3/4″	19.00	100		100.0
1/2″	12.50	100	90	94.6
3/8″	9.50	90		81.0
#4	4.75			54.4
#8	2.36	58	28	32.9
#16	1.18			22.4
#30	0.60			16.2
#50	0.30			11.0
#100	0.150			7.6
#200	0.075	10	2	5.5

Mixing, Short-Term Oven Aging, Compaction, and Air Voids

The HMAC mixture mixing and compaction temperatures shown in Table 3-5 are consistent with the TxDOT Tex-205-F and Tex-241-F test specifications for PG 64-22 and PG 76-22 binders (TxDOT 2003b). Prior to binder-aggregate mixing, the limestone and gravel aggregates were pre-heated to a temperature of 144 °C and 163 °C, respectively, for at least 4 hr to remove moisture. The binder was also heated at the mixing temperature for at most 30 min before mixing to liquefy it.

Table 3-5. HMAC Mixture Mixing and Compaction Temperatures

Process	**HMAC Mixture Temperature (°C)**	
	Bryan Mixture	**Yoakum Mixture**
Aggregate pre-heating	144 (291 °F)	163 (325 °F)
30 min binder pre-heating	144 (291 °F)	163 (325 °F)
Binder-aggregate mixing	144 (291 °F)	163 (325 °F)
4 hr short-term oven aging	135 (275 °F)	135 (275 °F)
Compaction	127 (261 °F)	149 (300 °F)

HMAC mixture STOA lasted 4 hr at a temperature of 135 °C (275 °F) consistent with the AASHTO PP2 standard aging procedure for Superpave mixture performance testing (AASHTO 1994). STOA simulates the time between HMAC mixing, transportation, and placement in the field (AASHTO 1994).

Gyratory Compaction

All the cylindrical HMAC specimens for the dynamic modulus and CMSE/CM tests were gyratory compacted using the standard Superpave Gyratory Compactor (SGC) shown in Fig. 3-6. Compaction parameters were 1.25° compaction angle and 600 kPa vertical pressure at a rate of 30 gyrations per minute.

Fig. 3-6. Superpave Gyratory Compactor (SGC)

Kneading Beam Compaction

Beam HMAC specimens for the flexural bending beam fatigue tests were compacted using the linear kneading compactor shown in Fig. 3-7 up to the target AV content consistent with the specified beam thickness at a maximum compaction pressure of 6,900 kPa (Tayebali et al. 1992, AASHTO 1996a).

Fig. 3-7. Linear Kneading Compactor

All HMAC specimens were compacted to a target AV content of 7±0.5%, as stated previously, to simulate after in situ field construction and trafficking when fatigue resistance is considered critical.

Specimen Sawing, Coring, Handling, and Storage

HMAC cylindrical specimens were gyratory compacted to a size of 165 mm height by 150 mm diameter, while actual test specimens were sawn and cored to a 150 mm height and 100 mm diameter. HMAC beam specimens were kneading compacted to a size of 457 mm length by 150 mm width by 63 mm thickness, and test specimens were sawn to a 380 mm length by 63 mm width by a 50 mm thickness (AASHTO 1996a). Fig. 3-8 shows the dimensions of the final test specimens.

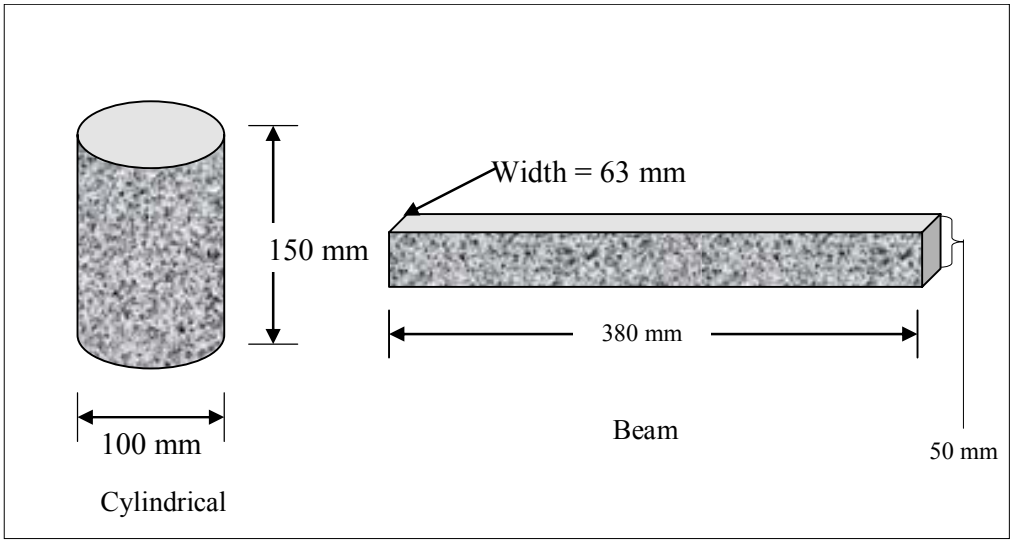

Fig. 3-8. Laboratory Test Specimens (Drawing Not to Scale)

After the specimens were sawn and cored, volumetric analysis based on the fundamental principle of water displacement was completed to determine the actual specimen AV. HMAC specimens that did not meet the target AV content were discarded or used as dummies in trial tests. In total, a cylindrical specimen took approximately 40 hr to fabricate, while a beam specimen, because of the difficulty in sawing, took an additional 5 hr. While beam specimens require delicate handling, the cylindrical specimens are not as sensitive to handling. Prior to laboratory testing, specimens were generally stored on flat surfaces in a temperature-controlled room at approximately 20±2 °C.

BINDER AND HMAC MIXTURE AGING CONDITIONS

Three laboratory aging exposure conditions listed in Table 3-6 were utilized in this study for both the binder and HMAC compacted specimens. Consistent with the Superpave procedure, all loose HMAC mixtures were subjected to 4 hr STOA (discussed previously) prior to room aging of the compacted HMAC specimens for the three selected aging conditions (AASHTO 1994).

Table 3-6. Laboratory Aging Conditions for Binders and HMAC Compacted Specimens

Laboratory Aging Condition	Aging Process	Description
0 months	4 hr AASHTO PP2 STOA of loose HMAC mix at 135 °C plus 0 months aging of compacted HMAC specimens at 60 °C in an environmental temperature-controlled room	Simulates the time period just after HMAC in situ field construction at the end of compaction (AASHTO 1994)
3 months	4 hr AASHTO PP2 STOA of loose HMAC mix at 135 °C plus 3 months aging of compacted HMAC specimens at 60 °C in an environmental temperature-controlled room	Simulates 3 to 6 years of Texas HMAC environmental exposure (Glover et al. 2005)
6 months	4 hr AASHTO PP2 STOA of loose HMAC mix at 135 °C plus 6 months aging of compacted HMAC specimens at 60 °C in an environmental temperature-controlled room	Simulates 6 to 12 years of Texas HMAC environmental exposure (Glover et al. 2005)

The laboratory aging process for HMAC specimens involved keeping the compacted HMAC specimens in a temperature-controlled room at 60 °C (140 °F) and at the same time allowing the heated air to circulate freely around the specimens. This allowed for accelerated oxidative aging of the binder within the HMAC specimens. An aging temperature of 60 °C was selected to accelerate aging because this temperature realistically simulates the critical pavement service temperature in Texas for HMAC aging. Based on previous research, the process also simulates the field HMAC aging rate (Glover et al. 2005). After HMAC mixture testing, the aged binders were extracted from tested HMAC specimens for binder testing by CMAC to characterize the binder's chemical and physical properties. In addition, CMAC also aged some binders in thin films in a stirred air flow test (SAFT) and the pressure aging vessel (PAV*) alongside HMAC mixtures to simulate the hot-mix process for short-term aging comparisons with the AASHTO PP2 aging procedure (Vassiliev et al. 2002).

Fig. 3-9 is a schematic illustration of the HMAC specimen aging conditions considered in each respective fatigue analysis approach. The M-E Pavement Design Guide software encompasses a global aging model that takes into account the binder aging effects, discussed in Chapter VII. Therefore, it was deemed unnecessary to test aged HMAC specimens for the M-E Pavement Design Guide fatigue analysis.

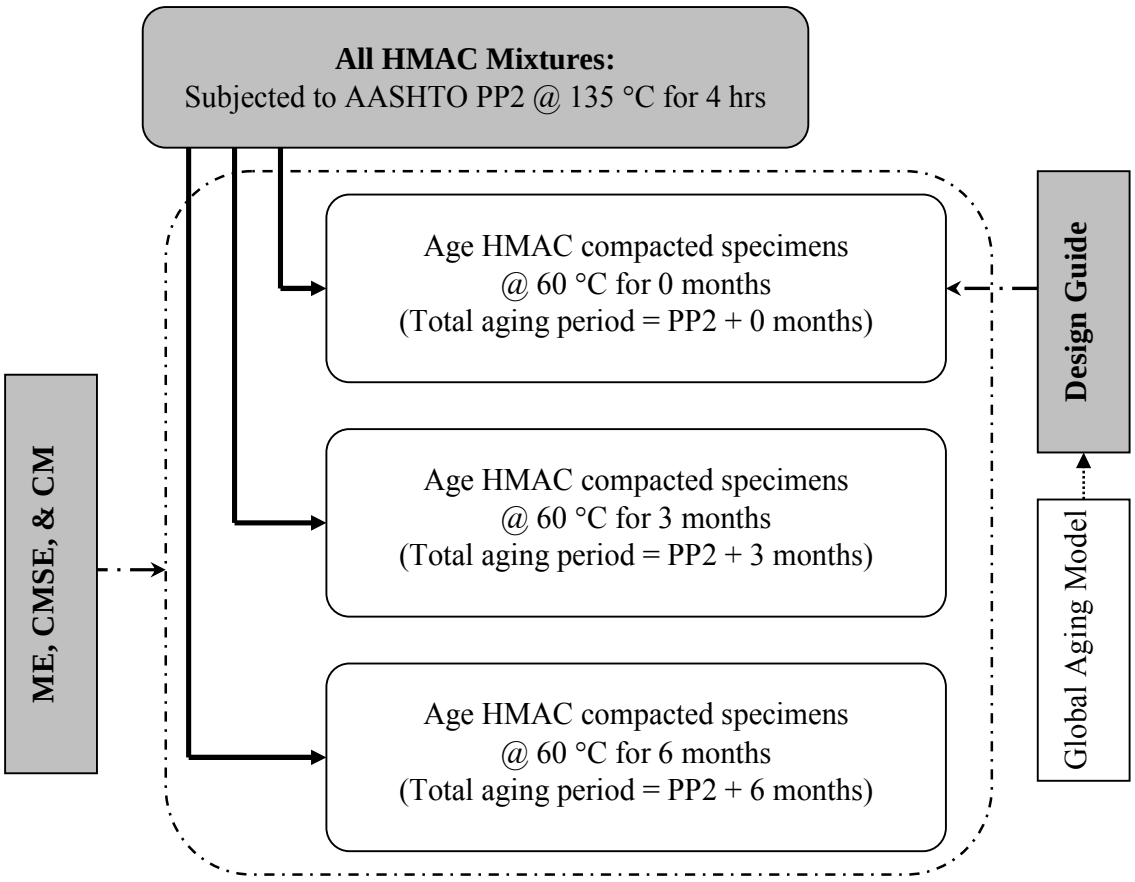

Fig. 3-9. Fatigue Analysis Approaches and HMAC Mixture Aging Conditions

HYPOTHETICAL FIELD PAVEMENT STRUCTURES AND TRAFFIC

Table 3-7 displays a list of the five selected TxDOT pavement structures (PS) and five associated traffic levels ranging between 0.25 to 11.00 × 10^6 ESALs over a design life of 20 yr that were considered in this study. These HMAC pavement structures represent actual material properties and layer thicknesses that are commonly used on TxDOT highways (Freeman 2004). Typical traffic loading conditions consisted of an 80 kN (18 kip) axle load, 690 kPa (100 psi) tire pressure, 97 km/hr (60 mph) speed, and 10% to 25% truck traffic over a design life of 20 yr (Freeman 2004). In Table 3-7, PS#5 represents the actual pavement structure where the Bryan mixture was used.

Table 3-7. Pavement Structures and Traffic

PS #	HMAC Surfacing	Base	Subbase	Subgrade	Traffic ESALs	Trucks
1	150 mm, 3447 MPa, ν = 0.33	Flex, 350 mm, 414 MPa, ν = 0.40	N/A	63 MPa ν = 0.45	5.0E+06	25%
2	50 mm, 3447 MPa, ν = 0.33	Flex, 250 mm, 414 MPa, ν = 0.40	Lime stab, 150 mm, 241 MPa, ν = 0.35	85 MPa ν = 0.45	1.4E+06	24%
3	50 mm, 3447 MPa, ν = 0.33	Flex, 150 mm, 345 MPa, ν = 0.40	Stab. sub, 127 mm, 207 MPa, ν = 0.40	69 MPa ν = 0.45	0.4E+06	11%
4	50 mm, 3447 MPa, ν = 0.33	Asphalt stab, 175 mm, 3447 MPa, ν = 0.35	Flex, 200 mm, 165 MPa, ν = 0.40	66 MPa ν = 0.45	7.2E+06	13%
5	100 mm, 3447 MPa, ν = 0.33	Cemented, 350 mm, 1034 MPa, ν = 0.35	N/A	103 MPa ν = 0.45	10.8E+06	15%

ENVIRONMENTAL CONDITIONS

Fig. 3-10 shows five Texas environmental zones based on annual precipitation, annual freezing index, and the number of wet days and freeze/thaw days (Freeman 2004). As shown in Fig. 3-10, the TxDOT districts have been grouped into five environmental zones: dry-cold (DC), wet-cold (WC), dry-warm (DW), wet-warm (WW), and moderate.

The italicized environmental zones (*DC*, *WW*, and *DW*) in Fig. 3-10 indicate zones that are critical to alligator (fatigue) cracking according to the TxDOT Pavement Management Information System (PMIS) report (TxDOT 2003a). About 20% to 100% of the PMIS pavement sections in these locations exhibited alligator cracking.

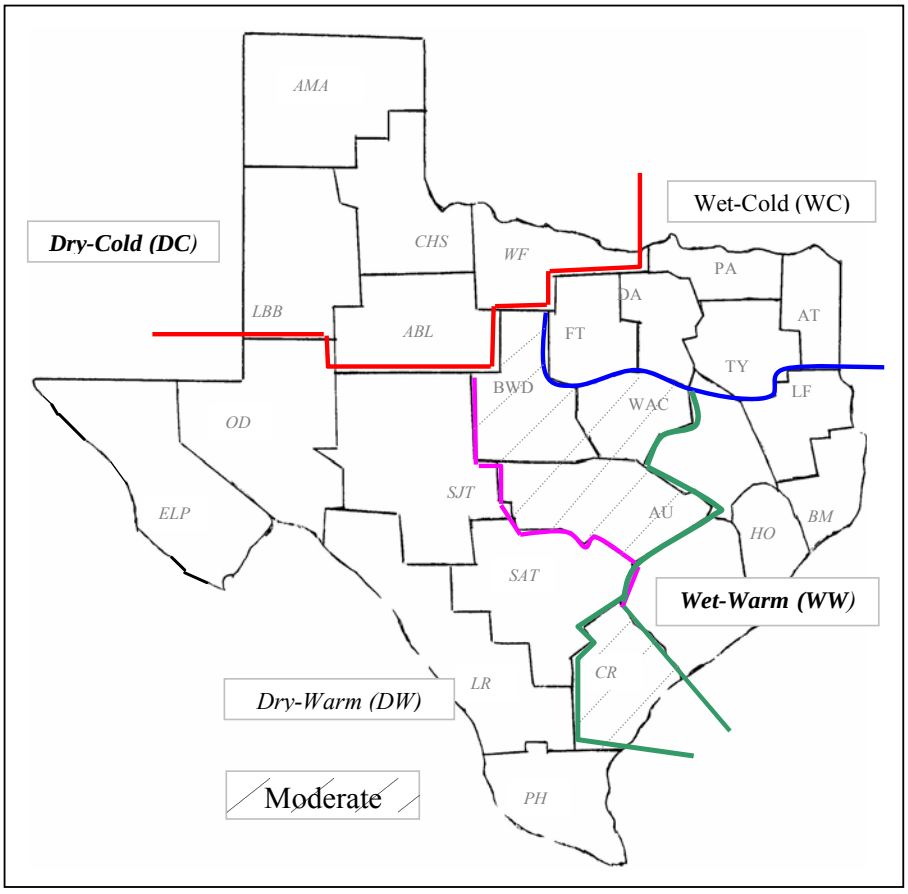

Fig. 3-10. Texas Environmental Zoning (Freeman 2004)

Pavement material performance depends on both traffic and environment. It is therefore not uncommon that for a given design traffic level, a material that performs well in a particular environment may perform poorly in a different environmental location. Material properties for pavement design and performance evaluation are thus generally characterized as a function of environmental conditions.

HMAC, for instance, is very sensitive to temperature changes, while unbound materials in the base, subbase, or subgrade are generally more sensitive to moisture variations. Most often, the HMAC elastic modulus is characterized as a function of seasonal or monthly temperature variations, with the critical pavement temperature being at the mid-depth or two-thirds depth point of the HMAC layer. This pavement temperature generally (but not always) exhibits a decreasing trend with depth. The subgrade elastic modulus is normally characterized as a function of the seasonal moisture conditions, with the wettest period of the year considered as the worst-case scenario assuming a conservative design approach. Note also that water seepage through cracks and/or accumulation in AV can accelerate damage, including fatigue cracking in HMAC materials.

In this study, two environmental conditions, WW and DC were considered (see Fig. 3-10). WW and DC are the two extreme Texas weather conditions considered to have a significant impact on HMAC mixture fatigue performance. In fact, the 2003 TxDOT "*Condition of Texas Pavements PMIS Annual Report*" indicates that HMAC highway pavements in these environmental locations (WW and DC) are comparatively more susceptible to fatigue-associated cracking (TxDOT 2003a).

RELIABILITY LEVEL

For this study, a 95% reliability level was utilized. This is a typical value often used for most practical HMAC pavement designs and analyses. In statistical terms, this means that for a given test or assessment criteria, there is 95% data accuracy, and that up to 5% failure or result inaccuracy is anticipated and tolerable. In other words, the acceptable risk level is 5%, which is better known as the level of significance "alpha" ($\alpha = 0.05$), in statistical language (Montgomery et al. 2002).

STRESS-STRAIN ANALYSIS

For the five selected hypothetical PSs and environmental conditions (WW and DC) considered, elastic ELSYM5 stress-strain computations were adjusted based on FEM simulations to account for the HMAC visco-elastic and plasticity behavior (Ahlborn 1969, Park 2004).

ELSYM5 Input and Output Data

The bullets below summarize the typical input data requirement for ELSYM5 stress-strain analysis:

- pavement structure (number of layers and layer thicknesses),
- material properties (elastic modulus and Poisson's ratio), and
- traffic loading (axle load and tire pressure).

Table 3-7 displays the PSs and the respective elastic moduli used for ELSYM5 analysis in this study. The axle load and tire pressure used were as discussed previously, 80 kN and 690 kPa. Typical Poisson's ratios used in the analysis were 0.33, 0.40, and 0.45 for the HMAC layer, the base, and subgrade, respectively (Huang 1993). The basic output response parameters from the ELSYM5 computational analysis include the stresses, strains, and deformations.

The strain response parameters from ELSYM5 were then adjusted according to FEM simulations discussed in the subsequent section to account for HMAC visco-elastic and plastic behavior. These tensile (ε_t) and shear (γ) strains constitute input parameters for the ME, CMSE, and CM fatigue analysis, respectively, discussed in Chapters IV through VI. Stress-strain computations for the M-E Pavement Design Guide (Chapter VII) are built into the analysis software.

FEM Strain Adjustment

The FEM strain-adjustment factor for elastic strain analysis to account for HMAC visco-elastic and plastic behavior was determined as follows:

$$S_{adj\,(VE)i} = \frac{Strain_{FEM}}{Strain_{ELSYM5}} \qquad (3\text{-}1)$$

where:

$S_{adj(VE)}$ = FEM strain-adjustment factor

$Strain_{FEM}$ = Strain (ε_t or γ) computed via FEM analysis (mm/mm)

$Strain_{ELSYM5}$ = Strain (ε_t or γ) computed via ELSYM5 analysis (mm/mm)

Subscript i = ε_t or γ

For this study, mean $S_{adj(VE)}$ values of 1.25 and 1.175 were used for ε_t and γ computations, respectively, based on the previous FEM work by Park (2004) (ABAQUS 1996). Note that while it is possible that these visco-elastic adjustments may vary for different HMAC mixtures, the adjustment from layered elastic to elasto-viscoplastic was assumed to be constant across both HMAC mixtures in this study. In addition, the elastic moduli values at 0 months laboratory aging for these two HMAC mixtures did not vary significantly. Thus for each computed ELSYM5 strain (ε_t and γ) for the PSs shown in Table 3-7, the $S_{adj(VE)i}$ was applied as shown in Eqs. (3-2) and (3-3) to obtain the critical design strains as listed in Table 3-8:

$$\varepsilon_t = S_{adj(VE)e_t} \times \varepsilon_{t(ELSYM5)} = 1.25\varepsilon_{t(ELSYM5)} \quad (3\text{-}2)$$

$$\gamma = S_{adj(VE)\gamma} \times \gamma_{(ELSYM5)} = 1.175\gamma_{(ELSYM5)} \quad (3\text{-}3)$$

Table 3-8. Computed Critical Design Strains

PS#	WW Environment		DC Environment	
	(ε_t)	(γ)	(ε_t)	(γ)
1	1.57×10^{-4}	1.56×10^{-2}	1.51×10^{-4}	1.51×10^{-2}
2	2.79×10^{-4}	1.98×10^{-2}	2.71×10^{-4}	1.89×10^{-2}
3	2.73×10^{-4}	1.91×10^{-2}	2.66×10^{-4}	1.86×10^{-2}
4	2.89×10^{-4}	2.06×10^{-2}	2.78×10^{-4}	1.96×10^{-2}
5	0.98×10^{-4}	1.41×10^{-2}	0.91×10^{-4}	1.46×10^{-2}

SUMMARY

Salient points from this chapter are summarized as follows:

- Two commonly used TxDOT HMAC mixtures, the Bryan (PG 64-22 + limestone) and Yoakum (PG 76-22 + gravel) mixtures were selected for fatigue analysis in this study. Bryan is a typical basic TxDOT Type C HMAC mixture while Yoakum is a rut-resistant 12.5 mm Superpave HMAC mixture. Both the binder and aggregate material properties were consistent with the Superpave PG and TxDOT standards.
- Two laboratory compactors, the standard SGC and kneading beam compactor, were utilized for compacting cylindrical and beam HMAC specimens, respectively.

- The target HMAC specimen fabrication AV content was 7±0.5% to simulate the in situ AV field compaction after construction and trafficking when fatigue resistance is considered critical.
- Three laboratory aging exposure conditions at a critical temperature of 60 °C were selected to investigate the effects of oxidative aging on binder and HMAC mixture properties including fatigue resistance. These aging conditions were 0, 3, and 6 months that simulate approximately up to 12 years of Texas HMAC field aging exposure (Glover et al. 2005).
- Five hypothetical standard TxDOT HMAC pavement structures with corresponding traffic levels of 0.25 to 11.00 million ESALs over a design life of 20 years were selected for analysis. Using layered elastic analyses (ELSYM5) and adjusting based on FEM simulations, tensile and shear strains within the pavement HMAC layer were determined and utilized as the failure load-response parameters associated with fatigue cracking when predicting the HMAC mixture fatigue resistance.
- Two Texas environmental conditions (wet-warm and dry-cold) that are considered critical to fatigue-associated (alligator) cracking in HMAC pavements were selected for the analysis.

CHAPTER IV
THE MECHANISTIC EMPIRICAL APPROACH

This chapter discusses the mechanistic empirical (ME) approach for HMAC pavement fatigue analysis. This includes the fundamental theory, input/output data, the flexural bending beam laboratory fatigue testing, the failure criteria, the analysis procedure, and statistical analysis.

FUNDAMENTAL THEORY

The selected SHRP A-003A ME approach in this study utilizes the flexural bending beam fatigue test (third-point loading) and considers bottom-up cracking to determine an empirical fatigue relationship of the simple power form shown in Eq. (4-1) (Tayebali et al. 1992):

$$N = k_1 \varepsilon^{-k_2} \qquad (4\text{-}1)$$

where:

N = Number of load cycles to fatigue failure

ε = Applied tensile strain (mm/mm)

k_i = Laboratory-determined material constants

The SHRP A-003A fatigue analysis approach incorporates reliability concepts that account for uncertainty in laboratory testing, construction, and traffic prediction; and considers environmental factors, traffic loading, and pavement design. The SHRP A-003A is the ME fatigue analysis approach utilized in this study, and the flexural bending beam fatigue testing to determine the HMAC mixture fatigue empirical relationship shown in Eq. (4-1) was based on the AASHTO TP8-94 test protocol (AASHTO 1996a). The AASHTO TP8-94 test protocol is discussed later in this chapter.

HMAC specimen preparation by rolling wheel or kneading compaction is strongly recommended as part of this ME approach to simulate the engineering properties of extracted field HMAC pavement cores. Conditioning prior to laboratory testing to a representative or worst-case aging state is also suggested. The AASHTO TP8-94 test protocol requires testing conditioned HMAC specimens at least at two different controlled strain levels under sinusoidal repeated loading to generate an empirical fatigue relationship as shown in Eq. (4-1) (AASHTO 1996a).

Determination of the experimental fatigue relationship expressed by Eq. (4-1) constitutes the empirical part of the ME approach of fatigue modeling of HMAC mixtures. This empirical fatigue relationship (Eq. [4-1]) is then used in the design and analysis system illustrated schematically in Fig. 4-1.

The fatigue analysis system shown in Fig. 4-1 evaluates the likelihood that the selected design HMAC mixture will adequately resist fatigue cracking in a specific pavement structure under anticipated in situ conditions, including traffic loading and the environment. The designer must, however, select a specific level of reliability commensurate with the pavement site for which the HMAC mixture will be utilized, as well as the required level of service of the pavement structure.

An HMAC mixture is expected to perform adequately if the number of load repetitions sustainable in laboratory testing after correcting for field conditions exceeds the number of load repetitions anticipated in service. The design strain at which the pavement fatigue life must be estimated using the empirical fatigue relationship developed based on laboratory testing results is often computed using a simple multi-layer elastic theory. For this computation, the design strain of interest is the maximum principal horizontal-tensile strain at the bottom of the HMAC layer in the specific pavement structure, assuming the bottom-up mode of fatigue cracking. The determination of this critical design tensile strain within a representative field pavement structure at the bottom of the HMAC layer constitutes the mechanistic part of the ME approach.

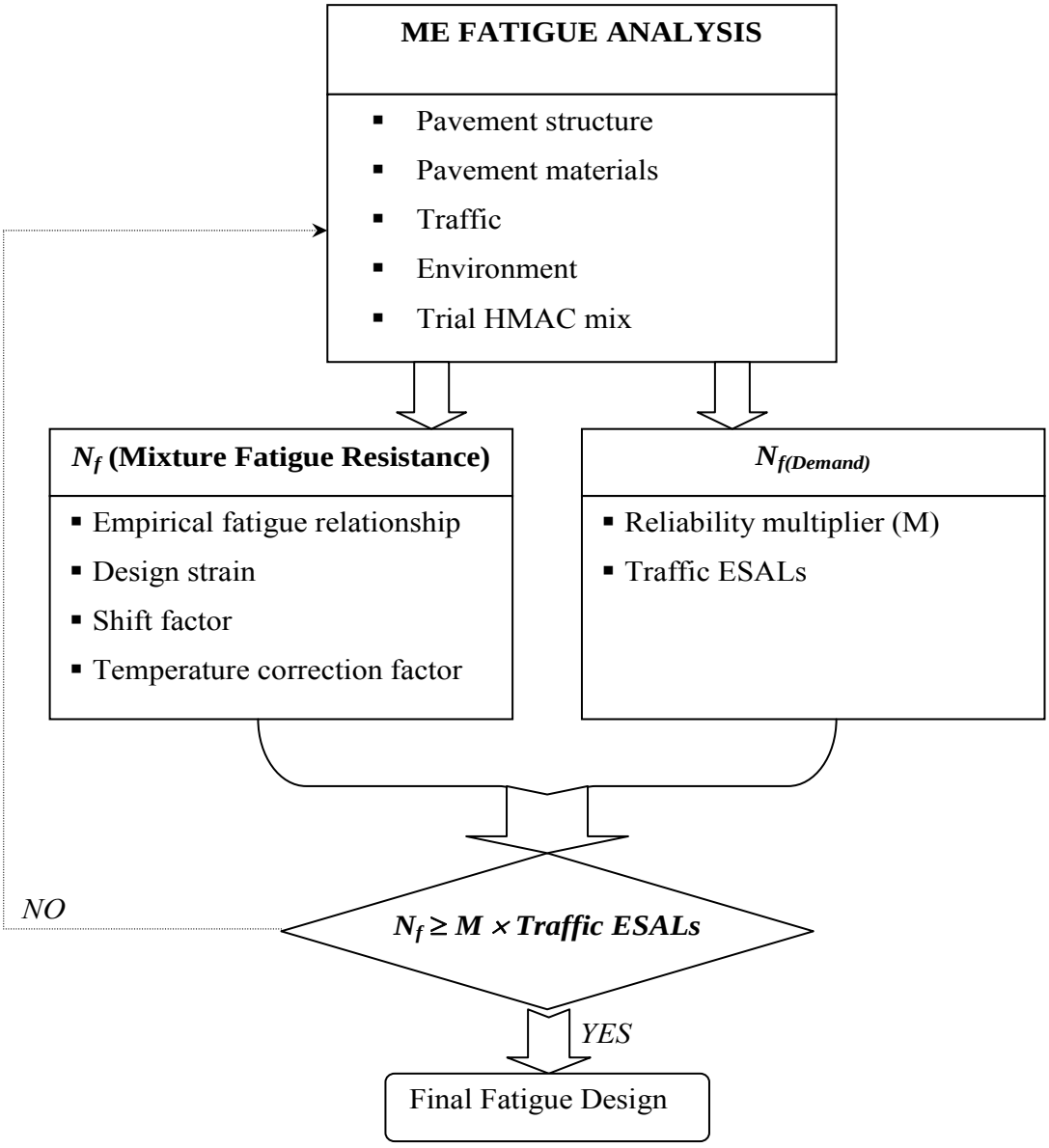

Fig. 4-1. The ME Fatigue Design and Analysis System

INPUT/OUTPUT DATA

Table 4-1 summarizes the general ME fatigue analysis input and the expected output data based on the SHRP A-003A approach and the AASHTO TP8-94 bending beam fatigue test protocol (Tayebali et al. 1992, AASHTO 1996a). These parameters and their respective components are discussed in more detail in subsequent sections.

Table 4-1. Summary of ME Fatigue Analysis Input and Output Data

Source	**Parameter**
Laboratory test data (HMAC mixture testing of beam specimens)	• Strain (ε_t) & stress • # of fatigue load cycles (N)
Analysis of laboratory test data	• Flexural stiffness or dissipated energy • Material regression constants (k_i) • Empirical fatigue relationship ($N = f(\varepsilon_t)$)
Field conditions (design data)	• Pavement structure (layer thickness) • Pavement materials (elastic modulus & Poisson's ratio) • Traffic (ESALs, axle load, & tire pressure) • Environment (temperature & moisture conditions) • Field correction/shift factors (i.e., temperature)
Computer stress-strain analysis	• Design tensile strain (ε_t) @ bottom of the top HMAC layer
Other	• Reliability level (i.e., 95%) • Reliability multiplier (M)
Output	• HMAC mixture fatigue resistance ($N_{f(Supply)}$) • Pavement fatigue life ($N_{f(Demand)}$) • Assessment of adequate or inadequate performance

LABORATORY TESTING

The flexural bending beam fatigue test including the test equipment, specimen setup, and data acquisition was conducted consistent with the AASHTO TP8-94 test procedure (Tayebali et al. 1992, AASHTO 1996a). This section discusses the flexural bending beam fatigue test protocol.

The Flexural Bending Beam Fatigue Test Protocol

The flexural bending beam (BB) fatigue test consists of applying a repeated constant vertical strain to a beam specimen in flexural tension mode until failure or up to a specified number of load cycles. In this study, the test was strain controlled and the input strain waveform was sinusoidal shaped, applied at a frequency of 10 Hz. The BB test device and the loading configuration are shown in Figs. 4-2 and 4-3, respectively.

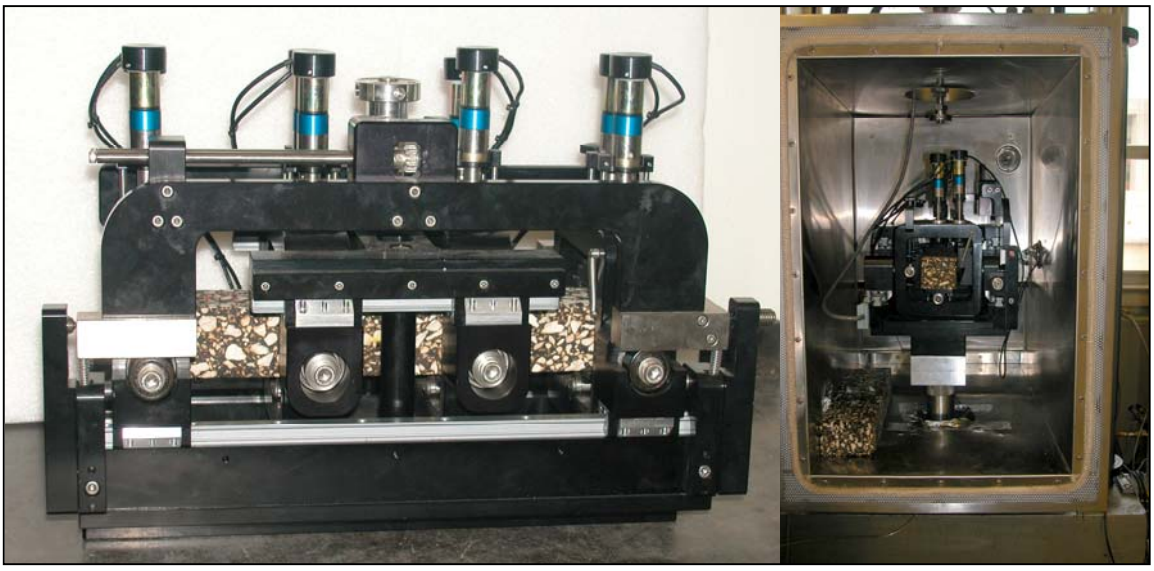

Fig. 4-2. The BB Test Device

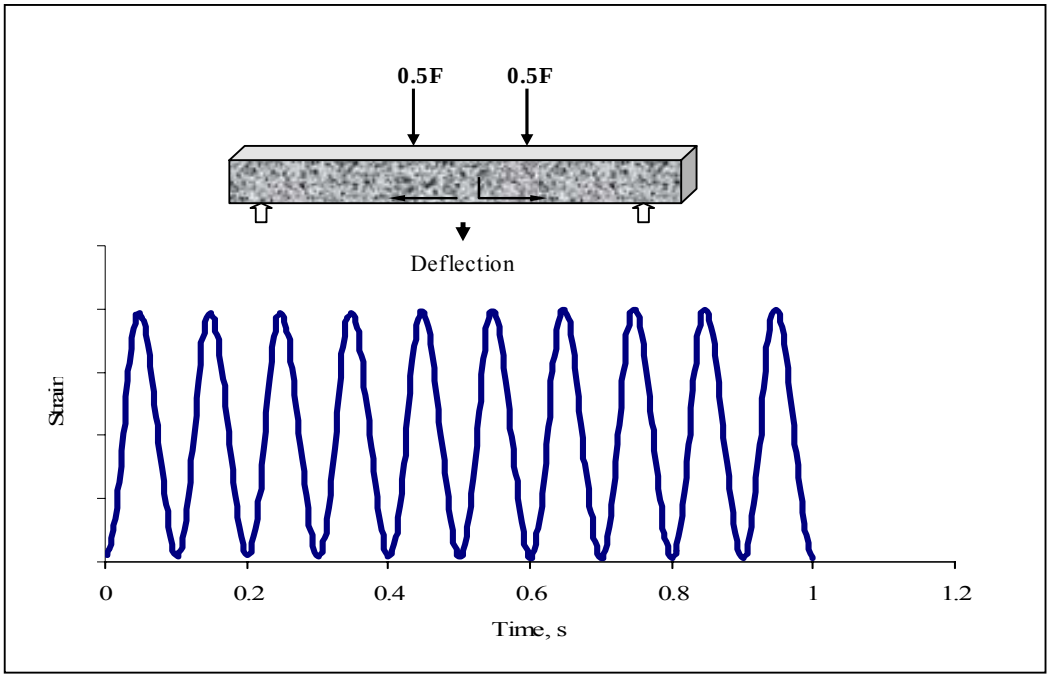

Fig. 4-3. Loading Configuration for the BB Fatigue Test

As evident in Fig. 4-3, repeated vertical loading causes tension in the bottom zone of the HMAC specimen, from which cracking will subsequently initiate and propagate to the top, thus simulating pavement fatigue failure under traffic loading. The test was conducted at two strain levels of approximately 374 and 468 microstrain consistent with the AASHTO TP8-94 test protocol to generate the required material N-ε_t empirical relationship shown in Eq. (4-1) (AASHTO 1996a). These test strain levels are within the recommended AASHTO TP8-94 test protocol range to reduce test time while at the same time capturing sufficient data for analysis.

A 10 Hz frequency (Fig. 4-3) without any rest period was used for the test. The average duration of each test was approximately 5 hr. Note that the BB test time is inversely proportional to the magnitude of the input strain wave. Testing can, however, be terminated either when the initial application load response (stress) recorded at the 50^{th} load cycle decreases to 50% in magnitude or when a preset number of load cycles such as 100,000 is reached. The former approach was used in this study.

Test Conditions and Specimens

HMAC is temperature sensitive, so the test was conducted in an environmentally controlled chamber at a test temperature of 20±0.5 °C, consistent with the AASHTO TP8-94 test procedure (AASHTO 1996a). The minimum HMAC specimen conditioning time was 2 hr. However, specimens were actually preconditioned at 20 °C on a more convenient 12 hr overnight-time period. The test temperature was monitored and recorded every 600 s via a thermocouple probe attached inside a dummy HMAC specimen also placed in the environmental chamber. Fig. 4-4 is an example of a temperature plot captured during BB testing at 20 °C.

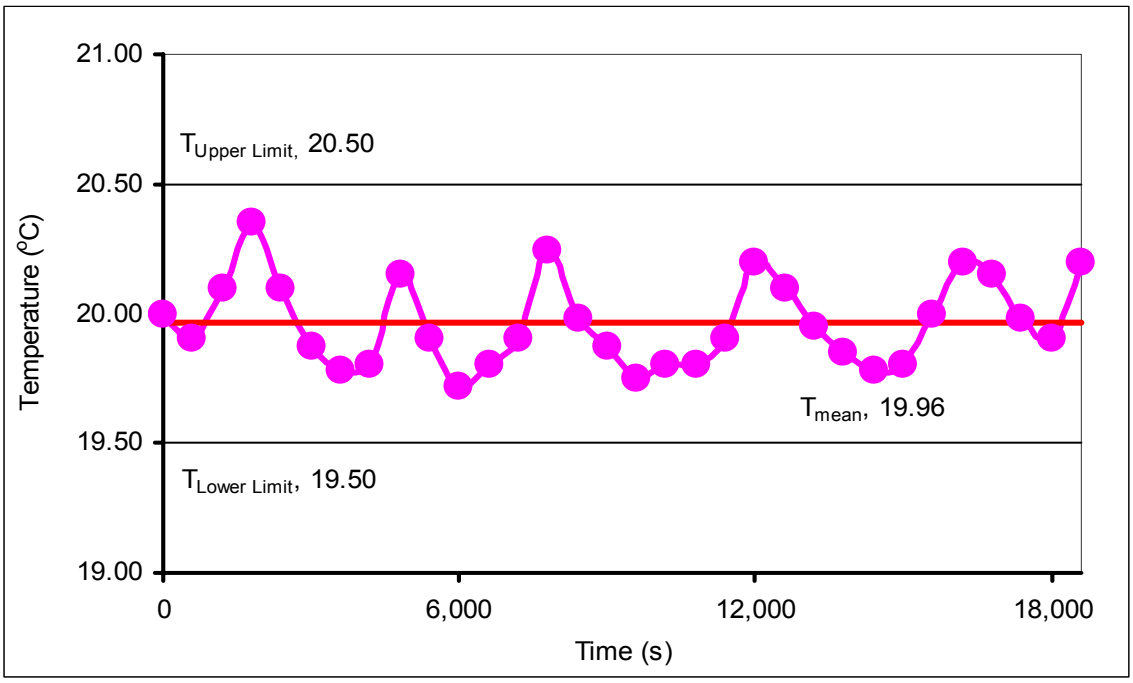

Fig. 4-4. Example of Temperature Plot for BB Testing at 20 °C

As evident in Fig. 4-4, the average temperature for this particular test was 19.96 °C with a coefficient of variation (COV) of 0.84%. Three replicate beam specimens were tested for each strain level, so a complete BB test cycle for low and high strain level tests required a minimum of six beam specimens per aging condition per HMAC mixture type.

Test Equipment and Data Measurement

A servo electric-hydraulic controlled material testing system (MTS) equipped with an automatic data measuring system applied the sinusoidal input strain waveform. Actual loading of the specimen was transmitted by the BB device shown in Fig. 4-2, to which the beam specimen was securely clamped. Loading data were measured via the MTS load cell, and flexural deflections were recorded via a single linear differential variable transducer (LVDT) attached to the center of the specimen. During the test, load and deformation data were captured electronically every 0.002 s. Fig. 4-5 is an example of the output stress response from the BB test at 20 °C based on a 374 test microstrain.

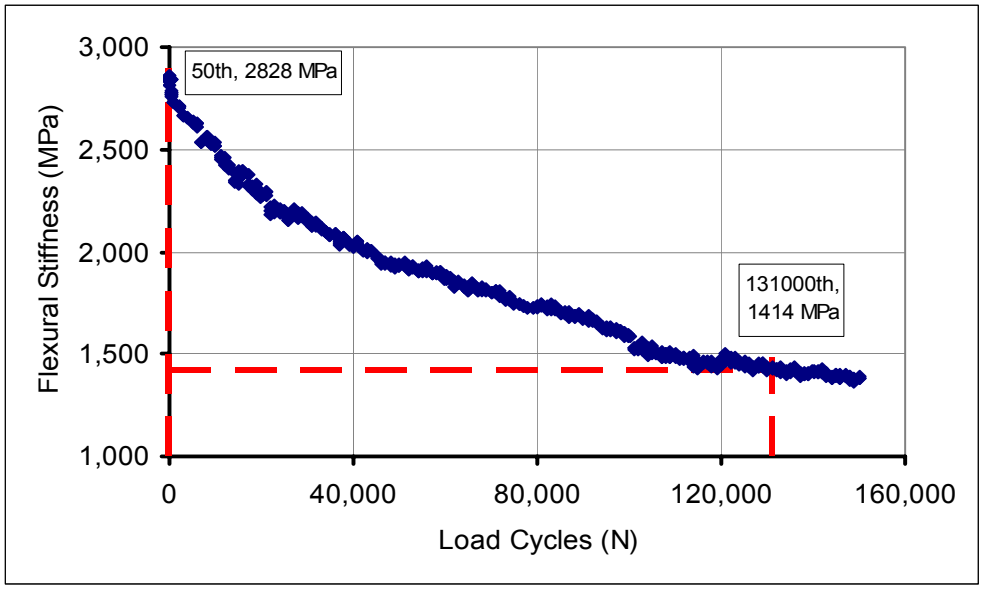

Fig. 4-5. Example of Stress Response from the BB Test at 20 °C (374 Test Microstrain)

FAILURE CRITERIA

For HMAC compacted specimens subjected to repeated flexural bending under strain-controlled loading mode, fatigue failure is defined as the point at which the specimen flexural stiffness is reduced to 50% of the initial flexural stiffness (Tayebali et al. 1992, AASHTO 1996a). This initial stiffness is generally defined as the specimen flexural stiffness measured at the 50^{th} load cycle, illustrated in Fig. 4-5. With this criterion, fatigue cracking was considered to follow the bottom-up adhesive failure mode assuming a service temperature of 20 °C.

ANALYSIS PROCEDURE

The ME fatigue analysis utilized in this study was a five-step procedure involving laboratory test data analysis to determine the HMAC N_f-ε_t empirical fatigue relationship expressed by Eq. (4-1), computer stress-strain analysis to determine the design maximum ε_t within a selected and representative pavement structure at the bottom of the HMAC layer, statistical analysis to predict the design HMAC mixture fatigue resistance, determination of the required pavement life, and finally a design check for adequate performance. These analyses, which are illustrated schematically in Fig. 4-1, are discussed in this section.

Step 1: Laboratory Test Data Analysis (N-ε_t Empirical Relationship)

Laboratory test data from the BB fatigue test was analyzed using the AASHTO TP8-94 calculation procedure. Eqs. (4-2) to (4-4) are the fundamental basis for BB test data analysis (AASHTO 1996a):

$$S = \frac{\sigma_t}{\varepsilon_t} \tag{4-2}$$

$$N_{50\%} = \frac{\ln\left(\frac{S_{50\%}}{A}\right)}{b} = -0.69315b^{-1} \tag{4-3}$$

where:

S = Flexural stiffness (MPa)
σ_t = Maximum measured tensile stress per load cycle (kPa)
ε_t = Maximum measured tensile strain per load cycle (mm/mm)
$N_{50\%}$ = Number of load cycles to failure during BB testing
$S_{50\%}$ = Flexural stiffness at failure during BB testing (MPa)
A = Initial peak flexural stiffness measured at the 50^{th} load cycle (MPa)
b = Exponent constant from log S versus log load cycles (N) plot

The solution of Eq. (4-3) for two different input strain levels (low and high), and a plot of the resultant $N_{50\%}$ versus the respective applied ε_t on a log-log scale, will generate the required empirical fatigue relationship of the simple power format shown in Eq. (4-1).

Step 2: Stress-Strain Analysis, $\varepsilon_{t\ (Design)}$

Following establishment of the HMAC N_f-ε_t empirical fatigue relationship through laboratory test data analysis, computer stress-strain analysis was executed to determine the actual maximum design ε_t of a given pavement structure at the bottom of the HMAC layer. Input parameters for this analysis include traffic loading, pavement structure (layer thicknesses), and material properties. Traffic loading data include the standard axle load (e.g., 80 kN [18 kip]), ESALs, and axle and tire configurations. Material properties including the elastic modulus and Poisson's ratio should be defined as a function of the environment in terms of temperature and subgrade moisture conditions. In this study, a simple multi-layer linear-elastic software, ELSYM5, was used for ε_t computations (Ahlborn 1969). Ideally, an FEM software that takes into account the visco-elastic and plasticity nature of the HMAC material is desired for this kind of analysis. Consequently, adjustments were applied to the ELSYM5 linear-elastic analysis results, consistent with the FEM adjustment criteria discussed in Chapter III.

Step 3: Statistical Prediction of HMAC Mixture Fatigue Resistance, $N_{f(Supply)}$

$N_{f(Supply)}$ is the laboratory design HMAC mixture fatigue resistance that was statistically determined as a function of the design ε_t (ELSYM5 analysis and FEM adjustment) and the laboratory-determined empirical fatigue N-ε_t (Eq. [4-1]) relationship at a given reliability level. This is discussed in detail in the subsequent section.

While $N_{f(Supply)}$ represents laboratory fatigue life, the final field fatigue life for the ME approach in this study was obtained as expressed by Eq. (4-4):

$$N_f = \frac{SF\left(k_i\left[\varepsilon_t\right]^{-k_2}\right)}{TCF} = \frac{SF \times N_{f(Supply)}}{TCF} \qquad (4\text{-}4)$$

where:

TCF = Temperature conversion factor to laboratory test temperature

SF = Composite shift factor that accounts for traffic wander, construction variability, loading frequency, crack propagation, and healing

Determination of TCF and SF generally requires calibration to local field conditions, which was beyond the scope of this study. However, a default TCF value of 1.0 is often used, while SF can often range from 0.33 to 150 depending on the HMAC mixture type, traffic loading, and environmental conditions under consideration (Lytton et al. 1993). However, SF values ranging between 13 and 26 have typically been used (Lytton 2004). For simplicity, TCF and SF values of 1.0 and 19, respectively, were used in this study (Tayebali et al. 1992, Deacon et al. 1994).

Step 4: Determination of the Required Pavement Fatigue Life, $N_{f(Demand)}$

$N_{f(Demand)}$ is the expected pavement fatigue life, which is representative of the actual applied traffic loading. It is a function of the total traffic ESALs summed over the entire pavement design life determined as expressed by Eq. (4-5):

$$N_{f(Demand)} = M \times Traffic\ ESALs_{(Design)} \tag{4-5}$$

where:

M = Reliability multiplier that is dependent on the reliability level selected

In this ME fatigue analysis approach, the safety factor associated with a specified level of reliability is defined in terms of a reliability multiplier (M) and is often applied to traffic demand (ESALs) as shown in Eq. (4-5) (Tayebali et al. 1992, Deacon et al. 1994). This factor accounts for HMAC mixture variability and the anticipated uncertainties in traffic estimate (demand), mixture fatigue resistance (supply), and performance during service. For a reliability level of 95%, some studies have used an M value of 3.57; this was the value used in this study (Tayebali et al. 1992, Deacon et al. 1994).

Step 5: Fatigue Design Check for Adequate Performance

An analytical fatigue design check for adequate performance requires that the HMAC mixture fatigue resistance given by Eq. (4-4) be greater than or equal to the required pavement fatigue life given by Eq. (4-5) as expressed by Eq. (4-6):

$$N_f \geq N_{f(Demand)} \Rightarrow N_f = \frac{SF\left[k_1\left(\varepsilon_t\right)^{-k_2}\right]}{M \times TCF} \geq Traffic\ Design_{ESALs} \tag{4-6}$$

If N_f is less than $N_{f(Demand)}$, a wide range of options including the following are available:

- redesigning the HMAC mixture by changing the binder content and/or type, AV, aggregate type, or gradation;
- redesigning the pavement structure by changing the layer thicknesses, for example,
- redesigning the underlying pavement materials including the subbase, base, and/or subgrade,
- reducing the pavement design life; and/or
- allowing an increased risk of premature failure.

VARIABILITY, STATISTICAL ANALYSIS, AND N_f PREDICTION

Precision is inversely proportional to uncertainty/variability in a testing method. If N is the measured fatigue life and $N_{\text{f(supply)}}$ is the predicted fatigue life at a given design strain level, then the precision of the method (on a log scale) can be represented by the estimated variance of $Ln\lfloor N_{\text{f(supply)}} \rfloor$ as follows:

$$s_{y^*}^2 = s^2\left(1 + \frac{1}{n} + \frac{(X-\bar{x})^2}{q\sum(x_p-\bar{x})^2}\right) \qquad (4\text{-}7)$$

where:

y^* = $Ln\lfloor N_{\text{f(supply)}} \rfloor$

$s_{y^*}^2$ = Estimated variance of $Ln\lfloor N_{\text{f(supply)}} \rfloor$

s^2 = $Var[Ln(N)]$

n = Number of test specimens

X = Ln[in situ strain] at which $Ln\lfloor N_{\text{f(supply)}} \rfloor$ must be predicted

$\bar{x}$ = Average *Ln*[test strain]

q = Number of replicate specimens at each test strain level

x_p = *Ln*[strain] at the *p*th test strain level

A prediction interval for $Ln\lfloor N_{\text{f(supply)}} \rfloor$ is another way of assessing the precision of the prediction. If the resulting interval is narrow, there is little uncertainty in $Ln\lfloor N_{\text{f(supply)}} \rfloor$, and the prediction is quite precise. An explicit formula for a 1-α prediction interval is as follows:

$$a + bX \pm t_{1-\alpha/2,n-2} s_{y^*} \tag{4-8}$$

where:

a, b = The estimated intercept and the estimated slope of the least squares line fitted on the $\left(Ln(strain), Ln\left(N_{f(\sup ply)}\right)\right)$ data

$t_{1-\alpha/2,n-2}$ = The *t*-critical value corresponding to the right tail probability of $\alpha/2$ of the *t* distribution with *n-2* degrees of freedom

$s^2_{y^*}$ = The estimated variance of $Ln\lfloor N_{\text{f(supply)}} \rfloor$ as given in Eq. (4-7)

The estimated intercept and the estimated slope, *a* and *b*, respectively, can also be given explicitly as follows:

$$a = \bar{y} + b\bar{x} \tag{4-9}$$

and

$$b = \frac{q\sum\left(x_p - \bar{x}\right)\left(y_p - \bar{y}\right)}{q\sum\left(x_p - \bar{x}\right)^2} \tag{4-10}$$

where:

y_p = $Ln(N)$ at the pth test strain level

$\bar{y}$ = Average $Ln(N\ )$

Note that the predicted fatigue life $Ln\lfloor N_{f(supply)} \rfloor$ or the prediction interval estimate $\lfloor a + bX - t_{1-\alpha/2,n-2} s_{y^*}, a + bX + t_{1-\alpha/2,n-2} s_{y^*} \rfloor$ can be back-transformed by taking exp( ) to provide the estimates in the original scale, but the variance estimate $s^2_{y^*}$ itself cannot be transformed in the same manner.

In summary, mean *Ln* $N_{f(supply)}$ values were predicted based on the least squares regression line approach (Montgomery et al. 2002). Next a 95% *Ln* N_f prediction interval was estimated based on the selected 95% reliability level. The predicted value and the prediction interval estimates for $N_{f(supply)}$ were then obtained by back-transformation analysis. As another measure of variability, a COV of *Ln* N_f was computed based on the estimated standard deviation for the predicted *Ln* N_f interval and the predicted mean *Ln* N_f value based on the normality distribution assumption.

SUMMARY

This section summarizes the ME fatigue analysis approach as utilized in this study:

- The ME approach utilized in this study is mechanistic empirical and based on the fundamental concepts that fatigue cracking in HMAC pavements occurs due to critical tensile strains (ε_t) at the bottom of the HMAC layer and that the predominant mode of crack failure is bottom-up crack growth.
- Laboratory determination of the experimental N-ε_t fatigue relationship (i.e., the k_i material regression constants) constitutes the empirical part of the ME approach, and determination of the critical design ε_t within a representative field pavement structure at the bottom of the HMAC layer constitutes the mechanistic part.

- The flexural bending beam fatigue test conducted at 20 °C and 10 Hz in sinusoidal strain-controlled mode is the principal HMAC mixture fatigue characterization test for the ME approach in the laboratory. Under this BB testing, kneading or rolling wheel compacted beam specimens are required.
- For HMAC compacted specimens subjected to repeated flexural bending under strain-controlled loading, fatigue failure according to the ME approach is defined as the number of repetitive load cycles at which the HMAC specimen flexural stiffness (S) is reduced to 50% of the initial flexural stiffness measured at the 50^{th} load cycle.

CHAPTER V
THE CALIBRATED MECHANISTIC APPROACH WITH SURFACE ENERGY MEASUREMENTS

In this chapter, the calibrated mechanistic approach with surface energy measurements, including the fundamental theory, input/output data, laboratory testing, failure criteria, analysis procedure, and statistical analysis are discussed.

FUNDAMENTAL THEORY AND DEVELOPMENT

HMAC is a complex composite material that behaves in a non-linear elasto-visco-plastic manner, ages, heals, and requires that energy be stored on fracture surfaces (or be expended) as load-induced damage in the form of fatigue cracking. Energy is also released (expended) from fracture surfaces during the healing process. HMAC mixture resistance to fatigue cracking thus consists of two components, resistance to fracture (both crack initiation and propagation) and the ability to heal; processes that both change over time. Healing, defined as the closure of fracture surfaces that occurs during rest periods between loading cycles, is one of the principal components of the laboratory-to-field shift factor used in traditional empirical fatigue analysis. Prediction of fatigue life or the number of cycles to failure (N_f) must account for this healing process that affects both the number of repetitive load cycles for microcracks to coalesce to macrocrack initiation (N_i) and the number of repetitive load cycles for macrocrack propagation through the HMAC layer (N_p) that add to N_f. Both components of HMAC mixture fatigue resistance or the ability to dissipate energy that causes primarily fracture at temperatures below 25 °C, called dissipated pseudo strain energy (DPSE), can be directly measured in simple laboratory uniaxial tensile and compression tests (Jianlong and Francken 1997, Kim et al. 1997a, b, Little et al. 1998, 2000).

The CMSE approach is a fracture-damage micromechanics approach developed at Texas A&M University based on the SHRP A-005 results (Lytton et al. 1993, Little et al. 2000). Under this CMSE approach, HMAC is characterized both in terms of fracture and healing processes, and requires only creep or relaxation tests in uniaxial tension and compression, strength and repeated load tests in uniaxial tension, and a list of fracture and healing surface energy components of binders and aggregates measured separately. The approach utilizes Paris (1963)'s Law of fracture mechanics (Paris and Erdogan 1993), Schapery's (1984) work potential theory (WPT), the extended visco-elastic correspondence principle to remove the viscous effects, and monitoring of accumulated fracture damage through changes in DPSE under repeated uniaxial tension tests. The CMSE derivation of N_i and N_p based on Schapery's WPT and Paris' Law of fracture mechanics is contained in Appendix C. In this CMSE approach, HMAC behavior in fatigue is principally governed by the energy stored on or released from crack faces that drive the fracture and healing processes, respectively, through these two mechanisms of fracture and healing.

DPSE and pseudo strain are defined to quantify and monitor fracture and healing in HMAC mixtures. DPSE in an undamaged non-linear visco-elastic material is expected due to the viscous lag in material response. This pseudo strain energy is represented by the area in the pseudo hysteresis loop of a measured stress versus calculated PS after correcting for non-linearity, plotted as shown in Fig. 5-1. PS is determined by calculating the expected stress in a linear visco-elastic material under damaged conditions and dividing by a measured reference modulus (from the first stress cycle of a repeated load test), and a non-linearity correction factor ($\psi(t)$). This $\psi(t)$ is introduced to account for any non-linearity of the undamaged visco-elastic material (Si 2001). Any departure from the initial (first load cycle) pseudo hysteresis loop requires additional dissipated energy, indicating that fracture is occurring. As fracture progresses with additional load cycles, DPSE will increase. The healing process on the other hand produces opposite results, with DPSE decreasing.

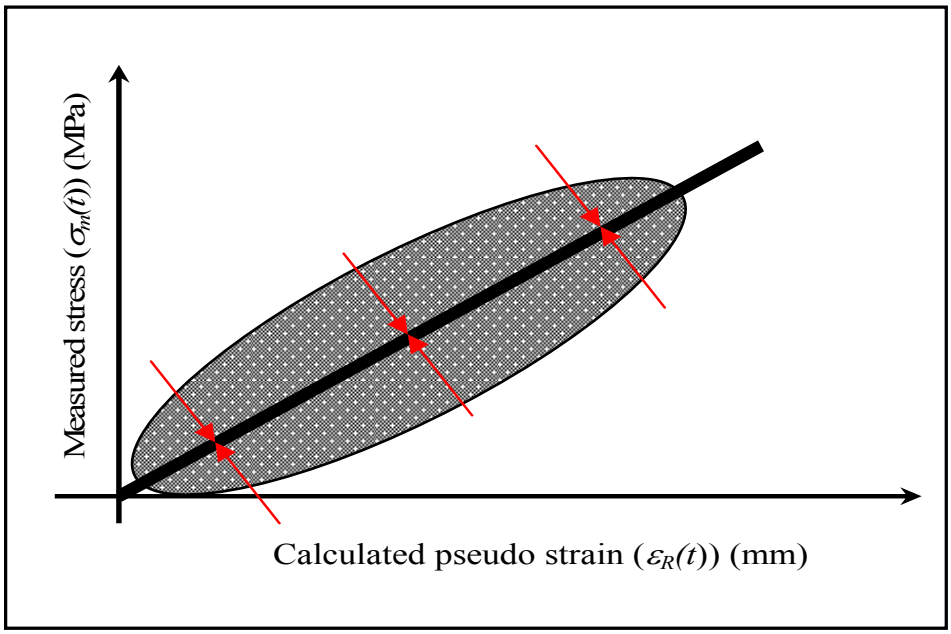

Fig. 5-1. Example of Hysteresis Loop (Shaded Area is DPSE)

Monitoring of both DPSE and PS in repeated uniaxial tension tests is required in this micromechanical CMSE approach. The relationship between DPSE and N is modeled using either of two functional forms: linear logarithmic or simple power law, and calibrated using measured data. In this study, the linear logarithmic function was used.

These calibration coefficients and Paris' Law fracture coefficients determined by monitoring both DPSE and PS with microcrack growth are required to determine N_i for macrocrack initiation at an average microcrack size of 7.5 mm (Jianlong and Francken 1997, Lytton 2000). This calibration is required because the coefficients of the equation for microcrack growth are not widely known as compared to those for macrocrack growth. The size and shape of a microcrack is controlled by microscopic quantities such as mastic film thickness, aggregate particle size, and the degree of bonding of crack-arresting obstacles dispersed in the mastic. Nevertheless, microcrack growth is still controlled by the rate of change of DPSE and indicated by a reduction in HMAC mixture stiffness.

N_p for microcrack propagation is a function of the difference between fracture and healing speed. This N_p is primarily quantified in terms of Paris' Law fracture coefficients (A and n) and the material failure load-response parameter, shear strain. Fracture speed depends on material properties determined in uniaxial tensile creep or relaxation and strength tests at multiple temperatures and total fracture surface energy.

Healing occurs as a result of both short-term and long-term rates of rest periods, and depends on traffic rest periods, healing surface energy components, and the material properties measured in creep or relaxation compression tests. Because the HMAC mixture healing properties are climatic dependent, fatigue healing calibration constants must be used to account for the climatic location of a given HMAC pavement structure (Jianlong and Francken 1997). In determining the final field N_f, an anisotropic shift factor (discussed subsequently) is also introduced to account for the anisotropic nature of HMAC.

The surface energies of the binder and aggregate in HMAC are made up of contributions from nonpolar short-range Lifshitz-van der Waals forces and longer-range polar acid-base forces mainly associated with hydrogen bonding (Good and Van Oss 1992, Si 2001, Cheng 2002). The polar acid-base surface energy is itself also a combination of the acid surface energy and the base surface energy. These polar forces typical of hydrogen bonding take longer to form and act perpendicular to the crack faces to actively pull them together, while the nonpolar tensile short-range and short-lived Lifshitz-van der Waals forces act in the plane of the crack face to form a contractile skin that resists healing (Good and Van Oss 1992, Lytton et al. 1993, Little et al. 2000, Si 2001, Cheng 2002).

The difference between the total fracture and healing surface energies lies in the measurement of the individual surface energy components using carefully selected materials with known surface energy component values. Fracture components are found when dewetting, and healing components are determined when wetting.

Summary of CMSE Fundamental Theory and Analysis System

The bullets below summarize the fundamental hypotheses upon which the CMSE fatigue analysis approach was formulated:

- HMAC is a complex composite material that behaves in a non-linear elasto-visco-plastic manner, exhibits anisotropic behavior, ages with time, and heals during traffic loading rest periods.
- HMAC requires that energy be expended to cause load-induced damage in the form of fracture cracking. Equally, energy must be expended to close up these fracture surfaces, a process called healing. The HMAC mixture is thus characterized in terms of fracture and healing processes, and requires only relaxation tests in uniaxial tension and compression, strength and repeated load tests in uniaxial tension, and a catalog of fracture and healing surface energy components of asphalt binders and aggregates measured separately.
- HMAC resistance to fracture cracking is governed by two processes; namely the number of repetitive load cycles for microcracks to coalesce to macrocrack initiation (N_i) and the number of repetitive load cycles for macrocrack propagation through the HMAC layer (N_p). These two processes constitute the HMAC mixture fatigue resistance that adds to N_f, after correcting for field traffic loading and environmental effects.
- The rate of fracture crack growth per load cycle is quantitatively a function of the stress intensity and distribution in the vicinity of the microcrack tip under repeated loading and unloading cycles. Consequently, Paris' Law of fracture mechanics and Schapery's modified work potential theory (WPT) for non-linear fracture mechanics (NLFM) analysis are utilized to model this relationship and the fracture energy that represents the work required to cause fracture cracking (Anderson 1995, Paris and Erdogan 1963, Schapery 1973, Lundström 2004).
- The HMAC fracture damage accumulation under laboratory repeated uniaxial tensile testing is a function of the dissipated pseudo strain energy (DPSE).

- The DPSE function is utilized based on Schapery's WPT and the extended visco-elastic correspondence principle because it allows to account for HMAC non-linearity and time-dependent visco-elastic effects. These corrections are achieved through the use of pseudo strain and a non-linearity correction factor.

Fig. 5-2 is a schematic illustration of the CMSE design and analysis system. Fig. 5-2 shows that if the predicted N_f is less than the design traffic ESALs, possible options include the following:

- modifying the pavement structure, materials, and reliability level;
- changing the HMAC mix-design and/or material type;
- reducing the pavement design life; and/or
- allowing an increased risk of premature failure, i.e., reducing the reliability level.

In this CMSE approach, the design shear strain (Fig. 5-2) computed within the HMAC layer of the pavement structure for N_p analysis constitutes the failure load-response parameter. This critical (maximum) design shear strain is determined at the edge of a loaded wheel tire using either a layered linear-elastic or visco-elastic model of material behavior. The utilization of calibration constants in modeling SF_h, N_i, and N_p constitutes the calibration part of the CMSE approach. This calibration simulates the field mechanism of microcrack growth in the HMAC layer thickness with respect to traffic loading and changing environmental conditions.

INPUT/OUTPUT DATA

Table 5-1 summarizes the general CMSE fatigue analysis input and the expected output data. These parameters and their respective components are discussed in more detail in subsequent sections.

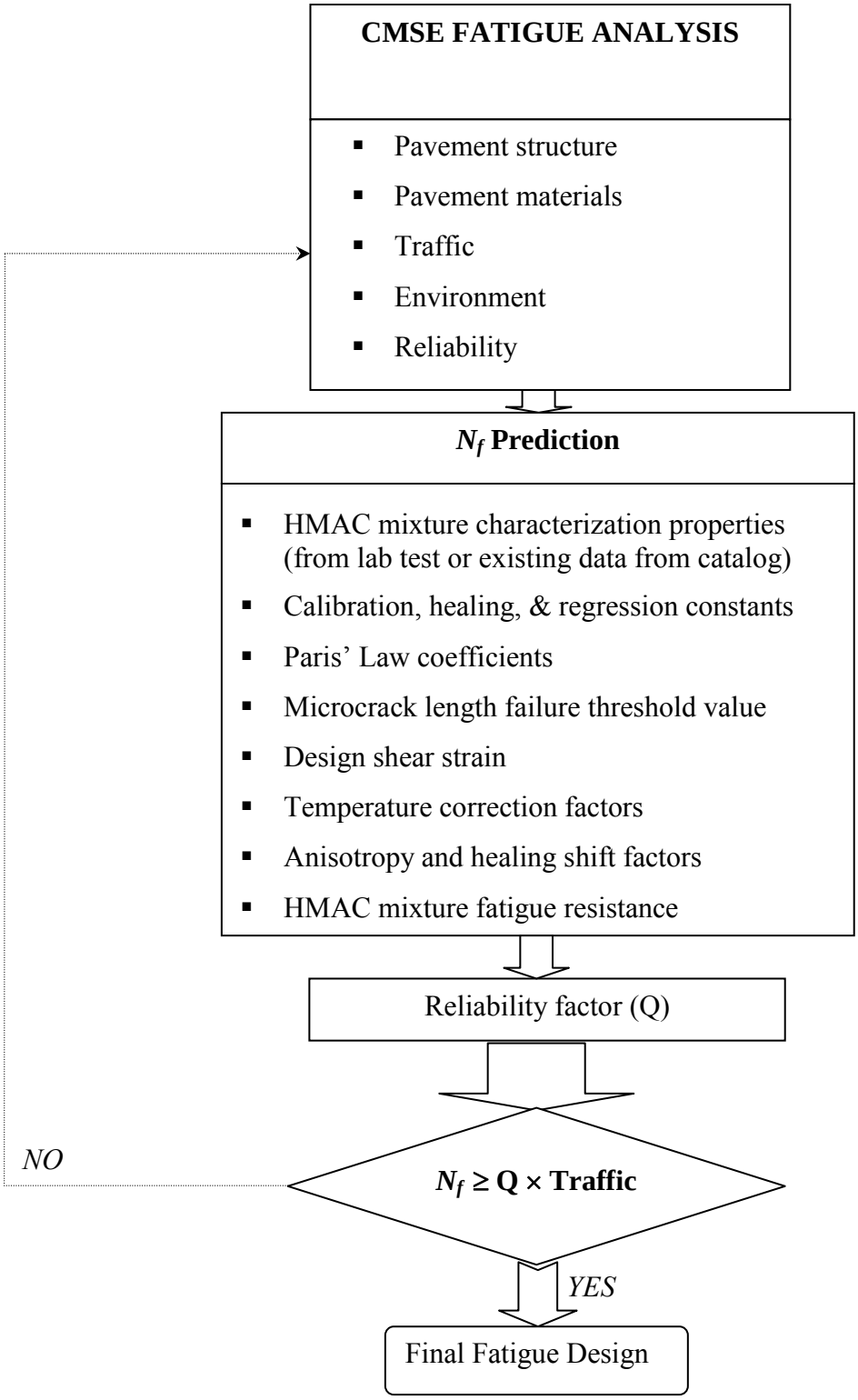

Fig. 5-2. The CMSE Fatigue Design and Analysis System

Table 5-1. Summary of CMSE Fatigue Analysis Input and Output Data

Source	Parameter
Laboratory test data (HMAC mixture testing of cylindrical specimens)	• Tensile stress & strain • Relaxation modulus (tension & compression) • Uniaxial repeated direct-tension test data (strain, stress, time, & N) • Anisotropic data (vertical & lateral modulus) • Dynamic contact angle for binder SE • Vapor pressure & adsorbed gas mass for aggregate SE
Analysis of laboratory test data	• Tensile strength • Relaxation modulus master-curves (tension & compression) • Non-linearity correction factor • DPSE & slope of DPSE vs. Log N plot • SE (ΔG_f & ΔG_h) for binder & aggregates • Healing indices & calibration constants • Creep compliance & shear modulus • Load pulse shape factor
Field conditions (design data)	• Pavement materials (E & ν) & structure (layer thickness) • Traffic (ESALs, axle load, & tire pressure) • Environment (temperature & moisture conditions.) • Field calibration coefficients • Temperature correction factor
Computer stress-strain analysis	• Design shear strain (γ) @ edge of a loaded tire
Others	• Reliability level (95%) • Crack density • Microcrack length • HMAC brittle-ductile failure characterization • Regression constants & material coefficients
Output	• Paris' Law fracture coefficients (A and n) • Shift factor due to anisotropy (SF_a) • Shift factor due to healing (SF_h) • Fatigue load cycles to crack initiation (N_i) • Fatigue load cycles to crack propagation (N_p) • HMAC mixture fatigue resistance (N_f)

LABORATORY TESTING

The required laboratory tests for the CMSE approach of HMAC mixture fatigue analysis include tensile strength, relaxation modulus in tension and compression, uniaxial repeated direct-tension, and surface energy (Lytton et al. 1993, Lytton 2000, Si 2001, Cheng 2002). These tests are described in this section. For each of these tests, at least two replicate cylindrical HMAC specimens were tested per aging condition per HMAC mixture type.

Tensile Strength Test

The tensile strength test was conducted to determine the HMAC mixture tensile strength (σ_t), which is a required input parameter for the CMSE fatigue analysis.

Test Protocol

The tensile strength (TS) test protocol involves applying a continuously increasing tensile load to a cylindrical HMAC specimen at a constant elongation (deformation) rate of 1.27 mm/min (0.05 in/min) until failure. This test is destructive and takes at most 2 min to complete the test. Fig. 5-3 shows the loading configuration for the TS test and typical results.

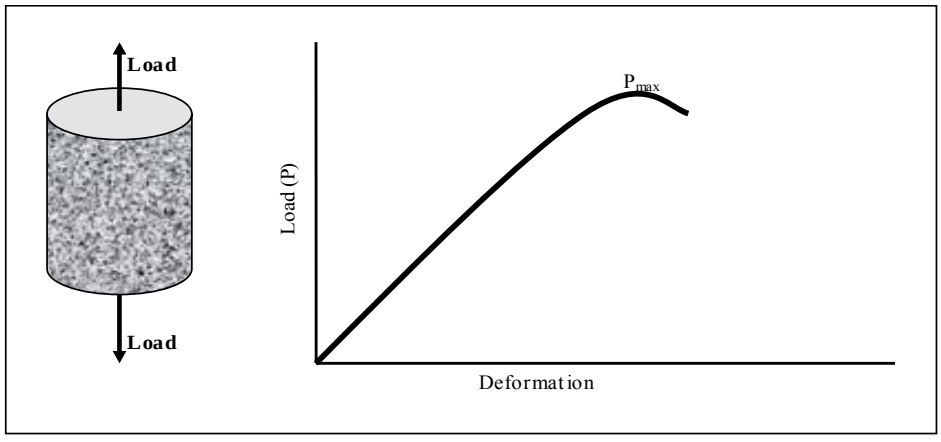

Fig. 5-3. Loading Configuration for the TS Test

Test Conditions and Data Acquisition

The TS test was conducted in an environmentally controlled chamber at a test temperature of 20±0.5 °C. Specimens were pre-conditioned to 20 °C for a minimum period of 2 hr. The temperature was monitored and controlled through a thermocouple probe attached inside a dummy HMAC specimen also placed in the environmental chamber. An MTS equipped with an automatic data measuring system applied the loading. Loading data were measured via the MTS load cell, and deformations were recorded via three LVDTs attached vertically to the sides of the specimen. During the test, load and axial deformation data were captured electronically every 0.1 s. Two replicate specimens were tested per aging condition per HMAC mixture type.

HMAC mixture tensile strength (σ_t) was calculated simply as the maximum tensile load at break divided by the specimen cross-sectional area as follows:

$$\sigma_t = \frac{P_{\max}}{\pi r^2} \tag{5-1}$$

where:

σ_t = Tensile strength (MPa)
P_{max} = Maximum tensile load at break (kN)
r = Radius of cylindrical HMAC specimen (mm)

Relaxation Modulus Test

The time-dependent elastic relaxation modulus ($E(t)$), modulus relaxation rate (m_i), and temperature correction factor (a_T) constitute input parameters for the CMSE fatigue analysis. These material properties were determined from the relaxation modulus test (Si 2001).

Test Protocol

Relaxation modulus (RM) is a strain-controlled test. The test involves applying a constant axial strain to a cylindrical HMAC specimen either in tension or compression for a given time period and then releasing the strain for another given time period, thereby allowing the specimen to rest or relax (elastic recovery). The test loading configuration is shown in Fig. 5-4.

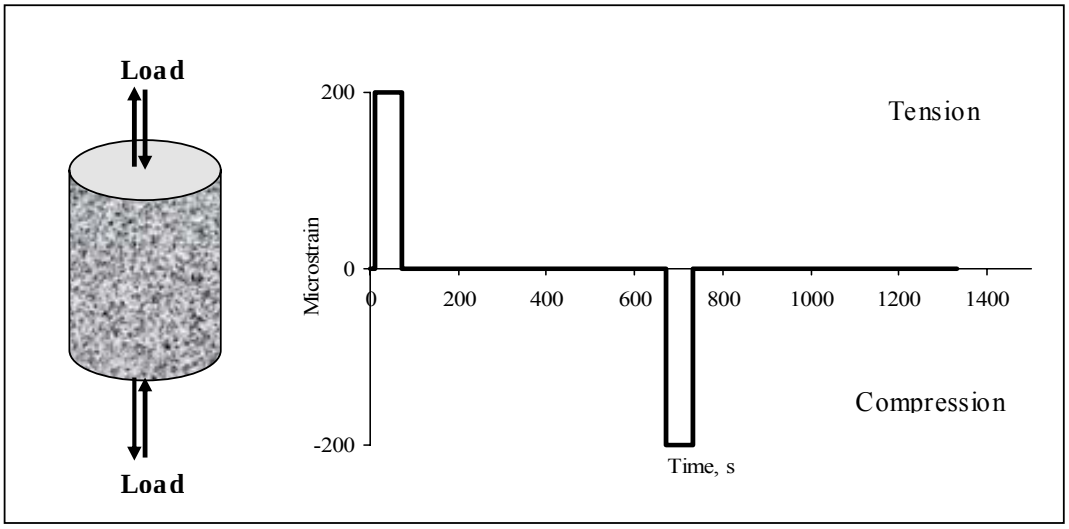

Fig. 5-4. Loading Configuration for the RM Test

As shown in Fig. 5-4, the loading sequence consisted of applying a 200 tensile microstrain for a period of 60 s, followed by a 600 s rest period and then application of a 200 compressive microstrain for 60 s, followed by another 600 s rest period. A 200 microstrain was selected because for the HMAC mixtures considered in this study, prior trial testing with microstrains above 200 proved to be destructive while those below 200 were too small to produce meaningful results. This input strain magnitude also simulated 20% of the HMAC mixture tensile strain at break at 20 °C for the 0 months aged HMAC specimens.

A 60 s strain loading time was considered adequate to prevent irrecoverable damage, while a 600 s rest period was considered adequate to allow for elastic recovery. The time interval for the strain load application from 0 to +200 or -200 microstrain was 0.6 s, and the input strain waveform was actually a trapezoidal shape. Thus, the total test time for both the tensile and compressive loading cycle for a given test temperature was approximately 25 min.

Test Conditions and Data Acquisition

RM testing was conducted in an environmentally controlled chamber at three temperatures: 10, 20, and 30 °C, to facilitate development of a time-dependent RM master-curve. This master-curve is a graphical representation of the HMAC mixture properties as a function of temperature and loading time. Note that HMAC is sensitive to both temperature and time of loading.

The temperatures were monitored and controlled at a tolerance of ±0.5 °C through a thermocouple probe attached inside a dummy HMAC specimen also placed in the same environmental chamber as the test specimen. For each temperature-test sequence, the minimum specimen conditioning time was 2 hr. The MTS provided the loading, while an automated data measurement system captured the data (time, load, and deformation) electronically every 0.5 s. Loading data were measured via the MTS load cell, and deformations were recorded via three LVDTs attached vertically to the sides of the specimen. Three replicate specimens were tested per aging condition per HMAC mixture type. Fig. 5-5 is an example of the output stress response from the relaxation modulus test at a single test temperature of 10 °C.

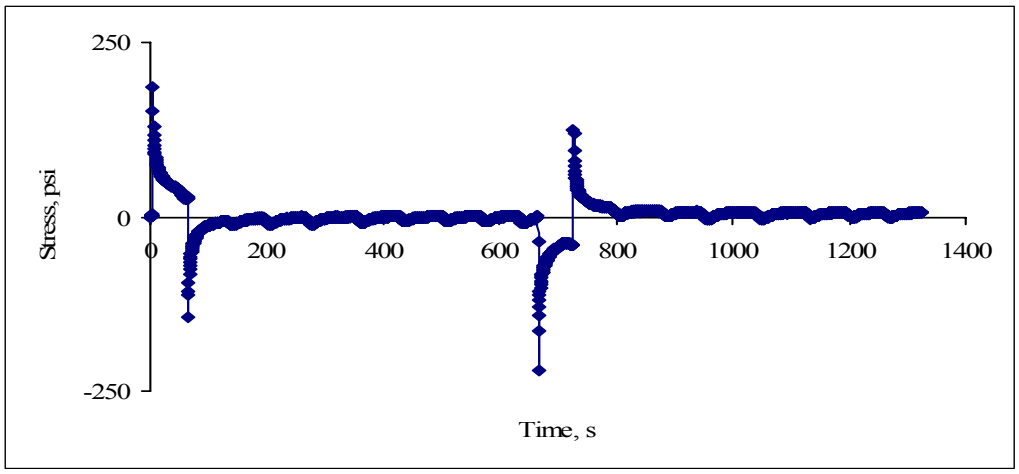

Fig. 5-5. Example of Stress Response from the RM Test at 10 °C

Eq. 5-2 was used to calculate the elastic relaxation modulus as a function of the measured load (stress) and strain:

$$E(t) = \frac{\sigma(t)}{\varepsilon} = \frac{P(t)}{\pi r^2 \varepsilon} \qquad (5\text{-}2)$$

where:

$E(t)$ = Elastic modulus (MPa)

P, ε = Load (kN) and strain (mm/mm)

A time-reduced superposition logarithmic analysis of the elastic modulus data for each test temperature to a reference temperature of 20 °C generates the required time-dependent RM master-curve. This master-curve is represented in the form of a simple power law and characterizes the HMAC visco-elastic properties. By the same logarithmic analysis, temperature correction factors (a_T) are determined, where a_T has a value of 1.0 for the 20 °C reference temperature.

Uniaxial Repeated Direct-Tension Test

The time-dependent tensile stress ($\sigma(t)$) is an input parameter required to calculate the rate of dissipation of PS energy (b) that is necessary to calculate N_i. This material property was determined from the uniaxial repeated direct-tension test discussed subsequently.

Test Protocol

Like the RM test, the uniaxial repeated direct-tension (RDT) test was conducted in a strain controlled mode. An axial direct tensile microstrain of 350 was applied repeatedly to a cylindrical HMAC specimen at a frequency of 1 Hz for a total of 1,000 load cycles. The input strain waveform was haversine shaped.

The actual loading time was 0.1 s with a 0.9 s rest period between load pulses. Thus, a complete load cycle including the rest period was 1.0 s. Fig. 5-6 shows the loading configuration. The 0.9 s rest period allowed for HMAC relaxation between the load pulses and prevented the buildup of undesirable residual stresses discussed subsequently. This rest period is also theorized to promote a limited amount of healing.

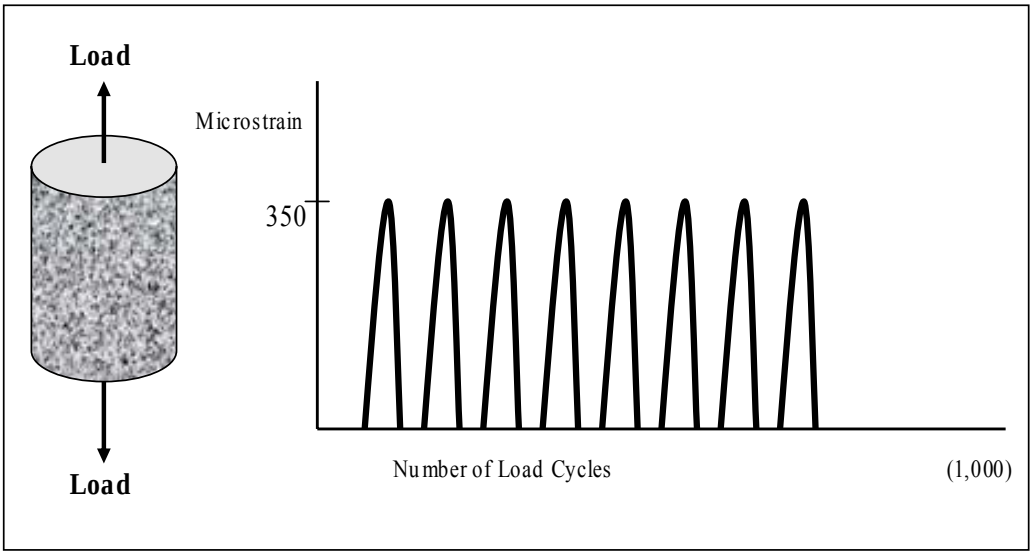

Fig. 5-6. Loading Configuration for the RDT Test

The haversine-shaped input strain waveform is representative of the field load pulse developed under moving wheel loads of commercial vehicles on interstate highways. A relatively high input strain magnitude of 350 microstrain was selected because this value (350 microstrain) was considered substantial enough to induce cumulative micro fatigue damage (microcracking) within the HMAC specimen during the test. In this test, while micro fatigue damage is desirable, an appropriate input strain level must be selected that will allow the test to continue to an appreciable number of load cycles to capture sufficient data for calculation of the *b* slope parameter needed in the CMSE analysis. In this study, testing was terminated at 1000 load cycles, during which time sufficient data had been captured for DPSE analysis and subsequent calculation of the constant *b*. A complete RDT test thus took at most 20 min.

Test Conditions and Data Acquisition

The haversine input strain waveform was supplied by the MTS, and axial deformations were measured via three LVDTs. Data (time, load, and deformations) were captured electronically every 0.005 s. The RDT test was conducted in an environmentally controlled chamber at a test temperature of 30±0.5 °C. The minimum conditioning period for the specimens was 2 hr. The temperature was monitored and controlled through a thermocouple probe attached inside a dummy HMAC specimen also placed in the same environmental chamber as the test specimen.

Three replicate cylindrical HMAC specimens that had previously been subjected to a series of RM tests at 10, 20, and 30 °C were used for this test for each aging condition and each HMAC mixture type. It should be noted that the RM test was assumed to be non-destructive in this study. However, the RDT test is a destructive test since some microdamage occurs within the HMAC specimen even though damage may not be physically visible.

Fig. 5-7 is an example of the stress response from the uniaxial repeated direct-tension test at 30 °C. The measured stress ($\sigma(t)$), strain ($\varepsilon(t)$), and time (t) are the required input parameters for CMSE fatigue analysis to calculate DPSE.

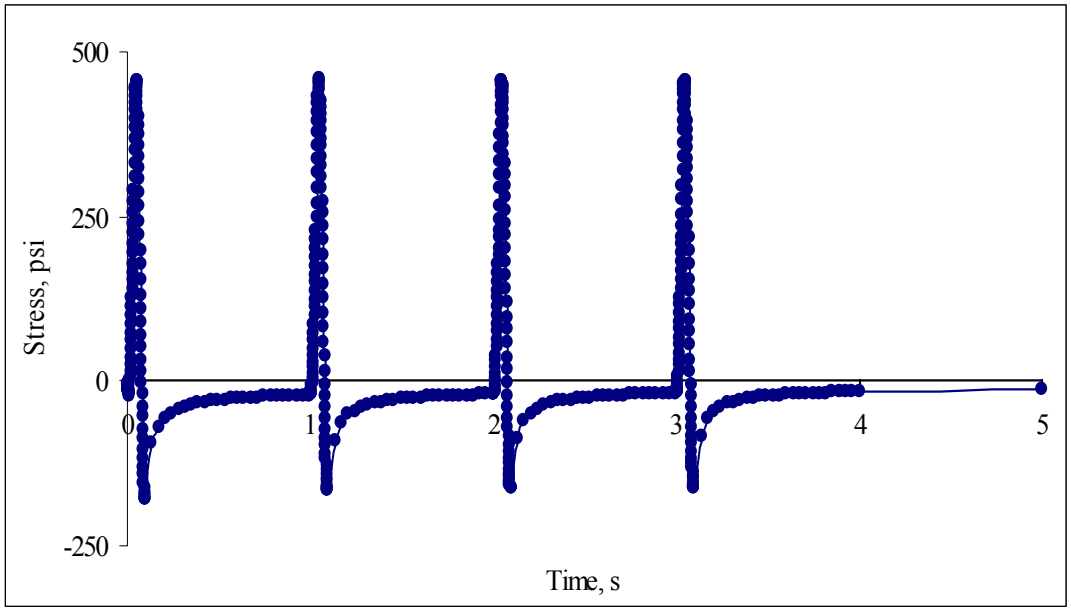

Fig. 5-7. Stress Response from the RDT Test at 30 °C

Anisotropic Test

The modulus of HMAC is an important input parameter used in predicting HMAC mixture fatigue properties. HMAC is not an isotropic material and therefore its mechanical properties (i.e., elastic modulus) are directionally dependent (Tashman et al. 2005, Arramon et al. 2000). The objective of the anisotropic test was therefore to measure the variation of HMAC modulus measured from different directions, vertical (E_z) and horizontal or lateral (E_x and E_y), which constitute input parameters for CMSE fatigue analysis. These data from the anisotropic (AN) test were used to determine the shift factor due to anisotropy (SF_a) discussed in the subsequent sections of this chapter.

Test Protocol

The AN test was conducted consistent with the HMAC elastic-resilient modulus test, but with both axial and radial deformation measurements for E_z and E_x determination, respectively (Huang 1993). AN is a destructive stress-controlled test with a sinusoidal-shaped input stress waveform. The test involved repeated application of a sinusoidal-shaped stress magnitude of 690 kPa at a loading frequency of 1 Hz for a total of 200 load cycles without any rest period. Fig. 5-8 shows the AN test loading configuration.

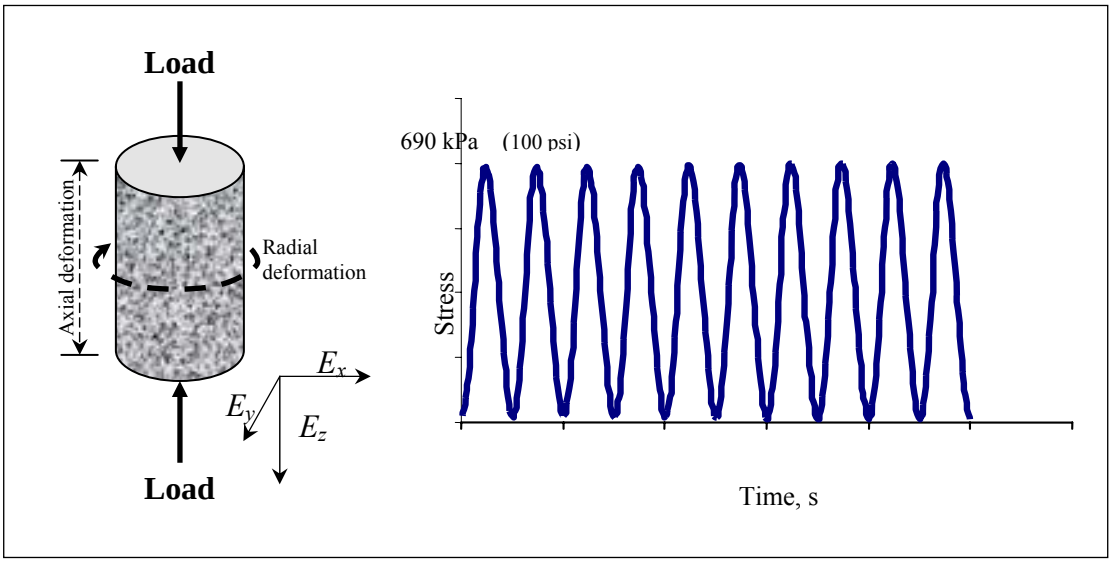

Fig. 5-8. Loading Configuration for the AN Test

An input stress magnitude of 690 kPa is a simulation of truck tire pressure on an in situ field HMAC pavement structure. For this study, AN testing was terminated at 200 load cycles, during which time sufficient data had been captured for moduli analysis. With a loading frequency of 1 Hz, the total AN test time was at most 5 minutes. Although AN is a destructive test, the 200 load cycles was in most cases not sufficient to cause visible damage to some specimens.

For AN testing of this nature, it is normal practice to subject the test specimens to lateral pressure confinement to simulate the field triaxial stress state, particularly when testing unbound granular materials (Adu-Osei 2000, Kim et al. 2004). In this study, the AN test was conducted under unconfined lateral pressure conditions. However, the AN analysis models were adjusted to the lateral pressure confinement conditions to simulate the laboratory triaxial stress state. This adjustment was achieved through trial testing of several HMAC specimens under both unconfined and confined laboratory lateral (345 kPa) pressure conditions and then comparing the moduli results. The moduli results measured without pressure confinement were then adjusted/modified to match the moduli results under lateral pressure confinement conditions, thus accounting for triaxial stress state conditions. Note that it is much more convenient, easier, and more practical to conduct the HMAC AN test under unconfined lateral pressure conditions.

Test Conditions and Data Acquisition

The sinusoidal input stress waveform was supplied by the MTS, while axial and radial deformations were measured via three LVDTs. Two LVDTs attached vertically to the sides of the specimen were used for axial measurements, and one LVDT attached radially around the center of the specimen was used for radial deformation measurements as shown in Fig. 5-8. Data (time, load, and deformations) were captured electronically every 0.02 s.

Like other HMAC mixture tests, the AN test was conducted in an environmentally controlled chamber at a test temperature of 20±0.5 °C. The minimum conditioning period for the specimens was 2 hours. The temperature was monitored and controlled through a thermocouple probe attached inside a dummy HMAC specimen also placed in the same environmental chamber as the test specimen. Three replicate specimens were tested per aging condition per HMAC mixture type.

Fig. 5-9 is an example of the strain responses from the AN test at 20 °C recorded for a period of 60 s. While the AN test gives both the elastic and plastic strain responses as shown in Fig. 5-9, the response component of interest that is critical to fatigue is the elastic strain. By contrast, the plastic strain is critical to permanent deformation, which was beyond the scope of this study.

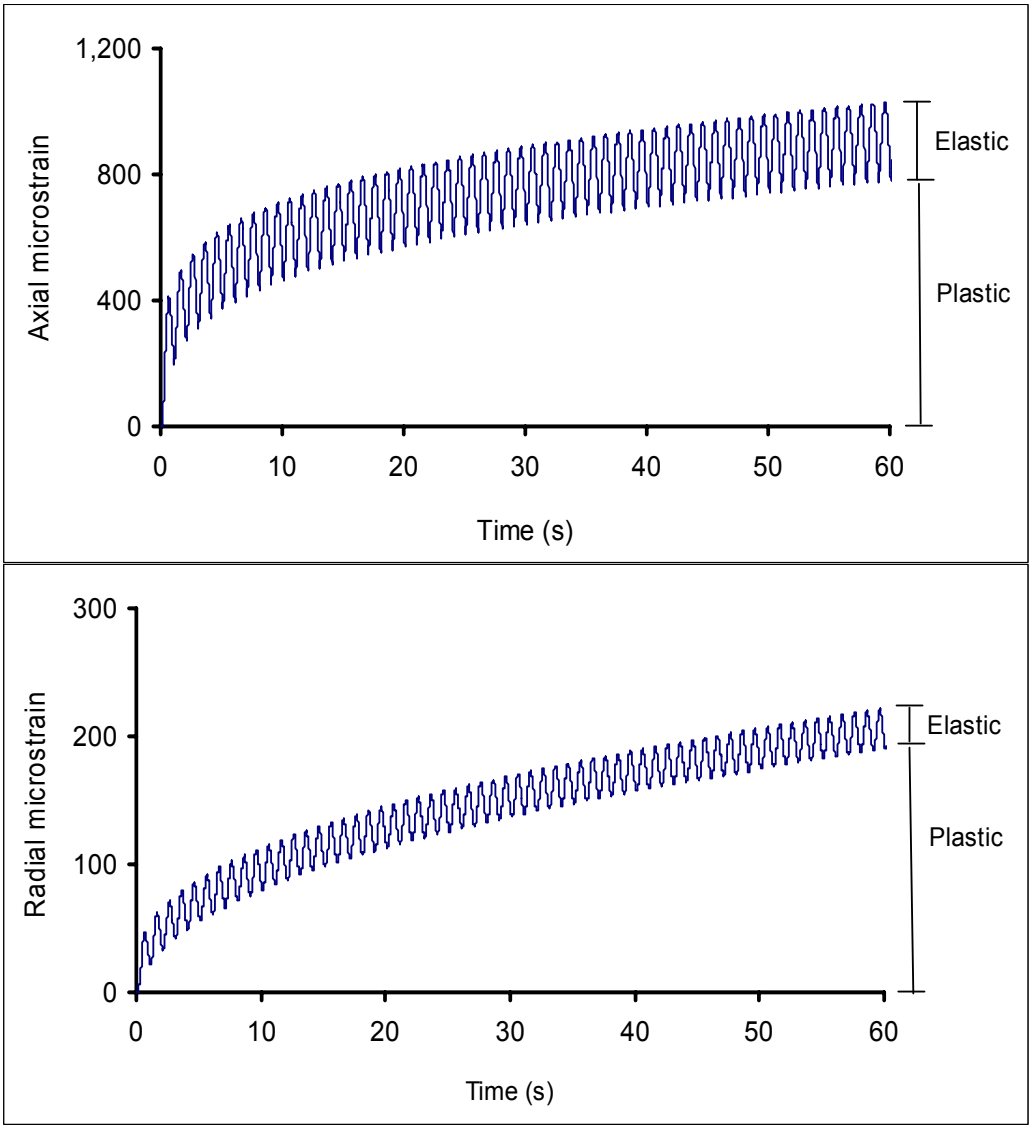

Fig. 5-9. Example of Strain Responses from AN Testing at 20 °C

From the measured AN test data, the elastic moduli were calculated as a function of the applied load (stress) and elastic strain response as expressed by Eqs. (5-3) and (5-4) (Huang 1993, Adu-Osei 2000, Kim et al. 2004). For simplicity, HMAC was assumed to be laterally isotropic, and therefore E_x was considered equivalent to E_y in magnitude.

$$E_z = a_z \frac{\sigma_z}{\varepsilon_z} \tag{5-3}$$

$$E_x = E_y = a_x \frac{\nu\sigma_z}{\varepsilon_x} \tag{5-4}$$

where:

E_z = Elastic modulus in the vertical direction (MPa)

E_x = Elastic modulus in the lateral direction (MPa)

σ_z = Applied compressive axial stress (MPa)

$\varepsilon_z, \varepsilon_x$ = Axial and radial deformation, respectively (mm/mm)

ν = Poisson's ratio ($\nu \cong 0.33$)

a_z, a_x = Anisotropic adjustment factors that simulate laboratory lateral pressure confinement conditions ($a_x \cong 1.15$, $a_z \cong 1.34$)

In this study, the mean a_x and a_z values were determined to be 1.15 and 1.34, respectively (for both HMAC mixtures), and these were the values used for moduli computations. Table 5-2 illustrates the determination of the a_i values.

Table 5-2. Determination of Anisotropic Adjustment Factors (a_i)

Test	Unconfined (MPa)		Confined (MPa)		$a_x = E_{x(c)}/E_{x(u)}$	$a_z = E_{z(c)}/E_{x(u)}$
	$E_{x(u)}$	$E_{z(u)}$	$E_{x(c)}$	$E_{z(c)}$		
1	1,789	3,399	1,940	4,450	1.08	1.31
2	1,569	2,980	1,785	3,927	1.14	1.32
3	1,678	3,188	1,963	4,320	1.17	1.35
4	1,589	3,219	1,900	4,180	1.20	1.30
5	1,498	2,846	1,760	3,972	1.17	1.40
Mean	1,625	3,127	1,870	4,170	1.15	1.34
Stdev	112	216	92	223	0.04	0.04
COV	6.90%	6.91%	4.91%	5.35%	3.76%	2.99%

Surface Energy Measurements for the Binder - The Wilhelmy Plate Test

The surface energy (SE) measurements for the binders in this study were completed using the Wilhelmy plate (WP) method (Si 2001, Cheng 2002). Compared to other methods such as the drop weight, Du Nouy ring, pendant drop, Sessile drop, capillary rise, and maximum bubble pressure, the WP method is relatively simple and does not require complex correction factors to the measured data (Si 2001, Cheng 2002).

The contact angle between binder and any liquid solvent can be measured using the Wilhelmy plate method. This method is based on kinetic force equilibrium when a very thin plate is immersed or withdrawn from a liquid solvent at a very slow constant speed, as illustrated in Fig. 5-10 (Maugis 1999).

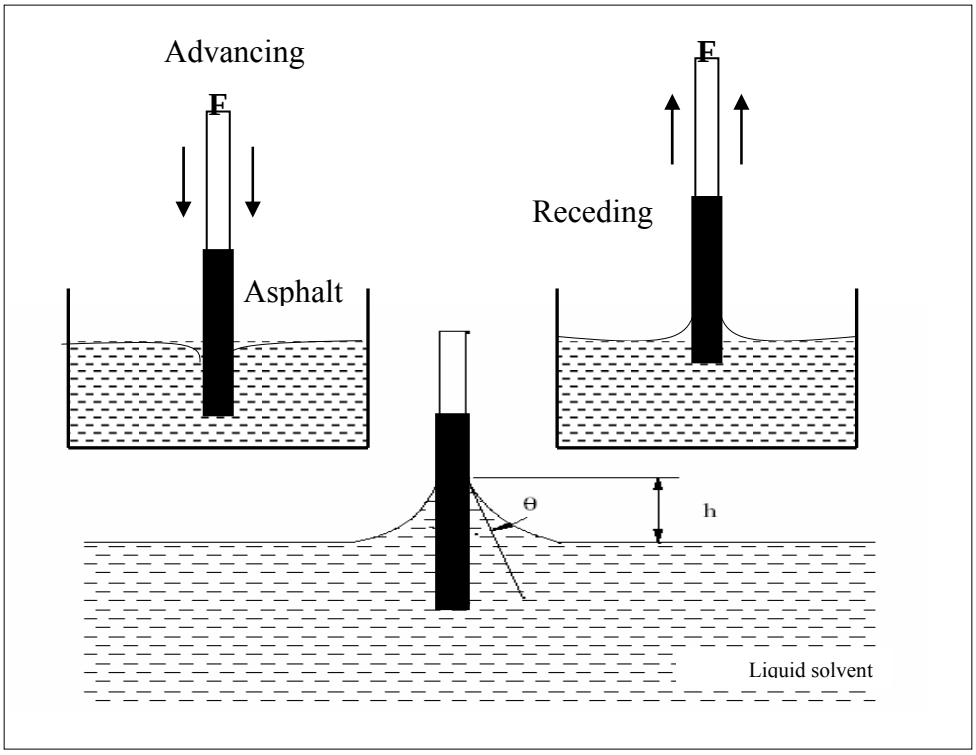

Fig. 5-10. Loading Configuration for the Wilhelmy Plate Test Method

The dynamic contact angle between binder and a liquid solvent measured during the immersing process is called the advancing contact angle, while the dynamic contact angle during the withdrawal process is called the receding contact angle.

The advancing contact angle, which is a wetting process, is associated with the healing process; the receding angle is associated with the fracture mechanism. The total surface free energy and its components for binder are calculated from these advancing and receding contact angles. The surface free energy calculated from the advancing contact angles is called the surface free energy of wetting (advancing) or healing, while the surface free energy computed from the receding contact angle is called the surface free energy of dewetting (receding) or fracturing.

Test Protocol and Data Acquisition

To complete the WP test, approximately 0.65 g of hot-liquid binder heated to 144 °C was coated onto glass plates 50 mm in length by 25 mm in width with a 0.15 mm thickness. By dipping the glass plate into a mass of hot-liquid binder to a depth of about 15 mm, a thin binder film of approximately 1 mm thickness was created on the glass plate after allowing the excess binder to drain off.

As shown in Fig. 5-7, the actual test protocol involves an automatically controlled cycle (s) of immersion and withdrawal (receding) processes of the binder-coated glass plates into a liquid solvent to a depth of about 5 mm at an approximate uncontrolled ambient temperature of 20±2 °C. The temperature is not tightly controlled in this test because previous research has indicated that the measurable contact angle, and consequently the surface free energy, are not very temperature sensitive (Si 2001, Cheng 2002). The total test time for both the immersion and withdrawal processes is approximately 15 min.

Prior to testing, the binder-coated glass plate must be vacuumed for about 12 hr in a diseccator to de-air the binder. Three test binder samples are required per test per three liquid solvents, and thus a total of nine samples were used per aging condition.

Distilled water, formamide, and glycerol were the three selected liquid solvents used in this study because of their relatively large surface energies, immiscibility with binder, and wide range of surface energy components. Table 5-3 lists the surface energy components of these three liquid solvents (distilled water, formamide, and glycerol) that were measured at 20 °C (Si 2001, Cheng 2002).

Table 5-3. Surface Energy Components of Water, Formamide, and Glycerol

Solvent	**Surface Free Energy Components (ergs/cm^2)**				
	Γ_{Li}	Γ_{Li}^{LW}	Γ_{Li}^{+}	Γ_{Li}^{-}	Γ_{Li}^{AB}
Distilled water	72.60	21.60	25.50	25.50	51.00
Formamide	58.00	39.00	2.28	39.60	19.00
Glycerol	64.00	34.00	3.60	57.40	30.00

During the test, the loading force for the immersion and receding processes was provided by an automatically controlled dynamic contact analyzer (DCA) balance shown in Fig. 5-11. Data (dynamic contact angle) were measured and captured electronically via the WinDCA software. Fig. 5-12 is an example of the measured dynamic advancing and receding contact angles at 20±2 °C.

Fig. 5-11. The DCA Force Balance and Computer Setup - Wilhelmy Plate Test

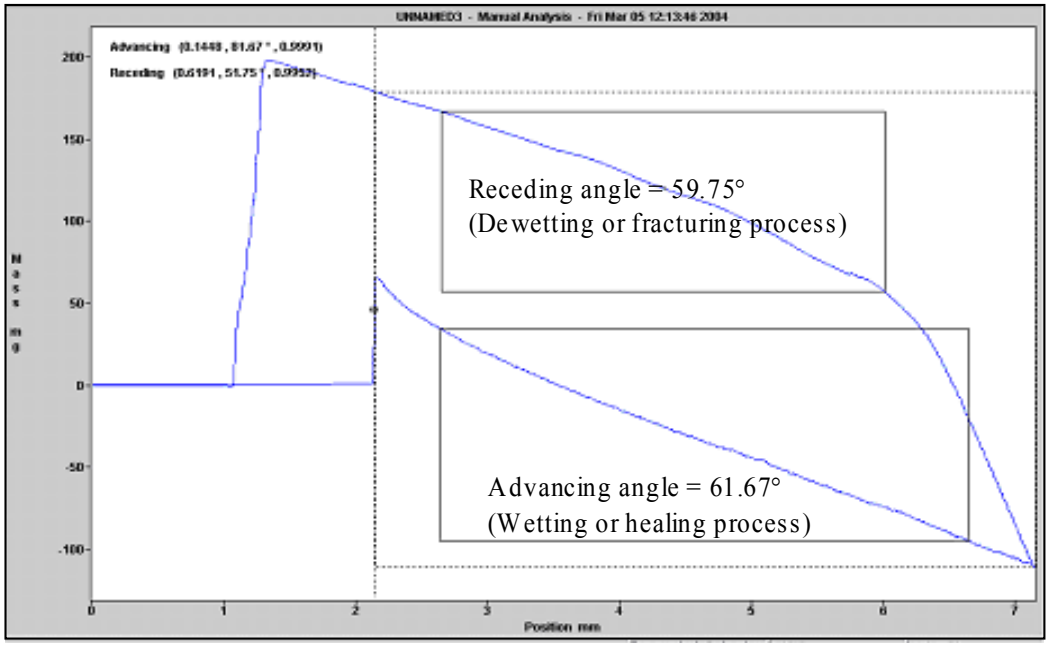

Fig. 5-12. Example of the DCA Software Display (Advancing and Receding)

For clarity, the vertical axis title in Fig. 5-12 is "mass" in mg with a scale of -100 to 200 mg, and the horizontal axis title is "position" in mm with a scale of 0 to 7 mm.

Binder Surface Energy Calculations

Eq. (5-5) is the force equilibrium equation resulting from the immersion (advancing) or the withdrawal (receding) processes during the WP test. Based on the Young-Dupre theory and the assumption that binder equilibrium film pressure is zero, Eq. (5-5) reduces to Eq. (5-6) (Cheng 2002):

$$\Delta F = P_t \Gamma_L Cos\theta - V\rho_L g + V\rho_{Air} g \qquad (5\text{-}5)$$

$$\Gamma_{L_i}\left(1 + Cos\theta_i\right) = 2\sqrt{\Gamma_i^{LW}\Gamma_{L_i}^{LW}} + 2\sqrt{\Gamma_i^{-}\Gamma_{L_i}^{+}} + 2\sqrt{\Gamma_i^{+}\Gamma_{L_i}^{-}} \qquad (5\text{-}6)$$

where:

F	=	Applied force (kN)
P_t	=	Perimeter of the binder-coated glass plate (m)
θ	=	Dynamic contact angle between binder and the liquid solvent, degrees (°)
V	=	Volume of immersed section of glass plate (m^3)
ρ	=	Density (subscript "L" for liquid solvent and "Air" for air) (g/cm^3)
g	=	Acceleration due to gravity (m/s^2)
Γ	=	Surface free energy ($ergs/cm^2$)

The dynamic contact angle θ (°) is the measurable parameter, either advancing (wetting) or receding (dewetting). Γ_{Li}^{LW}, Γ_{Li}^{+}, and Γ_{Li}^{-} are the known surface free energy components of the liquid solvent. Γ_i^{LW}, Γ_i^{+}, and Γ_i^{-} are the three unknown components of the binder surface free energy from Lifshtz-van der Waals forces, Lewis base, and Lewis acid, respectively, that need to be determined.

Mathematically, three liquid solvents of known surface free energies must be used to solve Eq. (5-6) for the three unknown parameters Γ_i^{LW}, Γ_i^{+}, and Γ_i^{-}. Algebraically, Eq. (5-6) can easily be transformed into a familiar matrix form of simple linear simultaneous equations expressed by Eq. (5-7) (Cheng 2002):

$$\begin{bmatrix} a_{11} & a_{12} & a_{13} \\ a_{21} & a_{22} & a_{23} \\ a_{31} & a_{32} & a_{33} \end{bmatrix} \begin{bmatrix} x_1 \\ x_2 \\ x_3 \end{bmatrix} = \begin{bmatrix} Y_1 \\ Y_2 \\ Y_3 \end{bmatrix} \tag{5-7}$$

$$a_{1i} = 2\frac{\sqrt{\Gamma_{L_i}^{LW}}}{\Gamma_{L_i}},\ a_{2i} = 2\frac{\sqrt{\Gamma_{L_i}^{+}}}{\Gamma_{L_i}},\ a_{3i} = 2\frac{\sqrt{\Gamma_{L_i}^{-}}}{\Gamma_{L_i}} \tag{5-8}$$

$$x_1 = \sqrt{\Gamma_i^{LW}},\ x_2 = \sqrt{\Gamma_i^{-}},\ x_3 = \sqrt{\Gamma_i^{+}} \tag{5-9}$$

$$Y_i(x) = 1 + Cos\,\theta_i \tag{5-10}$$

where:

a_{ki} = Known surface energy components of the three liquid solvents (distilled water, formamide, and glycerol) (ergs/cm^2) (see Table 5-2)

x_i = The unknown surface energy components (Γ_i^{LW}, Γ_i^{+}, and Γ_i^{-}) of the binder that need to be determined (ergs/cm^2)

$Y_i(x)$ = Known function of the measured contact angles of the binder in the three liquid solvents (θ_{Water}, $\theta_{Formamide}$, and $\theta_{Glycerol}$)

The solution of Eq. (5-10) provides the surface free energy components (Γ_i^{LW}, Γ_i^{+}, and Γ_i^{-}) of the binder required for the CMSE fatigue analysis.

Surface Energy Measurements for the Aggregate -The Universal Sorption Device

In this study, the universal sorption device (USD) was used for the surface energy measurements of aggregates. The USD method utilizes a vacuum gravimetric static sorption technique that identifies gas adsorption characteristics of selected solvents with known surface free energy to indirectly determine the surface energies of the aggregate. Sorption methods are particularly suitable for aggregate surface energy measurements because of their ability to accommodate the peculiarity of sample size, irregular shape, mineralogy, and surface texture associated with the aggregates (Cheng 2002).

Test Protocol and Data Acquisition

The USD setup is comprised of a Rubotherm magnetic suspension balance system, a computer system (with Messpro software), a temperature control unit, a high-quality vacuum unit, a vacuum regulator, pressure transducers, a solvent container, and a vacuum dissector. A schematic of the main components of the USD setup is illustrated in Fig. 5-13.

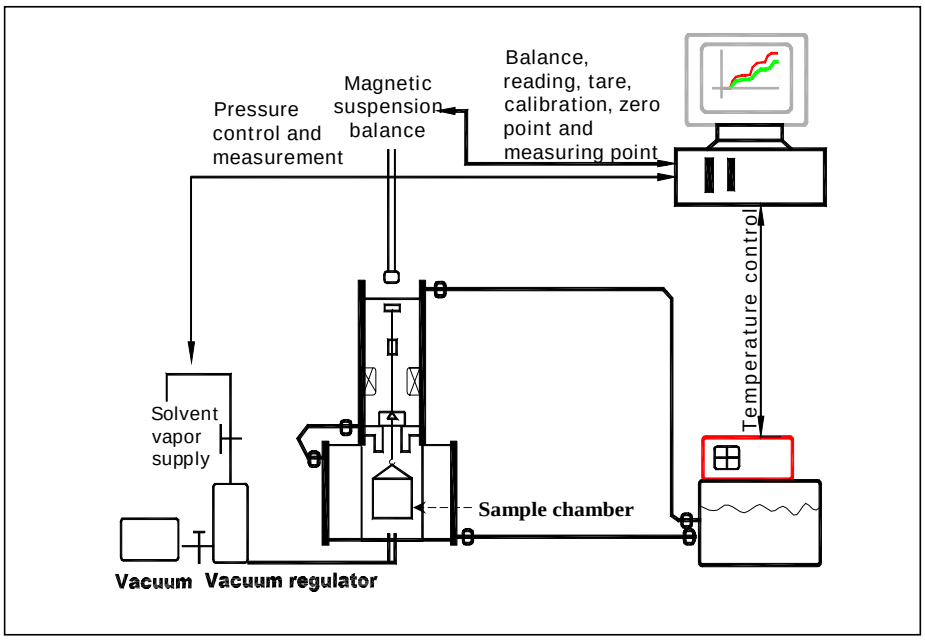

Fig. 5-13. The USD Setup (Cheng 2002)

A Mettler balance is securely established on a platform with the hang-down Rubotherm magnetic suspension balance and sample chamber beneath it. This magnetic suspension balance has the ability to measure a sample mass of up to 200 g to an accuracy of 10^{-5} g, which is sufficient for precise measurement of mass increase due to gas adsorbed onto the aggregate surface. The whole USD system is fully automated with about 8 to 10 predetermined pressure set points that automatically trigger when the captured balance readings reach equilibrium.

With this USD sorption method, an aggregate fraction between the 4.75 mm and 2.36 mm sieve sizes is suspended in the sample chamber in a special container. Essentially, the size of aggregate tested is that which passes the 4.75 mm sieve but is retained on the 2.36 mm sieve. Theoretically, the surface free energy of aggregate is not significantly affected by the size of the aggregate because size is accounted for during the SE calculation process. However, this aggregate fraction size (4.75 mm < aggregate size < 2.36 mm) used in the USD test is dictated by the limitation of the sample chamber size and the desired aggregate surface area for sufficient gas adsorption that is representative of all aggregate fractional sizes.

During the USD test process, once the chamber is vacuumed, a solvent vapor is injected into the aggregate system. A highly sensitive magnetic suspension balance is used to measure the amount of solvent adsorbed on the surface of the aggregate. The vapor pressure at the aggregate surface is measured at the same time. The surface energy of the aggregate is calculated after measuring the adsorption of three different solvents with known specific surface free energy components. In this study, three solvents; distilled water, *n*-Hexane, and Methyl Propyl Ketone 74 (MPK); with surface free energy components listed in Table 5-4 at 25 °C were used (Cheng 2002).

Table 5-4. Surface Energy Components of Water, n-Hexane, and MPK at 25 °C

Solvent	**Surface Free Energy Components (ergs/cm^2)**				
	Γ_{Li}	Γ_{Li}^{LW}	Γ_{Li}^{+}	Γ_{Li}^{-}	Γ_{Li}^{AB}
Distilled water	72.60	21.60	25.50	25.50	51.00
n-hexane	18.40	18.40	0.00	19.60	0.00
MPK	24.70	24.70	0.00	0.00	0.00

Like binder SE measurements, aggregate SE measurements are also insensitive to temperature, and so the USD test was conducted at an uncontrolled ambient temperature of approximately 25±2 °C. The total test time for a complete test set with three solvents is about 60 to 70 hr. For each solvent, a 50 g sample of aggregates was tested for the zero months aging condition only. Note that aggregates are by nature insensitive to aging, and thus aging was not considered for the aggregate SE measurements. Prior to testing, the aggregate sample was thoroughly cleaned with distilled water and oven dried (at about 120 °C for at least 8 hr) to remove any dusty particles and moisture that might negatively impact the results.

Data (vapor pressure, adsorbed gas mass, and test time) were measured and captured electronically via the Messpro software. Fig. 5-14 is an example of a typical output obtained from the USD adsorption test for n-hexane adsorption on limestone aggregate at 25 °C.

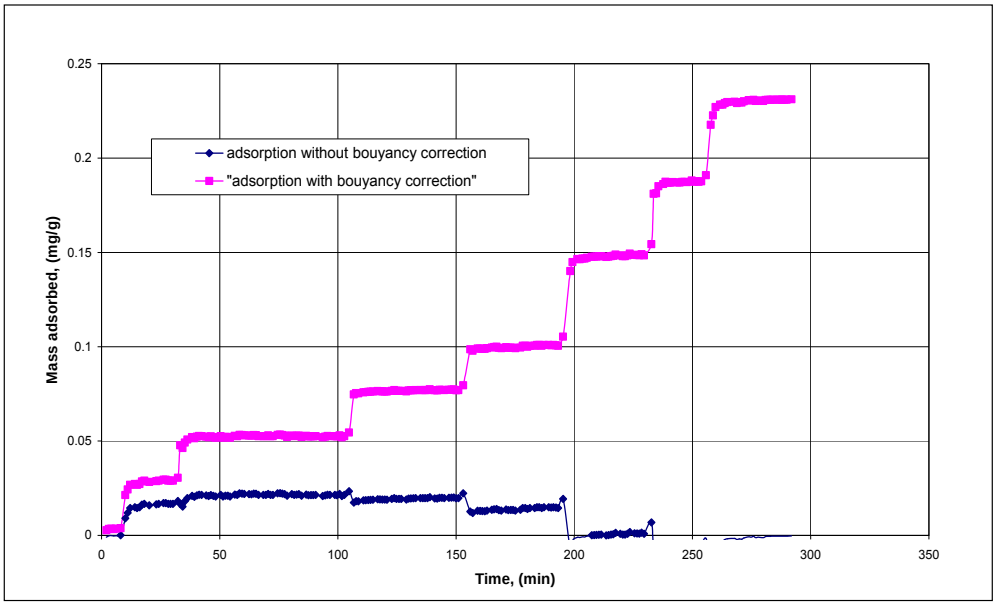

Fig. 5-14. Adsorption of n-Hexane onto Limestone under USD Testing (Cheng 2002)

Aggregate SE Calculations

Once the adsorbed solvent mass and vapor pressure on the aggregate surface have been measured and the adsorption data corrected for solvent vapor buoyancy using the generalized Pitzer correlation model, the specific surface area of the aggregate was then calculated using the Brunauer, Emmett, and Teller (BET) model shown by Eq. (5-11) (Si 2001, Cheng 2002):

$$\frac{P}{n(P_0 - P)} = \left(\frac{c-1}{n_m c}\right)\frac{P}{P_0} + \frac{1}{n_m c} \qquad (5\text{-}11)$$

where:

P	=	Vapor pressure (MPa)
P_0	=	Saturated vapor pressure of the solute (MPa)
n	=	Specific amount adsorbed on the surface of the absorbent (mg)
n_m	=	Monolayer capacity of the adsorbed solute on the absorbent (mg)
c	=	Parameter theoretically related to the net molar enthalpy of adsorption

For the type of isotherms associated with the pressure conditions in this USD test, n_m can be obtained from the slope and the intercept of the straight line that fits the plot of *P/n(P-Po)* versus *P/Po* best. The specific surface area (A) of the aggregate can then be calculated through the following Equation:

$$A = \left(\frac{n_m N_o}{M}\right)\alpha \qquad (5\text{-}12)$$

And for a hexagonal close-packing model;

$$\alpha = 1.091\left(\frac{M}{N_o \rho}\right)^{2/3} \tag{5-13}$$

where:

A = Specific surface area

α = Projected area of a single molecule (m^2)

N_o = Avogadros' number (6.02×10^{23})

M = Molecular weight (g)

ρ = Density of the adsorbed molecule in liquid at the adsorption conditions (g/cm^3)

The result from the BET in Eq. (5-11) is used to calculate the spreading pressure at saturation vapor pressure (π_e) for each solvent using Gibbs free energy in Eq. (5-14) (Cheng 2002):

$$\pi_e = \frac{RT}{A}\int_0^{P_0} \frac{n}{P} dP \tag{5-14}$$

where:

π_e = Spreading pressure of the solute at saturation vapor pressure of the solvent ($ergs/cm^2$)

R = Universal gas constant (83.14 cm^3 bar/mol.K)

T = Absolute temperature (Kelvin, K) ($K = 273 + ℃$)

The work of adhesion of a liquid on a solid (W_A) can be expressed in terms of the surface energy of the liquid (Γ_l) and the equilibrium spreading pressure of adsorbed vapor on the solid surface (π_e) as shown in Eqs. (5-15) and (5-16):

$$W_a = \pi_e + 2\Gamma_l \tag{5-15}$$

$$\pi_e + 2\Gamma = 2\sqrt{\Gamma_s^{LW}\Gamma_l^{LW}} + 2\sqrt{\Gamma_s^{+}\Gamma_l^{-}} + 2\sqrt{\Gamma_s^{-}\Gamma_l^{+}} \tag{5-16}$$

where:

Subscript s = Solid (aggregate)
Subscript l = Liquid (solvent)

From Eqs. (5-15) and (5-16), the surface energy components and the total surface energy of the aggregate can be determined by employing Eq. (5-17) through Eq. (5-20):

$$\Gamma_s^{LW} = \frac{\left(\pi_e + 2\Gamma_l\right)^2}{4\Gamma_l^{LW}} \tag{5-17}$$

Eq. (5-17) is used to calculate the Γ_s^{LW} of the surface for a non-polar solvent on the surface of the solid (aggregate). For a known mono-polar basic liquid vapor (subscript m) and a known bipolar liquid vapor (subscript b), the Γ_s^{+} and Γ_s^{-} values were calculated using Eqs. (5-18) and (5-19) as follows:

$$\Gamma_s^{+} = \frac{\left(\pi_e + 2\Gamma_{lm} - \sqrt{\Gamma_s^{LW}\Gamma_{lm}^{LW}}\right)^2}{4\Gamma_{lm}^{-}} \tag{5-18}$$

$$\Gamma_s^- = \frac{\left(\pi_e + 2\Gamma_{lb} - \sqrt{\Gamma_s^{LW}\Gamma_{lb}^{LW}} - 2\sqrt{\Gamma_s^+\Gamma_{lb}^-}\right)^2}{4\Gamma_{lb}^+} \quad (5\text{-}19)$$

Finally, the total surface energy of the aggregate (Γ_s) is calculated as expressed by Eq. (5-20):

$$\Gamma_s = \Gamma_s^{LW} + 2\sqrt{\Gamma^+\Gamma^-} \quad (5\text{-}20)$$

Appendix D provides a summary of the current USD test protocol and SE analysis procedure as utilized in this study. Note that the current USD test protocol is still under development, in particular to improve its test time efficiency as well as a general review of the SE test protocol and data analysis procedure (Little et al. 2003). Presently, research is ongoing at TTI to explore the use of a new device called the Microcalorimeter to measure the aggregate SE. This device is hypothesized to be more time-efficient, less complex, and more accurate than the USD.

FAILURE CRITERIA

For the CMSE approach, fatigue failure is defined as crack initiation and propagation through the HMAC layer thickness. In this study, a maximum microcrack length of 7.5 mm was selected as the failure threshold value for crack initiation and propagation. This 7.5 mm threshold value was selected based on the work of Lytton et al. (1993) from extensive fatigue testing that indicated that crack propagation in the HMAC layer begins when microcracks grow and coalesce to form a small microcrack approximately 7.5 mm long.

CMSE ANALYSIS PROCEDURE

Eq. (5-21), which relates field fatigue life (N_f) to the number of load cycles to crack initiation (N_i) and crack propagation (N_p) as a function of shift factors (SF_i), is the fundamental principle of the CMSE approach for fatigue modeling of HMAC mixtures (Lytton et al. 1993):

$$N_f = SF_i\left(N_i + N_p\right) \tag{5-21}$$

where:

N_f = Fatigue life or number of load cycles to fatigue failure

SF_i = Product of the shift factors that include HMAC anisotropy (SF_a), healing (SF_h), and aging (SF_{ag})

N_i = Number of load cycles to crack initiation

N_p = Number of load cycles to crack propagation

Each of the terms in Eq. (5-21) is discussed in the subsequent subsections. In Eq. (5-21), the sum ($N_i + N_p$) constitutes the laboratory fatigue life, and the product of the shift factors (SF_i) and the sum ($N_i + N_p$) constitute the field fatigue life.

Shift Factor Due to Anisotropic Effect, SF_a

Anisotropy arises due to the fact that HMAC is not isotropic as often assumed. The HMAC mixture stiffness (modulus) in the lateral (horizontal) direction is not equal to that in the vertical direction due to the differences in the particle orientation during compaction/construction. During construction, there is always a high compactive effort in the vertical direction relative to other directions. So the HMAC behavior or response to loading and/or the environment is different in different directions. Consequently, the HMAC anisotropy must be considered in fatigue analysis. However, most laboratory test protocols measure only the vertical stiffness and assume isotropic behavior.

In the CMSE analysis, SF_a takes care of the anisotropic behavior of the HMAC mixture. Eq. (5-22) shows the relationship between the vertical (E_z) and horizontal (E_x) moduli used in this study. E_z and E_x are measurable parameters from the AN test.

$$SF_a = \left(\frac{E_z}{E_x} \right)^{1.75} \tag{5-22}$$

where:

SF_a = Shift factor due to HMAC anisotropy, ranging between 1 and 5
E_z = Elastic modulus in the vertical direction (MPa)
E_x = Elastic modulus in the lateral or horizontal direction (MPa)

Generally, because of the vertical orientation of the compactive effort during field construction or laboratory compaction, E_z is always greater than E_x, on the order of magnitude of about 1.5 times, at a temperature of around 20 °C (Khanal and Mamlouk 1995). For simplicity purposes, HMAC was assumed to be laterally isotropic, and therefore E_x was considered equivalent to E_y in magnitude.

Shift Factor Due to Healing Effect, SF_h

Due to traffic loading rest periods and temperature variations, the asphalt binder has a tendency to heal (closure of fracture surfaces), which often results in improvement in the overall HMAC mixture fatigue performance. The CMSE approach takes this into account and relates healing to traffic rest periods and temperature as expressed by Eq. (5-23) (Lytton et al. 1993, Cheng 2002):

$$SF_h = 1 + g_5 \left(\frac{\Delta t_r}{a_{TSF}} \right)^{g_6} \tag{5-23}$$

$$\Delta t_r = \frac{31.536 \times 10^6 P_{DL}}{80kN \text{ Traffic ESALs}} \tag{5-24}$$

$$g_5 = a(h_o)^{g_6} \tag{5-25}$$

$$h_o = \dot{h}_2 + \left(\frac{\dot{h}_1 - \dot{h}_2}{1 + \left[\left(\frac{\dot{h}_1 - \dot{h}_2}{h_\beta} \right) \left(\frac{\Delta t C_{sr}}{a_{TSF}} \right) \right]} \right) \tag{5-26}$$

$$\dot{h}_1 = \left(\frac{C_1}{\left[\Delta G_h^{LW} E_c \right]^{\left(\frac{1}{m_c} \right)}} \right) \tag{5-27}$$

$$\dot{h}_2 = \left(\left[C_2 \left(\frac{\Delta G_h^{AB}}{E_c} \right) \right]^{\left(\frac{1}{m_c} \right)} + C_3 \right) \tag{5-28}$$

$$h_\beta = C_4 \left(\frac{\Delta G_h^{AB}}{\Delta G_h^{LW}} \right) \left(\frac{C_5}{m_c} \right) \tag{5-29}$$

where:

SF_h = Shift factor due to healing, ranging between 1 and 10

Δt_r = Rest period between major traffic loads (s)

Δt = Loading time (s)

a_{TSF} = Temperature shift factor for field conditions (~1.0)

C_{sr} = Square rest period factor (~1.0)

a, g_5, g_6 = Fatigue field calibration constants

h_0, $\dot{h}_{1-2}$, h_β = Healing indices

P_{DL} = Pavement design life in years

$ESALs$ = Equivalent single axle loads over a given pavement design period

$C_{1\text{-}5}$ = Healing constants

E_c = Elastic relaxation modulus from compression RM master-curve (MPa)

m_c = Exponent from compression RM master-curve

ΔG_h^i = Surface energy due to healing or dewetting (ergs/cm^2)

In Eq. (5-23), Δt_r represents the field long-term rest period and depends on the pavement design life and traffic expressed in terms of ESALs. The numerical value of 31.536×10^6 in Eq. (5-24) represents the total time in seconds for a 365-day calendar year. The parameter a_{TSF} is a temperature shift factor used to correct for temperature differences between laboratory and field conditions. For simplicity, an a_{TSF} value of 1.0 was used, but this value can vary depending on the laboratory and field temperature conditions under consideration. C_{sr} represents the shape of the input strain wave rest period during the RDT test. As discussed previously, the periodic time interval between the input strain waveforms for the RDT test in this study simulated a square-shaped form, with a total duration of 0.9 s. This 0.9 s periodic time interval was considered a square- shaped rest period, so a C_{sr} value of 1.0 was used in the analysis (Lytton 2001). As stated previously, this rest period allowed for HMAC relaxation and healing, and prevented the buildup of undesirable residual stresses during RDT testing.

The parameters a, g_5, g_6, h_0, $\dot{h}_{1-2}$, and h_β are fatigue field calibration constants/coefficients and healing indices. These parameters quantify the HMAC mixture healing properties as a function of climatic location of a specific pavement structure, ΔG_h, due to healing and HMAC mixture elastic properties (E_c and m_c) obtained from compression RM tests. These calibration constants and healing indices also represent the HMAC mixture short-term rest periods and binder healing rates, both short-term and long-term, respectively (Lytton et al. 1993). In particular, h_β is a healing index ranging between 0 and 1.0 that represents the maximum degree of healing achievable by the asphalt binder (Cheng 2002).

The fatigue calibration constants g_5 and g_6 are climatic dependent. In this study, values shown in Table 5-5 were used assuming wet-no-freeze and dry-no-freeze climates. Table 5-6 provides an additional set of g_i values based on accelerated laboratory testing. Note that the g_i values in Tables 5-5 and 5-6 do not differ significantly. These values were established by Lytton et al. (1993) in their extensive field calibration study of fatigue cracking through Falling Weight Deflectometer (FWD) tests in the field and accelerated laboratory tests. In their (Lytton et al. 1993) findings, these calibration constants provided a good fit between measured and predicted fatigue cracking.

Table 5-5. Fatigue Calibration Constants Based on Backcalculation of Asphalt Moduli from FWD Tests (Lytton et al. 1993)

Coefficient	**Climatic Zone**			
	Wet-Freeze	**Wet-No-Freeze**	**Dry-Freeze**	**Dry-No-Freeze**
g_0	-2.090	-1.615	-2.121	-1.992
g_1	1.952	1.980	1.707	1.984
g_2	-6.108	-6.134	-5.907	-6.138
g_3	0.154	0.160	0.162	1.540
g_4	-2.111	-2.109	-2.048	-2.111
g_5	0.037	0.097	0.056	0.051
g_6	0.261	0.843	0.642	0.466

Table 5-6. Fatigue Calibration Constants Based on Laboratory Accelerated Tests (Lytton et al. 1993)

Coefficient	Climatic Zone			
	Wet-Freeze	**Wet-No-Freeze**	**Dry-Freeze**	**Dry-No-Freeze**
g_0	-2.090	-1.429	-2.121	-2.024
g_1	1.952	1.971	1.677	1.952
g_2	-6.108	-6.174	-5.937	-6.107
g_3	0.154	0.190	0.192	1.530
g_4	-2.111	-2.079	-2.048	-2.113
g_5	0.037	0.128	0.071	0.057
g_6	0.261	1.075	0.762	0.492

The SE and RM tests were discussed in previous sections of this chapter. ΔG_h, E_c, and m_c are material (binder, aggregate, and HMAC mixture) dependent, but also vary with the aging condition of the binder and/or HMAC mixture, which has a net impact on SF_h and N_f. As discussed in subsequent chapters, this study has shown that the variation of these parameters (ΔG_h, E_c, and m_c) with 3 and 6 months aging of the binder and HMAC mixture at 60 °C reduced the value of SF_h considerably, particularly the resultant N_f. Analysis procedures for ΔG_h, E_c, and m_c are discussed subsequently.

The healing constants C_1 through C_5 were backcalculated from regression analysis as a function of the measured E_c, ΔG_h due to healing, and the healing rates (h_i) using a spreadsheet sum of square error (SSE) minimization technique (Lytton et al. 1993, Si 2001, Cheng 2002).

Other Shift Factors

The shift factor due to aging (SF_{ag}) is discussed in Chapters X and XI of this dissertation. In the current CMSE analysis, other shift factors including residual stress, stress state, dilation, and traffic wander were not considered or were simply assigned a numerical value of 1.0 based on the assumptions discussed in this section. In fact, some of these factors are already included in the SF_a and SF_h shift factors. Nonetheless, future CMSE studies should consider the possibility of exploring these shift factors in greater detail.

Residual Stresses, SF_r

In the field, because of incomplete elastic relaxation/recovery and short time intervals between some traffic load applications (axles of the same vehicle), residual stresses can remain in the pavement after the passage of each load cycle and may thus pre-stress the HMAC layer so that the stresses that occur with the next load cycle cause less, equivalent, or more damage. If present, these residual stresses occur either in tension or compression depending, among other factors, on the magnitude of the load and the pavement structure. On the same principle, residual stresses can also build-up in laboratory test fatigue specimens, particularly if there is an insufficient rest period between load applications or if the specimens are not properly loaded during the test. Eqs. (5-30) and (5-31) show the estimation of SF_r according to Tseng and Lytton (1990):

$$SF_r = \left(\frac{1}{1 \pm P_o t^{-m}} \right)^{k_{21}} = \left(1 \pm P_o t^{-m}\right)^{\left(\frac{-2}{m}\right)} \qquad (5\text{-}30)$$

$$P_o = \frac{\sigma_r(t)}{\varepsilon_t E(t)} \qquad (5\text{-}31)$$

where:

P_o	=	The percent of total strain remaining in the pavement as residual strain after passage of the traffic load (%)
t	=	Loading duration (s) (e.g., 0.1 s)
m	=	Stress relaxation rate (i.e., from tensile RM master-curve)
k_{21}	=	Laboratory-determined material constant as a function of m
$\sigma_r(t)$	=	Residual stresses (tensile or compressive) at time t (MPa)
ε_t	=	Total tensile strain (mm/mm)
$E(t)$	=	HMAC elastic modulus at time t (MPa)

Note that the expression $k_{21} = 2/m$ may be valid only for HMAC subjected to uniaxial strain-controlled loading tests. A different expression may be required for stress-controlled loading tests.

According to Lytton et al. (1993), SF_r commonly ranges between 0.33 and 3.0 depending on whether the residual stresses are tensile or compressive. In the absence of sufficient field data to accurately predict the magnitude and/or determine whether these residual stresses (or strains) will be tensile or compressive, and in recognition of the fact that there was insignificant residual stress build-up in the CMSE laboratory fatigue specimens in the RDT test (i.e., $\sigma_r(t) \cong P_o \cong 0.0$), a SF_r value of 1.0 was not an unreasonable assumption in this study. In fact, Eqs. (5-30) and (5-31) also show that if there are no residual stresses ($\sigma_r(t) \cong 0.0$) as in the case of the RDT test in this study, P_o will be 0.0, and SF_r will have a numerical value of 1.0.

The RDT test in this study was conducted with a 0.9 s rest period between load pulses, while the actual loading time was 0.1 s. The RDT output stress response indicated that this 0.9 s rest period sufficiently allowed for HMAC relaxation and subsequent prevention of residual stress buildup. Note also that the CMSE fatigue analysis approach used in this study assumes that there are no residual stresses due to construction compaction in the field or SGC compaction in the laboratory.

Stress State, SF_{ss}

In a pavement structure under traffic loading, a triaxial stress state exists. The continuum nature of the pavement material tends to transfer the applied stress in all three coordinate directions (x, y, and z) based on the Poisson's ratio and the interlayer bonding conditions. In the laboratory, the stress state can be uniaxial, biaxial, or triaxial depending on the test protocol. A shift factor is thus required to account for this difference in stress state between laboratory and field conditions.

In a linear elastic stress-strain analysis, Al-Qadi and Nassar (2003) found that a shift factor based on strain energy that accounts for the differences between laboratory and field pavement stress state can vary between 1.0 and 6.0. With sufficient laboratory and field data, Al-Qadi and Nassar (2003) proposed that SF_{ss} can be approximated by Eq. 5-32 as follows:

$$SF_{ss} = \frac{W_{Lab}}{W_{Field}} = \frac{\sum_{i=x}^{y}\left(E_i \varepsilon_i\right) + \sigma_z^2 E_z}{\sum_{i=x}^{y}\left(E_i \varepsilon_i\right) + \sigma_z^2 E_z} \qquad (5\text{-}32)$$

where:

W_{Lab} = Total work done by laboratory loading ≅ strain energy (J/m^3)

W_{Field} = Total work done by traffic loading in the field ≅ strain energy (J/m^3)

σ, E, ε = stress (MPa), elastic modulus (MPa), and strain (mm/mm)

i = Subscript i, for x, y, and z coordinate directions

However, for the current CMSE analysis, the effect of differences in stress state between laboratory and field loading conditions was assumed to be directly tied to the anisotropic response of HMAC. For example, the response behavior of HMAC in terms of the elastic modulus under loading is directionally dependent, which is a function of the stress state. Therefore, the effect of stress state was considered to be indirectly incorporated in the SF_a factor.

Resilient Dilation, SF_d

Consistent with the theoretical definition of ν, resilient dilation will occur only for ν values greater than 0.5. For pavement material subjected to vertical loading, dilation occurs when the lateral deformation is greater than the vertical deformation, often as a result of inadequate lateral confinement or support. This tendency to dilate is generally caused by the motion of particles that tend to roll over one another (Lytton et al. 1993).

Dilation is often very critical in unbound granular materials, and the subgrade and base can often have a very significant impact on the overall fatigue performance of the pavement structure in terms of stress-strain response. HMAC, on the other hand, is a bound material and is not very sensitive to dilation. However, its stress-strain response to traffic loading and overall performance can be greatly affected if the underlying pavement layers have the potential to dilate.

SF_d often ranges between 1.0 and 5.0 depending upon how much larger the Poisson's ratio (ν) is greater than 0.5. Since in this study all the values of ν used were less than 0.5 (Chapter III), a minimum value of 1.0 for SF_d was assumed.

Traffic Wander, SF_{tw}

Controlled laboratory fatigue testing applies loading repetitively to the same exact location on the specimen. However, traffic loading in the field does not constrain itself to the same position in the wheelpath. Accordingly, SF_{tw} is needed to account for the traffic wander when modeling pavement response to loading.

Blab and Litzka (1995) postulated that the vehicle positions within the wheelpaths follow a Laplace distribution function. Al-Qadi and Nassar (2003) assumed a normal distribution around the wheelpath with a mean of zero and a standard deviation σ. Based on transverse strain measurements in the wheelpath, Al-Qadi and Nassar. (2003) derived SF_{tw} values ranging between 1.6 and 2.7 for a σ range of 0.5 to 1.0.

Also, Al-Qadi and Nassar (2003)'s study seems to indicate that with the assumption of normal traffic distribution in the wheelpath and a relatively small value of σ (i.e., σ < 0.5), a SF_{tw} value of 1.0 can possibly be derived. In this study, traffic wander was not, however, directly taken into account.

Number of Load Cycles to Crack Initiation, N_i

N_i is defined as the number of load cycles required to initiate and grow a microcrack to 7.5 mm in length in the HMAC layer and was derived as explained in Appendix C. In the CMSE analysis, N_i is determined as a function of crack density, HMAC specimen cross-sectional area, Paris' Law fracture coefficients, and the rate that damage accumulates as indicated by the DPSE during RDT testing (Lytton et al. 1993, Jacobs et al. 1996, Simons and Seaman 2000, Daniel and Kim 2002):

$$N_i = \left(\frac{\overline{C}_{\max}^{(1+2n)}}{A}\right)\left(\left[\frac{4\pi A_c}{b}\right]^n\right)(C_D)^n \tag{5-33}$$

$$n = \left(\frac{1}{m_t}\right) \tag{5-34}$$

$$A = \frac{k}{\sigma_t^2 I_i}\left(\left[\frac{D_1^{(1-m_t)} E_t}{\Delta G_f}\right]^{\left(\frac{1}{m_t}\left[\frac{1}{(n_{BD}+1)}\right]\right)}\right)\int_0^{\Delta t} w^n(t)\,dt \tag{5-35}$$

$$D_1 = \left(\frac{1}{E_t}\right)\left(\frac{Sin[m_t\pi]}{m_t\pi}\right) \tag{5-36}$$

$$I_i = \frac{2}{(1+n_{BD})} \tag{5-37}$$

$$\int_0^{\Delta t} w^n(t).dt = \int_0^{\Delta t} \left(Sin^{2n}\left[\frac{\pi}{\Delta t} t \right] \right) dt = 0.5042 - 0.1744 \ln(n) \qquad (5\text{-}38)$$

where:

$\overline{C}_{max}$ = Maximum microcrack length (mm) (i.e., 7.5 mm)

A, n = Paris' Law fracture coefficients

A_c = HMAC specimen cross-sectional area (m^2)

b = Rate of accumulation of dissipation of pseudo strain energy

C_D = Crack density (m/m^2)

m_t = Exponent obtained from the tension RM master-curve (slope of the log relaxation modulus versus log time graph)

D_1 = Time-dependent creep compliance at 1.0 s (MPa^{-1})

E_t = Elastic modulus from tension RM master-curve (MPa)

k = Material coefficient (~0.33)

ΔG_f = Surface energy due to fracture or dewetting ($ergs/cm^2$)

σ_t = Maximum HMAC mixture tensile strength at break (kPa)

I_i = Dimensionless stress integral factor in crack failure zone, ranging between 1 and 2

n_{BD} = Dimensionless brittle-ductile factor, ranging between 0 and 1

Δt = Repeated loading time (s) (~0.01 s)

$\int_0^{\Delta t} w^n(t)dt$ = Load pulse shape factor, ranging between 0 and 1

t = Time (s)

The parameter $\overline{C}_{max}$ defines the CMSE maximum microcrack length at the point of crack initiation and subsequent propagation through the HMAC layer thickness. The crack density (C_D) and rate of accumulation of dissipation of pseudo strain energy (b) are discussed in the subsequent subsections of this chapter.

The parameters A and n are Paris' Law fracture coefficients for material fracture properties, which quantify the HMAC mixture's susceptibility to fracturing under loading. According to Paris' Law and Schapery's WPT theory, the coefficient n can be defined simply as the inverse of the stress (tensile) relaxation rate (m_t) as expressed by Eq. (5-34) (Paris and Erdogan 1963, Schapery 1984, Si 2001, Cheng 2002). This assumption is valid for linear visco-elastic HMAC materials under a constant strain-controlled RDT test (Si 2001, Cheng 2002). The Paris' Law fracture coefficient A (Eq. [5-33)) on the other hand is a function of many parameters including k, D_1, E_t, m_t, n_{BD}, ΔG_f, σ_t, I_i, and $w^n(t)$. Based on Eq. (5-33), a small value of A is desirable in terms of HMAC mixture fatigue resistance. Numerical analysis, however, indicated that this coefficient A is very sensitive to n_{BD} and σ_t if other factors are held constant.

The parameter k is a material coefficient relating the length of the fracture process zone ($\propto$) to strain energy and tensile strength. While k is a measurable parameter, a value of 0.33 was used based on the work of Lytton et al. (1993) and the assumption that k does not vary significantly with microcrack length in the fracture process zone.

As expressed by Eq. (5-36), the time-dependent creep compliance, D_1, was determined as a function of E_t and m_t at 1.0 s. Although an exact value of D_1 can be measured from uniaxial creep tests, this less costly and simple approximation produces reasonable results that are sufficient for use in HMAC mixture characterization analysis.

The numerical integration of $w^n(t)$ (Eq. [5-38)) with respect to time (t) describes the shape of the input load pulse as a function of material fracture coefficient n (Paris' Law). This integral exhibits a linear proportional relationship with the Paris' Law fracture coefficient A, as evident from Eq. (5-35), and has a subsequent inverse relationship with N_i.

For a haversine-shaped input strain waveform for the RDT test, as in this study, the integral reduces to a simple linear logarithmic form shown in Eq. (5-38) with n as the only variable. Note that material response to loading is not only magnitude dependent but is also dependent on the shape of the applied load form. As discussed previously, a haversine-shaped input load form is a close simulation of HMAC load response under a moving wheel load (Lytton et al. 1993, Si 2001). The parameters E_t, m_t, ΔG_f, and σ_t are discussed subsequently.

I_i is an elasticity factor due to the integration of the stresses near the microcrack tip over a small region in the microcrack failure zone (Lytton et al. 1993, Si 2001, Cheng 2002). This factor I_i, which quantifies the materials' elasticity, ranges between 1.0 and 2.0 for perfectly linear-elastic (brittle) and rigid-plastic (ductile) materials, respectively (Lytton 2004). Generally, a lower value (i.e., more brittle) of I_i is indicative of high susceptibility to fatigue damage. As expressed by Eq. (5-37), I_i was quantified simply as a function of n_{BD} in this study. This brittle-ductile factor n_{BD}, which ranges between 0.0 for perfectly plastic materials and 1.0 for brittle materials, is an age-related adjustment factor that accounts for the brittleness of the HMAC mixture in terms of stress-strain response under loading. In this study, unaged HMAC specimens were assumed to exhibit plastic behavior and were subsequently assigned an n_{BD} value of 0.0. All the aged HMAC specimens were assumed to exhibit a more brittle behavior lying somewhere between perfectly plastic and brittle behavior, and were thus assigned n_{BD} values of 0.5 and 0.75 for 3 and 6 months aging conditions, respectively. Fig. 5-15 illustrates the HMAC brittle-ductile characterization as a function of σ_t and ε_t.

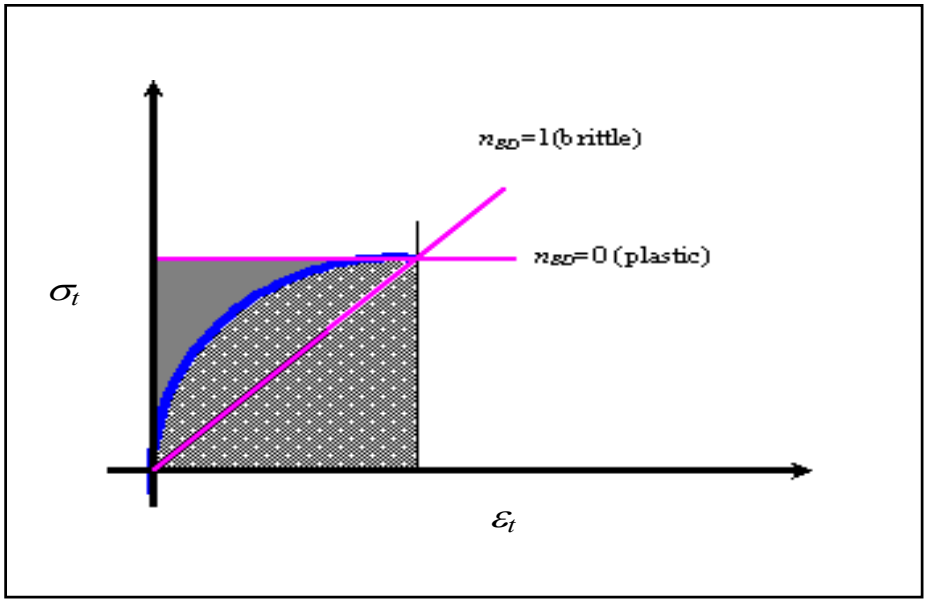

Fig. 5-15. HMAC Brittle-Ductile Characterization

Based on this σ_t-ε_t plot, the lower the n_{BD} value, the more plastic and ductile the material is and vice versa. Note that the n_{BD} value can be likened to the slope of the σ_t-ε_t plot and the steeper the slope, the more brittle the material is. According to Fig. 5-15, a perfectly plastic-ductile material will have a minimum n_{BD} value of 0.0 and a maximum n_{BD} value of 1.0 for a perfectly elastic-brittle material. Notice also from Eq. (5-39) that as n_{BD} increases from 0.0 to 1.0, I_i will in contrast decrease from 2.0 to 1.0, indicating an increase in HMAC brittleness. In Fig. 5-15, the shaded area (A_{shaded}) is given by Eq. (5-39) below:

$$A_{shaded} = \frac{\sigma_t \varepsilon_t}{2}\left[\frac{2}{n_{BD}+1}\right] = \frac{\sigma_t^2 D_1}{2}\left[\frac{2}{n_{BD}+1}\right] \qquad (5\text{-}39)$$

The area represented by Eq. (5-39) can be likened to a simplified representation of the actual physical energy that will be expanded to cause fracture failure or break under tensile loading. When the product $\sigma_t \times \varepsilon_t$ is normalized to 1.0, A_{shaded} is simply I_i.

Eq. (5-39) further indicates that as HMAC approaches a brittle state (i.e., n_{BD} approaches 1.0), A_{shaded} will decrease to almost half the magnitude when n_{BD} is zero, indicating a decrease in the amount of actual physical energy expended to cause fracture failure. This response is theoretically expected as brittle materials are more susceptible to fracture damage and subsequently require less energy to induce and cause fracture failure.

Number of Load Cycles to Crack Propagation, N_p

N_p refers to the number of load cycles required to propagate a 7.5 mm microcrack through the HMAC layer thickness and its derivation is included in Appendix C. As expressed by Eq. (5-40), N_p is determined as a function of the maximum microcrack length, HMAC layer thickness, shear modulus, Paris' Law fracture coefficients, and a design shear strain (Lytton et al. 1993, Si 2001, Cheng 2002):

$$N_p = \left(\frac{d^{\left(1-\frac{n}{2}\right)}}{\left[A(2r)^n (SG)^n (1-nq)\right]} \right) \left(1 - \left[\frac{\overline{C}_{\max}}{d} \right]^{(1-nq)} \right) \left(\frac{1}{\gamma} \right)^n \tag{5-40}$$

$$S = \frac{(1-\nu)}{(1-2\nu)} \tag{5-41}$$

$$G = E_t \left(\frac{G_{xz}}{E_z} \right) \tag{5-42}$$

where:

A, n	=	Paris' Law fracture coefficients
r, q	=	Regression constants for stress intensity factor (~4.40, 1.18)
S	=	Shear coefficient
G	=	Shear modulus (MPa)

$\overline{C}_{\max}$ = Maximum microcrack length (mm) (i.e., 7.5 mm)

d = HMAC layer thickness (mm)

γ = Maximum design shear strain at the edge of a loaded tire (mm/mm)

ν = Poisson's ratio

G_{xz} = Resilient shear modulus (MPa)

E_t = Elastic modulus from tensile RM master-curve (MPa)

If the elastic modular ratio G_{xz}/E_z in Eq. (5-42) is unknown, Eq. (5-43) below can be used to approximate G (Lytton 2001). Eq. (5-43) is a simple shear-elastic modulus relationship based on elastic theory:

$$G = \frac{E_t}{2(1+\nu)} \tag{5-43}$$

The parameters A, n, and C_{max} were discussed in the previous subsections, and γ is discussed in the subsequent text. Like N_i, an inverse relationship exists between A and N_p, indicating that a small value of A is desired in terms of HMAC mixture fatigue resistance. The failure load-response parameter γ also exhibits an inverse relationship with N_p.

Unlike for N_i, d is introduced in N_p because during the microcrack propagation process, for fatigue failure to occur, a microcrack length of a defined threshold value must actually propagate through the HMAC layer thickness. By contrast, the prediction relationship for N_i is a fatigue model for microcrack initiation and is independent of the parameter d.

Parameters r and q are regression constants that are a function of the stress intensity distribution in the vicinity of the microcrack tip. In this study, values of 4.40 and 1.18 were used, respectively, based on the work of Lytton et al's through FEM analysis (1993). S is a shear coefficient, which as defined by Eq. (5-41) is a function of the Poisson's ratio.

Surface Energies, ΔG_h^{AB}, ΔG_h^{LW}, and ΔG_f

To cause load-induced damage in the form of fatigue cracking, energy must be expended, and equally energy must be expended to close the fracture surfaces. Surface energy data thus constitute input parameters for the healing, crack initiation, and propagation calculations in the CMSE fatigue analysis (Eqs. [5-44] through [5-50]). The respective equations for the SE data analysis required for the CMSE approach based on an adhesive mode of fracturing under dry conditions are described in this subsection.

$$\Delta G_h^{LW} = -\Gamma_{ij}^{LW} + \Gamma_i^{LW} + \Gamma_j^{LW} \tag{5-44}$$

$$\Delta G_h^{AB} = -\Gamma_{ij}^{AB} + \Gamma_i^{AB} + \Gamma_j^{AB} \tag{5-45}$$

$$\Delta G_h = \Delta G_h^{LW} + \Delta G_h^{AB}$$

$$\begin{aligned} \Delta G_f &= \Delta G_f^{LW} + \Delta G_f^{AB} \\ &= \left[-\Gamma_{ij}^{LW} + \Gamma_i^{LW} + \Gamma_j^{LW}\right] + \left[-\Gamma_{ij}^{AB} + \Gamma_i^{AB} + \Gamma_j^{AB}\right] \end{aligned} \tag{5-46}$$

And,

$$\Gamma_{ij}^{LW} = \left(\sqrt{\Gamma_i^{LW}} - \sqrt{\Gamma_j^{LW}}\right)^2 \tag{5-47}$$

$$\Gamma_i^{AB} = 2\left(\sqrt{\Gamma_i^+ \Gamma_i^-}\right) \tag{5-48}$$

$$\Gamma_{ij}^{AB} = 2\left(\sqrt{\Gamma_i^+} - \sqrt{\Gamma_j^-}\right)\left(\sqrt{\Gamma_i^-} - \sqrt{\Gamma_j^-}\right) \tag{5-49}$$

$$\Gamma_j^{AB} = 2\left(\sqrt{\Gamma_j^+ \Gamma_j^-}\right) \tag{5-50}$$

where:

Γ	=	Surface free energy component of the binder or aggregate (ergs/cm^2)
i,j	=	Subscript "i" for binder (healing or fracture) and "j" for aggregate
h,f	=	Subscript "h" for healing and "f" for fracture
LW	=	Superscript "LW" for Lifshitz-van der Waals (LW) component
AB	=	Superscript "AB" for acid-base (AB) component
$+$	=	Superscript "+" for Lewis acid component of surface interaction
$-$	=	Superscript "–" for Lewis base component of surface interaction
Γ_{ij}	=	Interfacial surface energy between binder and aggregate due to "LW" or "AB" (superscripts) components (ergs/cm^2)
ΔG	=	Total surface free energy due to "h" or "f" (subscripts) for "LW" and/or "AB" (superscripts) components (ergs/cm^2)

Eqs. (5-44) through (5-48) are the non-polar surface bond energy for healing, the polar surface bond energy for healing, the interactive term for the non-polar *LW* surface bond energy component, and the polar surface energy component for binder, respectively. These equations quantify the bond strength within the binder mastic and the binder-aggregate adhesion.

Eq. (5-46) is the total bond strength energy for fracture, which is made up of the LW nonpolar energy components and the AB polar energy components. Eq. (5-46) is also commonly known as the total bond strength or Gibbs free energy of fracture for the binder (Lytton 2004).

According to Lytton et al. (1993), greater resistance to fracture, is provided by larger bond strength (cohesive or adhesive), and a greater healing capacity is promoted by the smallest *LW* bond strength and the largest *AB* bond strength. On this basis, the lower the value of ΔG_h, the greater the potential to self-heal and the higher the value of ΔG_f, the greater the resistance to fracture for HMAC.

In the simplest fundamental theory of energy, if a relatively higher amount of energy is required or must be expended to cause fracture damage (i.e., initiate and propagate a microcrack through the HMAC layer), then the HMAC mixture is substantially resistant to fracture damage. If, on the other hand, a higher amount of energy is required or must be expended to repair the fracture damage (i.e., healing defined as the closure of fracture surfaces) that occurred during the fracturing process, then the HMAC mixture has relatively less potential to self-heal.

Relaxation Modulus, E_i, Exponent, m_i, and Temperature Correction Factor, a_T

The elastic relaxation modulus ($E(t)$) and exponent (m_i) were determined from RM master-curves of log modulus ($E(t)$) versus log time (t) obtained from tension and compression RM test data at a reference temperature of 20 ^{o}C (Si 2001). From the RM master-curve, a simple power function of relaxation modulus and loading time was generated as follows:

$$E(t) = E_i \xi^{-m_i} \tag{5-51}$$

$$\xi = \frac{t}{a_T} \tag{5-52}$$

where:

$E(t)$ = Time-dependent elastic relaxation modulus (MPa)

E_i = $E(t)$ at ξ = 1.0 s (MPa) tension (E_t) or compression (E_c)

ξ, t = Reduced and actual RM test time, respectively (s)

m_i = Exponential stress relaxation rate ($0 \leq m_i < 1$)

i = Subscript “t” for tension and “c” for compression

Eq. (5-51) is a simple power law relationship that is valid for most HMAC materials at intermediate and/or long times of loading (Si 2001). The exponent m_i refers to the rate of stress relaxation. The temperature correction factors (a_T) were obtained through utilization of the SSE regression optimization technique using the spreadsheet "Solver" function and the Arrhenius time-temperature superposition model shown in Eq. (5-53) (Francken and Clauwert 1988). The reference temperature was 20 °C, and thus the a_T for 20 °C was 1.0.

$$Log(a_T) = A_a\left[\left(\frac{1}{T} - \frac{1}{T_{ref}}\right)\right] \qquad (5\text{-}53)$$

where:

A_a = Material regression constant obtained from spreadsheet regression SSE optimization analysis

T = Test temperature in degrees Kelvin ($K = 273 + °C$)

T_{ref} = Reference temperature of interest ($°K$) ($K_{ref} = 273 + 20 = 293$)

Dissipated Pseudo Strain Energy (DPSE) and Constant, *b*

Using Schapery's (1984) WPT and the extended visco-elastic correspondence principle, DPSE was utilized as a representative measure of HMAC damage under RDT testing. This DPSE was used to describe cumulative fracture damage within the HMAC specimens instead of the physically measured dissipated energy because the DPSE approach allows for a more accurate and appropriate characterization of the fracture damage process by eliminating the time-dependent linear visco-elastic effects and non-linearity of the material (Cleveland et al. 2003). The slope of a plot of DPSE versus load cycles (N) from the RDT test is defined as the rate of fracture damage accumulation or energy dissipation denoted as the constant *b*.

This constant b is basically a representation of the rate at which the specimen is accumulating fracture damage during RDT testing. Both DPSE and the constant b were determined from a combination of the RM test data (E_t and m_t) in tension and the RDT test data. The steps and associated numerical models used for DPSE analysis in this study are discussed in the subsequent text.

For any selected load cycle, the time-dependent linear visco-elastic stress (under damaged or undamaged conditions) was calculated using the Boltzmann superposition constitutive equation as a function of the RM and the RDT test data (Lytton 2001, Si 2001, Daniel and Kim 2002, Wen and Kim 2002). A temperature correction factor (a_T) was also introduced into the constitutive equation to normalize the calculated stress to a given reference temperature. In this study, a_T was obtained from RM analysis, and the selected reference temperature was 20 °C. This temperature is a realistic simulation of field service temperatures at which HMAC is susceptible to fracture damage under traffic loading. The RDT test was conducted at 30 °C, and therefore the calculated stress had to be normalized to 20 °C.

Secondly, pseudo strain for damaged conditions was calculated as a function of the normalized calculated linear visco-elastic stress for damaged conditions, the reference modulus (E_R), and a non-linearity correction factor, $\psi(t)$ (Si 2001). In the analysis, calculated PS rather than physically measured strain is used to characterize damage and healing to separate and eliminate the time-dependent visco-elastic behavior of the HMAC material from real damage during the strain-controlled RDT test (Si 2001).

E_R is the modulus of the undamaged material determined from the first load cycle of the RDT test. Note that no significant fracture damage was considered to occur during the first RDT load cycle. This E_R can be an arbitrary constant introduced primarily to remove the stress dimension in the pseudo strain analysis. However, the selected E_R in this study also allows the linear visco-elastic material behavior to be treated as elastic during the damage development process due to the elastic visco-elastic correspondence principle.

The $\psi(t)$ is introduced primarily to account for any non-linearity of the undamaged visco-elastic material. This $\psi(t)$ is a function of the measured and calculated stress at the first RDT load cycle in an assumed undamaged condition. The principal concept of $\psi(t)$ is to collapse the hysteresis loop of the first RDT load cycle into a straight line as illustrated in Fig. 5-1 so that the DPSE of the first RDT load cycle is equal or close to zero. This $\psi(t)$ concept is based on the theoretical assumption that no fracture damage occurs during the first RDT load cycle and thus the DPSE should essentially be zero if the assumption of linear elastic behavior is upheld.

Finally, DPSE was then calculated as a product of the measured stress and the calculated PS for damaged conditions using the double meridian distance method (DMD) for traverse area determination (Kissam 1956, Si 2001). This DPSE is simply the area in the pseudo hysteresis loop of the measured tensile stress versus the calculated PS plotted as shown in Fig. 4-1. The value of DPSE is supposed to be close or equal to zero for the first RDT load cycle. The respective equations are:

$$DPSE = \sum \left(\varepsilon_R^d(t) \times \sigma_m^d(t) \right) \tag{5-54}$$

$$\varepsilon_R^d(t) = \psi(t) \left[\frac{\sigma_c^d(t)}{E_R} \right] \tag{5-55}$$

$$\Psi(t) = \frac{\sigma_{c(1)}^u(t)}{\sigma_{m(1)}^u(t)} \tag{5-56}$$

$$\sigma_c^u(t) \neq \sigma_m^u(t) \, , \sigma_c^d(t) \neq \sigma_m^d(t) \tag{5-57}$$

$$\sigma_{c(1)}^u(t) = \sigma_{c(1)}^d(t) \neq \sigma_{c(2...N)}^d(t) \ , \ \sigma_{m(1)}^u(t) = \sigma_{m(1)}^d(t) \neq \sigma_{m(2...N)}^d(t) \tag{5-58}$$

$$\sigma_c(t) = \int_0^t E(t-\tau)\frac{\partial \varepsilon(\tau)}{d\tau} d\tau \tag{5-59}$$

The convolution integral Eq. (5-59) is the general uniaxial stress-strain relationship applicable to most linear visco-elastic materials including HMAC and is generally compatible with changing boundary conditions such as damage growth during transient loading (Schapery 1984, Cleveland et al. 2003). For a haversine-shaped input strain waveform, Eq. (5-59) can be written in the simple approximate numerical-integration form shown in Eq. (5-60):

$$\sigma_c(t_{i+1}) = \sum_{k=0}^{k=i+1}\left(C_k \Delta\tau\left[E_\infty + E_1\left(t_{i+1} - t_k\right)^{-m}\right]\right) \tag{5-60}$$

Assuming E_∞ is zero, and using E_t and m_t for undamaged conditions and a_T from RM analysis, Eq. (5-60) reduces to Eq. (5-61) shown below:

$$\sigma_c(t_{i+1}) = \sum_{k=0}^{k=i+1}\left(C_k \Delta\tau\left[E_t\left(\frac{(t_{i+1} - t_k)}{a_T}\right)^{-m_t}\right]\right) \tag{5-61}$$

$$\sigma_c(t_{i+1}) = \Delta\tau E_t \sum_{k=0}^{k=i+1}\left(C_k\left(\frac{(t_{i+1} - t_k}{a_T}\right)^{-m_t}\right) \tag{5-62}$$

where:

$\sigma^u_{c(1)}(t)$ = Calculated time-dependent linear visco-elastic tensile stress in an assumed undamaged condition at the first load cycle (kPa)

$\sigma^d_c(t)$ = Calculated time-dependent linear visco-elastic tensile stress under damaged conditions at any load cycle other than the first (kPa)

t_{i+1}, t_k = Present and previous time, respectively (s)

τ = Loading time history (e.g., 0.0 to 0.10 s at which strains were measured) (s)

$\Delta\tau$ = Time increment (s) (e.g., 0.005 s)

$E(t-\tau)$ = Tensile relaxation modulus in an assumed undamaged condition at time t-τ (MPa)

$\varepsilon(\tau)$ = Measured strain at previous time, τ (mm/mm)

C_k = Mean slope of any segment of the haversine input strain waveform

$\varepsilon_R^d(t)$ = Calculated pseudo strain for damaged conditions (mm/mm)

E_R = Reference modulus for an assumed undamaged material calculated from the first load cycle (MPa)

$\psi(t)$ = Dimensionless non-linearity correction factor (NLCF)

$\sigma_{m(1)}^u(t)$ = Measured tensile stress for assumed undamaged condition at the first load cycle (MPa)

$\sigma_m^d(t)$ = Measured tensile stress for damaged conditions (kPa)

a_T = Temperature correction factor (from relaxation modulus analysis)

$DPSE$ = Dissipated pseudo strain energy (J/m^3)

g = Acceleration due to gravity (m/s^2)

For a haversine-shaped input strain waveform, both the measured and approximate (calculated) stress should exhibit a shape of the form shown in Fig. 5-16.

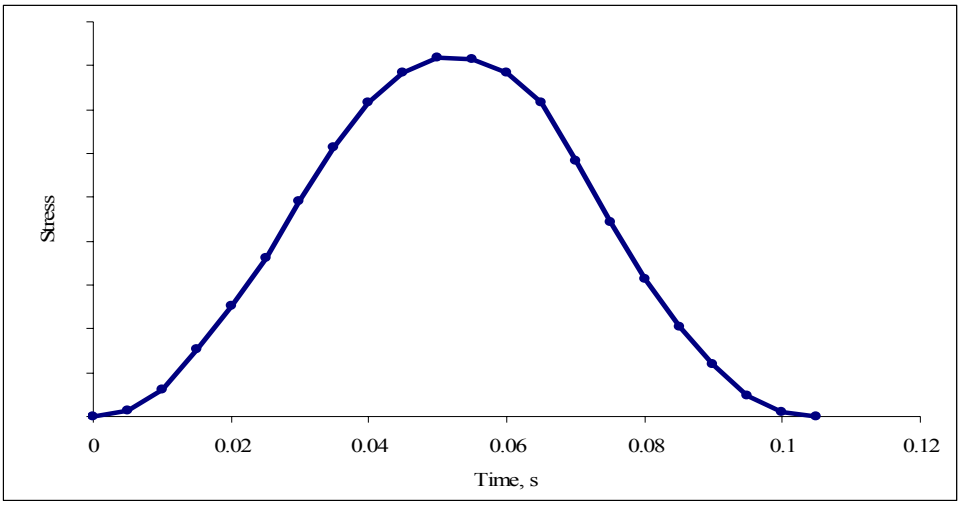

Fig. 5-16. Output RDT Stress Shape Form

DPSE for selected laboratory test load cycles (N) was then plotted against log N to generate a linear logarithmic function of the form shown in Eq. (5-63). The constant b in Eq. (5-63), also defined as the rate of change in DSPE during microcrack growth, is simply the slope of the DPSE versus log N plot, which is the required input parameter for the CMSE fatigue analysis (Si 2001).

$$W_R = a + bLog(N) \tag{5-63}$$

where:

W_R = DPSE (J/m^3)
a = Constant or DPSE at the first load cycle
b = Slope of W_R-log N plot
N = Load cycle

A plot of DPSE versus log N should exhibit a simple linear graph of the form shown in Fig. 5-17.

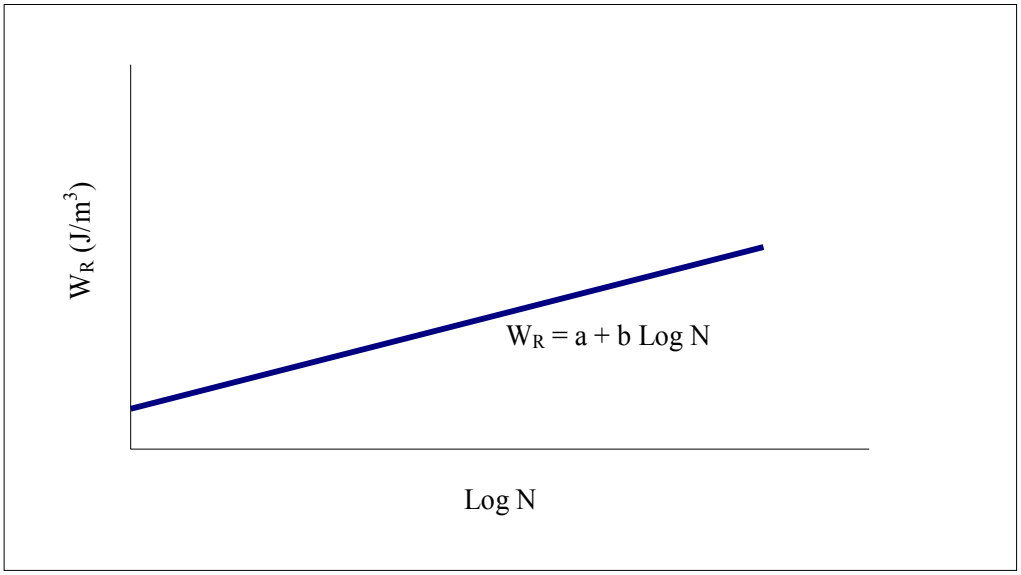

Fig. 5-17. Example of W_R - Log *N* Plot

The constant *b* is inversely related to the HMAC mixture fatigue resistance. Generally, a comparatively small value of *b* is indicative of a relatively low rate of accumulation of micro-fatigue damage and consequently high HMAC mixture fatigue resistance.

Crack Density, C_D

Crack density calculations were based on the cavitation analysis by Marek and Herrin (1986) assuming a brittle mode of crack failure for the HMAC specimen as shown in Fig. 5-18. In their analysis, Marek and Herrin (1986) used an average microcrack length of 0.381 mm based on 281 HMAC specimens. Using these data, microcrack density was calculated as a function of the number of cracks per specimen cross-sectional area to be 2.317 mm^{-2}. This is the crack density value (2.317 mm^{-2}) used for the CMSE fatigue analysis in this study.

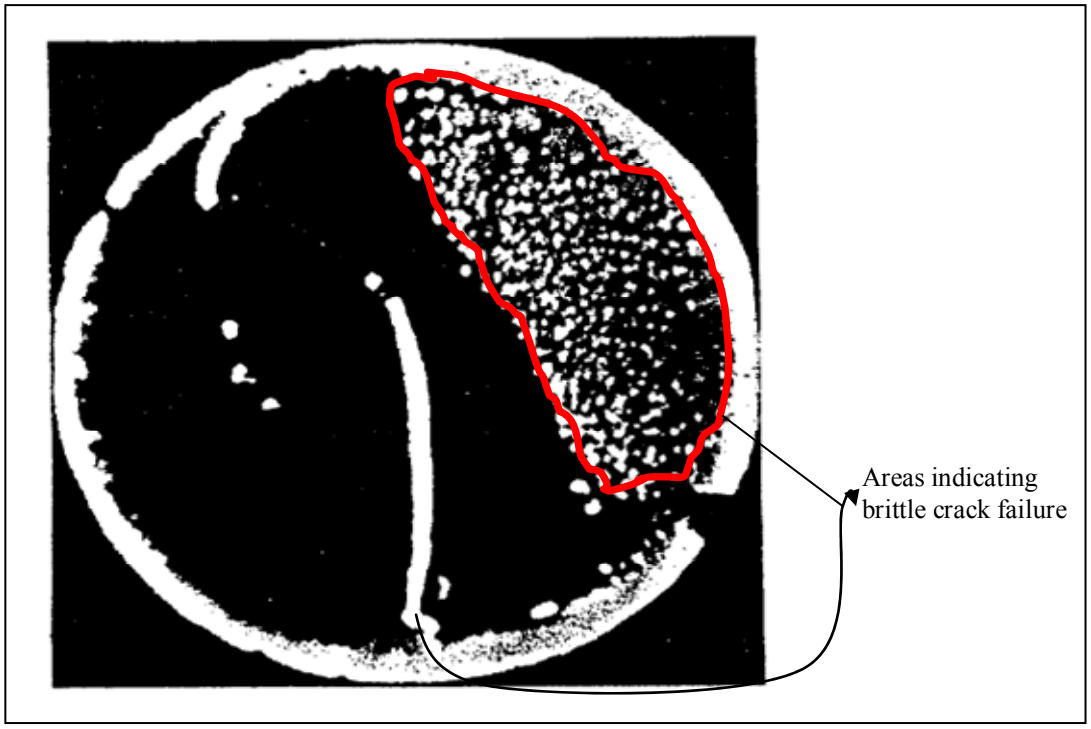

Fig. 5-18. Brittle Crack Failure Mode (Marek and Herrin 1968)

Shear Strain, γ

FEM analysis software that takes into account the visco-elastic nature of HMAC is desirable for pavement stress-strain analysis to determine the maximum design shear strain γ at the edge of a loaded tire. If linear elastic analysis software such as ELSYM5 (Ahlborn 1969) is used, an adjustment to the calculated γ must be done to account for the visco-elastic and plastic nature of HMAC. In this study, computed linear elastic γ was adjusted consistent with the FEM adjustment criteria discussed in Chapter III.

Input parameters for the stress-strain analysis included traffic loading (ESALs and the axle and tire configuration), pavement structure and material properties defined as a function of environment (temperature and subgrade moisture conditions), and desired response locations. If linear-elastic conditions are assumed, Eq. 5-64 can be used to approximate γ (Lytton 2001). In this study, the former analysis procedure as discussed in Chapter III was used.

$$\gamma = \frac{\sigma_p}{S \times G} \tag{5-64}$$

where:

σ_p = Tire pressure (kPa) (~690 kPa)
S = Shear coefficient
G = Shear modulus (MPa)

VARIABILITY, STATISTICAL ANALYSIS, AND N_f PREDICTION

In this study, a COV was utilized as an estimate of the variability of *Ln* N_f predicted by the CMSE approach. The COV expresses the standard deviation as a percent of the mean as follows:

$$COV = \frac{100s}{\bar{x}} \tag{5-65}$$

where:

s = Sample standard deviation
$\bar{x}$ = Sample mean, calculated based on replicate measurements of N_f

The COV is basically a measure of relative variation, and it says that the measurements lie, on the average, within approximately COV percent of the mean (Montgomery et al. 2001). Replicate N_f predictions obtained by varying the material input parameters based on actual laboratory-measured replicate values also provided a reasonable measure of variability and precision for the CMSE approach.

For this CMSE approach, mean *Ln* N_f values were predicted from laboratory-measured material properties (i.e., tensile strength [σ_t]) on at least two replicate specimens. For this analysis, a typical spreadsheet descriptive statistics tool was utilized. A 95% confidence interval (CI) for the mean *Ln* N_f was then computed as expressed by Eq. (5-66) under a normality assumption on the distribution of *Ln* N_f. These statistical analyses were also supplemented and counterchecked with a one-sample t-test for an assumed t-value of zero. A statistical software, Statistical Package for Social Sciences (SPSS V11-5), was utilized for the one-sample t-test analysis (Montgomery et al. 2001).

$$95\%\ N_f\ \text{CI} = \bar{x} \pm t_{\frac{\alpha}{2},n-2}\left[\frac{s}{\sqrt{n}}\right] \tag{5-66}$$

where:

CI	=	Confidence interval
$\bar{x}$	=	Mean *Ln* N_f value
s	=	Standard deviation of *Ln* N_f
α	=	Level of significance, i.e., 0.05 for 95% reliability level
n	=	Number of replicate specimens

SUMMARY

The following bullets summarize the CMSE fatigue analysis approach as utilized in this study:

- The CMSE approach was formulated on the fundamental concepts of continuum micromechanics and energy theory and utilizes the visco-elastic correspondence principle, Paris' Law fracture mechanics, and Schapery's work potential theory to monitor cumulative fracture damage in HMAC mixtures.

- The CMSE approach utilizes the fundamental HMAC mixture properties including tensile strength, fracture, healing, visco-elasticity, anisotropy, crack initiation, and crack propagation to estimate N_f.
- The energy theory in this CMSE approach is conceptualized on the basis that energy must be expended to cause load-induced damage in the form of fracture cracking, and, equally, energy must be expended to close up these fracture surfaces, a process called healing.
- The computation of the critical design shear strain at the edge of a loaded tire within a representative field HMAC pavement structure for N_p analysis constitutes the failure load-response parameter for this approach. The utilization of field calibration constants *for* N_f (SF_h, N_i, and N_p) constitute the calibration part.
- For this CMSE approach, the HMAC material is characterized in terms of fracture and healing processes and requires only relaxation tests in uniaxial tension and compression, tensile strength tests, repeated load tests in uniaxial tension, and a list of fracture and healing surface energy components of asphalt binders and aggregates measured separately.
- HMAC mixture characterization by CMSE laboratory testing utilizes gyratory-compacted cylindrical HMAC specimens under strain and temperature-controlled conditions.
- Fatigue failure according to the CMSE approach in this study was defined as the number of repetitive load cycles that are required to initiate and propagate a 7.5 mm microcrack through the HMAC layer thickness.

CHAPTER VI
THE CALIBRATED MECHANISTIC APPROACH WITHOUT SURFACE ENERGY MEASUREMENTS

The calibrated mechanistic approach without surface energy measurement measurements follows the same analysis concept and failure criteria as the CMSE approach except for a few differences. Laboratory testing differences include the absence of SE measurements and RM testing in compression. The analysis is slightly different to account for the fact that some of the input data (i.e., SE and RM in compression) is not measured. Fig. 6-1 and Table 6-1 summarize the CM fatigue design and analysis system, and input/output data, respectively.

The fundamental concepts, failure criteria, statistical analysis, and N_f prediction are similar to the CMSE approach (Chapter V) and are therefore not discussed in detail again in this chapter. The CM approach is essentially postulated to be a simplified version of the CMSE approach, with reduced laboratory testing and analyses.

LABORATORY TESTING

Unlike the CMSE approach, SE measurements (for both binders and aggregates) and mixture RM tests in compression are not required in the CM approach. These laboratory tests are briefly discussed in the subsequent text in this chapter.

However, all other laboratory test protocols are similar to that of the CMSE approach. These laboratory tests include the TS, RM (tension), and RDT and will not be discussed again in this chapter.

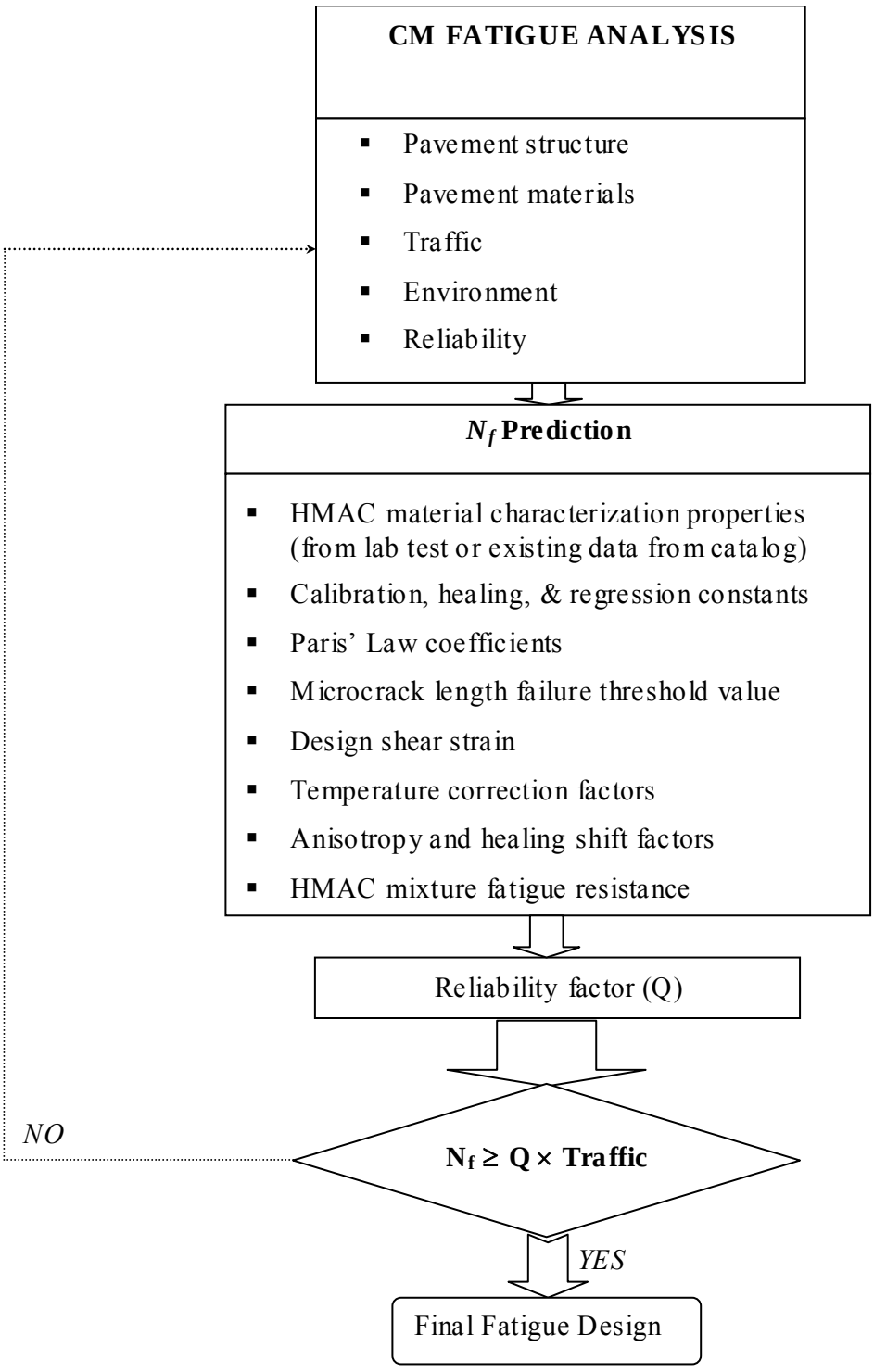

Fig. 6-1. The CM Fatigue Design and Analysis System

Table 6-1. Summary of CM Fatigue Analysis Input and Output Data

Source	**Parameter**
Laboratory test data (HMAC mixture testing of cylindrical specimens)	• Tensile stress & strain • Relaxation modulus (tension only) • Uniaxial repeated direct-tension test data (strain, stress, time, & N) • Anisotropic data (vertical & lateral modulus)
Analysis of laboratory test data	• Tensile strength • Relaxation modulus master-curves (tension only) • Non-linearity correction factor • DPSE & slope of DPSE vs. Log N plot • Healing indices & calibration constants • Creep compliance • Shear modulus • Load pulse shape factor
Field conditions (design data)	• Pavement structure (i.e., layer thickness) • Pavement materials (i.e., elastic modulus & Poisson's ratio) • Traffic (i.e., ESALs, axle load, & tire pressure) • Environment (i.e., temperature & moisture conditions) • Field calibration coefficients • Temperature correction factor
Computer stress-strain analysis	• Design shear strain (γ) at edge of a loaded tire
Others	• Reliability level (i.e., 95%) • Crack density • Microcrack length • HMAC brittle-ductile failure characterization • Stress intensity factors • Regression constants • Shear coefficient
Output	• Paris' Law fracture coefficients (A, n) • Shift factor due to anisotropy (SF_a) • Shift factor due to healing (SF_h) • Fatigue load cycles to crack initiation (N_i) • Fatigue load cycles to crack propagation (N_p) • HMAC mixture fatigue resistance (N_f)

SE Measurements for Binders and Aggregates

The complete CMSE analysis procedure involves the determination of the surface energies of both binder and aggregate. The required SE input parameters for N_f prediction in the CMSE approach are used to calculate ΔG_f and ΔG_h. Determination of the SE components required for determining these inputs (ΔG_f and ΔG_h) is a time-consuming process using the current SE test protocol (the WP and USD), which requires approximately up to 70 hours to complete (see Chapter V).

Therefore, in order to improve the practicality of the CMSE approach, N_f was predicted using the CM procedure without using SE (ΔG_f and ΔG_h) as an input parameter. Consequently, no SE measurements are required in this CM approach.

RM Test in Compression

Mixture RM data in compression are required in the CMSE approach primarily to compute the SF_h. As discussed in the subsequent section, SF_h computation in the CM procedure does not require RM data in compression (i.e., E_{1c} and m_c) as input parameters.

ANALYSIS PROCEDURE

In terms of analysis, the major difference between the CMSE and CM approaches is in the computation of SF_h and Paris' Law fracture coefficients A and n. These differences are illustrated subsequently.

Shift Factor Due to Healing, SF_h

Eq. (6-1) expresses the computation of SF_h in the CM approach:

$$SF_h = 1 + g_5 \left(\frac{\Delta t_r}{a_{TSF}} \right)^{g_6} \tag{6-1}$$

$$\Delta t_r = \frac{31.536 \times 10^6 P_{DL}}{80kN \text{ Traffic ESALs}} \tag{6-2}$$

where:

Δt_r = Rest period between major traffic loads (s)

a_{TSF} = Temperature shift factor for field conditions (≅1.0)

g_i = Fatigue field calibration constants

P_{DL} = Pavement design life (i.e., 20 years)

It is clear that unlike the CMSE approach, ΔG_f, E_{1c}, and m_c are not required as input parameters for the computation of SF_h in the CM approach.

Paris' Law Fracture Coefficients, *A* and *n*

The modified and CMSE calibrated empirical Eqs. (6-3) and (6-4) based on the work of Lytton et al. (1993) show the computation of Paris' Law fracture coefficients A and n, respectively, according to the CM approach:

$$n = g_o + \left(\frac{g_1}{m_t}\right) \tag{6-3}$$

$$A = 10^{1+\left\{g_2+\frac{g_3}{m_t}\log\left(\frac{Sin(m\pi)}{m\pi E_t}\right)+g_4\log(\sigma_t)\right\}} \tag{6-4}$$

where:

A, n = Paris' Law fracture coefficients

g_i = Fatigue field calibration constants

m_t = Stress relaxation rate from the tension RM master-curve

E_t = Elastic modulus from tension RM master-curve (MPa)

σ_t = Mixture maximum tensile strength at break (kPa)

Fracture coefficients A and n are required as inputs for the determination of N_i and N_p, and subsequently N_f. The fatigue calibration coefficients g_i are climatic dependent values that were established by Lytton et al. (1993) and shown in Table 5-4 in Chapter V.

Note that empirical Eqs. (6-1) through (6-4) in this study were calibrated to the CMSE approach by comparing the actual calculated numerical values to the corresponding values obtained via the CMSE approach. Eq. (6-4), for instance, is the modification of the original equations from Lytton et al. (1993):

$$A = 10^{\left\{g_2 + \frac{g_3}{m_t}\log\left(\frac{Sin(m\pi)}{m\pi E_t}\right) + g_4\log(\sigma_t)\right\}} \qquad (6\text{-}5)$$

The A values computed using this empirical Eq. (6-5) differed from the CMSE A values by about 10 times (i.e., $A_{CMSE} \cong 10 \times A_{CM}$). Consequently, Eq. (6-5) was modified as shown in Eq. (6-4) to match the CMSE results. However, more HMAC fatigue characterization is required to further validate this simplified CM approach.

SUMMARY

The CM fatigue analysis approach as utilized in this study is summarized as follows:

- The CM approach follows the same concepts, failure criteria, and N_f prediction procedure as the CMSE approach. The major differences stem from a reduced laboratory testing program and resulting changes in the analysis procedure.
- The CM approach does not require SE measurements (both binder and aggregates) and RM tests in compression. Instead, these data inputs can be interpolated based on existing material empirical relationships or obtained from existing catalogued data if available.

- The SF_h is computed primarily as a function of traffic rest periods, temperature shift factor, fatigue calibration constants, pavement design life, and the design traffic ESALs. In contrast to the CMSE approach, ΔG_f, E_{1c}, and m_c are not required as input parameters for the computation of SF_h in the CM approach.
- Paris' Law fracture coefficients A and n are computed as a function of the material tensile strength (σ_t), RM data in tension (E_{1t}, m_t), and fatigue field calibration constants (g_i) using empirically developed relationships that were calibrated to the CMSE approach.

CHAPTER VII
THE PROPOSED NCHRP 1-37A 2002 PAVEMENT DESIGN GUIDE

This chapter summarizes the relevant aspects of the proposed NCHRP 1-37A 2002 Pavement Design Guide as utilized in this study. Further details can be found elsewhere (Superpave Models Team 2000, Witczak 2001, AASHTO 2004).

FUNDAMENTAL THEORY

The proposed NCHRP 1-37A 2002 Pavement Design Guide (MEPDG) adopts a mechanistic empirical (ME) approach for the structural design of HMAC pavements (Superpave Models Team 2000, Witczak 2001, AASHTO 2004). There are two major aspects of ME-based material characterization: pavement response properties and major distress/transfer functions. Pavement response properties are required to predict states of stress, strain, and displacement (deformation) within the pavement structure when subjected to external wheel loads. These properties for assumed elastic material behavior are the elastic modulus and Poisson's ratio (ν).

The major distress/transfer functions for HMAC pavements are load-related fatigue fracture, permanent deformation, and thermal cracking. However, the focus of this study was on fatigue characterization of HMAC mixtures, and therefore only the fatigue analysis component of the MEPDG is discussed in this chapter. Fig. 7-1 is a schematic illustration of the fatigue design and analysis system for the MEPDG as utilized in this study. Fig. 7-1 shows that if the N_f prediction by the MEPDG software in terms of traffic ESALs is less than the actual design traffic ESALs, the following options are feasible:

- reviewing/modifying the input data including the pavement structure, materials, traffic, environment, reliability level, pavement design life, and analysis parameters (distress failure limits); and
- changing the HMAC mix-design and/or the material types.

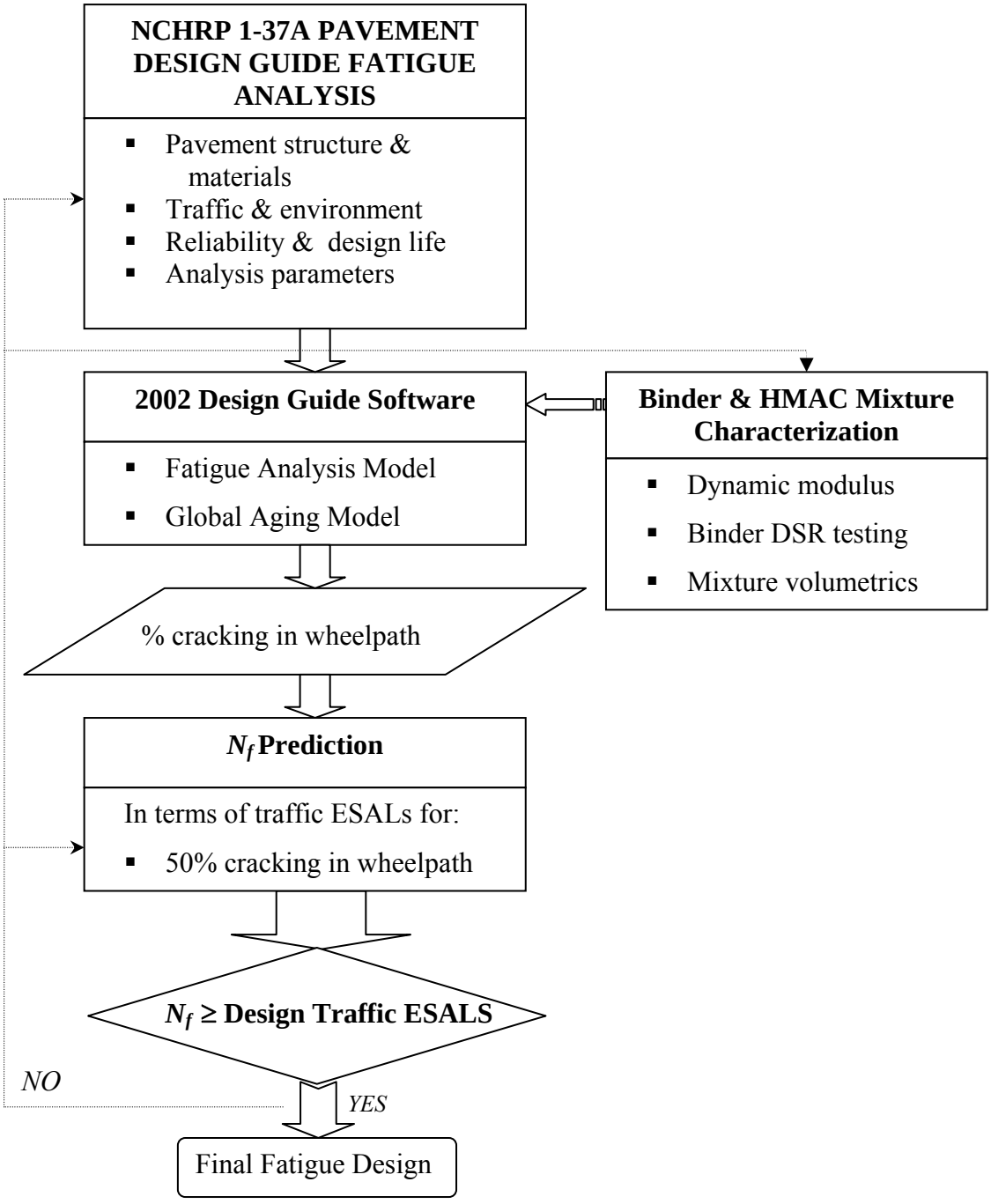

Fig. 7-1. The Fatigue Design and Analysis System for the MEPDG as Utilized in this Study

INPUT/OUTPUT DATA

The MEPDG utilizes a hierarchical system for materials characterization and analysis. This system has three input levels. Level 1 represents a design philosophy of the highest practically achievable reliability, and Levels 2 and 3 have successively lower reliability. The Level 1 fatigue design procedure used in this study requires mixture volumetrics, dynamic modulus (DM) values for HMAC mixtures, and a complex shear modulus for unaged binder as input parameters. The binder data are used in the MEPDG software to predict mixture aging using the Global Aging Model (GAM) (Mirza and Witczak 1995). Field input data include traffic, pavement structure, environment, and pavement design life. These input data are summarized in Table 7-1.

Table7-1. Input and Output Data for the MEPDG Software

Source	Parameter
Laboratory test data	• Dynamic modulus test data (i.e., temp., freq., & |E*| values) • Binder DSR test data (i.e., temperature, G*, & δ values) • Mixture volumetrics (i.e., binder content & AV)
Data analysis	• All calculations are software based
Field conditions (design data)	• Pavement structure (i.e., layer thickness) • Pavement materials (i.e., material type, elastic modulus, Poisson's ratio, gradations, & plasticity indices) • Traffic (i.e., AADT, axle load, & tire pressure) • Environment (i.e., climatic location) • Pavement design life (i.e., 20 years)
Computer stress-strain analysis	• All calculations are software based (utilized bottom-up crack failure mode in this study)
Other	• Reliability level (i.e., 95%) • Analysis parameters (i.e., distress failure limits)
Output	• Percentage cracking in wheelpath • N_f in terms of traffic ESALs for 50% wheelpath cracking • Assessment of adequate or inadequate fatigue performance

For the output data in terms of fatigue cracking (alligator cracking), the MEPDG software predicts the percentage of fatigue cracking (along with other distresses) at any age of the pavement for a given structure and traffic level at a particular environmental location. The failure criteria can be set in two ways: setting the limit of percentage of cracks in the wheelpath for a given number of traffic loads or determining the number of traffic loads in terms of ESALS to reach a certain percentage of cracks in the wheelpath at a certain age of the pavement. In this study, the former failure criterion was used.

The output data in this study thus consisted of percentage cracking in the wheelpath for at least two input traffic levels of 2.5 and 5.0 million traffic ESALs. Thereafter, N_f in terms of traffic ESALs was statistically determined for 50% cracking in the wheelpath.

LABORATORY TESTING

Characterization of the HMAC mixture and binder for Level 1 fatigue analysis in the MEPDG software requires the laboratory tests described in this section.

Dynamic Shear Rheometer Test

Binder dynamic shear complex modulus (G^*) and phase angle (δ) required for Level 1 fatigue analysis were measured using the standard Dynamic Shear Rheometer (DSR) consistent with AASHTO TP5-98 (AASHTO 1998). A minimum of two binder samples were tested, and test results are shown in Table 2-1 (Chapter III).

Dynamic Modulus Test

For Level 1 fatigue analysis, the MEPDG software requires the dynamic modulus of the HMAC mixture measured over a range of temperatures and frequencies using the dynamic modulus (DM) test. A typical DM test is performed over a range of different temperatures by applying sinusoidal axial loading at different frequencies to an unconfined specimen.

Test Protocol

In this study, the DM test was conducted in accordance with the AASHTO TP 62-03 Standard Method of Test for Determining Dynamic Modulus of Hot Mix Asphalt Concrete Mixtures at five test temperatures of -10, 4.4, 21.1, 37.8, and 54.4 °C and six loading frequencies of 25, 10, 5, 1, 0.5, and 0.1 Hz (AASHTO 2003).

DM is a stress-controlled test using compressive axial loading, and the test protocol in this study involved applying a sinusoidal dynamic compressive stress to gyratory-compacted cylindrical HMAC specimens of 150 mm in height by 100 mm in diameter. Fig. 7-2 shows the DM loading configuration.

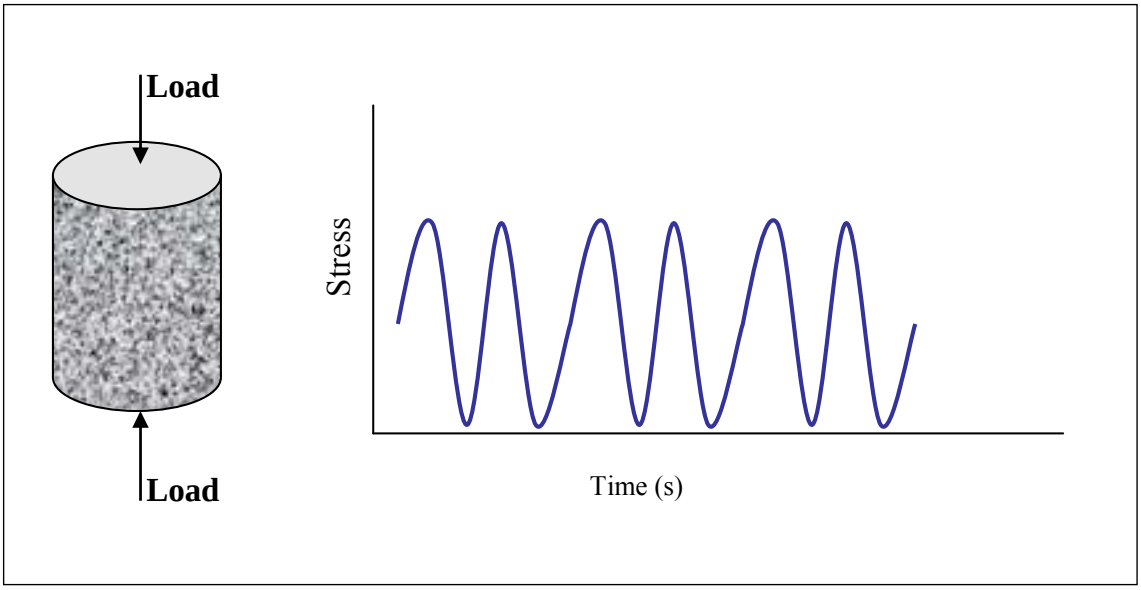

Fig. 7-2. Loading Configuration for the DM Test

The stress level for measuring the DM was chosen in order to maintain the measured resilient strain (recoverable) within 50 to 150 microstrain consistent with the TP 62-03 test protocol (AASHTO 2003). The order for conducting each test sequence was from lowest to highest temperature and highest to lowest frequency of loading at each temperature to minimize specimen damage. For each temperature-frequency test sequence, the test terminates automatically when a preset number of load cycles have been reached (AASHTO 2003).

Test Conditions and Data Acquisition

The sinusoidal axial stress waveform was supplied by the Universal Testing Machine (UTM-25) shown in Fig. 7-3. Axial deformations were measured via three LVDTs. The DM test was conducted in an environmentally temperature-controlled chamber. For each test temperature, the specimens were subjected to six consecutive loading frequencies of 25, 10, 5, 1, 0.5, and 0.1 Hz.

Fig. 7-3. The Universal Testing Machine (UTM-25)

The minimum conditioning period for the specimens for each test temperature was 2 hr. This temperature was monitored and controlled through a thermocouple probe attached inside a dummy HMAC specimen also placed in the same environmental temperature-controlled chamber as the test specimen. For each HMAC mixture type, three replicate HMAC specimens were tested, but only for the 0 months aging condition. Note that the MEPDG software encompasses a GAM that takes into account aging in the fatigue analysis (Mirza and Witczak 1995).

During the DM tests, data (time, load, and deformations) were captured electronically every 0.001 s. Fig. 7-4 is an example of the compressive axial strain response from DM testing at 4.4 °C.

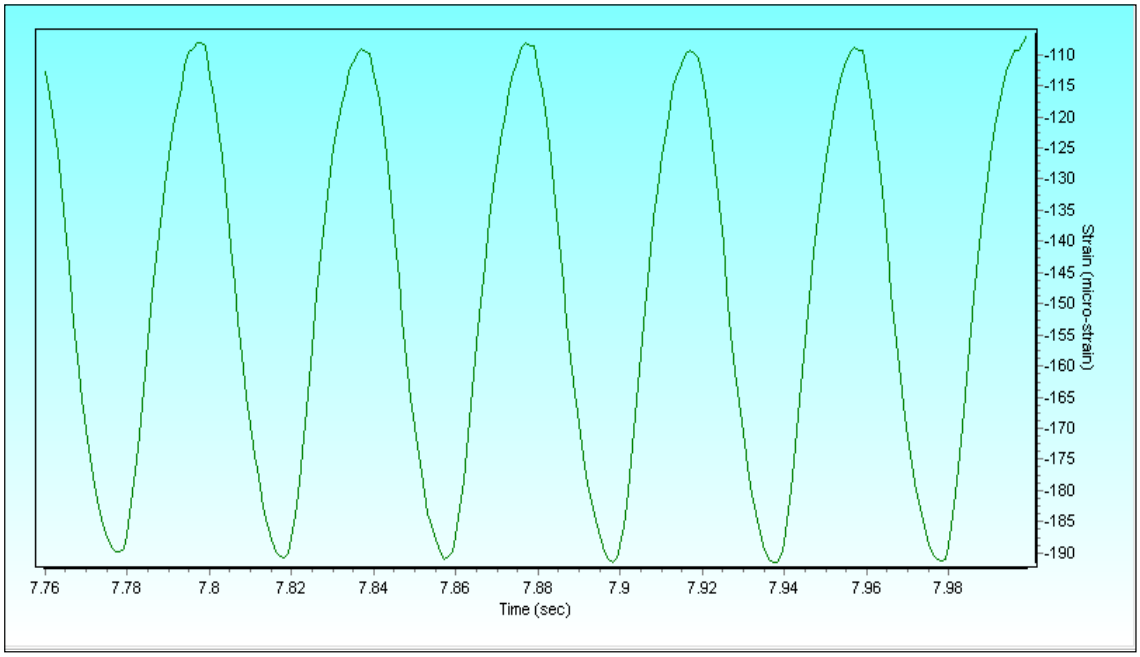

Fig. 7-4. Compressive Axial Strain Response from DM Testing at 4.4 °C

The typical parameters that result from DM testing are the complex modulus ($|E^*|$) and the phase angle (δ) that characterizes the HMAC visco-elastic properties for Level 1 MEPDG analysis. The |E*| data are used for generation of a HMAC master-curve for pavement performance prediction. The $|E^*|$ is a function of the storage modulus (E') and loss modulus (E''). The magnitude of $|E^*|$ is represented as shown in Equation 7-1:

$$|E^*| = \frac{\sigma_0}{\varepsilon_0} \tag{7-1}$$

$$E' = |E^*| Cos\delta \,,\; E'' = |E^*| Sin\delta \tag{7-2}$$

where:

$|E^*|$ = Dynamic complex modulus (MPa)

σ_0 = Axial stress (MPa)

ε_0 = Axial strain (mm/mm)

E', E'' = Storage (elastic) and loss (viscous) modulus, respectively (MPa)

δ = Phase angle (°)

However, the $|E^*|$ calculations were automatically done concurrently via the UTM-25 software during DM testing. Table 7-2 is an example of the output data from DM testing using the UTM-25 test setup and UTM-25 software. The $|E^*|$, frequency, and temperature are the actual input data for the MEPDG software.

Table 7-2. Example of Output Data from DM Testing at 4.4 °C

Parameter (summed average)	**Frequency (Hz)**					
	25	**10**	**5**	**1**	**0.5**	**0.1**
Dynamic modulus (|E*|) (MPa)	19,056	17,538	16,078	13,343	12,118	9,432
Phase angle (°)	5.24	8.31	9.84	13.15	14.95	18.99
Dynamic stress (kPa)	1,567.7	1,713.6	1,653.9	1,683.0	1,607.7	1,505.6
Recoverable axial microstrain	82.3	97.7	102.9	126.1	132.7	150.6
Permanent axial microstrain	106.6	152.1	160.9	173.7	175.4	271.1
Temperature (°C)	4.4	4.4	4.4	4.4	4.4	4.4

For generating the |E*| master-curve as a function of loading time or frequency, the following time-temperature superposition signomoidal model as demonstrated by Pellinen and Witczak (2002) is often used and is in fact built into the MEPDG software:

$$Log(|E^*|) = \delta + \frac{\alpha}{1 + e^{\beta - \gamma \log(\xi)}} \qquad (7\text{-}3)$$

where:

$|E^*|$ = Dynamic modulus (MPa)

ξ = Reduced frequency (Hz)

δ = Minimum modulus value (MPa)

α = Span of modulus values

β = Shape parameter

γ = Shape parameter

FAILURE CRITERIA

The fatigue failure criteria for the MEPDG software in this study was defined as the number of traffic ESALs required to cause 50% fatigue (alligator) cracking (bottom-up) on a 152.4 m (500 ft) stretch of the wheelpath. This 50% threshold value is consistent with the TxDOT fatigue cracking tolerable limits in the wheelpath based on the 2003 TxDOT PMIS report (TxDOT 2003b). The fatigue failure mode was considered adhesive bottom-up cracking, with horizontal tensile strain is the primary mechanistic failure load-response parameter associated with crack growth (AASHTO 2004).

ANALYSIS PROCEDURE

The fatigue analysis procedure for the MEPDG is a step-by-step computerized process based on the modified Asphalt Institute fatigue predictive model incorporated in the software (Asphalt Institute 1991, Bonnaure et al. 1980):

$$N_f = \beta_{f1} k_1 \left(\varepsilon_t\right)^{-\beta_{f2} k_2} \left(E\right)^{-\beta_{f3} k_3} \qquad (7\text{-}4)$$

where:

N_f = Number of repetitions to fatigue cracking
ε_t = Tensile strain at the critical location of the HMAC layer
E = Stiffness of the HMAC mixture
β_{fi} = Calibration parameters
k_i = Laboratory regression coefficients

The β_{fi} calibration parameters incorporate state/regional/national calibration coefficients and are utilized to account for environmental conditions. Although these parameters are changeable, default national calibration factors that are built into the MEPDG software were used in this study.

The regression coefficients k_i are coefficients that relate to material properties. E is the stiffness of the HMAC mixture that is a function of the DM test data. The horizontal tensile strain (ε_t) constitutes the mechanistic failure load-response parameter and was computed at the bottom of the HMAC layer in this study.

As pointed out previously, the MEPDG software incorporates a GAM that takes into account the effects of binder aging with time in the overall fatigue analysis process (Mirza and Witczak 1995, Superpave Models Team 2000, Witczak 2001, AASHTO 2004). This model utilizes empirically developed equations and is based on the change in binder viscosity as a function of pavement age, AV, environment, traffic loading, and pavement depth. The model accounts for both the short-term aging that occurs during HMAC mixing and construction operations and HMAC long-term aging during service. The output of the GAM is basically a prediction of the binder viscosity at any time and any depth in the pavement system, which is ultimately incorporated in the overall fatigue analysis process.

VARIABILITY, STATISTICAL ANALYSIS, AND N_f PREDICTION

For traffic input levels of 2.5 and 5.0 million ESALs and for each HMAC mixture type in each pavement structure and under each environmental condition, percentage cracking in the wheelpath was predicted for at least three HMAC specimens using the MEPDG software. Using these percentages of cracking output from the MEPDG software for these specimens, mean N_f values in terms of traffic ESALs were statistically predicted for 50% cracking in the wheelpath using the least squares regression line regression approach and statistical analysis software SPSS V11.5 (Montgomery et al. 2001, 2002). A 95% prediction interval (PI) for the N_f were also determined.

SUMMARY

The bullets below summarize the fatigue analysis component of the proposed MEPDG as utilized in this study:

- The proposed MEPDG adopts an ME approach for the structural design of HMAC pavements. In terms of fatigue analysis, the MEPDG software utilizes the modified Asphalt Institute fatigue damage predictive equation with tensile strain as the primary mechanistic failure load-response parameter associated with crack growth.
- The MEPDG software incorporates aging effects using a Global Aging Model. It also incorporates comprehensive traffic and climatic analysis models.
- The MEPDG characterizes pavement materials in a three-level hierarchical system, with Level 1 representing the highest possible achievable reliability level.
- For Level 1 input data and fatigue analysis, HMAC mixture characterization through dynamic modulus testing at five different temperatures and six loading frequencies utilizes gyratory-compacted cylindrical HMAC specimens. Other required material tests include mixture volumetrics and binder DSR data.
- Fatigue failure for the MEPDG software analysis was defined as the number of applied repetitive load cycles expressed in terms of traffic ESALs required to cause 50% cracking in the wheelpath consistent with TxDOT tolerable limits. The fatigue failure mode was considered adhesive bottom-up cracking.

CHAPTER VIII
HMAC MIXTURE PROPERTY RESULTS AND ANALYSIS

This chapter presents the laboratory test results for the HMAC mixture properties and analysis including the effects of binder oxidative aging for both the Bryan and Yoakum mixtures, respectively. These results include:

- the BB testing,
- tensile strength,
- relaxation modulus ,
- dissipated pseudo strain energy,
- surface energy,
- anisotropy, and
- dynamic modulus.

In general, these laboratory test results represent mean values of at least two replicate measurements. Because HMAC fatigue cracking is generally more prevalent at intermediate pavement service temperatures, most of the laboratory tests were conducted at 20 °C. Otherwise, the test data were normalized to 20 °C during the analysis phase.

THE BENDING BEAM TEST RESULTS

The BB fatigue test results conducted at two test strain levels of 374 and 468 microstrain at 20 °C and a 10 Hz loading frequency are discussed in this section. Detailed results are attached in Appendix E.

HMAC Mixture Flexural Stiffness (*S*)

Fig. 8-1 is an example of a plot of flexural stiffness (*S*) versus load cycles (*N*) during BB testing and illustrates the 50% stiffness reduction criteria. Fig. 8-2 is a plot of the average initial *S* measured at the 50^{th} *N* as a function of the aging condition on a semi-log scale. From Fig. 8-1, the declining *S* trend with increasing *N* is evident as expected. This was the observed trend for all the BB tests except that the rate of *S* decline increased with aging of the specimens.

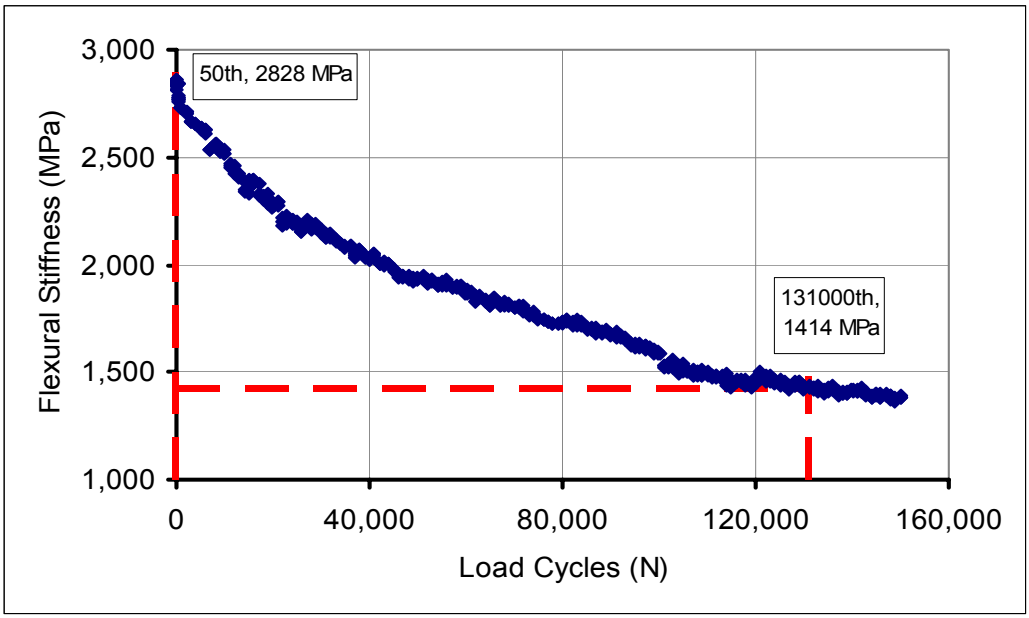

Fig. 8-1. Flexural Stiffness versus Load Cycles at 20 °C (Bryan Mixture, 0 Months)

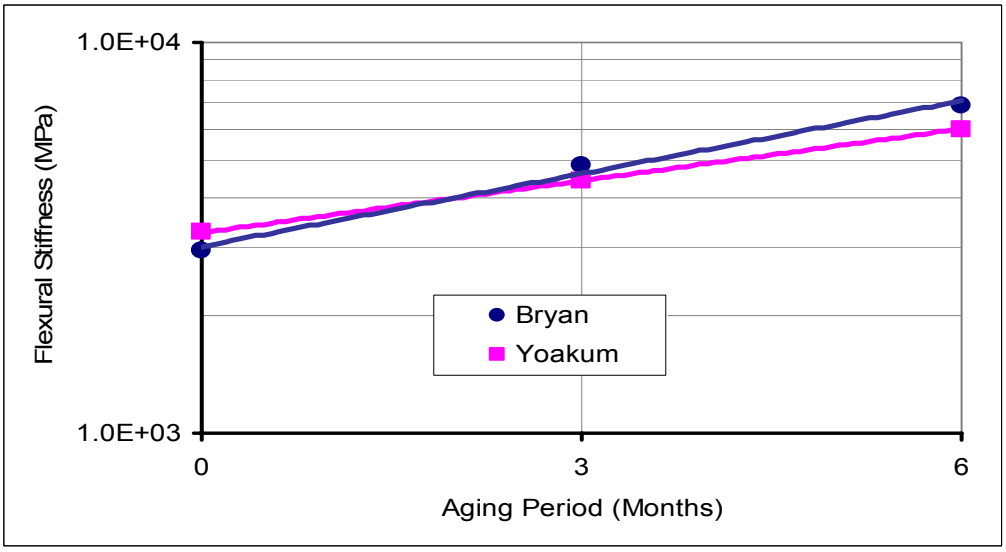

Fig. 8-2. Initial HMAC Mixture *S* (MPa) versus Aging Condition at 20 °C

Fig. 8-2 shows that while the Yoakum mixture exhibited a relatively higher *S* value at 0 months aging condition, both the *S* magnitude and the rate of *S* increase (about 1.4 times based on the slopes of the graphs in Fig. 8-2) for the Bryan mixture were higher than that of the Yoakum mixture after aging. For the laboratory test conditions considered in this study, this result suggests that the Bryan mixture with the softer unmodified binder was more susceptible to stiffness age-hardening compared to the Yoakum mixture. Theoretically, rapid stiffness age-hardening is often associated with a subsequent decline in HMAC mixture fatigue resistance due to a decreased ability to flow and relieve the applied stresses.

BB Testing and Number of Load Cycles to Failure (*N*)

Table 8-1 is a summary of the laboratory test results in terms of *N* to fatigue failure during BB testing. These results represent average values of at least two replicate measurements per test strain level per mixture type per aging condition. As shown in Table 8-1a, while *N* decreased significantly with aging for both mixtures, the Yoakum mixture sustained higher *N* values at both test strain levels for all aging conditions compared to the Bryan mixture. This reduction in *N*, which is approximately 25% and 50% after 3 and 6 months aging, respectively, indicates that aging has a very significant effect on the HMAC mixture fatigue resistance subjected to repeated flexural loading.

By contrast, however, there was generally a higher variability in the *N* results for the Yoakum mixture in terms of the COVs shown in Table 8-1. The COV ranges are from 4.8% to 21.3% and 14.4% to 28% (Table 8-1) for the Bryan and Yoakum mixtures, respectively. This result is in agreement with Rowe and Bouldin's (2000) suggestion that while the current ME test protocols and analysis procedures may work well for unmodified binders (Bryan mixture), it may not be so with modified binders (Yoakum mixture), and thus the results must be analyzed and interpreted cautiously. This problem is not surprising because the majority of the ME fatigue analysis approaches/models were formulated based on laboratory testing and field performance monitoring of unmodified binders.

Table 8-1. BB Laboratory Test Results at 20 °C

Aging Condition @ 60 °C	Test Microstrain Level	Measured Mean *N* Value		Stdev		COV	
		Bryan	Yoakum	Bryan	Yoakum	Bryan	Yoakum
0 months	374	127,000	223,790	6,082	32,229	4.8%	14.4%
	468	50,667	105,350	4,509	14,354	8.9%	13.6%
3 months	374	80,187	172,167	9,702	17,848	12.0%	18.6%
	468	39,833	86,187	7,522	16,389	18.9%	19.1%
6 months	374	53,000	108,200	11,314	30,739	21.3%	28.0%
	468	27,500	47,150	4,947	12,092	18.0%	25.6%

Surprisingly for each mixture type, however, this variability in terms of COV values tended to increase with aging (Table 8-1), probably arising from the differences in the degree of oxidative aging of the individual beam specimens. The assumption here is that although subjected to similar aging conditions, the degree and extent of oxidative aging may vary from specimen to specimen depending on the actual specimen AV content and mixture heterogeneity. Note that high variability has generally been reported with BB testing primarily arising from high AV variability, aggregate segregation, and mixture heterogeneity (Tayebali et al. 1992).

HMAC Mixture Empirical Fatigue Relationships

Fig. 8-3 is a plot of the average *N* versus test ε_t on a log-log scale and shows that for the same test strain level, *N* decreased with aging. While the Yoakum mixture exhibited higher *N* values, *N* generally exhibited a decreasing trend with an increase in test ε_t as expected.

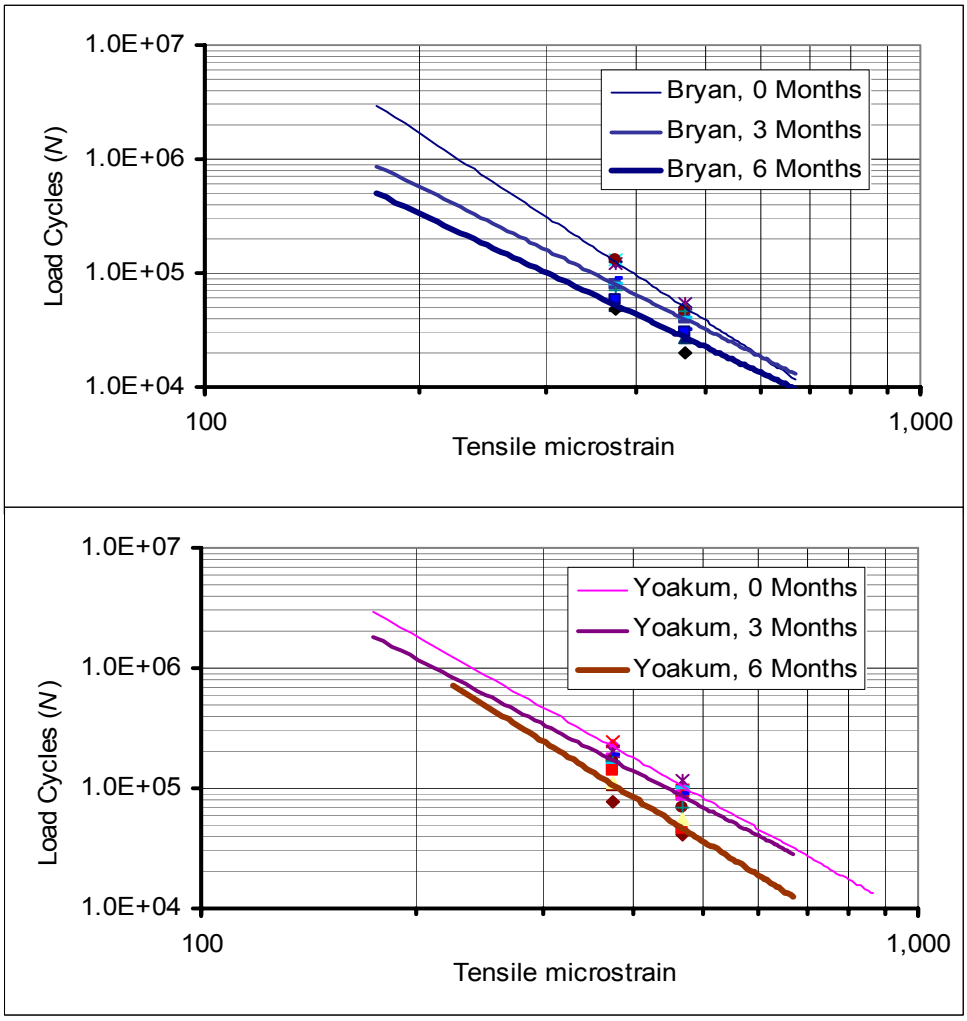

Fig. 8-3. Plot of BB Load Cycles versus Test Tensile Microstrain at 20 °C

Note that the fatigue results in Fig. 8-3 were based on two test strain levels for each mixture type per aging condition. For better N_f predictions and statistical analysis, more data points (collected at more than two test strain levels) and more replicates are recommended with the recognition that BB testing is time consuming.

Based on Fig. 8-3 and utilizing a statistical least square line regression approach and natural logarithmic back-transformation analysis, laboratory empirical fatigue relationships of the power functional form shown in Table 8-2 were derived.

Table 8-2. HMAC Mixture Empirical Fatigue Relationships at 20 °C

Aging Condition @ 60 °C	Mixture	Lab N_f Model	Materials Constants		Correlation Coefficient (R^2)
			k_1	k_2	
0 months	Bryan	$N_f = 1\times10^{-9}(\varepsilon_t)^{-4.0984}$	1×10^{-9}	4.0984	0.98
	Yoakum	$N_f = 7\times10^{-7}(\varepsilon_t)^{-3.3603}$	7×10^{-7}	3.3603	0.97
3 months	Bryan	$N_f = 2\times10^{-6}(\varepsilon_t)^{-3.1205}$	2×10^{-6}	3.1205	0.99
	Yoakum	$N_f = 5\times10^{-6}(\varepsilon_t)^{-3.0861}$	5×10^{-6}	3.0861	0.96
6 months	Bryan	$N_f = 5\times10^{-6}(\varepsilon_t)^{-2.9263}$	5×10^{-6}	2.9263	0.95
	Yoakum	$N_f = 2\times10^{-8}(\varepsilon_t)^{-3.7047}$	2×10^{-8}	3.7047	0.98

Note that the natural logarithmic (*Ln*) transformation of Eq. (4-1) in Chapter IV reduces to a simple linear regression model of the format shown in Eq. (8-1).

$$Ln(N_f) = Ln(k_1) - k_2[Ln(\varepsilon_t)] \qquad (8\text{-}1)$$

Therefore, all test data (the test strain and the measured *N*) were converted to the *Ln* format for least square line regression analysis and *Lab* N_f predictions using the statistical analysis software SPSS V11.5 (Montgomery et al. 2001). Table 8-3 provides an example of *Ln* transformation analysis of the BB test data for the Bryan mixture at 0 months aging condition. An example of the detailed *Ln* transformation analysis is included in Appendix E. Table 8-4 is an extract of the output from the SPSS V11.5 software analysis at 95% reliability for the Bryan mixture at 0 months aging. The table displays the computed k_i values and the coefficient of determination (R^2) associated with the model, and the predicted lab N_f and its 95% prediction interval.

Table 8-3. Example of *Ln* Transformation Analysis of BB Test Data

(Bryan Mixture, 0 Months)

Replicate Specimen#	**Test Strain**	**Measured *N***	***Ln* (Test Strain)**	***Ln* (*N*)**
1	374×10^{-6}	131,000	-7.89	11.78
2	374×10^{-6}	120,000	-7.89	11.70
3	374×10^{-6}	130,000	-7.89	11.78
Mean		127,000		11.75
Stdev		6,083		
COV		4.8%		
1	468×10^{-6}	55,000	-7.67	10.92
2	468×10^{-6}	51,000	-7.67	10.84
3	468×10^{-6}	46,000	-7.67	10.74
Mean		50,667		10.83
Stdev		4,509		
COV		8.9%		

Table 8-4. Extract of SPSS V11.5 Least Squares Line Regression Analysis

(Bryan Mixture, 0 Months)

Parameter	**Value**
Ln (k_1)	-20.63 ($k_1 \cong 1 \times 10^{-9}$)
95% *Ln* (k_1) prediction interval	$-26.26 \le Ln\ (k_1) \le -14.99$ ($3.93 \times 10^{-12} \le k_2 \le 3.09 \times 10^{-7}$)
k_2	4.098
95% k_2 prediction interval	$3.38 \le k_2 \le 4.83$
Coefficient of determination, R^2	0.98
Prediction design strain	*Ln* (ε_t) = *Ln* (157×10^{-6}) $\cong$ -8.76
Predicted *Lab Ln* (N_f) @ $\varepsilon_t = 157 \times 10^{-6}$	15.32 ($N_f \approx 4.48 \times 10^6$)
95% lab *Ln* (N_f) prediction interval @ $\varepsilon_t = 157 \times 10^{-6}$	$14.57 \le Lab\ Ln(N_f) \le 16.06$ ($2.12 \times 10^6 \le$ lab $N_f \le 9.46 \times 10^6$)

The Material Constants k_2-k_1 Relationship

From Table 8-2, the dependency of the material constants k_i on mixture type and aging condition is evident. For the Bryan mixture with the unmodified binder, the variation of k_i with aging follows a consistent trend as shown in Fig. 8-4 (i.e., k_1 is increasing and k_2 is decreasing with aging, respectively), which is not the case for the Yoakum mixture with a modified binder.

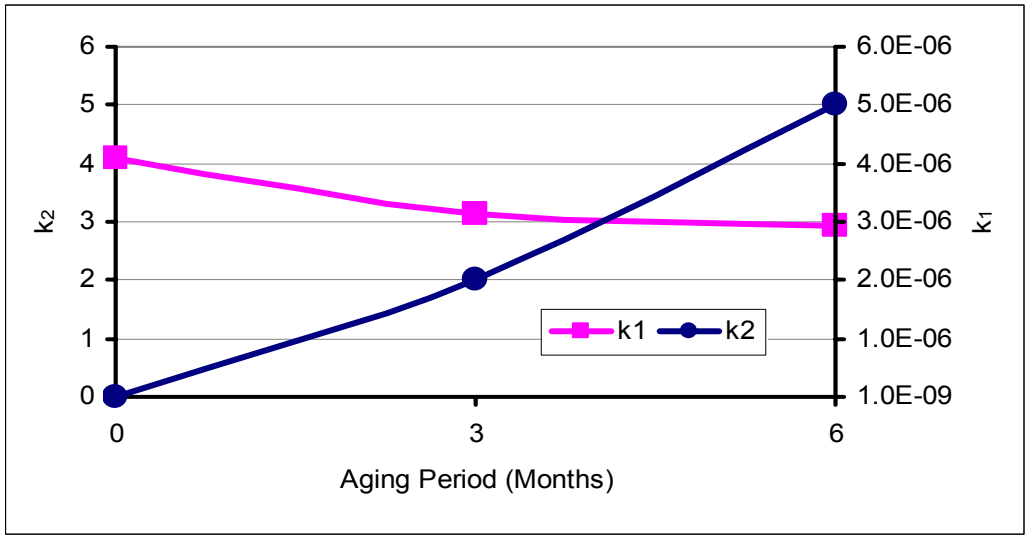

Fig. 8-4. Plot of k_i versus Aging for the Bryan Mixture

For both HMAC mixtures, however, there seems to exist an interrelationship between k_1 and k_2, such that a smaller k_1 value is often associated with a relatively larger k_2 value and vice versa. Eq. (8-2) shows the generalized k_2-k_1 logarithmic relationship based on the Bryan and Yoakum mixtures plotted in Fig. 8-5:

$$k_2 = -aLn(k_1) + b \qquad (8\text{-}2)$$

where:

a, b = Regression constants

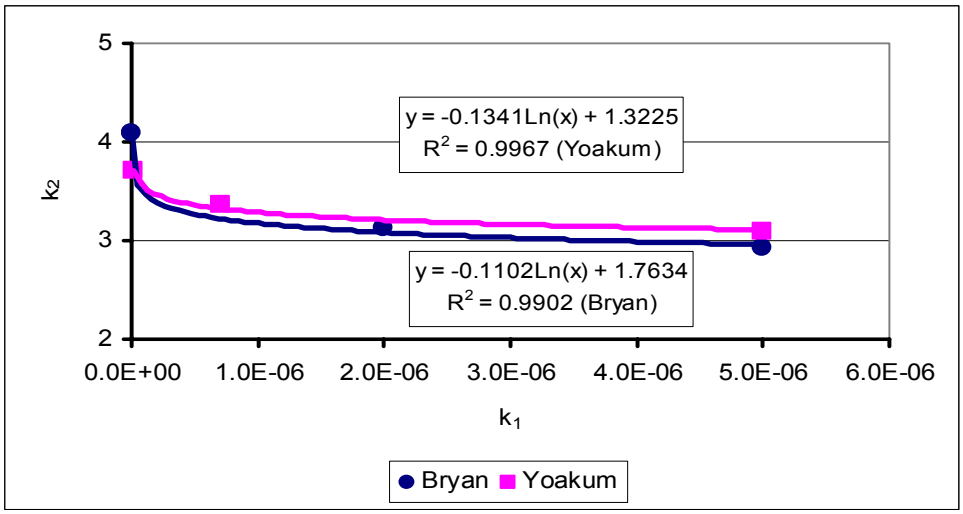

Fig. 8-5. The k_2-k_1 Relationship

As with the k_i values in Table 8-2 and Fig. 8-5, literature reports state that k_2 usually ranges from 3 to 6 while k_1 may vary by several orders of magnitude (Ghuzlan and Carpenter 2002). However, the Bryan mixture's k_2 value exhibits a distinctively decreasing trend with aging (Fig. 8-4), and it is doubtful if it will remain in this range (3 to 6), particularly if the mixture were to be subjected to longer laboratory aging periods greater than 6 months. Furthermore, although the BB test in this study was conducted at a single temperature of 20 °C and a loading frequency of 10 Hz, these material constants are also temperature and loading mode dependent as reported by Ghuzlan and Carpenter (2002). This variation of the k_i constants should not be surprising but merely signifies the importance of characterizing fatigue performance among other variables as a function of HMAC mixture type, aging condition, temperature, and loading mode.

HMAC MIXTURE TENSILE STRENGTH (σ_t)

Table 8-5 is a summary of the average σ_t results measured at 20 °C. Fig. 8-6 is an example of plots of tensile stress and strain at break under tensile loading as a function of aging condition for each mixture type.

Table 8-5. HMAC Mixture Tensile Strength Results at 20 °C

Aging Condition @ 60 °C	Mixture	Mean σ_t @ Break (kPa)	Mean Tensile Strain (ε_f) @ Break	Statistical Analysis for σ_t	
				Stdev	COV
0 months	Bryan	725	$1{,}245 \times 10^{-6}$	16.81	2.32%
	Yoakum	849	$3{,}483 \times 10^{-6}$	54.36	6.40%
3 months	Bryan	770	689×10^{-6}	33.69	4.38%
	Yoakum	1,049	$2{,}342 \times 10^{-6}$	25.91	2.47%
6 months	Bryan	1,080	401×10^{-6}	42.03	3.89%
	Yoakum	1,270	851×10^{-6}	83.58	6.58%

Table 8-5 indicates that as the HMAC ages, it becomes more brittle, thus breaking under tensile loading at a lower strain level (Fig. 8-6). For both mixtures, while the σ_t was within the test variability (Medani et al. 2004), the ε_f at break decreased significantly on the order of at least 30% due to an increase in mixture brittleness from oxidative aging of the binder. In terms of HMAC mixture comparison, the σ_t and ε_f values for the Yoakum mixture were higher than that of the Bryan mixture at all aging conditions, indicating that for the test conditions considered in this study:

- the Yoakum mixture was more ductile than the Bryan mixture and
- the Yoakum mixture had a better resistance to tensile stress than the Bryan mixture.

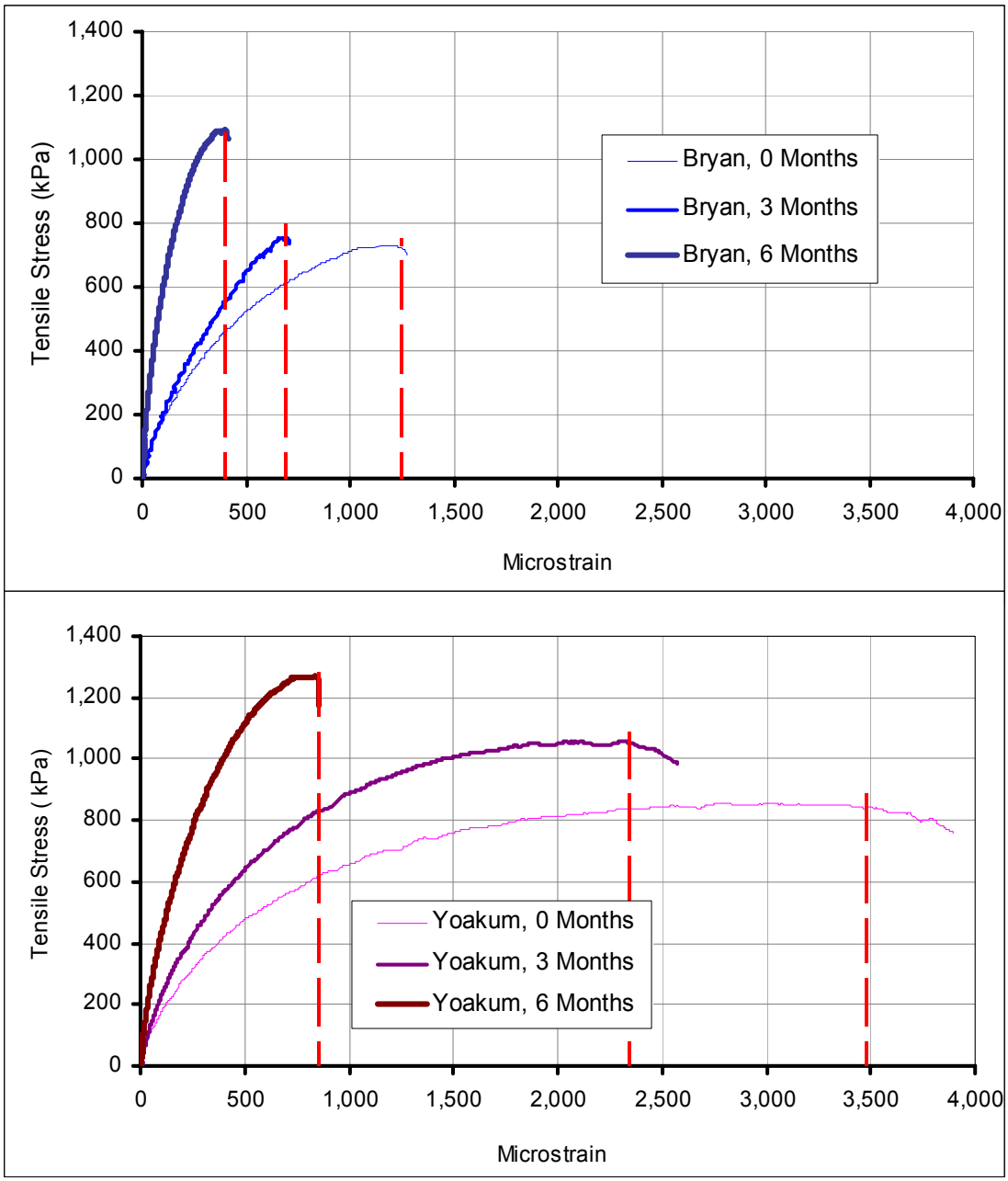

Fig. 8-6. HMAC Mixture Tensile Stress at 20 °C

Fig. 8-7 is a plot of the ε_f values as a function of aging condition. The figure shows the expected decreasing trend of the failure strain (ε_f values) at 20 °C as a function of binder oxidative aging due to increasing mixture brittleness. The increased ductility of the Yoakum mixture is apparent and is indicated by the comparatively higher ε_f values at all aging conditions, which are almost double the Bryan mixture ε_f values. In general, the decreasing ε_f trend with aging indicates that aging reduces mixture ductility.

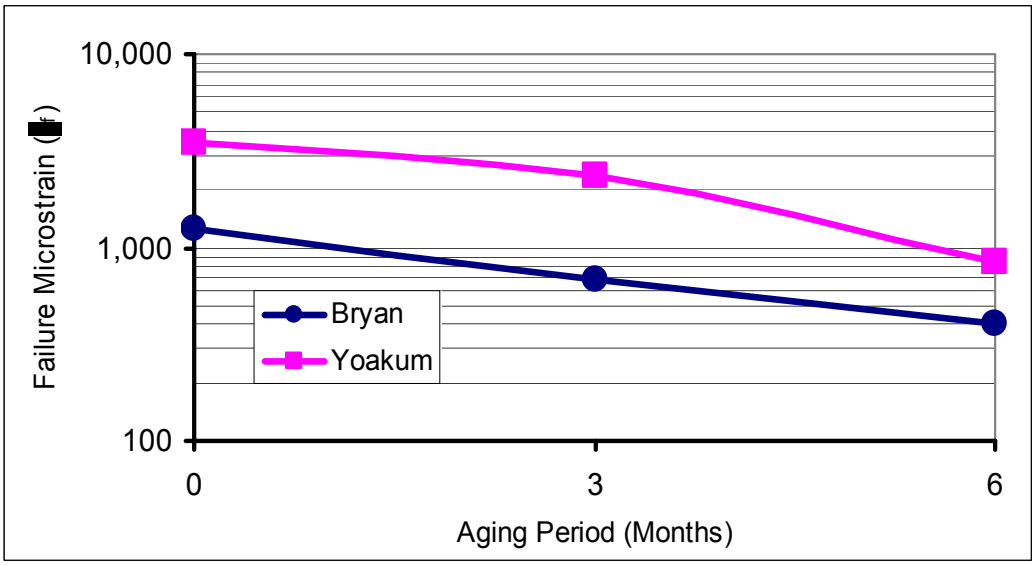

Fig. 8-7. HMAC Mixture Failure Tensile Microstrain at Break at 20 °C

Tensile strength is a significant material property often utilized as an indicator of HMAC mixture ductility and cracking potential. A high ε_f at failure indicates that a particular HMAC mixture can tolerate higher strains before failing under tensile loading. This means that it is more likely to resist cracking than an HMAC mixture with a lower ε_f at failure under similar loading and environmental conditions. Thus, aging reduces HMAC mixture ductility and resistance to cracking as indicated by the decreasing ε_f values with aging for both mixtures.

RELAXATION MODULUS (*E(t)*)

The RM test results in terms of *E(t)* and *m* values are summarized in Figs. 8-8 and 8-9, and relaxation modulus master-curves are presented graphically in Figs. 8-10 and 8-11 on a log-log scale. Note that the *E(t)* at 1.0 s and the *m* values in Figs. 8-8 and 8-9 were obtained from simple power functional trend lines fitted through the RM master-curves as shown by Eq. (8-3) and illustrated in Fig. 8-10:

$$E(t) = E_1 \xi^{-m} \tag{8-3}$$

where:

$E(t)$	=	Time-dependent elastic relaxation modulus (MPa)
E_1	=	Time-dependent elastic relaxation modulus at 1.0 s (MPa)
ξ	=	Reduced time (s)
m	=	Stress relaxation rate (slope of RM master-curve)

As expected, *E(t)* increased with aging due to HMAC hardening and stiffening effects from oxidation of the binder. This stiffening effect, however, also causes the material property parameter *m,* which describes the rate at which the mixture relaxes the applied stress, to decrease. For visco-elastic materials like HMAC, the higher the *m* value, the higher the ability of the mixture to relax the stress and the greater the resistance to fracture damage. Generally, the magnitude of *m* ranges from 0 to 1 (i.e., $0 < m \geq 1.0$).

Table 8-6 is a summary of the computed Paris' Law fracture coefficient *n* based on *m* values from Fig. 8-9. Based on the *n-m* relationship described in Chapter V, *n* exhibits an inverse relationship with mixture fracture resistance (see also Appendix C). Based on this relationship, Table 8-6 indicates that the HMAC mixture fracture resistance declines with aging and that that the Yoakum mixture had better fracture resistant properties than the Bryan mixture. Note that the range of *n* is $1.0 \leq n < \infty$ based on the *n-m* relationship in Chapter V.

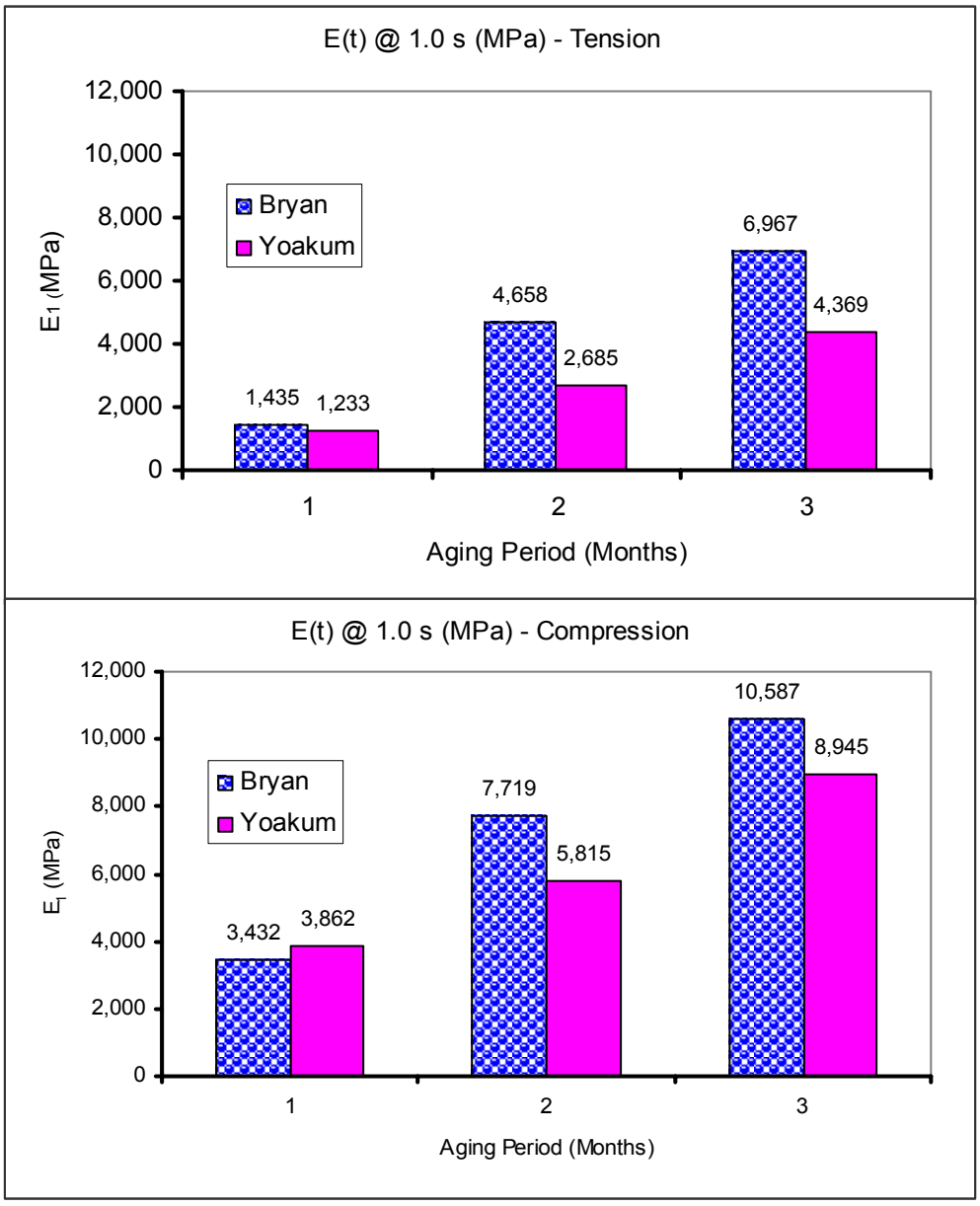

Fig. 8-8. Mean *E(t)* at 1.0 s at 20 °C

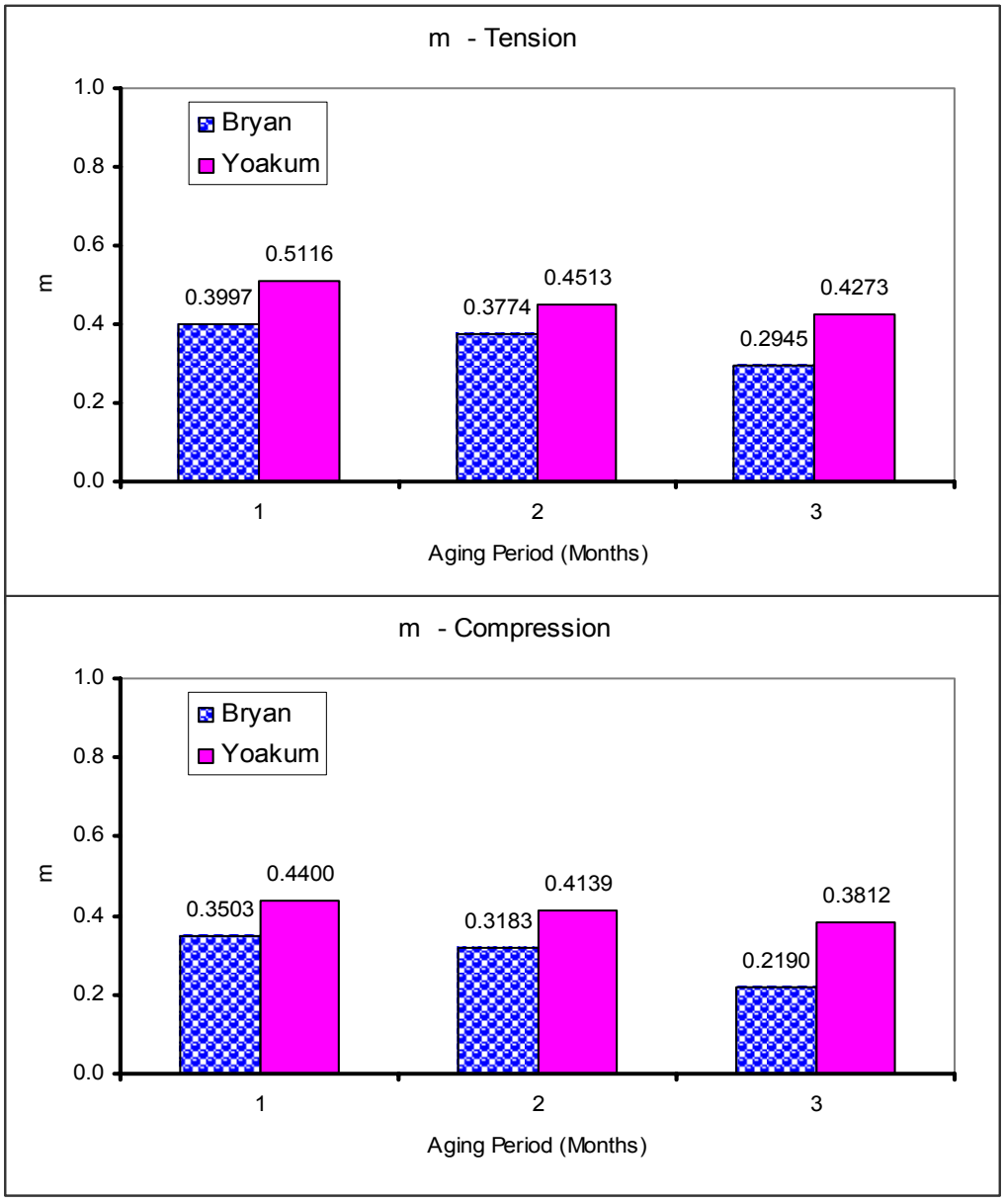

Fig. 8-9. Mean m Values at 20 °C

Table 8-6. Paris' Law Fracture Coefficient, *n*

Aging Condition @ 60 °C	***n=(1/m)* (Tension)**	***n=(1/m)* (Tension)**	***n=(1/m)* (Compression)**	***n=(1/m)* (Compression)**
	Bryan	**Yoakum**	**Bryan**	**Yoakum**
0 months	2.50	1.95	2.85	2.27
3 months	2.65	2.22	3.14	2.42
6 months	3.40	2.34	4.57	2.62

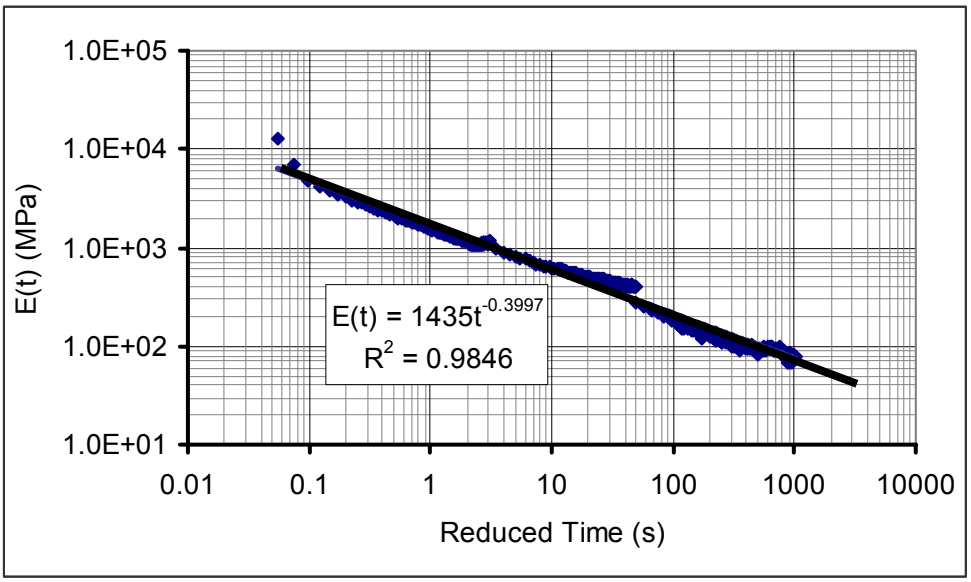

Fig. 8-10. RM (Tension) Master-Curve at 20 °C (Bryan Mixture, 0 Months)

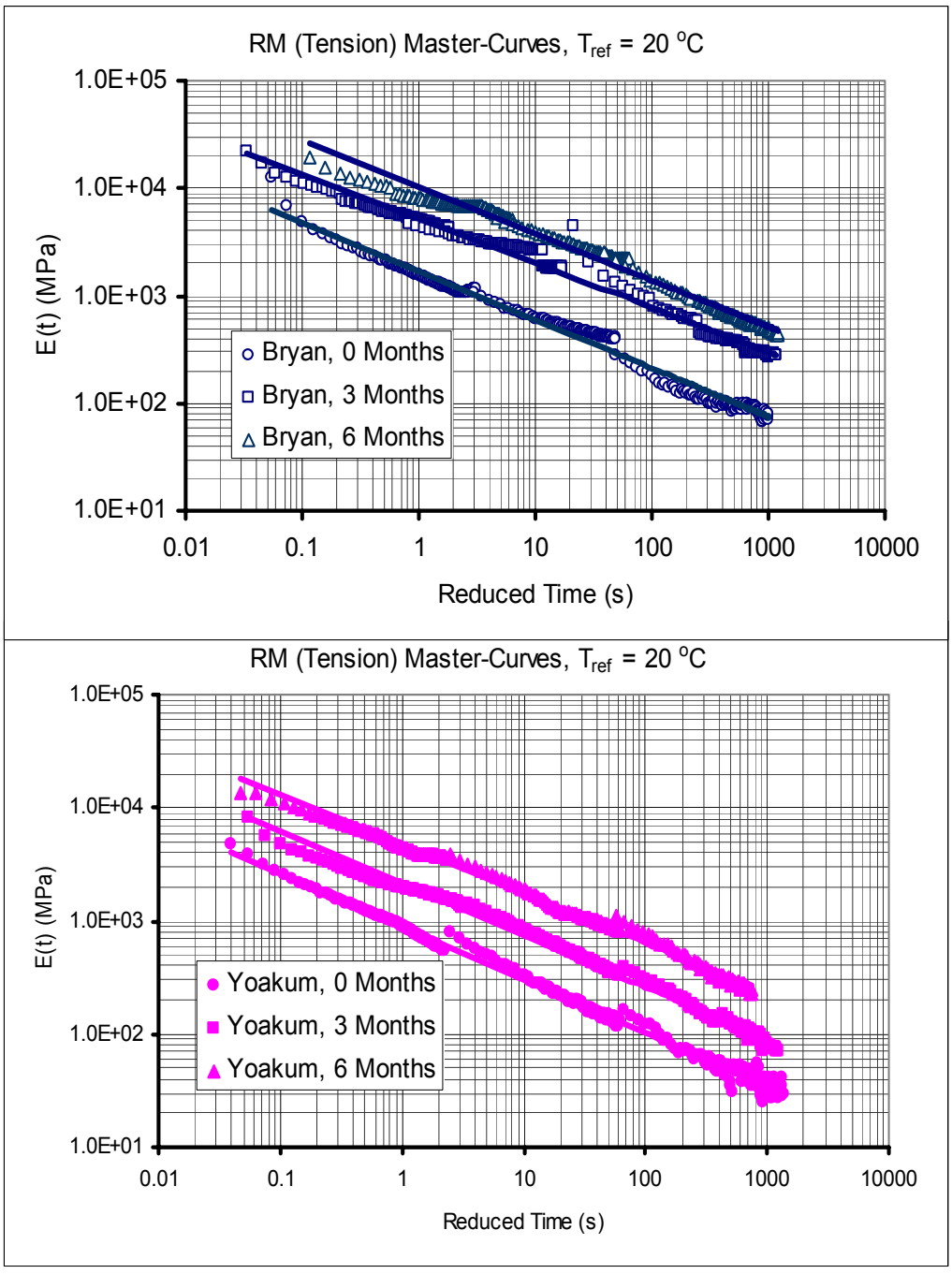

Fig. 8-11. RM (Tension) Master-Curves at 20 °C

From Figs. 8-8 and 8-11, it is clear that the Bryan mixture although designed with a softer PG 64-22 binder, was relatively stiffer than the Yoakum mixture. The difference in the stiffness is particularly more pronounced with aging, indicating that the Bryan mixture was probably more susceptible to stiffness age-hardening compared to the Yoakum mixture. While the Yoakum mixture exhibited comparatively lower *E(t)* values at 1.0 s, it exhibited higher *m* values at all aging conditions (Fig. 8-9). This result indicates that the Yoakum mixture had a relatively better potential to relax the applied stress than the Bryan mixture.

Note also that for all aging conditions, the *E(t)* values at 1.0 s in compression were higher than the corresponding values in tension and vice versa for the *m* values (Figs. 8-8 and 8-9). This is an expected material response due to the generally higher compactive effort in the vertical direction and confirms the anisotropic nature of HMAC.

RM Temperature Shift Factors, a_T

The a_T values plotted in Fig. 8-12 were computed when generating the RM master-curves at a reference temperature of 20 °C using the Arrehnius time-temperature superposition model via spreadsheet SSE regression optimization analysis (Lytton et al. 1993). The almost overlapping graphs in Fig. 8-12 indicate that the a_T values are not very sensitive to HMAC aging. These values, however, exhibit a linear relationship with temperature. Several researchers including Christensien and Anderson (1992) have reported similar findings. Looking at Fig. 8-12, the a_T values seem to be material (mixture) dependent as evident in Eqs. (8-4) and (8-5):

- Bryan mixture : $Log(a_T) = -0.1095T + 2.1978,\ R^2 = 0.998$ (8-4)
- Yoakum mixture: $Log(a_T) = -0.132T + 2.6711,\ R^2 = 0.996$ (8-5)

where:

a_T = Temperature shift factor

T = Temperature of interest (°C)

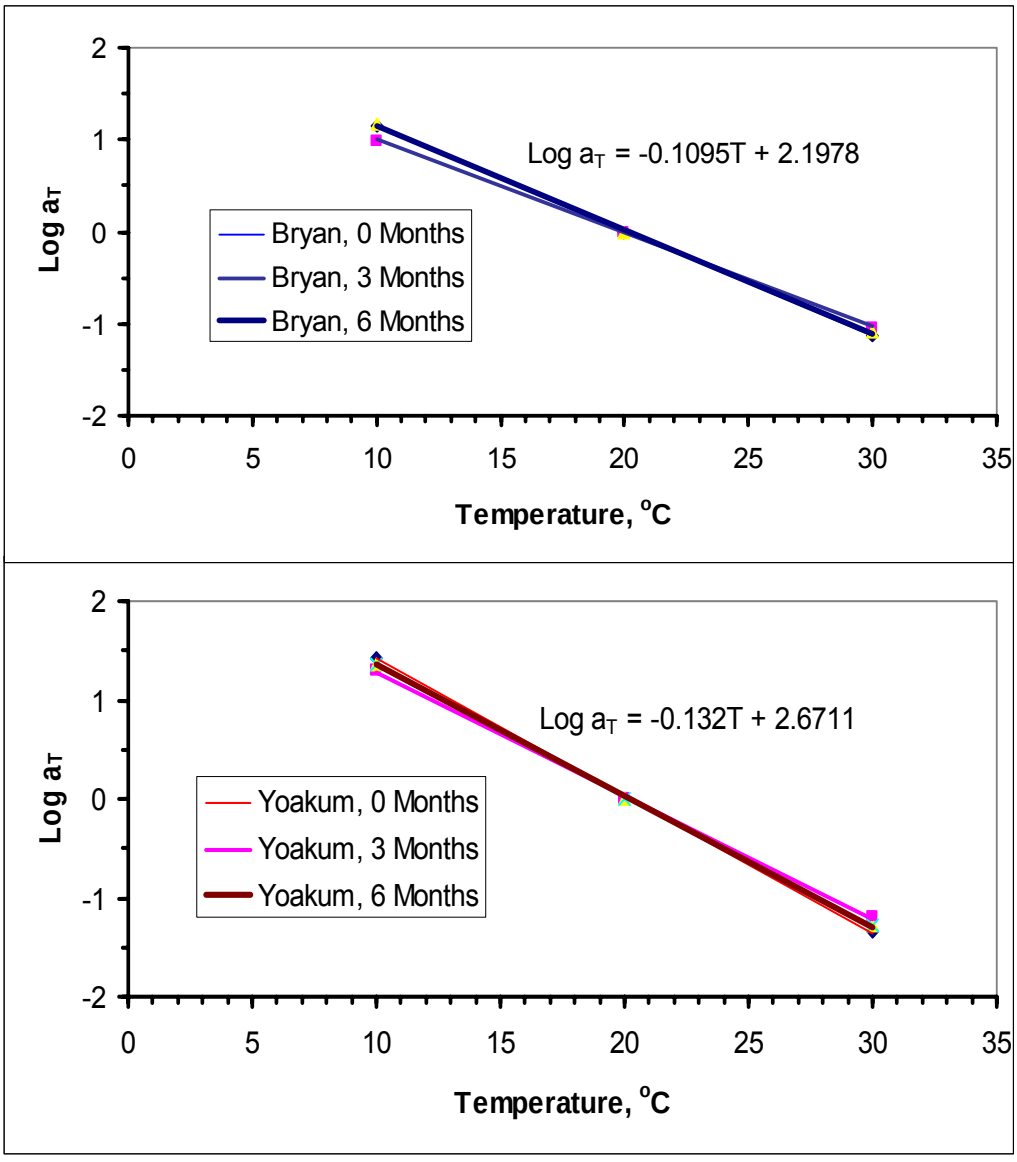

Fig. 8-12. RM Temperature Shift Factors, a_T at $T_{ref=20\ ^\circ C}$

DISSIPATED PSEUDO STRAIN ENERGY (DPSE)

Fig. 8-13 is a plot of the DPSE versus log *N* during RDT testing at 30 °C with the test data normalized to 20 °C. This DPSE was calculated as a function of the measured time-dependent tensile stress during RDT testing and the pseudo strain discussed in Chapter V.

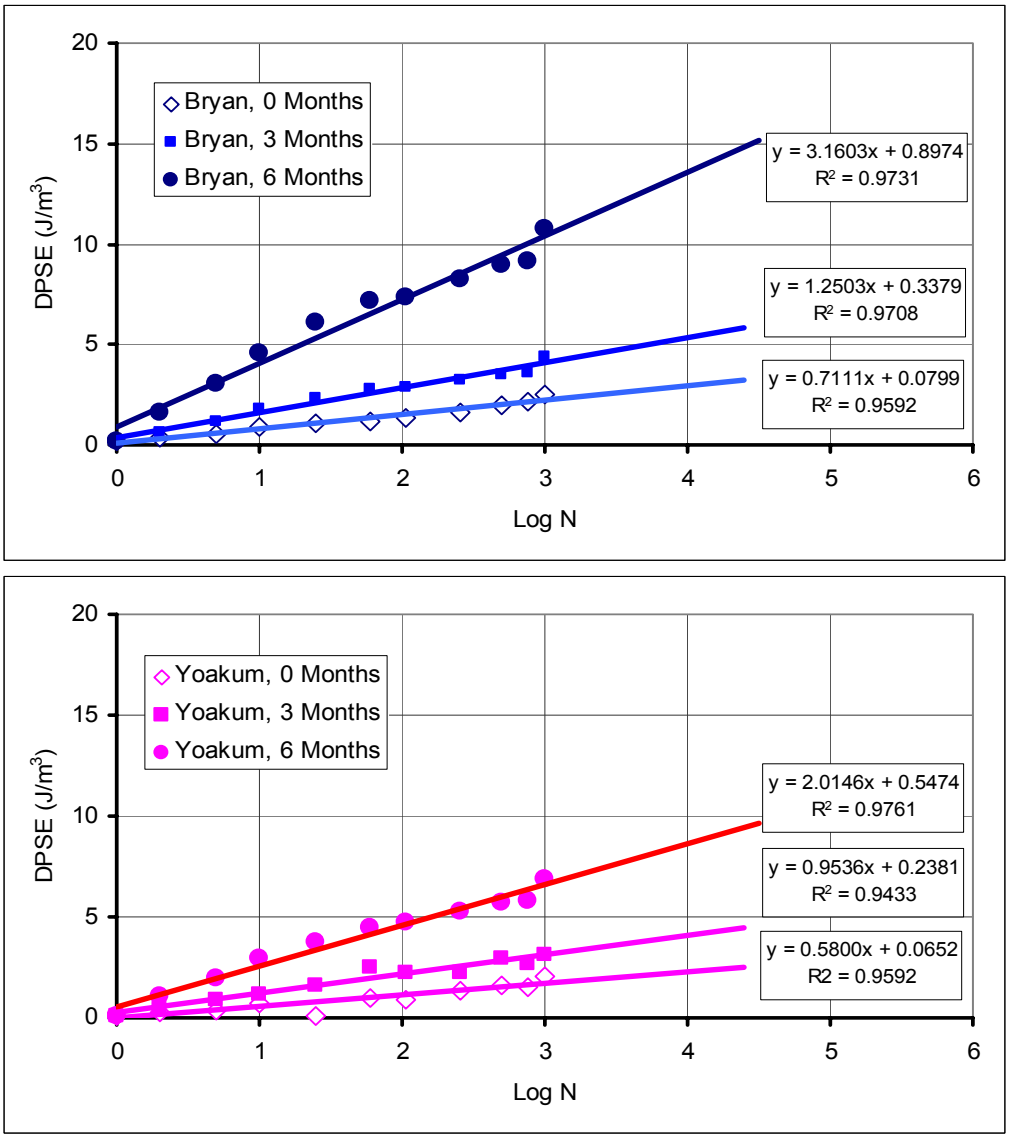

Fig. 8-13. Plot of DPSE versus Log *N* at 20 °C

Fig. 8-13 shows an increasing DPSE trend (in magnitude) with *N*, signifying the occurrence of fracture damage as the HMAC specimen is repeatedly loaded in a uniaxial tensile mode. In terms of damage, the higher the DPSE magnitude, the greater the fracture damage sustained. On this basis and considering similar loading conditions, the aged HMAC specimens appear to have sustained more fracture damage compared to the unaged (0 months) HMAC specimens. On the same basis, the Bryan mixture appears to have sustained more fracture damage compared to the Yoakum mixture.

The slopes *b* of DPSE versus log *N* for each mixture type and aging condition are plotted in Fig. 8-14. This parameter *b* is an indicator of the rate of fracture damage accumulation during RDT testing and was determined from Fig. 8-13 as expressed by the linear logarithmic relationship shown in Eq. (8-6) (Chapter V):

$$W_R(DPSE) = a + bLog(N) \qquad (8\text{-}6)$$

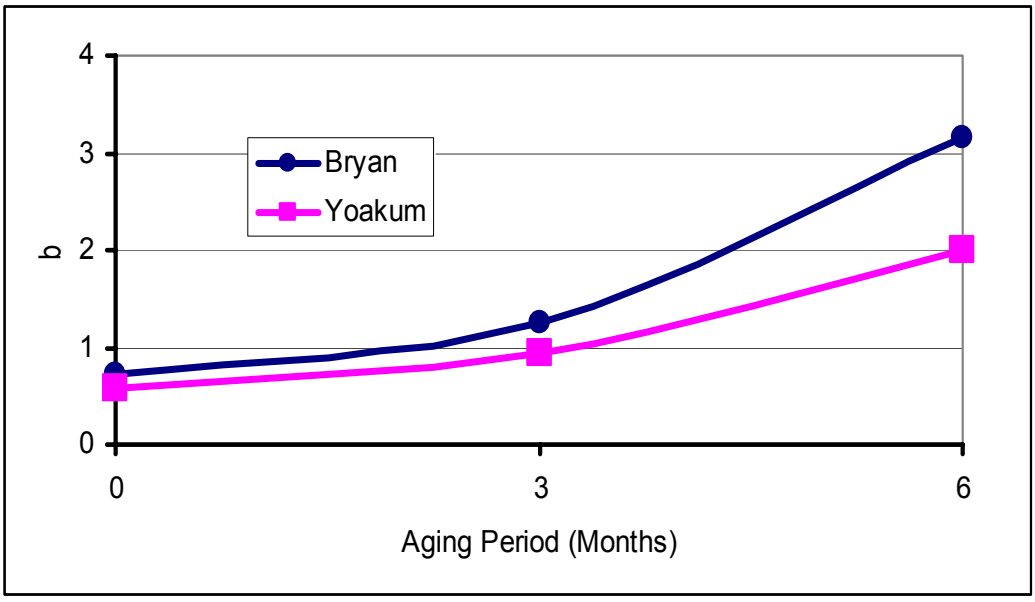

Fig. 8-14. Plot of the Parameter *b* versus Aging Condition

The increasing trend of the *b* value in Fig. 8-14 for both mixtures is indicative that the rate of fracture damage accumulation increased with aging. The relatively higher *b* values and greater rate of change (slope of the graphs in Fig. 8-14) of the *b* value with aging indicates that the Bryan mixture was accumulating fracture damage at a much faster rate. This observation is evidence that the Bryan mixture was perhaps more susceptible to fracture damage under RDT testing than the Yoakum mixture.

SURFACE ENERGY (SE)

The average measured SE results in terms of the binder and aggregate surface energy components (Γ_i) are summarized in Tables 8-7, 8-8, and 8-9. The calculated ΔG_f and ΔG_h based on the binder and aggregate surface energy components (Γ_i) in Tables 8-7, 8-8, and 8-9 are shown in Fig. 8-15 as a function of aging condition. The SE results shown in Fig. 8-15 represent the HMAC mixture adhesive bond strengths under dry conditions in the absence of water at an ambient temperature of approximately 20 °C.

Based on simple energy theory concepts, the higher the ΔG_f value, the greater the resistance to fracture damage; the lower the ΔG_h value, the greater the potential to self-heal. In simpler terms, ΔG_f is a representative measure of the bond strength between the binder and the aggregate and is associated with the energy that is required to break up this bond or create a fracture crack. On the other hand, ΔG_h is related to the affinity between the binder and aggregate and is associated with energy that is required to create a binder-aggregate bond or close up a fracture crack.

With these relationships, the Yoakum mixture has a better adhesive bond strength to resist fracture damage and a stronger potential to self-heal as indicated by the relatively higher fracture and lower healing energies, respectively, compared to the Bryan mixture. Also Fig. 8-15 shows that ΔG_f exhibits a decreasing trend with aging and vice versa for ΔG_h.

Table 8-7. SE Components for the Binder (Advancing ≈ Wetting ≈ Healing)

SE Component (ergs/cm^2)	PG 64-22 (Bryan Mixture)		
	0 Months	**3 Months**	**6 Months**
Γ_s^{LW}	4.28	6.10	9.78
Γ_s^-	4.43	2.42	8.21
Γ_s^+	1.83	7.55	2.35
Γ_s^{AB}	8.87	15.15	6.57
Γ_s^{Total}	13.16	6.10	17.13
PG 76-22 (Yoakum mixture)			
Γ_s^{LW}	13.63	24.53	44.16
Γ_s^-	2.28	3.19	4.47
Γ_s^+	1.15	1.50	1.94
Γ_s^{AB}	4.23	3.81	3.43
Γ_s^{Total}	17.15	22.30	28.98

Table 8-8. SE Components for the Binder (Receding ≈ Dewetting ≈ Fracturing)

SE Component (ergs/cm^2)	PG 64-22 (Bryan Mixture)		
	0 Months	**3 Months**	**6 Months**
Γ_s^{LW}	20.01	18.84	15.54
Γ_s^-	7.05	17.33	15.04
Γ_s^+	2.06	3.65	3.08
Γ_s^{AB}	10.58	15.76	16.53
Γ_s^{Total}	30.60	34.60	38.67
PG 76-22 (Yoakum Mixture)			
Γ_s^{LW}	76.92	35.03	31.53
Γ_s^-	9.42	23.53	58.81
Γ_s^+	4.48	6.14	11.05
Γ_s^{AB}	5.98	16.85	25.27
Γ_s^{Total}	17.15	46.69	52.76

Table 8-9. SE Components for the Aggregate

SE Component, ergs/cm^2	Γ^+	Γ^-	Γ^{AB}	Γ^{LW}	Γ^{Total}	SSA (m^2/gm)
Gravel (Victoria, Texas)	1.10	426.85	43.31	81.34	124.65	1.57
Limestone (Caldwell, Texas)	1.62	362.71	48.51	79.89	128.4	0.68

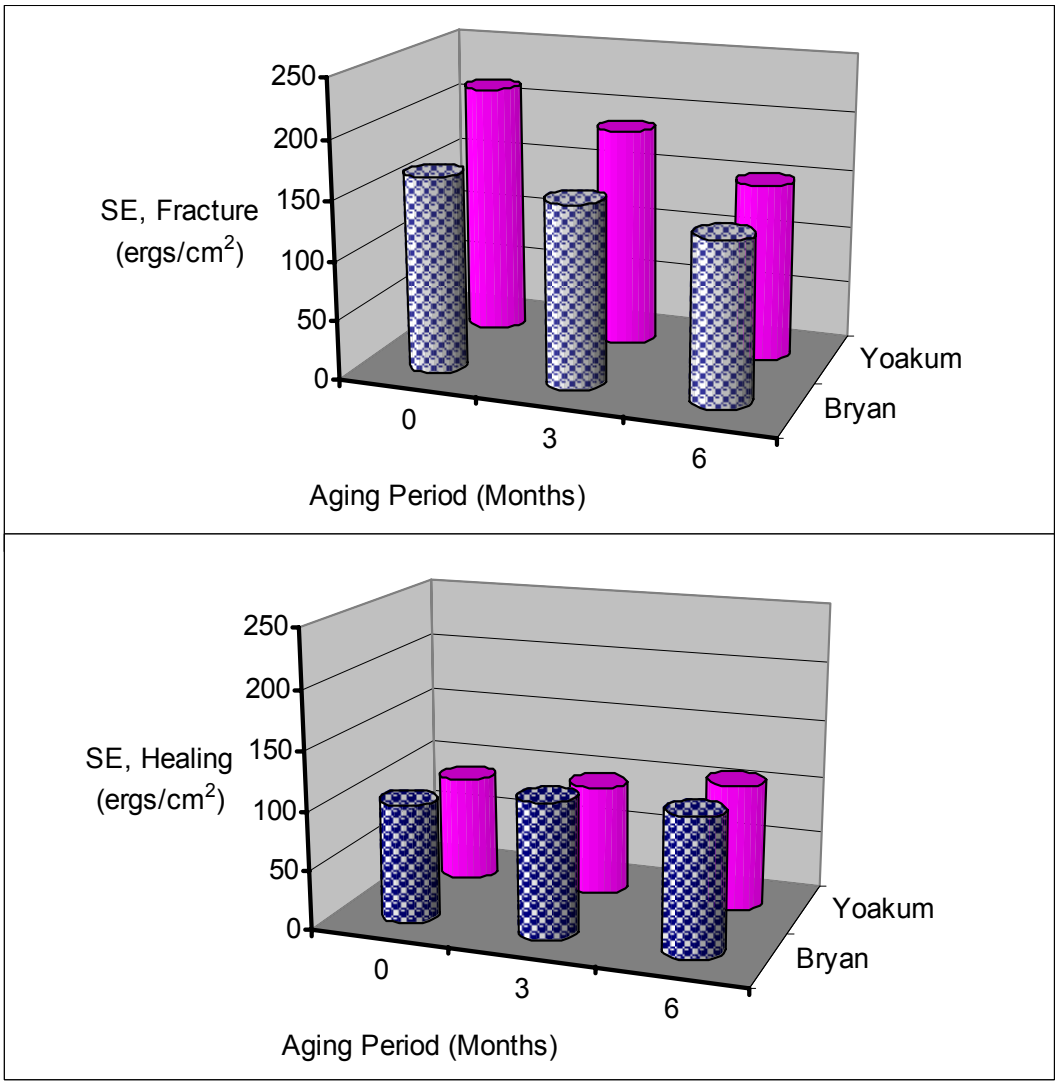

Fig. 8-15. HMAC Mixture Surface Energy at 20 °C

From the SE results in Fig. 8-15, the effect on SF_h and Paris' Law fracture coefficient A were determined as shown in Table 8-10. Table 8-10 shows that aging has a very significant effect on these parameters (A increased while SF_h decreased with aging). Generally, a lower value of A and higher value of SF_h are indicative of greater resistance to fracture damage and ability to self-heal, respectively.

Table 8-10. Paris' Law Fracture Coefficient A and SF_h Values at 20 °C

Parameter	**Mixture**	**Aging Condition @ 60 °C**		
		0 Months	**3 Months**	**6 Months**
A	Bryan	6.27×10^{-8}	16.00×10^{-8}	23.43×10^{-8}
	Yoakum	5.31×10^{-8}	14.01×10^{-8}	20.64×10^{-8}
SF_h	Bryan	6.73	4.74	3.07
	Yoakum	7.26	4.76	3.81

For the test conditions considered in this study, these SE results indicate that:

- ΔG_f decreases and ΔG_h increases with aging,
- binder oxidative aging reduces HMAC mixture resistance to fracture and ability to self heal, and
- as indicated by the relatively higher ΔG_f and lower ΔG_h values, respectively, the Yoakum mixture had a relatively better resistance to fracture damage and potential to self-heal than the Bryan mixture.

In terms of the Yoakum mixture exhibiting relatively better fracture and healing potential properties, the PG 76-22 plus gravel aggregate for the Yoakum mixture as indicated by the SE results exhibits a better adhesive bond strength with the corresponding binder than the component material combination for the Bryan mixture.

In other words, the PG 76-22 binder and gravel aggregates were perhaps more compatible in terms of adhesive bond strength than the PG 64-22 and limestone aggregates for the Bryan mixture. Note that SE data are also often used as a measure of material compatibility for HMAC mixture characterization with respect to moisture damage.

HMAC MIXTURE ANISOTROPY (AN)

The measured elastic moduli (E_i) values from the AN test at 20 °C are shown in Fig. 8-16. The expected difference in the E_x and E_z values (Fig. 8-16) is due to the anisotropic nature of the HMAC material under loading. For analysis simplicity based on elastic theory, the HMAC was assumed to be laterally isotropic and therefore E_x was considered equal to E_y in magnitude.

From Fig. 8-16, the increasing E_i trend with aging due to stiffness age-hardening is evident and again shows that the Bryan mixture was more susceptible to stiffness-age hardening than the Yoakum mixture. While in both cases (E_x and E_z), the E_i values at 0 months did not differ significantly, the E_i values for the Bryan mixture increased substantially after aging, more than the Yoakum E_i values. This result is evidence that the Bryan mixture was stiffening at a much faster rate than the Yoakum mixture. As expected, Fig. 8-16 further shows that the E_z values were higher that the E_x values at all aging conditions for both mixtures.

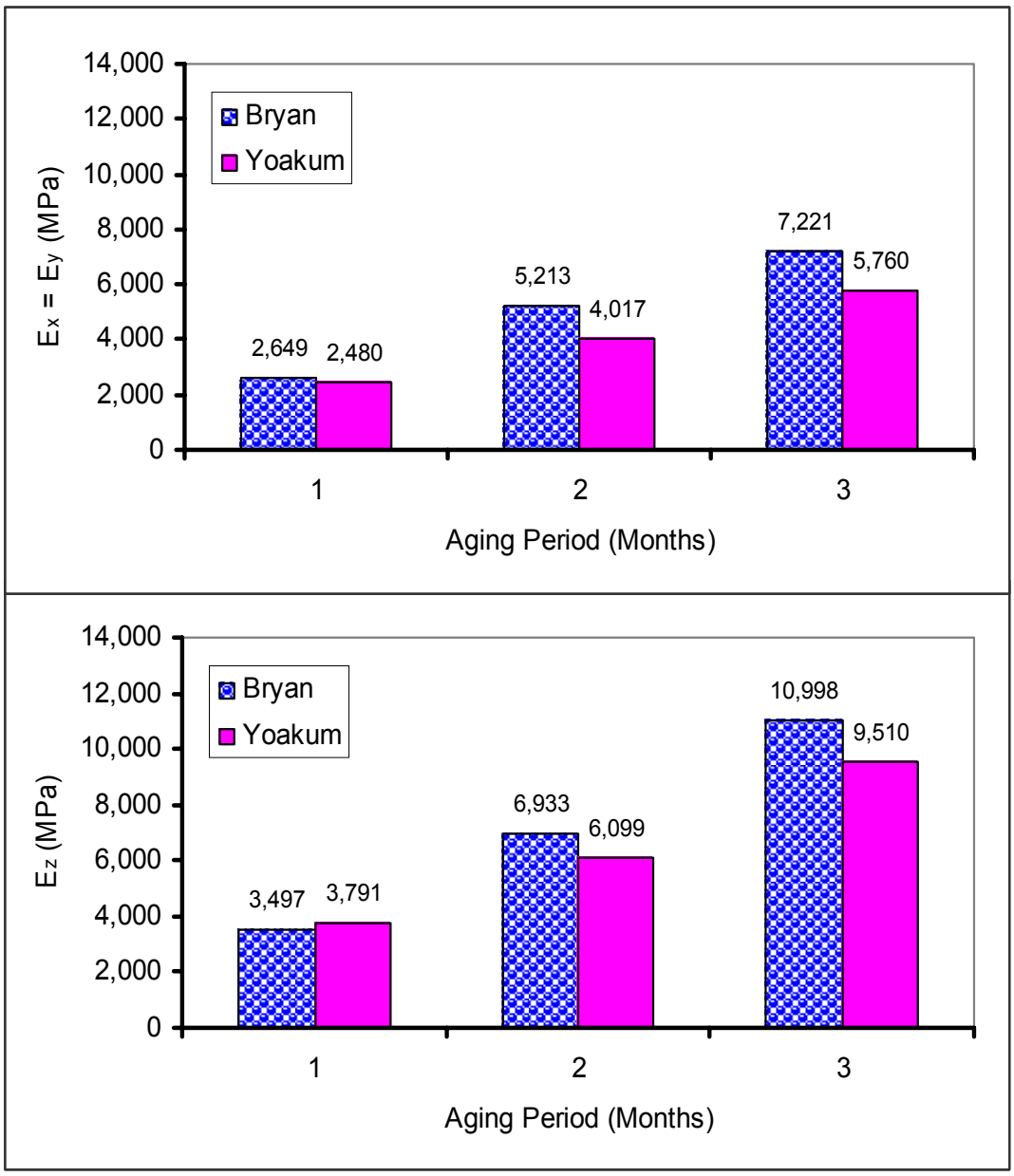

Fig. 8-16. HMAC Mixture Anisotropic Test Results at 20 °C

Elastic Modular Ratio (E_z/E_x)

Fig. 8-17 is a plot of the elastic modular ratio calculated based on the E_i values in Fig. 8-16. The range of the elastic modular ratio is from 1.32 to 1.65 with mean values of 1.39 (COV = 8.2%) and 1.57 (COV = 4.7%) for the Bryan and Yoakum mixtures, respectively. The overall mean elastic modular ratio for both HMAC mixtures at 20 °C was calculated to be 1.48 with a COV of 8.7%.

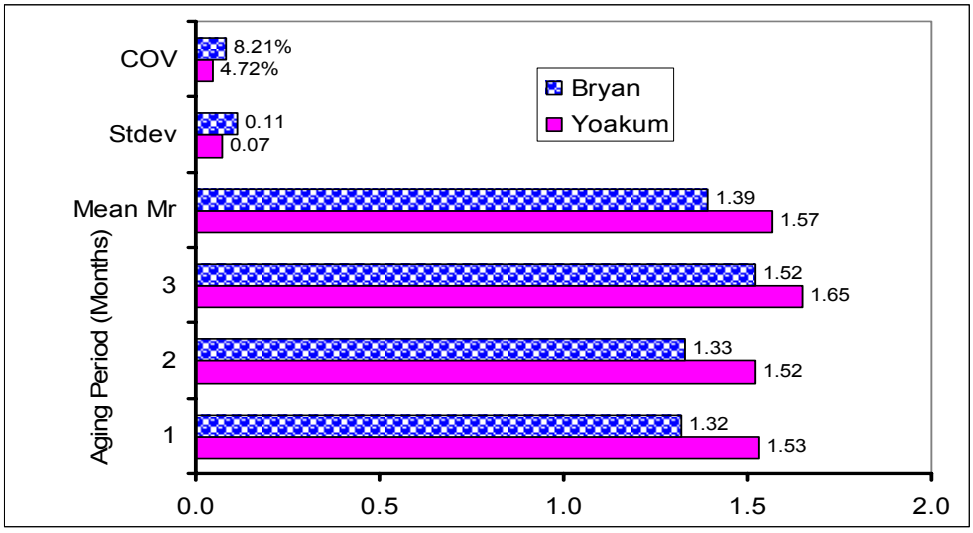

Fig. 8-17. Elastic Modular Ratio at 20 °C

In general, these elastic modular ratio results do not differ significantly from those reported by other researchers. In their studies, Khanal and Mamlouk (1995) and Al-Qadi and Nassar (2003) found that the resilient compression modulus was approximately 1.50 and 1.46 times that in tension, respectively, at 25 °C. Thus, E_z may be equated to $1.48E_x$ at 25 °C. Through extensive dynamic modulus testing, Kallas (1970) found that E_z was about 1.5 to 2 times the value of E_x at 21 °C. Based on HMAC dynamic modulus back-calculation analysis at an assumed temperature of 20 °C, Oh (2004) approximated E_z to be about 1.26 times E_x (i.e., $E_z = 1.26E_x$).

Shift Factor Due to Anisotropy (SF_a)

Table 8-11 shows the calculated SF_a values based on E_i values in Fig. 8-16. Note that anisotropy arises due to the fact that the HMAC mixture properties such as the elastic modulus are directionally dependent.

Table 8-11. Shift Factor Due to Anisotropy (SF_a) at 20 °C

Aging Condition @ 60 °C	$SF_a = (E_z/E_x)^{1.75}$	
	Bryan	**Yoakum**
0 months	1.63	2.10
3 months	1.65	2.08
6 months	2.09	2.40
Mean	1.79	2.19
Stdev	0.26	0.18
COV	14.6%	8.4%

Table 8-11 shows some degree of differences in the SF_a results as a function of mixture type and aging condition. Since anisotropy is predominantly controlled by particle orientation due to compaction, the theoretical assumption is that a particular HMAC mixture should exhibit similar anisotropic response under all aging conditions. Therefore, the cause of discrepancy could be related to test variability.

The calculated maximum COV for these measurements was approximately 14.6%, which is within the acceptable ±15% error tolerance due to HMAC mixture inhomogeneity and test variability (Medani et al. 2004). Assuming that the SF_a differences are primarily due to test variability and HMAC mixture inhomogeneity, the mean SF_a values for the Bryan and Yoakum mixtures were averaged to be 1.79 and 2.19, respectively, for all aging conditions within an error tolerance of 15% (Medani et al. 2004).

In terms of the effect of HMAC mixture type, some difference in the SF_a values can be expected due to the differences in the aggregate gradation that has an effect on the particle orientation during compaction. However, since the 1.79 and 2.19 values do not differ by more than 15%, a mean SF_a value of 2.0 is not unreasonable for both the Bryan and Yoakum mixtures for all aging conditions. Aparicio (2003) and Oh (2004) have reported similar findings.

DYNAMIC MODULUS (DM) RESULTS

Table 8-12 is a summary of the mean |E*| values at 0 months aging condition based on three replicate measurements per mixture type included in Appendix E. These |E*| results represent input data required for Level 1 fatigue analysis in the MEPDG software for estimating *Field* N_f. Because the MEPDG software incorporates GAM analysis in overall *Field* N_f prediction, DM testing of aged mixtures (HMAC specimens) was considered unnecessary.

Table 8-12. Mean |E*| Values from DM Testing (0 Months)

Temperature		**Mean |E*| (MPa) - Bryan Mixture**					
°C	**°F**	**0.1 Hz**	**0.5 Hz**	**1.0 Hz**	**5.0 Hz**	**10 Hz**	**25 Hz**
-10	14	16,698	19,833	20,916	23,860	24,929	26,632
4.4	40	8,595	11,162	12,386	15,204	16,686	18,616
21.1	70	3,066	4,518	5,381	7,600	8,877	11,038
37.8	100	1,035	1,625	1,920	3,196	4,043	5,680
54.4	130	443	602	679	1,101	1,456	2,269
Temperature		**Mean |E*| (MPa) - Yoakum Mixture**					
°C	**°F**	**0.1 Hz**	**0.5 Hz**	**1.0 Hz**	**5.0 Hz**	**10 Hz**	**25 Hz**
-10	14	9,320	12,602	14,068	18,062	19,797	22,128
4.4	40	6,654	9,419	10,656	13,914	15,317	17,232
21.1	70	1,705	3,086	3,942	6,408	7,836	9,873
37.8	100	438	723	895	1,658	2,268	3,684
54.4	130	260	340	374	672	933	1,624

From Table 8-13, the calculated |E*| variability in terms of COVs ranged from 0.1% to 19.3% for the Bryan mixture and from 18.1% to 42.8% for the Yoakum mixture. These results show a high variability in the Yoakum |E*| results, with the highest COVs associated with the extreme test temperatures of 10 and 54.4 °C, respectively.

Table 8-13. COV of |E*| Results from DM Testing (0 Months)

Temperature		**COV - Bryan Mixture**					
°C	**°F**	**0.1 Hz**	**0.5 Hz**	**1.0 Hz**	**5.0 Hz**	**10 Hz**	**25 Hz**
-10	14	15.2%	15.3%	14.5%	13.8%	12.9%	12.7%
4.4	40	10.3%	8.0%	7.4%	5.2%	4.7%	2.8%
21.1	70	6.0%	3.8%	3.6%	2.1%	0.9%	0.1%
37.8	100	15.8%	16.0%	16.5%	18.1%	16.3%	19.3%
54.4	130	17.0%	13.2%	12.1%	12.1%	10.1%	12.9%
Temperature		**COV - Yoakum Mixture**					
°C	**°F**	**0.1 Hz**	**0.5 Hz**	**1.0 Hz**	**5.0 Hz**	**10 Hz**	**25 Hz**
-10	14	30.2%	26.6%	24.2%	20.5%	18.5%	18.6%
4.4	40	23.1%	21.5%	20.2%	18.2%	18.2%	18.1%
21.1	70	24.9%	23.7%	23.1%	22.1%	21.3%	22.7%
37.8	100	24.0%	28.0%	27.5%	30.2%	29.7%	31.1%
54.4	130	29.8%	25.6%	25.9%	35.4%	38.0%	42.8%

DM Master-Curves

Fig. 8-18 shows an example of |E*| master-curves plotted as a function of reduced time and normalized to a reference temperature of 20 °C on a semi-log scale. These master-curves together with the respective a_T values were generated using the signomoidal time-temperature superposition model discussed in Chapter VII via spreadsheet regression SSE optimization analysis with the "Solver" function (Pellinen and Witczak 2002).

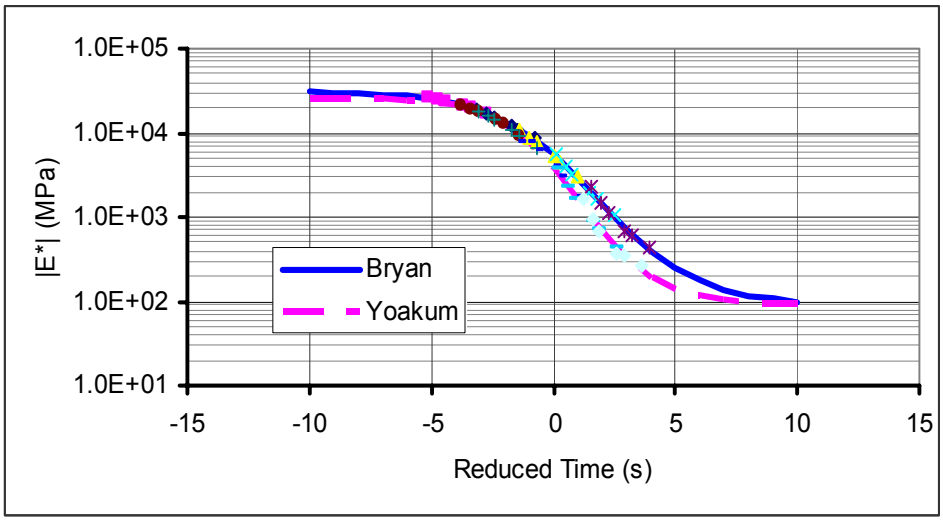

Fig. 8-18. Mixture |E*| Master-Curves at 20 °C

According to the modified Asphalt Institute fatigue predictive model (Chapter VII) incorporated in the MEPDG software, |E*| exhibits an inverse relationship with mixture fatigue resistance. Therefore, the relatively lower |E*| values of the Yoakum mixture at some loading frequencies (reduced time) may be indicative of superior fatigue resistance compared to the Bryan mixture. Although theoretically unexpected since the Yoakum mixture was designed with a stiffer binder, these results do concur with other mixture property results reported in this dissertation.

Because of the stiffer SBS modified PG 76-22 binder in the Yoakum mixture, higher |E*| values were theoretically expected for this mixture at all loading conditions compared to the Bryan mixture. This contrasting result, however, shows that binder stiffness alone may not be used as the sole measure or indicator of the overall HMAC mixture stiffness and fatigue resistance. Mix-design characteristics and other material properties such as aggregate gradation, binder content, AV, voids in mineral aggregate (VMA), voids filled with asphalt (VFA), and aggregate type may also play a significant role in the stiffening effect of the overall HMAC mixture and need to be carefully evaluated.

DM Temperature Shift Factors, a_T

Like for the RM test data, the natural logarithm of a_T plotted as shown in Fig. 8-19 exhibited a linear relationship with temperature, with R^2 values of 99.15% and 98.75% for the Bryan and Yoakum mixtures, respectively.

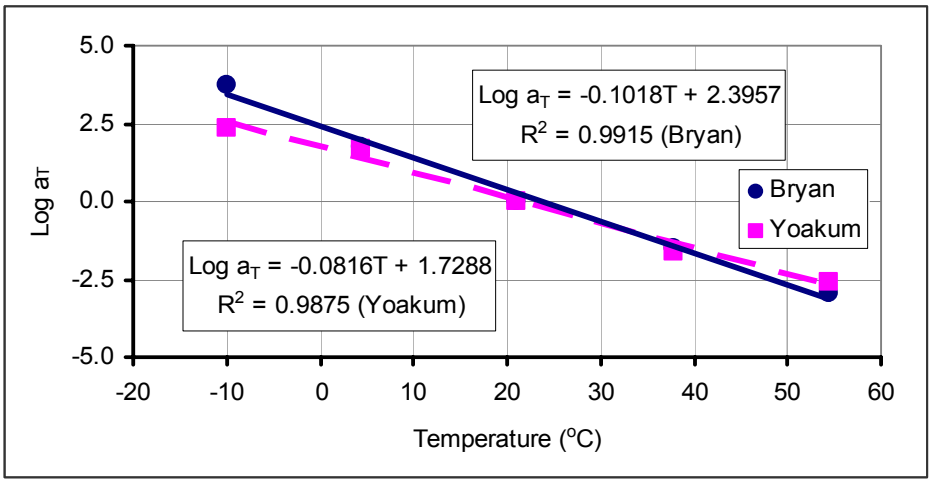

Fig. 8-19. Mixture a_T at $T_{ref=20\ ^\circ C}$ for |E*| Master-Curves

Although the coefficients of the fitted logarithmic trend lines of the mixtures do not differ significantly, it is apparent from Fig. 8-19 that the a_T may be sensitive to mixture type.

EFFECTS OF AGING ON HMAC MIXTURE PROPERTIES

Table 8-14 summarizes the effects of binder oxidative aging on the HMAC mixture properties and fatigue resistance.

Table 8-14. Effects of Binder Oxidative Aging on HMAC Mixture Properties

Parameter	Mixture	Value			Trend with Aging	Effect on N_f
		0 Months	3 Months	6 Months		
ΔG_f (erg/cm^2)	Bryan	165.66	154.66	138.00	Decrease	Reduce
	Yoakum	253.14	187.00	151.00		
ΔG_h (erg/cm^2)	Bryan	101	115	117	Increase	
	Yoakum	90	95	108		
σ_t (kPa)	Bryan	725	770	1,080	Increase	
	Yoakum	849	1,049	1,270		
ε_f (microstrain)	Bryan	1,245	689	401	Decrease	
	Yoakum	3,483	2,342	851		
$E(t)$ @ 1 s (MPa)	Bryan	1,435	4,658	6,967	Increase	
	Yoakum	1,233	2,685	4,369		
m	Bryan	0.3997	0.3774	0.2945	Decrease	
	Yoakum	0.5116	0.4513	0.4273		
b	Bryan	0.71	1.25	3.16	Increase	
	Yoakum	0.58	0.95	2.01		
I_i	Bryan/ Yoakum	2.00	1.33	1.14	Decrease	
n_{BD}	Bryan/Yoakum	0.00	0.50	0.75	Increase	
A (1×10^{-8})	Bryan	6.27	16.00	23.43	Increase	
	Yoakum	5.31	14.01	20.64		
n	Bryan	2.50	2.65	3.40	Increase	
	Yoakum	1.95	2.22	2.34		
SF_a	Bryan	1.63	1.65	2.09	No significant effect	
	Yoakum	2.10	2.08	2.40		
SF_h	Bryan	6.73	4.74	3.07	Decrease	Reduce
	Yoakum	7.26	4.76	3.81		

Based on simple energy theory concepts, the higher the ΔG_f value, the greater the resistance to fracture damage, and the lower the ΔG_h value; the greater the potential to self-heal. With this relationship, Table 8-14 shows that both mixture resistance to fracture damage and potential to self-heal decreases with aging and that the Yoakum mixture had better adhesive bond strength to resist fracture damage and potential to heal than the Bryan mixture at all aging conditions. The decrease in the potential to self-heal is further indicated by the SF_h parameter, which exhibits a decreasing trend with aging.

As the HMAC ages, it becomes more brittle (less ductile), thus breaking under tensile loading at a lower strain level. For both mixtures, Table 8-14 shows that while the σ_t was within the test variability (Medani et al. 2004), the ε_f at break decreased significantly on the order of over 30% due to an increase in mixture brittleness from oxidative aging of the binder. This increase in brittleness is also indicated by the increasing n_{BD} value with aging. In terms of HMAC mixture comparison, the σ_t and ε_f values for the Yoakum mixture were higher than that of the Bryan mixture at all aging conditions, indicating that for the test conditions considered in this study, the Yoakum mixture was more ductile and had a better resistance to tensile stress than the Bryan mixture. As expected, $E(t)$ increased with aging due to HMAC hardening and stiffening effects from oxidation of the binder, which inevitably resulted in a decreased ability to relax the applied stress as indicated by the decreasing m value. The increasing trend of the b value for both mixtures indicates that the rate of fracture damage accumulation increased with aging. Again, the results show an increased ability for the Yoakum mixture to relax the applied stress and a lower susceptibility to fracture damage under RDT testing than the Bryan mixture. Paris' Law fracture coefficient A is inversely related to HMAC mixture fracture resistance. Based on this relationship, the increasing A trends in Table 8-14 are indicative of declining HMAC mixture fracture resistance with aging. The Yoakum mixture's better fracture properties in terms of A and n magnitude is again clearly evident. The mixture property SF_a, however, did not vary significantly as a function of binder oxidative aging condition. In general, Table 8-14 shows that aging has a detrimental effect on HMAC mixture fatigue properties and N_f.

SUMMARY

In this chapter, the HMAC mixture property results were presented and the following bullets summarize the key findings based on the test conditions considered in the study.

BB Testing

- The number of laboratory load cycles to fatigue failure under BB testing decreased with binder oxidative aging.
- The Yoakum mixture performed better in terms of N during BB testing at 20 °C.
- While other researchers have demonstrated that the material constants k_i are temperature and loading-mode dependent, this study showed that these material constants are also mixture type and aging condition dependent. This result signifies the importance of characterizing fatigue performance among other variables as a function of mixture type, aging condition, temperature, and loading mode.
- For the test conditions considered in this study, the material constants k_1 and k_2 exhibited a linear logarithmic relationship.

Tensile Stress

- Due to more brittle behavior with binder oxidative aging, the mixture tensile failure strain (ε_f) at break under tensile loading at 20 °C decreased significantly with aging.
- Based on the higher ε_f values, the Yoakum mixture exhibited more ductility at all aging conditions compared to the Bryan mixture.
- With aging, the failure mode under tensile loading for both mixtures changed from ductile to brittle.
- The decreasing ε_f trend with aging is an indicator of decreased mixture ductility and resistance to fracture damage under tensile loading.

Relaxation Modulus

- While the mixture elastic relaxation modulus (*E(t)*) increased with binder oxidative aging due to stiffening effects, the RM results indicated that the Yoakum mixture had a better potential to relax stress than the Bryan mixture based on a larger *m* value. However, as expected, the ability to relax the stress (*m* value) generally decreased with aging for both mixtures.
- Due to HMAC anisotropy, the *E(t)* values in compression were generally higher than the *E(t)* values in tension and vice versa for the *m* value.
- Although designed with a relatively softer PG 64-22 binder, the relaxation modulus (*E(t)*) of the Bryan mixture was relatively higher than that of the Yoakum mixture designed with a stiffer SBS-modified PG 76-22 binder, particularly after aging. These results suggests that for the test conditions considered in this study, the Bryan mixture was perhaps more susceptible to stiffness age-hardening due to binder oxidative aging.
- The logarithm of the temperature shift factor (*Log* a_T) determined when generating the RM master-curves exhibited a linear relationship with temperature, but this parameter exhibited less dependence on binder oxidative aging conditions. By contrast, *Log* a_T exhibited some degree of sensitivity to HMAC mixture type.

DPSE and SE Results

- The DPSE results indicated that the Bryan mixture was more susceptible to fracture damage than the Yoakum mixture and that the rate of fracture damage accumulation generally increased with aging.
- The SE results indicated better adhesive bond strength for the Yoakum mixture relative to the Bryan mixture and that mixture resistance to fracture and potential to heal generally decreased with aging.

HMAC Mixture Anisotropy

- A mean modular ratio value of 1.48 was determined for both mixtures at 20 °C.
- Within a ±15% error tolerance, mixture anisotropy (SF_a) was observed to be insignificantly affected by binder oxidative aging and did not vary substantially as a function of mixture type. Consequently, a mean SF_a value of 2.0 was proposed for both the Bryan and Yoakum mixtures for all aging conditions.

Dynamic Modulus

- Contrary to theoretical expectations, dynamic modulus results indicated that while the Yoakum mixture was designed with a stiffer polymer modified binder (PG 76-22); the overall mixture stiffness was not greater than that of the Bryan mixture designed with a relatively softer binder (PG 64-22) at certain loading times. These DM results indicate that the wide spectrum of mixture properties (such as aggregate gradation, binder content, AV, VMA, and VFA) other than just binder and/or aggregate type may play a significant role in the stiffening effect of HMAC mixtures. Note that the mix-design characteristics for each mixture type were different.
- When generating the DM master-curves, the logarithmic of temperature shift factors (i.e. $Log\ a_T$) exhibited a linear relationship with temperature, but were insensitive to binder oxidative aging conditions. By contrast, $Log\ a_T$ exhibited sensitivity to HMAC mixture type.

CHAPTER IX
PREDICTION OF HMAC MIXTURE FATIGUE LIVES

This chapter presents the HMAC mixture fatigue resistance expressed in terms of laboratory fatigue life (*Lab* N_f) and field fatigue life (*Field* N_f) magnitude, analyzed at a typical 95% design reliability level. In the study, *Lab* N_f was defined as the estimated HMAC mixture fatigue resistance without inclusion of any shift factors to simulate field conditions and environmental exposure. *Field* N_f was then calculated as a product of the field shift factors (SF_i) and *Lab* N_f as illustrated below:

$$Field\ \ N_f = SF_i \times Lab\ \ N_f \qquad (9\text{-}1)$$

where:

Field N_f	=	Fatigue life expressed in terms of traffic ESALs to fatigue failure
SF_i	=	Field shift factors that include healing, anisotropy, aging, temperature correction, and reliability multiplier
Lab N_f	=	Fatigue life expressed in terms of allowable laboratory load repetitions to fatigue failure

Throughout this chapter and subsequent chapters, the units of fatigue life (*Lab* N_f and *Field* N_f) are defined and expressed in terms of the number of allowable load repetitions to fatigue failure in the laboratory or traffic ESALs in the field, respectively. The reference temperature for all the N_f (lab and field) analysis in this study was 20 °C, and the analysis reliability level for all the fatigue approaches was 95%. In the analysis of *Field* N_f, 0 months aging at 60 °C was considered equivalent to 0 years, 3 months to 6 years, and 6 months to 12 years, respectively, in terms of field HMAC pavement age (Glover et al. 2005). For the fatigue analysis approaches, detailed life *Lab* N_f and *Field* N_f results are include in Appendix F and G, respectively.

THE ME APPROACH

The calculated mixture *Lab* N_f and *Field* N_f consistent with the ME fatigue analysis models discussed in Chapter IV are presented in this section.

ME *Lab* N_f Results

The predicted *Lab* N_f results from the ME analysis based on Eq. 9-2a and the SPSS V11.5 least square line regression analysis discussed in Chapters IV and VIII are included in Appendix F. The definition of the parameters in Eq. (9-2) is found in Chapter IV.

$$Lab\ N_f = k_1\left(\varepsilon_t\right)^{-k_2} \tag{9-2}$$

The results in Appendix F represent mean values of at least two test measurements per mixture type per aging condition per strain level for the five pavement structures and two environmental conditions considered. The COV of *Ln* N_f considering both mixtures (Bryan and Yoakum) and environmental conditions (WW and DC) at 95% reliability level ranged between 2.5% and 6.8%. Although these COVs seem to be relatively lower when expressed in terms of *Ln* N_f, the 95% N_f PI margin is wide suggesting a high statistical variability and low precision in the predicted *Lab* N_f results. Table 9-1 provides a summary of the mean *Lab* N_f and 95% N_f PI for five pavement structures under WW environment for both mixtures for the 0 months aging condition.

In terms of the mixture *Lab* N_f comparison and the effects of aging, Fig. 9-1 is a diagrammatic illustration for one pavement structure designated as PS#1 (Table 3-7) under the WW environment.

Table 9-1. Summary of ME Mean *Lab* N_f and 95% N_f PI

PS	Mean Lab N_f		95% N_f PI Range			
	Bryan	Yoakum	Bryan [Lower]	Bryan [Upper]	Yoakum [Lower]	Yoakum [Upper]
1	4.48E+06	4.11E+06	2.12E+06	9.46E+06	0.27E+06	62.99E+06
2	0.42E+06	0.60E+06	0.29E+06	0.61E+06	0.17E+06	2.16E+06
3	0.42E+06	0.64E+06	0.32E+06	0.67E+06	0.17E+06	2.43E+06
4	0.36E+06	0.53E+06	0.26E+06	0.51E+06	0.16E+06	1.75E+06
5	29.83E+06	No data	10.20E+06	87.25E+06	No data	No data

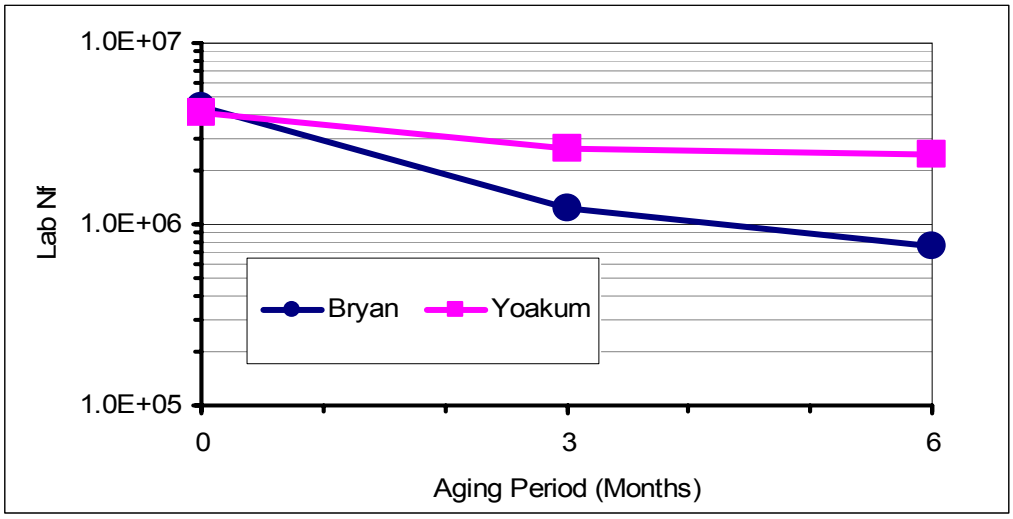

Fig. 9-1. ME *Lab* N_f for PS#1, WW Environment

For both mixtures, Fig. 9-1 shows that *Lab* N_f decreases with aging and that the Yoakum mixture generally exhibited relatively higher N_f values compared to the Bryan mixture. This trend was observed for all pavement structures in both the WW and DC environmental conditions and is consistent with the prediction from the material property results reported in Chapter VIII.

Ln N_f variability in terms of COV was, however, comparatively higher for the Yoakum mixture, on the order of about 10% more than that of the Bryan mixture. This high variability is also evident from the 95% PI in Table 9-1 and Appendix F when comparing the Bryan mixture to the Yoakum mixture. These results concur with the variability results reported in Chapter VIII for the HMAC mixture properties.

ME *Field* N_f Results

Fig. 9-2 shows an example of a plot of the *Field* N_f results as a function of aging condition expressed in terms of pavement age for PS#1 under the WW environment. Note that 0, 3, and 6 months aging at 60 °C were considered equivalent to up to 12 years of HMAC pavement field aging in Texas (Glover et al. 2005).

Detailed *Field* N_f results are contained in Appendix G. These *Field* N_f predictions were determined simply as a function of shift factor (*SF*), temperature correction factor (*TCF*), reliability multiplier (*M*), and the estimated *Lab* N_f as described in Chapter IV and illustrated in Eq. (9-3) where the parameters are defined in Chapter IV. In this study, values of SF = 19, M = 3.57, and TCF = 1.0 were used (Tayebali et al. 1992).

$$Field\ \ N_f = \frac{SF}{M \times TCF}\left[Lab\ N_f\right] \tag{9-3}$$

Like for the *Lab* N_f results, Fig. 9-2 shows that N_f exponentially decreases with aging for both mixtures and that the Yoakum mixture exhibited relatively better fatigue resistance in terms of higher *Field* N_f values compared to the Bryan mixture. The calculated rate of N_f decline based on the slopes of the exponential trend lines fitted through the N_f data points in Fig. 9-2 were 0.15 and 0.04 for the Bryan and Yoakum mixture, respectively. Thus the rate of *Field* N_f decline for the Bryan mixture was considerably higher (about 3.75 times) than that of the Yoakum mixture, which is consistent with the mixture property results reported in Chapter VIII.

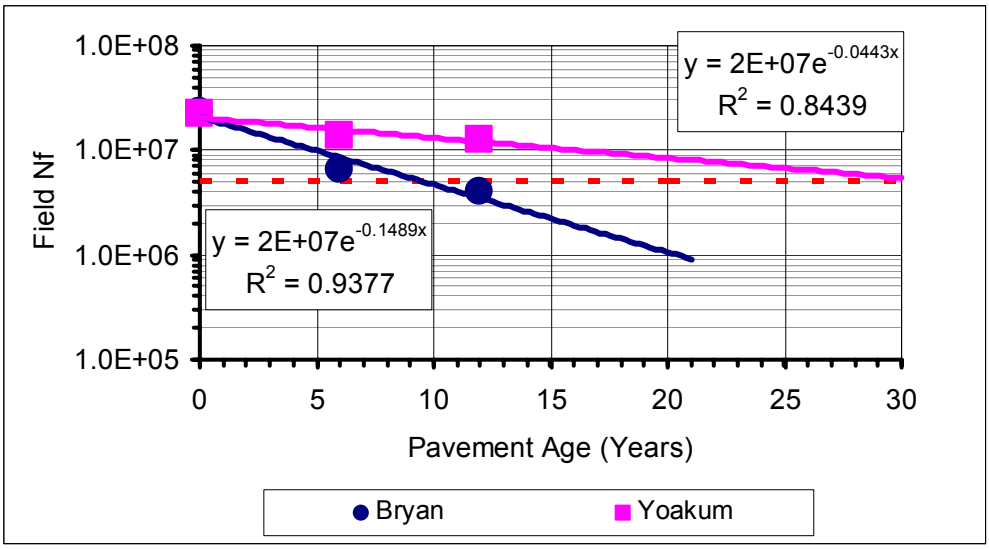

Fig. 9-2. ME *Field* N_f for PS#1, WW Environment

Eq. (9-4) shows the generalized exponential relationship between *Field* N_f and aging as a function of time (t) in years based on Fig. 9-2.

$$N_f = ae^{-bt} \tag{9-4}$$

where:

a, b = Material regression constants

Assuming that *Field* N_f exhibits an exponential functional relationship with pavement age as fitted in Fig. 9-2 consistent with Eq. 9-4, the *Field* N_f predictions at year 20 are 1.03×10^6 and 8.30×10^6 for the Bryan and Yoakum mixture, respectively. Thus the results indicate inadequate and adequate theoretical fatigue performance for the Bryan and Yoakum mixtures, respectively, based on the 5×10^6 design traffic ESALs and 20 years service life at 95% reliability level for this particular pavement structure (PS#1).

According to this analysis, the Bryan mixture will theoretically fail prematurely based on Fig. 9-2, approximately in the 10th year of service. The Yoakum mixture on the other hand will theoretically sustain the design traffic for the entire 20-year design period up to about the 29th year. Mean ME *Field* N_f results and the 95% PI for all pavement structures at year 20 are listed in Appendix G. On comparative basis, Appendix G indicate better fatigue resistance for the Yoakum mixture in terms of *Field* N_f magnitude, but relatively high statistical variability in terms of the COV and 95% PI.

THE CMSE APPROACH

This section presents the mixture *Lab* and *Field* N_f results for the CMSE fatigue analysis approach discussed in Chapter V. A methodology for developing a CMSE/CM aging shift factor based on binder shear properties is also presented.

CMSE *Lab* N_f Results

Appendix F contains a list of the mixture *Lab* N_f results consistent with the CMSE analysis procedure described in Chapter V and illustrated by Eq. (9-5).

$$Lab\ N_f = \left[N_i + N_P\right] \tag{9-5}$$

Like for the ME approach, these results were analyzed at 95% reliability level using a typical spreadsheet descriptive statistics tool and the SPSS V11.5 software based on a one-sample t-test statistical analysis (Montgomery et al. 2001). The results represent mean values of, at most, eight individual *Lab* N_f predictions based on actual material properties such as σ_t, DPSE (b), E_i, and m values measured from at least two test specimens per mixture type per aging condition. Table 9-2 illustrates this statistical analysis, and Table 9-3 is an example of a typical SPSS V11.5 one-sample t-test statistical analysis (with an assumed t- value of zero) for the Bryan mixture (0 months) at a 95% reliability level for PS#1 under the WW environment.

Table 9-2. Example of CMSE Statistical Analysis (Spreadsheet Descriptive Statistics)

#	**Material Property Combination**	**Lab N_f**	**Ln (Lab N_f)**
1	$[\sigma_{t1}]$, $[b_1]$, $[E_1,m_1]$	N_1	Ln N_1
2	$[\sigma_{t1}]$, $[b_1]$, $[E_2,m_2]$	N_2	Ln N_2
3	$[\sigma_{t1}]$, $[b_2]$, $[E_2,m_2]$	N_3	Ln N_3
4	$[\sigma_{t1}]$, $[b_2]$, $[E_1,m_1]$	N_4	Ln N_4
5	$[\sigma_{t2}]$, $[b_1]$, $[E_1,m_1]$	N_5	Ln N_5
6	$[\sigma_{t2}]$, $[b_1]$, $[E_2,m_2]$	N_6	Ln N_6
7	$[\sigma_{t2}]$, $[b_2]$, $[E_2,m_2]$	N_7	Ln N_7
8	$[\sigma_{t2}]$, $[b_2]$, $[E_1, m_1]$	N_8	Ln N_8
Mean Ln (Lab N_f)			$\bar{x}$
Stdev			σ
COV (%)			$\frac{100\sigma}{\bar{x}}$
95% PI			$\bar{x} \pm t_{\frac{\alpha}{2},n-2}\left(\frac{\sigma}{\sqrt{n}}\right)$

Table 9-3. Example of SPSS V11.5 Analysis (Bryan Mixture, 0 Months, PS# 1, WW)

#	**Material Property Combination**	**Calculated Lab N_f ($N_i + N_p$)**	**SPSS Input Data (Ln [Lab N_f])**
1	$[\sigma_{t1}]$, $[b_1]$, $[E_1,m_1]$	6.28 E+06	15.65
2	$[\sigma_{t1}]$, $[b_1]$, $[E_2,m_2]$	5.70 E+06	15.56
3	$[\sigma_{t1}]$, $[b_2]$, $[E_2,m_2]$	7.65 E+06	15.85
4	$[\sigma_{t1}]$, $[b_2]$, $[E_1,m_1]$	6.30 E+06	15.66
5	$[\sigma_{t2}]$, $[b_1]$, $[E_1,m_1]$	8.50 E+06	15.96
6	$[\sigma_{t2}]$, $[b_1]$, $[E_2,m_2]$	4.28 E+06	15.27
7	$[\sigma_{t2}]$, $[b_2]$, $[E_2,m_2]$	5.00 E+06	15.42
8	$[\sigma_{t2}]$, $[b_2]$, $[E_1,m_1]$	8.04 E+06	15.90
SPSS V11.5 Output Data @ 95% Reliability Level (One-Sample T-Test Analysis)			
Mean Ln (Lab N_f)			15.658 (6.31 E+06)
95% lower Ln (Lab N_f)PI			15.458 (5.17 E+06)
95% upper Ln (Lab N_f)PI			15.859 (7.71 E+06)
Stdev			0.240
COV of Ln (*Lab N_f*)			1.53%

In terms of statistical variability, the overall COV of *Ln* N_f ranged between 1.53% and 2.9%. The overall 95% *Lab* N_f PI range was 0.80×10^6 to 13.12×10^6 (Appendix F). Considering HMAC mixture inhomogeneity, test variability, and experimental errors, these results are reasonable and indicate better repeatability and precision compared to the ME approach.

Fig. 9-3 is a plot of the *Lab* N_f as a function of aging condition and indicates that mixture *Lab* N_f decreases significantly with aging and that the Yoakum mixture exhibited better fatigue resistance in terms of higher *Lab* N_f values at all aging conditions. Like for the ME approach, this trend was observed for all pavement structures in both the WW and DC environmental conditions and was consistent with the measured CMSE mixture material properties reported in Chapter VIII. Fig. 9-3 further shows that the rate of the Bryan mixture's N_f decline due to binder oxidative aging was relatively higher than that of Yoakum mixture, indicating that it (the Bryan mixture) was probably more sensitive to aging.

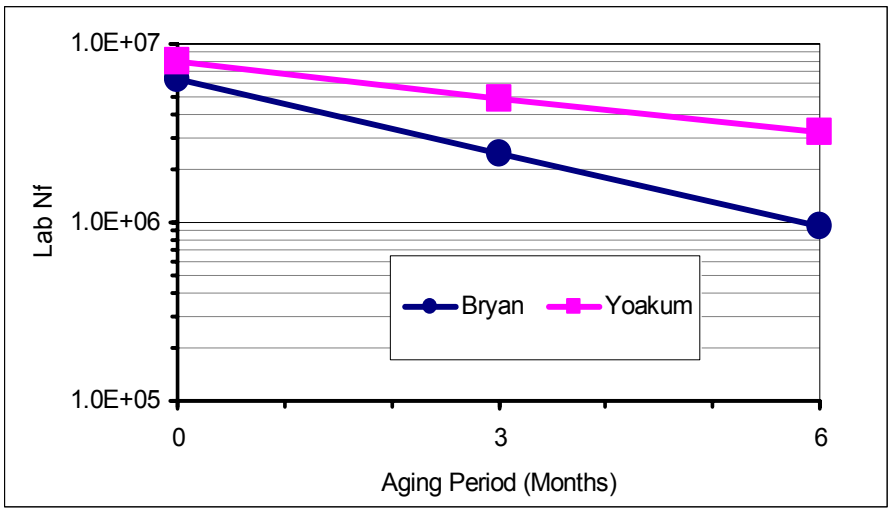

Fig. 9-3. CMSE *Lab* N_f for PS#1, WW Environment

CMSE *Field* N_f Results

Fig. 9-4 is a plot of the *Field* N_f on a semi-log scale as a function of the pavement age based on the 0, 3, and 6 months laboratory aging exposure conditions.

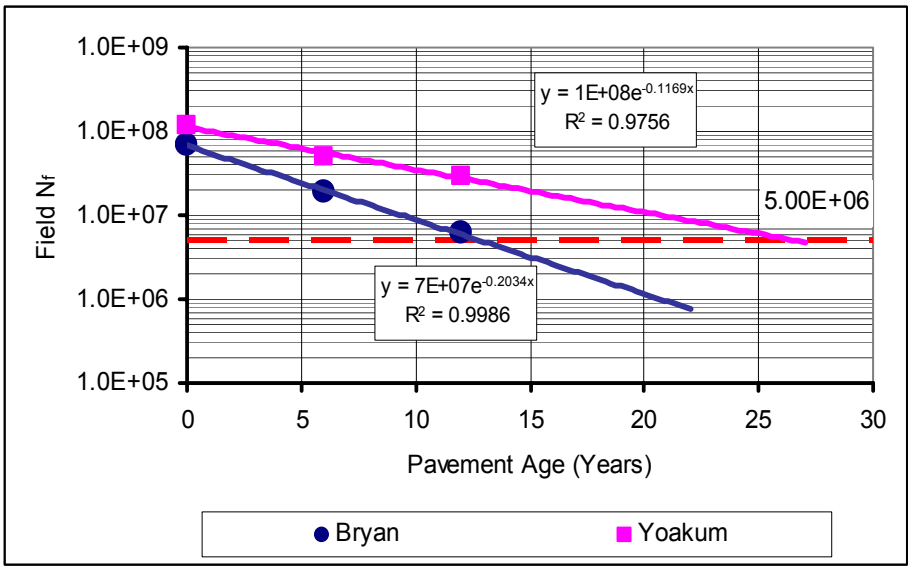

Fig. 9-4. CMSE *Field* N_f for PS#1, WW Environment

Detailed *Field* N_f results for other PSs are contained in Appendix G. These *Field* N_f predictions were determined from *Lab* N_f and the shift factors discussed in Chapter VIII. The CMSE computation of *Field* N_f is illustrated in Eq. (9-6). Definitions of the parameters in this equation can be found in Chapter V.

$$Field\ N_f = SF_a \times SF_h \left[Lab\ N_f \right] = SF_a \times SF_h \left[N_i + N_P \right] \qquad (9\text{-}6)$$

Fig. 9-4 indicates an exponentially declining N_f trend with aging for both mixtures and that the rate of N_f decay is mixture dependent based on the slopes of the exponential trend lines fitted through the N_f data points.

For mixture comparison, the better fatigue resistance of the Yoakum mixture in terms of *Field* N_f magnitude is clearly evident. Based on the 5×10^6 design traffic ESALs over a 20-year service life at a 95% reliability level, Fig. 9-4 indicate inadequate and adequate theoretical fatigue performance for the Bryan and Yoakum mixture, respectively. According to this analysis, the Bryan mixture will theoretically fail prematurely based on Fig. 9-4, approximately in the 13^{th} year of service, whereas, the Yoakum mixture will sustain the applied traffic ESALs up to about the 26^{th} year of service.

THE CM APPROACH

In this section, the N_f results based on the CM analysis are presented. Note that the analysis procedure for both *Lab* and *Field* N_f is similar to the CMSE approach except for the absence of SE and RM data in compression in the CM analysis.

CM *Lab* N_f Results

The CM *Lab* N_f results are contained in Appendix F and do not differ significantly from the CMSE results both in terms of the N_f magnitude and variability. Fig. 9-5 is an example of the CM *Lab* N_f plot for PS#1 under the WW environment. The decreasing N_f trend with aging is again evident, with the Yoakum mixture exhibiting better fatigue resistance in terms of N_f magnitude.

Table 9-4 is a summary comparison of the CMSE-CM results for PS#1 under the WW environment. For these two HMAC mixtures under consideration, the CM results are insignificantly different from the CMSE results. The difference based on the CMSE results as a benchmark is less than 10%.

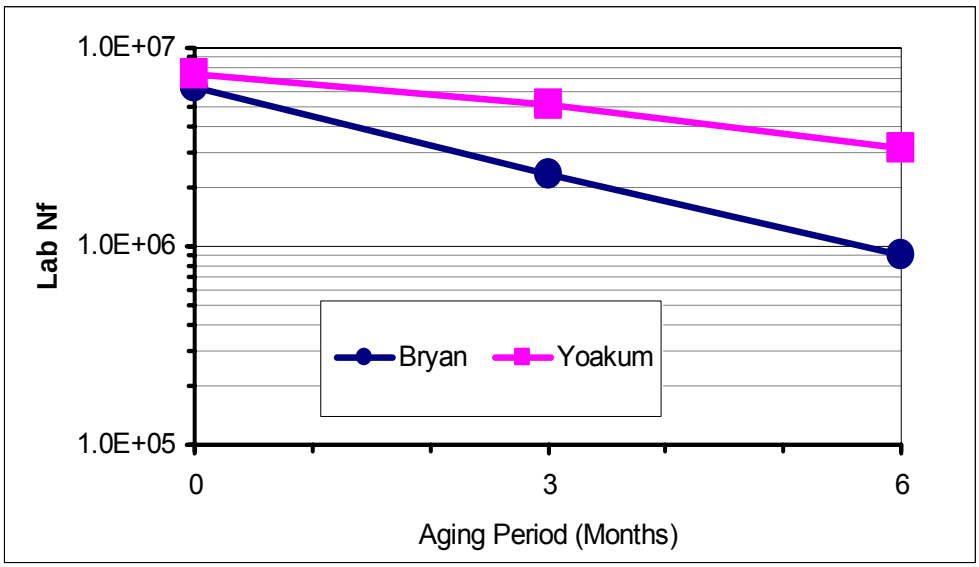

Fig. 9-5. CM *Lab* N_f for PS#1, WW Environment

Table 9-4. Comparison of CMSE-CM N_f Results for PS#1, WW Environment

Aging Condition	Mixture	Mixture *Lab* N_f		Difference
		CMSE	CM	
0 months	Bryan	6.31 E+06	6.29 E+06	-0.32%
	Yoakum	7.88 E+06	7.28 E+06	-7.61%
3 months	Bryan	2.42 E+06	2.31 E+06	-4.55%
	Yoakum	4.95 E+06	5.17 E+06	+4.44%
6 months	Bryan	0.94 E+06	0.91 E+06	-3.19%
	Yoakum	3.23 E+06	3.13 E+06	-3.10%

Overall, this correlation between the CM and CMSE *Lab* N_f results suggests that the CM approach can be utilized for mixture fatigue analysis in lieu of the CMSE approach. This may in turn minimize costs in terms of both laboratory testing and data analysis. Note that SE measurements (binder and aggregate) and RM tests in compression are not required in the CM approach.

The correlation (Table 9-4) between the CM and CMSE results was expected because the CM empirical analysis models were modified and calibrated to the CMSE approach. Consequently, more independent HMAC mixtures need to be characterized to validate this correlation.

CM *Field* N_f Results

CM *Field* N_f results are contained in Appendix G. Like for the *Lab* N_f, the mixture performance trend and fatigue resistance measured in terms of *Field* N_f magnitude were similar to the CMSE predictions and did not differ by more than 10%.

Fig. 9-6 is a plot of the CM *Field* N_f for PS#1 in the WW environment and is consistent with the CMSE predictions in Fig. 9-4.

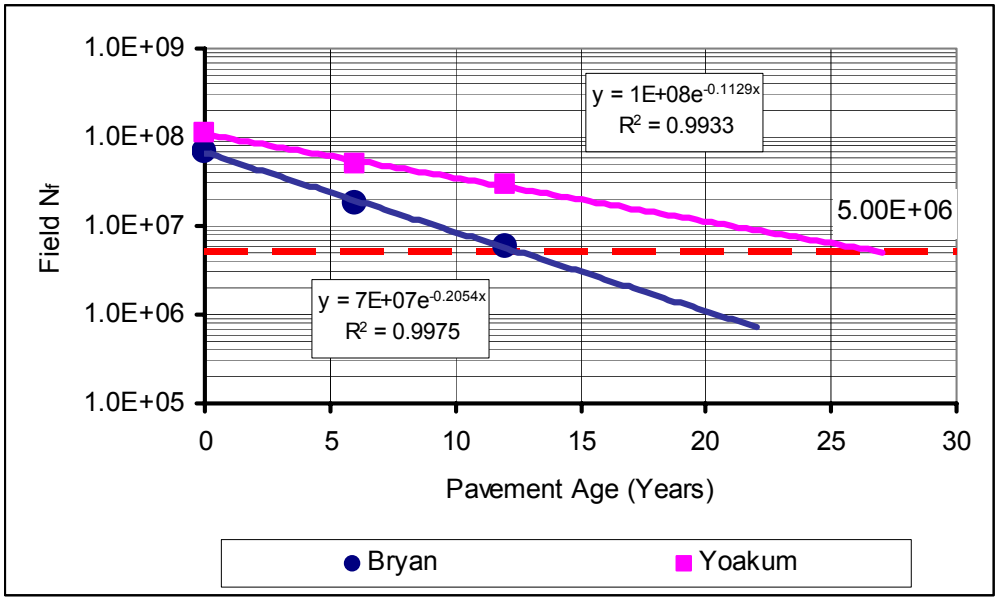

Fig. 9-6. CM *Field* N_f for PS#1, WW Environment

Like for the CMSE approach, Fig. 9-6 shows poor fatigue resistance for the Bryan mixture with inadequate theoretical fatigue performance based on 5×10^6 design traffic ESALs over a 20-year service life at a 95% reliability level. Fig. 9-6 also exhibits an exponential relationship between N_f and pavement age with an R^2 value of greater than 95% for both mixtures.

DEVELOPMENT OF A CMSE/CM SHIFT FACTOR DUE TO AGING

As part of this study's secondary objective, an attempt was made to develop a shift factor (SF_{ag}) that accounts for binder oxidative aging when predicting mixture *Field* N_f using the CMSE and CM approaches. This section discusses the SF_{ag} development based on the binder DSR tests that were conducted by CMAC (Walubita et al. 2005). The CMSE and CM *Field* N_f predictions using the developed SF_{ag} and *Field* N_f at 0 months are also provided.

Theoretical Basis and Assumptions

In this analysis, the SF_{ag} was solely based on neat binder shear properties and the following assumptions; where neat binder refers to binder not mixed with aggregate but that directly aged in thin films:

- SF_{ag} was considered as a multiplicative factor that tends to reduce N_f, and therefore its magnitude was postulated to range between 0 and 1 ($0 < SF_{ag} \leq 1$). A numerical SF_{ag} value of 1 represents unaged conditions or no consideration of aging effects in N_f analysis.
- SF_{ag} was only considered as a function of the neat binder properties in terms of the DSR function (DSR_f) and oxidative aging period (time). The hypothesis is that only the binder in the HMAC mixture ages, and therefore it is not unreasonable to determine SF_{ag} solely based on binder properties. The idea is that researchers and/or end users would only measure unaged and aged binder properties without having to measure aged mixture properties, and thereafter

estimate SF_{ag} and ultimately predict aged mixture *Field* N_f from unaged mixture *Field* N_f.

- The DSR_f was utilized on the hypothesis that this function provides a better representation of the binder shear properties in terms of ductility and durability; properties that are considered critical to fatigue performance for aged field HMAC pavements (Glover et al. 2005).
- The binder oxidative aging conditions as conducted by CMAC were consistent with the SAFT and PAV* procedures to simulate both short-term aging that occurs during the hot-mixing process and construction operations and long-term aging during service (Vassiliev et al. 2002). These laboratory aging conditions were SAFT + PAV* 0 hr, SAFT + PAV* 16 hr, and SAFT + PAV* 32 hr, respectively, and simulate approximately up to 6 years of Texas field HMAC aging exposure (Glover et al. 2005, Walubita et al. 2005). In contrast to the standard PAV aging, PAV* involve aging of the binder in 1 mm thin films.
- In contrast to SAFT + PAV* laboratory aging of binders, field aging is a relatively complex process involving fluctuating environmental conditions (e.g., varying temperatures) and a general decreasing AV content due to traffic compaction. These factors were not directly taken into account by the SF_{ag} developed in this study. It must also be emphasized that the effect of aging on HMAC mixture fatigue resistance is hypothetically considered a three-stage process involving binder oxidation, binder hardening, and mixture *Field* N_f decay. Additionally, mixture design parameters such as binder content and polymer modification probably also play a significant role in these three processes.

SF_{ag} Formulation and the Binder DSR Master-Curves

In this study, the SF_{ag} was formulated as a function of the DSR data from the binder DSR master-curve as shown by Eq. (9-7):

$$SF_{ag} = u\left[\chi(t)\right]^{w} \tag{9-7}$$

$$\chi(t) = \left(\frac{m'@t_i}{m'@t_0}\right)\left(\frac{DSR_{f(1)}@t_0}{DSR_{f(1)}@t_i}\right) \quad (9\text{-}8)$$

$$DSR_f = \left[G'/(\eta'/G')\right] \quad (9\text{-}9)$$

$$DSR_f(\varpi) = DSR_{f(1)}(\varpi)^{m'} \quad (9\text{-}10)$$

Where:

SF_{ag} = Shift factor due to binder oxidative aging

$\chi(t)$ = Material property ratio that relates the aged to the unaged binder shear properties as a function of time

u, w = Material regression constants

m' = Slope of the binder $DSR_f(\omega)$ master-curve within a reduced angular frequency range of 1 E-06 to 1 E+02 rad/s at 20 °C

ϖ = Reduced angular frequency (rad/s)

$DSR_{f(1)}$ = $\left[G'/(\eta'/G')\right]$ at 1 rad/s (Pa·s)

G', η' = Elastic dynamic shear modulus (MPa) and dynamic viscosity (Pa·s)

Fig. 9-7 is a plot of the binder DSR master-curves on a log-log scale in the form of a power function expressed by Eq. (9-10). Note that these DSR master-curves were generated from DSR test data that were measured by CMAC, including laboratory aging of the binders (Walubita et al. 2005).

For analysis simplicity, SAFT + PAV* 0 hr was assumed to be equivalent to 1 year Texas field HMAC exposure, SAFT + PAV* 16 hr to 2 years, and SAFT + PAV* 32 hr to 6 years (Glover et al. 2005). The SF_{ag} at 0 years field HMAC exposure was arbitrarily assigned a numerical SF_{ag} value of 1 on the premise that no significant aging occurs during this period. Based on the data from Fig. 9-7 and using Eq. (9-7), SF_{ag} values were estimated as a function of pavement age as shown in Table 9-5.

Table 9-5. CMSE-CM SF_{ag} Values

Pavement Age (Years)	SF_{ag}	
	PG 64-22 (Bryan)	PG 76-22 (Yoakum)
0	1.000	1.000
1	0.854	0.783
2	0.330	0.303
6	0.160	0.221
12	0.073	0.109
18	0.049	0.081
20	0.045	0.070

Note that SF_{ag} values beyond 6 years field HMAC exposure were determined based on the SAFT + PAV* 0hr, SAFT + PAV* 16 hr, and SAFT + PAV* 32 hr data. Additional laboratory aging conditions are recommended, i.e., SAFT + PAV* 64 hr and SAFT + PAV* 128 hr, that may be realistically close to a 20-year field HMAC exposure, which is consistent with typical HMAC pavement design periods. But this is of course bearing in mind that over aged binders may be impractical to test in the DSR test protocol due to high stiffness values.

CMSE-CM *Field* N_f Prediction Using SF_{ag}

Using the SF_{ag} data in Table 9-5 and the *Field* N_f at 0 years field HMAC aging exposure, the *Field* N_f at any pavement age can be estimated using the following relationship:

$$Field\ N_{f(t_i)} = SF_{ag(t_i)} \times Field\ N_{f(t_0)} \tag{9-11}$$

Table 9-6 provides an example of the estimated *Field* N_f at year 20 for PS#1 and the WW environment at a 95% reliability level. Predictions for other PSs and the DC environment are contained in Appendix G.

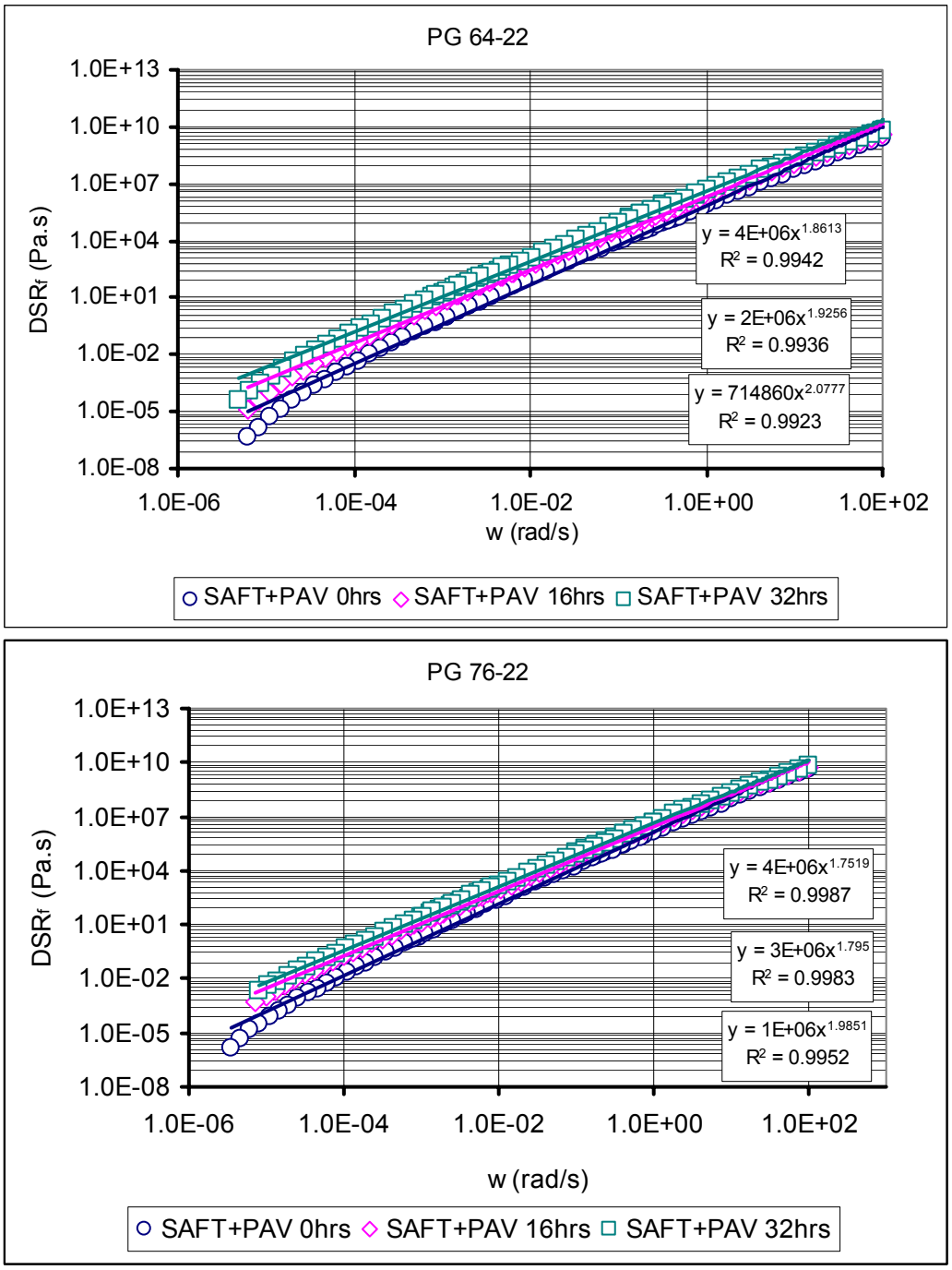

Fig. 9-7. Binder $DSR_f(\omega)$ Master-Curves at 20 °C

Table 9-6. *Field* N_f Predictions at Year 20 for PS#1, WW Environment

Approach	Mixture	*Field* N_f at Year 20 and 95% Reliability Level		
		Mean N_f	COV of ($Ln\ N_f$)	95% PI
CMSE	Bryan	3.11 E+06	2.81%	3.08 – 3.21 E+06
	Yoakum	8.40 E+06	3.92%	6.95 – 9.82 E+06
CM	Bryan	3.10 E+06	2.93%	2.98 – 4.47 E+06
	Yoakum	7.77 E+06	3.98%	6.12 – 8.08 E+06
Design traffic ESALs over 20-year design period at 95% reliability level: 5.00 E+06				

From Table 9-6, both the N_f magnitude and statistical variability from the two approaches do not differ significantly. In fact, both approaches indicate inadequate and adequate theoretical fatigue performance for Bryan and Yoakum mixtures, respectively.

Overall, while the SF_{ag} methodology utilized in this study produced reasonable results, validation of these concepts is still required through testing of additional binders and HMAC mixtures, possibly with longer laboratory aging periods that realistically simulate current HMAC pavement design practices. The further development of representative SF_{ag}, particularly as a function of time, with more research will inevitably allow for realistic N_f predictions at any desired pavement age.

THE MEPDG APPROACH (*FIELD* N_f)

The mixture *Field* N_f results from the MEPDG software analysis are presented in Appendix G as mean values of at least three test specimens per mixture type. These *Field* N_f values were back-calculated from the percentage cracking output from the MEPDG software analysis based on a 50% cracking failure criteria using the statistical analysis software SPSS V11.5. Table 9-7 illustrates an example of the MEPDG software analysis for the Bryan mixture based on a 20-year design period, 95% reliability level, and the WW environment for PS#1 (Table 3-7, Chapter III).

Table 9-7. Example of the MEPDG Software Analysis (Bryan Mixture)

PS#	HMAC Specimen	AV	Environment	Traffic ESALs	Output % Cracking in Wheelpath
1	BDM0001	6.6%	WW	2.50E+06	26.80%
1	BDM0002	7.5%	WW	2.50E+06	38.30%
1	BDM0003	6.9%	WW	2.50E+06	31.80%
1	BDM0001	6.6%	WW	5.00E+06	45.60%
1	BDM0002	7.5%	WW	5.00E+06	59.90%
1	BDM0003	6.9%	WW	5.00E+06	51.60%

Details of the MEPDG software analysis for other pavement structures and environmental conditions for both the Bryan and Yoakum mixtures are included in Appendix G. From this analysis, the actual *Field* N_f were then back-calculated based on the input traffic ESALs and output percent cracking in the wheelpath using the statistical analysis software SPSS V11.5 (Montgomery et al. 2001). Linear regression was utilized for SPSS V11.5 analysis. Essentially, both the traffic ESALs and the output percentage cracking from the MEPDG software analysis constitute input data for the SPSS V11.5 software.

Table 9-8 shows an example of the SPSS V11.5 *Field* N_f prediction for the Bryan mixture based on the data from Table 9-7. For this study, the cracking failure criterion was bottom-up 50% cracking in the wheelpath at a 95% reliability level.

Table 9-8. Example of SPSS V11.5 Analysis (Bryan Mixture)

SPSS V11.5 Input Data (from MEPDG Software Analysis)		
Data#	**Cracking (%)**	**Field N_f (Traffic ESALs)**
1	26.80%	2.50E+06
2	38.30%	2.50E+06
3	31.80%	2.50E+06
4	45.60%	5.00E+06
5	59.90%	5.00E+06
6	51.60%	5.00E+06
7	*50.00%*	*(SPSS prediction point)*
Reliability level = 95%		
SPSS V11.5 Output Data @ 95% Reliability Level (Linear Regression Analysis)		
Field N_f prediction at 50% cracking		4.71E+06
95% lower prediction interval		1.93E+06
95% upper prediction interval		9.74E+06

According to Table 9-8 based on input data from Table 9-7, the predicted *Field N_f* at 50% cracking and 95% reliability level is 4.71×10^6 with a 95% PI range of 1.93×10^6 to 9.74×10^6. The results in Table 9-8 and those in Appendix G represent *Field N_f* values that incorporate laboratory-to-field shift factors and aging effects over a 20-year design period based on the GAM incorporated in the software. Essentially, these *Field N_f* results represent the number of traffic ESALs that the HMAC pavement structure can carry over a 20-year design life prior to 50% fatigue cracking in the wheelpath at 95% reliability level. Fig. 9-8 is an example of the mixture *Field N_f* results from the MEPDG software analysis for PS#1 under the WW Environment for both mixtures.

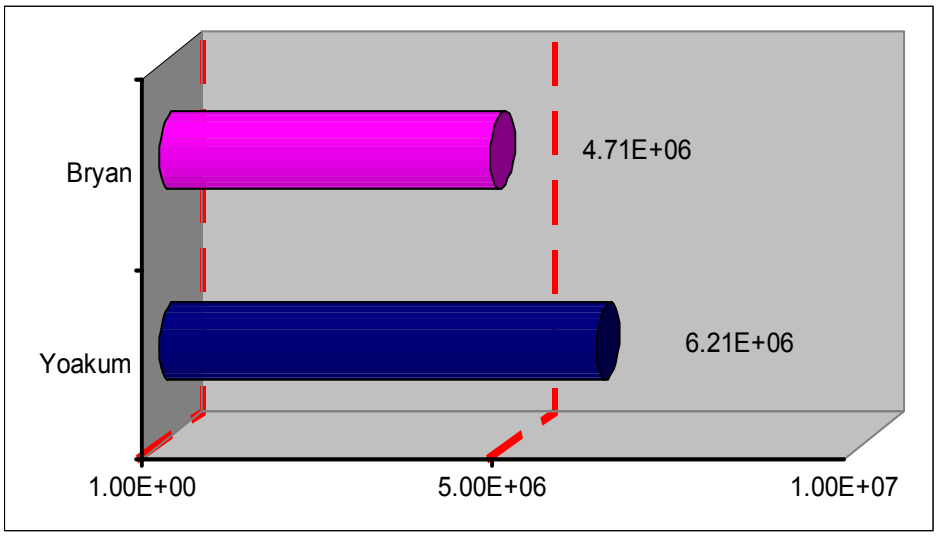

Fig. 9-8. *Field* N_f for PS#1, WW Environment

The comparatively higher *Field* N_f value of the Yoakum mixture for PS#1 under the WW environment shown in Fig. 9-8 is consistent with the predictions made by the other fatigue analysis approaches discussed in this dissertation. Considering a 20-year design service life with traffic design ESALs of 5.0×10^6, Fig. 9-8 shows that only the Yoakum mixture passes the 50% wheelpath cracking failure criterion at a 95% reliability level.

Generally, the MEPDG software predicted higher *Field* N_f values for the Yoakum mixture in all the pavement structures and environmental conditions (see Appendix G) considered. This improved fatigue resistance of the Yoakum mixture in terms of higher *Field* N_f values was attributed to the higher binder content in the mixture. Note that binder content is a direct input parameter in the MEPDG software, and therefore *Field* N_f can be tied directly to this parameter. In this study, the MEPDG software was generally observed to exhibit greater sensitivity to mixture volumetrics such as binder content and AV, and also showed high N_f statistical prediction variability for the HMAC mixture (Yoakum) designed with a modified binder. Table 9-9 illustrates the N_f statistical variability in terms of the 95% N_f PI for the WW environment.

Table 9-9. Summary of MEPDG Mean *Field* N_f and 95% *Field* N_f PI (WW)

PS#	Mean Field N_f		95% Field N_f PI Range			
	Bryan	**Yoakum**	**Bryan [Lower]**	**Bryan [Upper]**	**Yoakum [Lower]**	**Yoakum [Upper]**
1	4.71E+06	6.21E+06	1.93E+06	9.74E+06	2.04E+06	15.34E+06
2	4.05E+06	5.75E+06	2.00E+06	6.35E+06	2.35E+06	10.54E+06
3	1.93E+06	3.41E+06	0.00E+06	3.74E+06	0.14E+06	7.77E+06
4	2.02E+06	2.97E+06	0.28E+06	3.56E+06	0.35E+06	6.00E+06
5	19.29E+06	----------	14.20E+06	24.83E+07	----------	----------

Clearly, Table 9-9 shows a relatively higher 95% N_f PI range for the Yoakum mixture. This result further suggests that the software might be more sensitive to modified binders. In terms of AV sensitivity, Table 9-10 shows that a difference of approximately 1% in specimen AV content results in about 5% difference in the predicted *Field* N_f for the Bryan mixture and correspondingly 10% difference for the Yoakum mixture (Table 9-10). Based on this analysis, these results show that AV has a significant effect on both the *Field* N_f magnitude and statistical variability.

Table 9-10. Example of Effects of AV on N_f Prediction (Bryan Mixture)

PS	HMAC Specimen	AV	Environment	Predicted N_f
1	BDM0001	6.6%	WW	5.64E+06
1	BDM0002	7.5%	WW	3.67E+06
1	BDM0003	6.9%	WW	4.80E+06
Mean *Field* N_f				4.70E+06
95% PI				1.93 – 9.74 E+06

Table 9-11. Example of Effects of AV on N_f Prediction (Yoakum Mixture)

PS	HMAC Specimen	AV	Environment	Predicted N_f
1	YDM0001	6.80%	WW	7.93E+06
1	YDM0002	6.90%	WW	6.47E+06
1	YDM0003	7.30%	WW	4.24E+06
Mean *Field* N_f				6.21E+06
95% PI				2.04 – 15.34 E+06

Fig. 9-9 illustrates the N_f-AV relationship for both the Bryan and Yoakum mixtures, respectively. Clearly, the software N_f predictions show greater dependence on the AV content, and the predicted N_f decreases almost exponentially as the specimen AV content increases. Notice also that both Tables 9-10 and 9-11 and Fig. 9-9 show comparatively greater N_f variability and AV sensitivity for the Yoakum mixture. Like binder content, specimen AV content is a direct input parameter in the MEPDG software for Level 1 analysis. Ultimately, these results show that mixture volumetrics play a significant role in the fatigue performance of HMAC pavements.

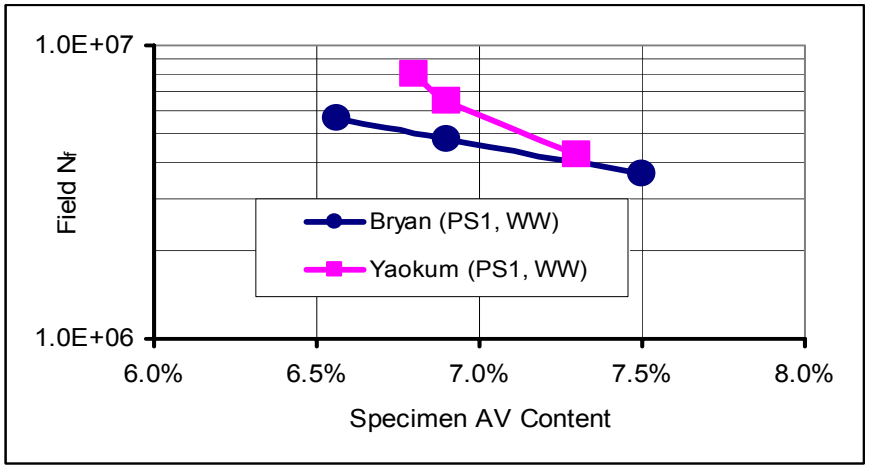

Fig. 9-9. *Field* N_f-AV Relationship for PS#1, WW Environment

COMPARISON OF HMAC MIXTURE FATIGUE RESISTANCE

Generally, all fatigue analysis approaches predicted higher N_f (both lab and field) values for the Yoakum mixture under all aging and environmental conditions for all the pavement structures. Mixture property results discussed in Chapter VIII also indicated better fatigue-resistant properties for the Yoakum mixture than the Bryan mixture, and therefore better performance in terms of N_f (lab or field) magnitude under the test conditions considered in this study was expected. Fig. 9-10 is an example of the mixture field N_f comparison for WW environmental conditions for PS#1.

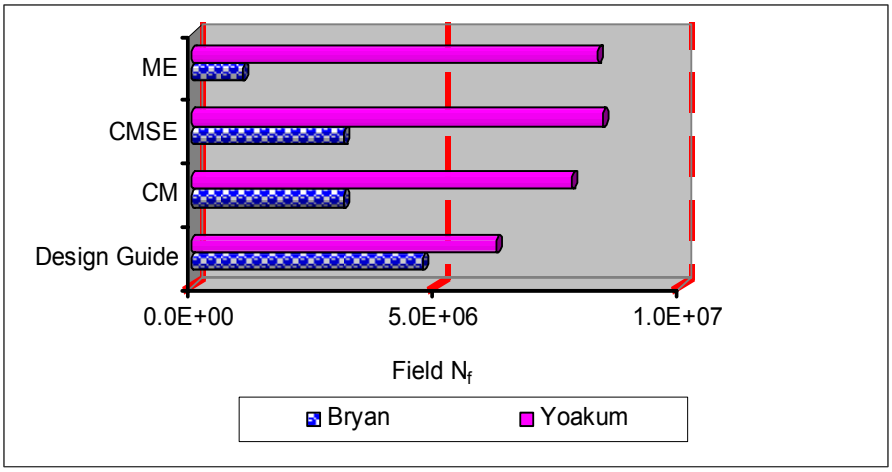

Fig. 9-10. *Field N_f* for PS#1, WW Environment

For all the fatigue analysis approaches, Fig. 9-10 shows better fatigue resistance for the Yoakum mixture in terms of *Field N_f* magnitude compared to the Bryan mixture. Based on the 5×10^6 design traffic ESALs and 20-year service life at a 95% design reliability level for this PS and the environmental conditions under consideration, all the fatigue analysis approaches (although with different failure criteria) indicate inadequate and adequate theoretical fatigue performance for the Bryan and Yoakum mixtures, respectively.

In summary, while the N_f predictions by all the fatigue analysis approaches were comparable, the Yoakum mixture generally exhibited better fatigue resistance in all the PSs and environmental conditions under consideration. The Bryan mixture, in contrast, exhibited the greatest rate of N_f decay, indicating a higher susceptibility to binder oxidative aging and consequently performed poorly in terms of N_f magnitude. Considering that the Yoakum mixture was designed with a stiffer SBS modified PG 76-22 binder, this relatively better fatigue resistance in terms of *Field* N_f results was theoretically unexpected. In fact, the theoretical expectation was that the Yoakum mixture's fatigue resistance in terms of *Field* N_f magnitude would be worse than the Bryan mixture. However, the actual response behavior was attributed to the following factors:

- Compared to the Bryan mixture, the Yoakum mixture had relatively higher binder content (5.6% versus 4.6% by weight of aggregate).
- Contrary to theoretical expectations based solely on binder stiffness, the SBS modifier probably improved the Yoakum mixture's fatigue resistance as well as reducing its susceptibility to binder oxidative aging.
- The Yoakum mixture incorporated 1% hydrated lime in the mix-design. Although lime is often added to improve mixture resistance to moisture damage, this lime perhaps increased the mixture's resistance to both fatigue damage and aging. Wisneski et al. (1996) made similar observations that lime tended to improve the fatigue performance of asphalt mixtures.
- SE results in Chapter VIII indicated a better fracture resistance and stronger potential to heal for the Yoakum mixture than for the Bryan mixture. Based on these SE results, it can be hypothesized that the PG 76-22 binder-gravel aggregate had an increased bond strength compared to that of the PG 64-22 binder-limestone aggregate combination. Note that one of the SE measurements' objectives is often to asses the affinity and bond (cohesive and/or adhesive) strength of binders and aggregates. Theoretically, a comparatively better bond

strength compatibility between the binder and aggregate (in this case for the Yoakum mixture) is generally expected to exhibit superior performance.

- Tensile strength and RM results in Chapter VIII indicated that the Yoakum mixture was more ductile and less susceptible to stiffness age-hardening compared to the Bryan mixture, properties which probably contributed to its higher *Field* N_f values. Additionally, the Yoakum mixture exhibited better potential to relax the applied stress as indicated by higher *m* values compared to the Bryan mixture.

Theoretically, stiffer HMAC mixtures are generally poor in fatigue, particularly for thin pavement structures where controlled strain is generally the applicable testing condition. By contrast, this finding suggests that an initially stiffer HMAC mixture or mixture designed with a stiffer binder may not necessarily perform poorer in fatigue or be more susceptible to aging, as may be theoretically expected compared to a less stiff (flexible) HMAC mixture or mixture designed with a softer binder subjected to similar loading and environmental conditions. As noted in Chapter VIII, the Bryan mixture designed with a softer binder stiffened much faster with oxidative aging than the Yoakum mixture. This finding signifies the importance of considering the stiffness age-hardening rate due to aging when comparatively evaluating the fatigue resistance of HMAC mixtures.

In performance comparison studies of this nature, the wide spectrum of HMAC mix-design characteristics and other material properties need to be evaluated. These properties include material type, binder content, aggregate gradation, rate of stiffness age-hardening (i.e., sensitivity to aging), binder film thickness, voids in mineral aggregate (VMA), and voids filled with asphalt (VFA). Binder stiffness or the initial mixture stiffness alone may not be used as the sole determinant/indicator of mixture fatigue resistance. For example, the calculated binder film thicknesses based on Eq. (9-12) were approximately 15.42 microns (μ) and 20.36 μ for the Bryan and Yoakum mixtures, respectively (Roberts et al. 1996):

$$T_F = 1000\left(\frac{V_{asp}}{SA \times W}\right) \quad (9\text{-}12)$$

where:

T_F = Average binder film thickness (microns)

V_{asp} = Effective binder volume (liters)

SA, W = Aggregate surface area (m^2/kg) and weight (kg), respectively.

According to Roberts et al. (1996), binder film thickness is generally correlated with performance/durability, and thin binder films are often more susceptible to oxidation than thicker binder films due to ease of air infiltration in the compacted HMAC mixture. Rapid binder oxidation often results in a more brittle HMAC mixture and consequently, a decreased resistance to fatigue damage. This perhaps explains the greater sensitivity of the Bryan mixture (with a relatively thin binder film thickness) to aging based on the mixture property results presented in Chapter VIII and the relatively poor fatigue performance in terms of N_f magnitude. By contrast, the Yoakum mixture with a relatively thicker binder film thickness performed comparatively better in terms of N_f magnitude. Generally, HMAC mixtures with thinner binder film thicknesses have been reported to exhibit greater susceptibility to traffic and environmental damage including fatigue, moisture damage, and raveling (Roberts et al. 1996).

Overall, these results suggest that binder stiffness or initial mixture stiffness alone may not be used as the sole determinant of mixture fatigue resistance or field fatigue performance. A mixture designed with a stiffer binder may not necessarily perform poorly in fatigue compared to a mixture designed with a softer binder. The entire mix-design matrix and other material properties need to be evaluated, particularly in performance comparison studies of this nature. Equally to be considered is the pavement structure, the environmental conditions, the HMAC mixture sensitivity to aging in terms of binder oxidation and stiffness age-hardening rate, and probably even the binder's potential to heal during traffic loading rest periods.

HMAC MIXTURE VARIABILITY AND STATISTICAL ANALYSIS

In general, higher statistical variability was observed in both mixture properties and N_f results for the Yoakum mixture. Compared to the Bryan mixture, the Yoakum mixture consists of a stiffer SBS modified PG 76-22 binder that is relatively harder to work with when mixing, compacting, and sawing/coring. Table 9-12 shows an example of the mixture AV variability associated with the laboratory HMAC specimen fabrication process.

Table 9-12. Example of HMAC Specimen AV Variability

Specimen	Mixture	Target AV	Average AV	Stdev	COV
Cylindrical	Bryan	7±0.5%	7.23%	0.20	2.81%
	Yoakum	7±0.5%	7.10%	0.35	5.94%
Beam	Bryan	7±0.5%	7.18%	0.29	4.04%
	Yoakum	7±0.5%	6.98%	0.55	7.87%

Table 9-12 represents the average AV content of 10 random sample HMAC specimens per specimen type per mixture type. Although the COV values are reasonably acceptable, Table 9-12 clearly shows the high variability in the AV content for the Yoakum mixture. Modified binders are generally more difficult to work with, and consequently it is more difficult to control the AV content, which was ultimately reflected in the high variability of the final N_f results.

From Table 9-12, it is also worthwhile to note the relatively high variability in the AV for the beam specimens. In this study, it was generally more difficult to control the AV for the beam specimens during compaction due to the nature of their shape and the kneading compaction method. This high variability in the AV content was also reflected in the final ME N_f results discussed previously.

The cylindrical HMAC specimens on the other hand are compact and easy to handle, and the gyratory compaction method allows for better control of the AV content. Mixture *Field* N_f results generally indicated higher variability with the Yoakum mixture and for the ME approach for all PSs, and environmental and aging conditions. Table 9-13 provides a summary example of the mixture *Field* N_f statistical analysis in terms of the COV of Ln N_f and the 95% PI for PS#1 and WW environment. More details are attached in Appendices E and G.

Table 9-13. Example of Mixture *Field* N_f Variability for PS#1, WW Environment

Approach	**Mixture**	***Field* N_f at Year 20 and 95% Reliability Level**		
		Mean N_f	**COV (Ln N_f)**	**95% PI**
ME	Bryan	1.03 E+06	6.87%	0.49 – 2.17 E+06
	Yoakum	8.30 E+06	9.85%	5.41 – 16.74 E+06
CMSE	Bryan	3.11E+06	2.81%	3.08 – 3.21 E+06
	Yoakum	8.40 E+06	3.92%	6.95 – 9.82 E+06
CM	Bryan	3.10 E+06	2.93%	2.98 – 4.47 E+06
	Yoakum	7.77 E+06	3.98%	6.12 – 8.08 E+06
MEPDG	Bryan	4.71 E+06	N/A	1.93 – 9.74 E+06
	Yoakum	6.21 E+06	N/A	2.04 – 15.34 E+06
Design traffic ESALs over 20 year design period at 95% reliability level: 5.00 E+06				

From Table 9-13, it is evident that variability in terms of COV of *Ln* N_f and 95% PI is relatively higher for the Yoakum mixture. These COV values seem low because they are expressed in terms of logarithmic response which provides a better statistical analysis in terms of an assumed normal distribution. However, they nonetheless provide a comparative basis for the approaches.

Note that no COV of *Ln* N_f values are reported for the MEPDG in Table 9-13. This is due to the nature of the back-calculation analysis of *Field* N_f at 50% cracking using percentage cracking output values from the MEPDG software. The N_f backcalculation analysis does not allow for a realistic determination of representative COVs.

Although, three DM specimens were used for each mixture, the output is just one single *Field* N_f value. From Table 9-13, it is clearly evident that the ME exhibited the highest statistical variability both in terms of the COV values and 95% PI range (particularly for the Yoakum mixture). The CMSE in contrast exhibited the least statistical variability.

EFFECTS OF OTHER INPUT VARIABLES

Among other variables, mixture fatigue resistance is dependent on the pavement structure and environment. The effect of these variables on mixture *Field* N_f assuming similar traffic loading conditions is discussed in this section.

Pavement Structure

HMAC mixture *Field* N_f prediction and fatigue performance is a function of the strain (tensile or shear) as the failure load-response parameter. For any given pavement structure (assuming similar traffic loading and environmental conditions), the critical maximum design strain is computed as a function of the number of structural layers, layer thicknesses, and material properties (i.e., the E and ν values) of the respective layers. Fig. 9-11 is an example of the effect of pavement structure on the mixture *Field* N_f under WW environmental conditions based on the Bryan and Yoakum mixtures, respectively. Structural details of these pavement structures (PS#1, PS#4, and PS#5) are summarized in Table 3-7 (Chapter III). In terms of fatigue analysis, the optimum combination of the number of layers, layer thicknesses, and E_i values that gives the lowest critical maximum design strain will result in higher *Field* N_f values and better field fatigue performance. Because fatigue cracking initiates due to horizontal tensile and/or shear strains in the HMAC layer that exceed the capacity of the HMAC, pavement structures with higher values of the critical maximum design strain will generally be more susceptible to fatigue cracking than those with lower values when subjected to similar traffic loading and environmental conditions. Table 9-14 provides a summary of the design strains associated with each PS shown in Figs. 9-11 and 9-12.

Table 9-14. PS Design Strains (WW Environment)

PS	ε_t	γ
1	1.57×10^{-4}	1.56×10^{-2}
4	2.89×10^{-4}	2.06×10^{-2}
5	0.98×10^{-4}	1.41×10^{-2}

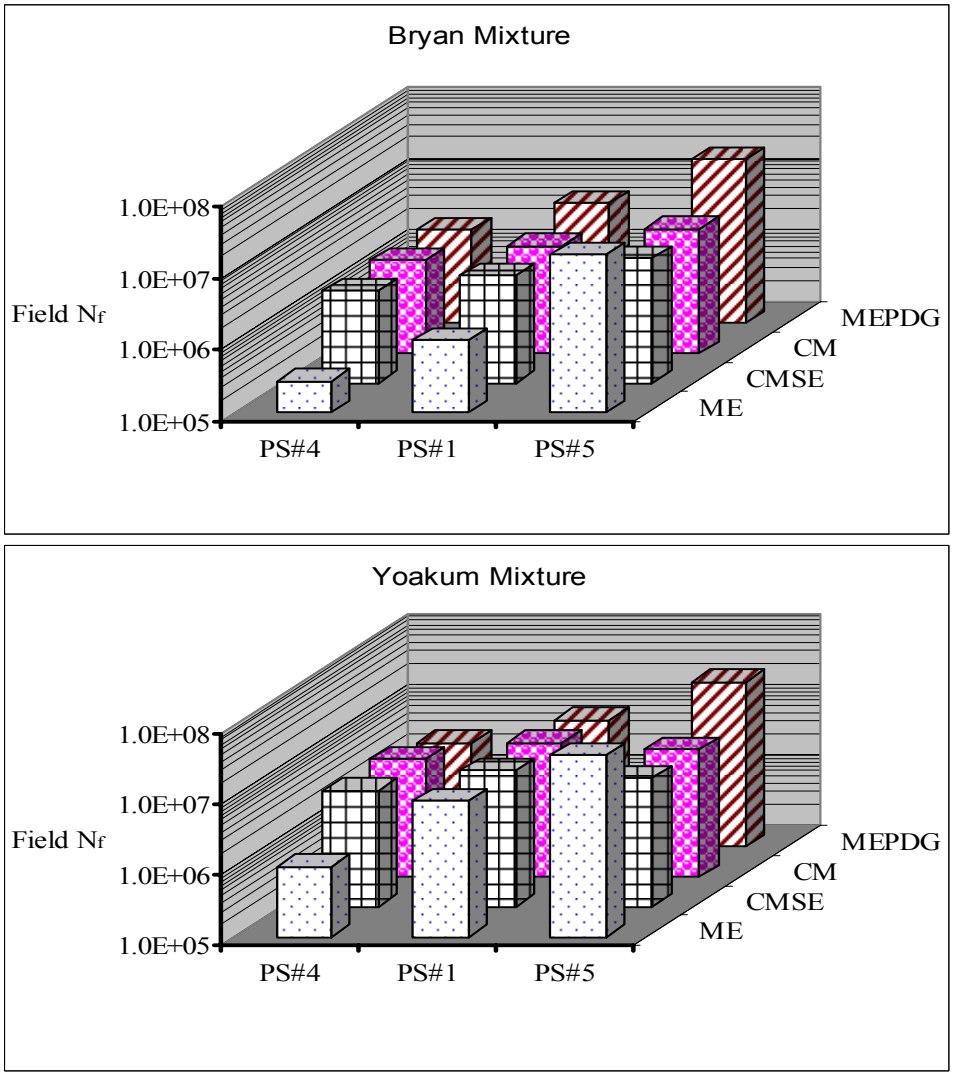

Fig. 9-11. Effect of Pavement Structure on *Field* N_f for WW Environment

As evident in Table 9-14, PS#5 has the least critical maximum design strain and therefore higher *Field* N_f values for all the fatigue analysis approaches as shown in Fig. 9-11. According to Table 3-7, PS#1 and PS#5 are three-layered pavement structures (including the subgrade), while PS#4 is four layered. However, the 100 mm (4 inch) thick HMAC layer in PS#5 is resting on a stiff cemented base that provides structural support for the loading and produces lower strains in the top HMAC layer and subsequently higher *Field* N_f values.

Environmental Conditions

As discussed in Chapters II and III, environmental conditions have a significant effect on the pavement material properties in terms of the E_i values. These E_i values in turn have an effect on the design strain that ultimately has an effect on N_f. Fig. 9-12 shows the effect of environmental conditions for PS#1 based on the MEPDG analysis that incorporates a very comprehensive climatic analysis model.

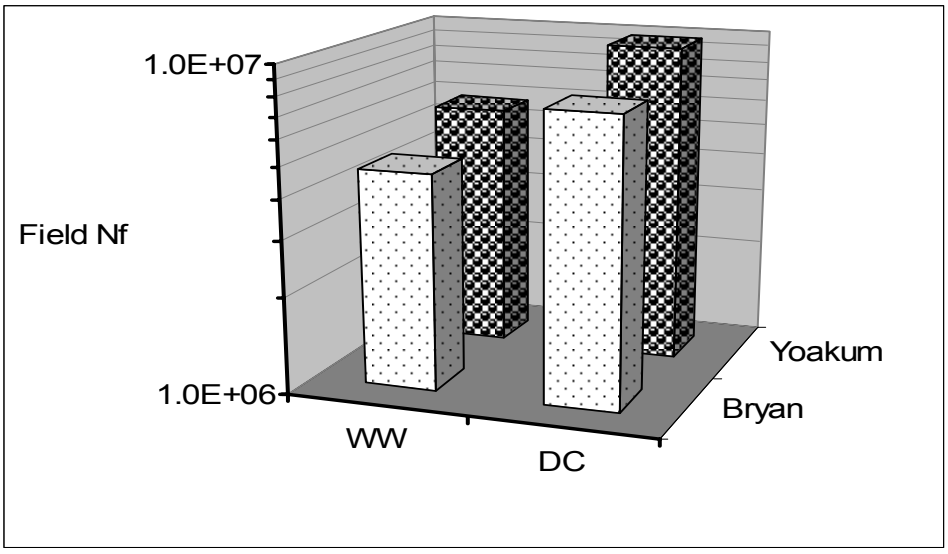

Fig. 9-12. Effect of Environmental Conditions on *Field* N_f for PS#1

From Fig. 9-12, both mixtures exhibited relatively higher field N_f values in the DC environment. The lower *Field* N_f values in the WW environment are possibly due to the wetting effect (presence of moisture) that had a significant effect on the E_i values of the unbound pavement layers including the subgrade. Note that the presence of moisture within and/or underneath a PS is to reduce the E value that ultimately results in a higher ε_t value in the HMAC layer.

Overall, these results indicate that HMAC mixture fatigue resistance depends on pavement structure and environmental location. This finding signifies the importance of adequately interfacing HMAC mixture fatigue characterization with pavement structural design and analysis to achieve adequate field fatigue performance.

SUMMARY

The bullets below summarize the findings based on the HMAC mixture fatigue life predictions using the four fatigue analysis approaches:

- HMAC mixture N_f predictions by all four fatigue analysis approaches (ME, CMSE, CM, and MEPDG) were comparable. However, the ME approach exhibited the highest statistical variability measured in terms of COV of *Ln* N_f and N_f 95% PI, particularly for the Yoakum mixture with the modified binder. The CMSE by contrast exhibited the least statistical variability, while the MEPDG exhibited the greatest potential and comprehensiveness in modeling traffic and environmental effects.
- In terms of the effects of binder oxidative aging under strain-controlled laboratory testing, the ME, CMSE, and CM approaches indicated an exponentially declining N_f trend with aging and that the rate of N_f decay is mixture dependent. This finding signifies the importance of incorporating aging effects into the fatigue design and analysis of HMAC mixtures to ensure adequate field fatigue performance.

- The CMSE/CM SF_{ag} concept utilized in the study to account for binder oxidative aging effects based on CMAC's DSR_f produced promising results. However, more research is recommended to better quantify the N_f-aging relationship and develop more representative SF_{ag} factors that will allow for realistic N_f predictions at any desired pavement age.
- As indicated by all the fatigue analysis approaches, the Yoakum (rut-resistant) mixture exhibited less sensitivity to binder oxidative aging and had better fatigue resistance measured in terms of N_f magnitude compared to the Bryan (Basic) mixture, possibly due to the higher SBS modified binder content and the 1% hydrated lime content.
- By contrast, the Bryan mixture was more susceptible to binder oxidative aging measured in terms of N_f decline, and this mixture also performed poorly in terms of N_f magnitude. Thus for mixture performance comparison studies of this nature, the entire spectrum of mix-design parameters and material properties for each respective HMAC mixture need to be evaluated.
- In terms of statistical analysis by each fatigue analysis approach, the Yoakum mixture exhibited the highest variability measured in terms of COV of $Ln\ N_f$ and N_f 95% PI range as compared to the Bryan mixture.
- As evident from the MEPDG analysis, mixture volumetrics have a significant effect on the fatigue resistance of HMAC mixtures and should be appropriately taken into account during HMAC pavement fatigue design and analysis. Note however that mixture volumetrics are not currently directly accounted for in the ME, CMSE, and CM analyses.
- The MEPDG results further indicated that HMAC mixture fatigue resistance depends on pavement structure and environmental location. This result signifies the importance of adequately interfacing HMAC mixture fatigue characterization with pavement structural design and analysis to achieve adequate fatigue performance.

CHAPTER X
COMPARISON AND EVALUATION OF THE FATIGUE ANALYSIS APPROACHES

This chapter presents a comparative evaluation of the fatigue analysis approaches including a recommendation of the best fatigue analysis approach based on a value engineering assessment criteria.

COMPARATIVE REVIEW OF THE FATIGUE ANALYSIS APPROACHES

Table 10-1 is a summary comparison of the four fatigue analysis approaches in terms of laboratory testing, equipment, input data, data analysis, failure criteria, and variability of the results.

Table 10-1. Summary Comparison of the Fatigue Analysis Approaches

Item	**Fatigue Analysis Approach**		
	MEPDG	**ME**	**CMSE/CM**
Concept	Mechanistic-empirically based	Mechanistic-empirically based	Continuum micromechanics & fundamental HMAC properties
Laboratory testing	Easy but lengthy temperature conditioning time	Rigorous & lengthy	Numerous but easy to run & less costly (no SE for CM approach)
Testing time	≅ 5 hr	≅ 30 hr	≅ 70 hr (≅ 5 hr for CM approach)
Equipment cost*	≅ $130,000 (minus the software)	≅ $155,000 (≅ $25,560 for BB device)	≅ $210,000 (≅ $80,000 for SE devices)
Input data	Comprehensive/flexible	Comparatively few	Comprehensive (no SE for CM approach)
COV of input data	≅ 5 - 23 %	≅ 5 - 28 %	≅ 4 - 12 %

Table 10-1 Continued

Item	Fatigue Analysis Approach		
	MEPDG	**ME**	**CMSE/CM**
Failure criteria	50% cracking in wheelpath	50% reduction in flexural stiffness	7.5 mm microcrack growth through HMAC layer thickness
Analysis procedure	Comprehensive but is software based	Relatively easy & straightforward	Comprehensive & lengthy
Analysis time**	≅ 4.5 hr	≅ 3 hr	≅ 6 hr (≅ 5 hr for CM)
Failure load-response parameter	Maximum critical design tensile strain (ε_t) @ bottom of HMAC layer	Maximum critical design tensile strain (ε_t) @ bottom of HMAC layer	Maximum critical design shear strain (γ) @ edge of loaded tire
Fatigue analysis model	$N_f = \beta_{f1} k_1 (\varepsilon_t)^{-\beta_{f2} k_2} (E)^{-\beta_{f3} k_3}$ $N_f \geq TrafficDesign_{ESALs}$	$N_f = SF\left[k_1 (\varepsilon_t)^{-k_2}\right]$ $N_f \geq M \times TrafficDesign_{ESALs}$	$N_f = SF_i (N_i + N_p)$ $N_p = k_1 (\gamma)^{-k_2}$ $N_f \geq Q \times TrafficDesign_{ESALs}$
Aging effects	Software incorporates a Global Aging model	None (but can possibly use Miner's hypothesis)	Shift factor (SF_{ag}) being developed
Mean field N_f value***	5.46 E+06	4.67 E+06	5.60 E+06
COV of Ln N_f (field)***	N/A	≅ 6.87- 9.85%	≅ 2.81 -3.98%
95% field N_f CI***	≅ 1.93 - 15.34 E+06	≅ 0.49 -16.74 E+06	≅ 2.98 -8.92 E+06

Note:
*Equipment costs were based on July 2004 estimates.
**Analysis time estimates based solely on author's experience with each approach
***Field N_f, COV, and 95% CI values were based on PS#1 and WW environment only.

Theoretical Concepts

Unlike the empirically based proposed MEPDG and ME approaches, the CMSE and CM approaches were formulated on the fundamental concepts of continuum micromechanics and energy theory with fracture and healing as the two primary mechanisms controlling HMAC mixture fatigue damage. The CMSE/CM approaches utilize fundamental HMAC mixture properties to estimate mixture N_f.

Input Data

The input data for the CMSE and CM approaches and associated laboratory tests are comprehensive, which is necessary to sufficiently and adequately predict N_f by considering all relevant factors that affect HMAC fatigue performance. The CMSE and CM approaches incorporate various material properties such as modulus, tensile strength, fracture, aging effects, healing, and anisotropy. Most of these material properties are not utilized in the ME approach.

The input data for the new MEPDG is also comprehensive but can be flexible depending on the level of analysis selected. Level 1 requires comprehensive input data in terms of traffic, environment, mixture volumetrics, and material properties with HMAC mixtures characterized in terms of the |E*| values measured from DM testing.

Laboratory Testing

The BB test for the ME approach is comparatively complex (in terms of test setup) and time consuming. Note also that the laboratory BB device is limited to only third-point loading HMAC beam fatigue testing in a flexural tension mode. The linear kneading compactor may also be limited to rectangular beam-shaped specimens, while most of the current Superpave HMAC mixture characterization tests use gyratory-compacted cylindrical specimens.

The CMSE laboratory tests may be numerous, but they are relatively simple to run and less time consuming. In fact, one of the concepts behind development of the CMSE/CM approaches is to be able to model HMAC fatigue behavior based on mixture properties obtained from routine laboratory material property tests that are relatively simple and less time consuming to run. With the exception of SE measurements, the average test time for CMSE testing was at most 5 hr including test setup. Additionally, CMSE cylindrical specimens are relatively easy to fabricate and handle. In the case of the CM approach, SE measurements (both for binder and aggregate) and RM tests in compression are not required, thus making the CM approach more practically advantageous in terms of laboratory testing and subsequent data analysis. However, with CMSE/CM uniaxial testing of the HMAC mixtures, it is imperative that the cylindrical specimens are properly aligned along the central loading axis (tensile or compressive) to prevent the induction of undesirable moments that can lead to erroneous results.

DM testing for Level 1 analysis of the MEPDG is relative easy and simple to run but very time consuming in terms of temperature conditioning time for the specimens. Since a complete DM test for a single cylindrical specimen is often conducted at five temperatures, the minimum total conditioning time in this study was 10 hr, i.e., a minimum of 2 hr for each test temperature.

BB testing with the ME approach utilizes kneading-compacted beam-shaped specimens that are comparatively difficult to fabricate, are time consuming to make, and require delicate handling and storage. Improper handling and/or storage can easily induce residual stresses within the specimen which can have a negative impact on the results. Also, the beam shape of the specimens and the linear compaction procedure makes it difficult to adequately control the AV content to the target level. For instance, the COV of the AV content for the beam specimens in this study ranged from 4% to 8%. While this COV range is within acceptable limits, it was nonetheless higher than the approximately 3% to 5% COV for the cylindrical specimens utilized in the MEPDG and CMSE/CM approaches. All these factors ultimately contributed to the relatively high statistical variability in both the input data and final N_f results for the ME approach.

Failure Criteria

The proposed M-E Design Guide failure criterion is based on a percentage cracking in the wheelpath. In this study, 50% was used as the threshold value consistent with the TxDOT tolerable limits (TxDOT 2003b). However, this percent cracking does not correlate well with the actual fatigue damage accumulation (i.e., crack growth through the HMAC layer) or crack severity in an in situ HMAC pavement structure. For instance, a severely cracked HMAC pavement structure with only 10% crack area coverage may be considered adequate according to this criterion whereas a 60% cracked pavement section with cracks only initiating (beginning) will be considered inadequate according to this criterion. Therefore, there may be a need to review this failure criterion.

In the case of the ME approach, the correlation between fatigue crack area and severity on an in situ pavement structure and/or crack length through the HMAC layer thickness and 50% flexural stiffness reduction is not well defined. As pointed out by Ghuzlan and Bouldin's (2000), 50% initial stiffness reduction for constant strain BB testing is an arbitrary failure criterion that does not correlate well to the actual damage accumulation in the HMAC material. These researchers instead proposed the use of energy concepts. Rowe and Bouldin's (2000) study also suggests that while this 50% stiffness reduction may work well for unmodified binders, it may not be applicable for modified binders, and thus results must be analyzed and interpreted cautiously. Note that the Yoakum mixture with the modified binder generally exhibited higher $Ln\ N_f$ variability in this study. Additionally, HMAC stiffness alone may not be sufficient to adequately characterize the mixture fatigue resistance and may probably lead to biased results. Other material properties such as ductility and fracture strength need to be considered. Also, the ME assumption of bottom-up crack failure mode due to horizontal ε_t as utilized in this study may not always be true, particularly for thick, stiff or thin, flexible HMAC pavement structures.

For the CMSE approach, the failure criterion provides a close simulation of a direct relationship between crack development and actual fatigue damage accumulation in an in situ HMAC pavement structure. However, the criterion needs to be further reviewed to establish the adequacy of assuming one microcrack (7.5 mm) initiating and propagating through the HMAC layer thickness as representative of the fatigue cracking process and crack distribution in the entire HMAC pavement structure.

Both the ME and the proposed MEPDG approaches utilize horizontal tensile strain as the failure load-response parameter (Superpave Models Team 2000, Witczak 2001, AASHTO 1996a). Though still subject to review, recent research including the preliminary observation of this study has shown that because of the anisotropic nature of the HMAC, this may not always be true, particularly for thick stiff HMAC pavement structures. Therefore, the use of ε_t at the bottom of the HMAC layer may provide an under- or over-estimation of the HMAC mixture fatigue resistance, particularly for pavement structures where ε_t at the bottom of the HMAC layer is not critical to fatigue performance. Based on this hypothesis, it appears that the ME approach may be applicable only to pavement structures where ε_t at the bottom of the HMAC layer is critical to fatigue performance. Otherwise, the ME approach tended to over-predict *Field* N_f particularly for pavement structures with ε_t less than 100 microstrain in this study. Various researchers including Nishizwa et al. (1997) have also reported infinite fatigue life at low strain levels less than 200 microstrain with the ME approach.

Data Analysis

In terms of analysis, the CMSE and CM approaches are comparatively complex and lengthy because of the comprehensive input data requirements. Inevitably, this type of analysis is necessary to adequately model the HMAC mixture fatigue resistance by analyzing and directly incorporating all the influencing factors. However, these numerical calculations can easily be simplified if a simple spreadsheet analysis program is developed for the computations, as was the case in this study.

Alternatively, CMSE/CM fatigue analysis software can be developed to simplify and reduce the time needed for these calculations. Nonetheless, a comprehensive sensitivity analysis of the CMSE/CM fatigue analysis procedure is strongly recommended to simplify the calculations by eliminating/reducing less critical and/or redundant variables. While the CMSE/CM analysis procedure produced reasonable results in this study, it should be noted that this is a relatively new fatigue analysis procedure and may therefore still be subject to review and modifications in continuing research work during the validation phase.

For the ME approach, the simplified AASHTO TP8-94 analysis procedure utilized in this study was relatively easy and straightforward probably because of relatively fewer input data required (AASHTO 1996a). For the proposed MEPDG, the fatigue analysis process is software based, but utilizes the ME concepts (Superpave Models Team 2000, Witczak 2001).

While the ME laboratory-to-field shift factors may be environmentally specific and require calibration to local conditions, the CMSE/CM calibration constants were developed based on a wider environmental spectrum covering the United States (Lytton et al. 1993), thus making the CMSE approach more flexible. By contrast the proposed MEPDG incorporates a comprehensive climatic model that computes the shift factors based on a specific environmental location (Superpave Models Team 2000, Witczak 2001). The MEPDG Level 1 fatigue analysis actually computes these calibration constants based on actual climatic (current or past) data from local weather stations. In this context, the proposed MEPDG may therefore be considered as being more accurate and realistic in terms of simulating field environmental conditions compared to the other fatigue analysis approaches. The MEPDG software also encompasses a comprehensive traffic analysis model that more closely simulates field traffic loading conditions as compared to the ME and CMSE/CM approaches (Superpave Models Team 2000, Witczak 2001).

Furthermore, the MEPDG software incorporates a GAM that takes into account the effects of aging in HMAC mixture fatigue analysis (Superpave Models Team 2000, Witczak 2001). By contrast, the ME approach does not directly incorporate the effects of aging in the analysis. In the case of the CMSE/CM approaches, attempts were made to develop shift factors due to binder oxidative aging (Chapter IX) and have been incorporated in the analysis. However, although promising results were obtained, more research work is still required in this area. For the ME approach, Miner's (1945) hypothesis can be utilized to develop and incorporate the effects of aging in *Field* N_f predictions, but this was beyond the scope of this study.

In the case of the MEPDG software, it also has the added advantage of simultaneously predicting other HMAC pavement distresses besides fatigue cracking. These include thermal cracking, rutting, and pavement roughness expressed in terms of the international roughness index (IRI).

Results and Statistical Variability

Although the computed mixture field N_f results presented in Chapter IX were comparable, the CMSE and CM approaches exhibited relatively low statistical variability measured in terms of the COV of Ln N_f and 95% PI compared to both the ME and the proposed MEPDG approaches. As highlighted in Table 9-7b, the ME approach exhibited the highest statistical variability both in terms of the COV of Ln N_f and 95% field N_f PI range.

Although this lower statistical variability may also indicate that the CMSE/CM test repeatability was better than that of the BB and DM tests, more comprehensive statistical analyses for the CMSE/CM approaches are required, including more laboratory HMAC mixture fatigue characterization and field validation.

Costs - Time Requirements for Laboratory Testing and Data Analysis

The cost comparisons in this study were evaluated in terms of billable time requirements for laboratory testing (specimen fabrication, machine setup, and actual test running time) and data analysis based on July 2004 cost estimates. These typical time estimates, based on at least four HMAC specimens for the ME and CMSE/CM approaches and at least two for the proposed MEPDG to obtain at least a single value of field N_f, are shown in Table 10-1.

Detailed time requirements are attached as Appendix H. Note that these time estimates were purely based on the work contained in this study, but actual time requirements for laboratory testing and data analysis may generally vary from one person to another and from machine to machine or computer to computer (e.g., in the case of the proposed MEPDG) or the complexity of the pavement structure under consideration. In Table 10-1, laboratory testing time does not include aggregate pre-heating, binder liquefying, short-term oven aging, heating for compaction, cooling after compaction, and temperature conditioning time of the specimens prior to testing because time for these processes was considered almost equal in each approach and may often not be billable.

Based on the billable time requirements in Table 10-1, the MEPDG was ranked as the cheapest (shortest billable time requirement) followed by the CM approach. Generally, the ME approach required more time for specimen fabrication, machine setup, and actual testing but less time for data analysis, primarily due to the simplified AASHTO (1996a) TP8-94 analysis procedure and fewer input data requirements. For the CMSE approach, SE values for binders and aggregates are required as input data. Though the current test protocol for aggregates might require a test time of 60 to 70 hr per aggregate, various alternate and time-efficient SE measurement methods are being investigated in other ongoing research studies and these include application of the Microcalorimeter test protocol (Little et al. 2003).

Despite the lengthy test time, however, CMSE SE measurements are only performed once for any binder or aggregate type from a particular source (as long as there are no major compositional changes). The SE data can then be utilized for numerous analysis applications including fatigue, permanent deformation, and moisture sensitivity modeling of HMAC mixtures. Thus SE measurements are actually efficient considering their repeated and widespread use for binder and aggregate materials that may be utilized in different HMAC mixture designs for different studies.

Costs - Equipment

In terms of equipment cost, the CMSE was ranked as the most expensive approach with an approximate total cost of $210,000 (with about $80,000 being for the SE equipment) followed by the ME approach, based on the July 2004 equipment cost estimates. Although the SE equipment appears costly, its versatility in terms of data measurements for HMAC mixture fatigue, permanent deformation, and moisture sensitivity analysis may actually offset the high initial cost. This is especially significant for numerous concurrent studies or projects.

The equipment costs for the proposed MEPDG (≅ $130,000) and the CM (≅ $210,000 - $80,000 = $130,000) approaches are similar (based on July 2004 cost estimates). However, the cost of the MEPDG software, which is not included in Table 10-1, may probably raise the proposed MEPDG total cost to a value higher than that of the CM approach. The ME equipment cost is lower than that of the CMSE, but it exceeds the proposed MEPDG and the CM approaches by approximately $25,560 based on the July 2004 cost estimate of the BB device (Table 10-1) (James Cox and Sons, Inc. 2004). The limited use of the BB device for fatigue testing in flexural tension mode only also indirectly makes the ME approach more costly.

RATING OF THE FATIGUE ANALYSIS APPROACHES

Table 10-2 summarizes the advantages and disadvantages of each fatigue analysis approach as observed in this study. The assessment and rating criteria including a TxDOT evaluation survey questionnaire to rate the assessment factors according to their degree of significance, are discussed in the subsequent text.

TxDOT Evaluation Survey Questionnaire

An evaluation survey questionnaire was conducted with TxDOT personnel to ascertain the degree of significance of the various factors to be used in evaluating and rating the four fatigue analysis approaches consistent with the TxDOT HMAC mixture fatigue characterization and pavement structural design for fatigue resistance. These factors include laboratory testing, material properties, input data variability, analysis, field N_f results, and associated costs. Appendix I is an example of the evaluation survey questionnaire and shows the sub-factors associated with each factor. For each factor and sub-factor, the rating score was from 1 to 10, with 10 representing the most significant factor/sub-factor and 1 being the least significant.

Fig. 10-1 summarizes these rating results in decreasing order of significance for both the factors and sub-factors. Based on these rating scores, the averaged weighting scores out of a total score of 100% were determined and are shown in parentheses in Fig. 10-1. According to these rating results, mixture field N_f results in terms of statistical variability and their tie to field performance are the most significant factor to consider when selecting and recommending an appropriate fatigue analysis approach to TxDOT. This factor has a weighting score of 22%. Material properties were considered the least significant factor with a total weighting score of 14%. Within the factor "material properties," mixture volumetrics (binder content and AV) and modulus/stiffness were considered the most significant sub-factors with an equal weighting score of 17%, while anisotropy was the least significant (9%). It is also worthwhile to note that the factors "analysis" and "laboratory testing" have the same degree of importance, with an equal weighting score of 15%.

Table 10-2. Advantages and Disadvantages of the Fatigue Analysis Approaches

Approach	Advantage	Disadvantage
CMSE	• Utilizes fundamental HMAC mixture properties to estimate N_f • Exhibits greater flexibility & potential to incorporate material properties that affect HMAC mixture fatigue performance • Utilizes shear strain as failure load-response parameter • Utilizes cylindrical specimens that are easy to fabricate & handle • Requires numerous tests that are easy & relatively less costly to run • Relates fatigue failure to damage accumulation within HMAC material • Produces N_f results that exhibits lower variability in terms of COV and 95% PI • Produces fatigue performance results as a function of microcrack growth through HMAC layer thickness • Utilizes calibration constants that were developed nationwide • Incorporates aging, healing, & anisotropic effects in N_f analysis • Laboratory tests & resultant data are versatile in their application	• More validity & applicability testing still required • More HMAC mixture characterization needed • Test protocols & analysis procedure subject to review • Lab testing - specimen alignment very critical to obtaining good results • Adequacy of failure criteria still need to be reviewed • Statistical analysis criteria need more review • SE testing is lengthy & costly
CM	• Same as CMSE but with no SE tests & reduced analysis	
MEPDG	• Ideal for pavement structures where tensile strain is critical to fatigue performance • Incorporates Global aging model • Predicts distress as a function of pavement age • Incorporates a comprehensive traffic and climatic analysis models • Utilizes cylindrical specimens that are easy to fabricate & handle • Tests are easy & less costly • Failure criteria is based on 50% cracking in wheelpath • Versatility - other tests & analyses (e.g., rutting and IRI)	• Mechanistic-empirically based • Global aging model may not be good for modified binders • No direct incorporation of healing nor anisotropy • Failure criteria does not clearly relate to field fatigue damage & severity • Only bottom-up cracking failure mode was considered in this study
ME	• Ideal for pavement structures where tensile strain is critical to fatigue performance • Requires local calibration to field conditions • Failure criteria is based on 50% stiffness reduction	• Empirically based • Beams specimen are difficult to fabricate and handle • Laboratory testing is lengthy • No direct incorporation of aging, anisotropy, & healing effects in analysis • High variability in results • Not applicable to pavement structures where tensile strain is not critical to fatigue performance • Test equipment is limited to BB testing only

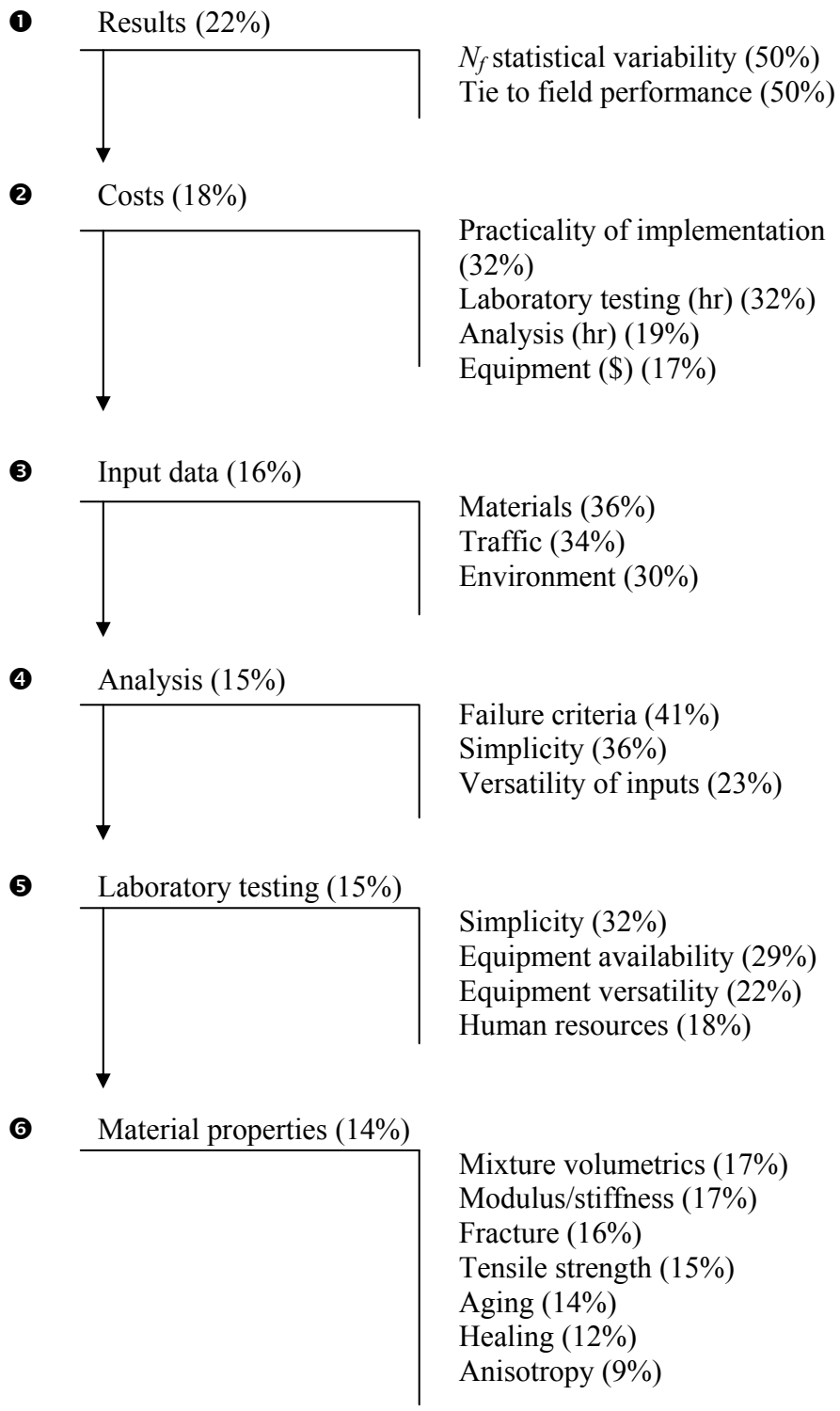

Fig. 10-1. Assessment Factors/Sub-factors and Associated Weighting Scores

Assessment and Rating Criteria of the Fatigue Analysis Approaches

Using Tables 10-1 and 10-2, scores (out of 10) were assigned to each sub-factor as shown in Appendix I. For this analysis, the scores (with a range of 0 to 10) for each sub-factor, e.g., those associated with the factor "results," were defined as follows:

- Variability: 10/10 ≅ low, 5/10 ≅ low to high, and 0/10 ≅ high variability.

- Tie to field performance: 10/10 ≅ high, 5/10 ≅ low to high, and 0/10 ≅ low degree of or poor tie to field performance.

Using Fig. 10-1, the weighted scores for each factor for each approach were summed up as shown in Appendix J. Table 10-3 provides an evaluation summary of the scores and ratings of the fatigue analysis approaches based on Appendix J.

Table 10-3. Weighted Scores and Rating of the Fatigue Analysis Approaches

Category	**Weight**	**Evaluation Score**			
		MEPDG	**ME**	**CMSE**	**CM**
Results	*22%*	11%	9%	14%	13%
Cost	*18%*	16%	10%	15%	16%
Input data variability	*16%*	12%	8%	10%	10%
Analysis	*15%*	9%	9%	11%	10%
Laboratory testing	*15%*	12%	6%%	12%	12%
Incorporation of material properties	*14%*	10%	8%	13%	12%
Total	*100%*	69%	50%	**75%**	73%

Table 10-3 showed the weighting scores associated with each factor and the actual score assigned for each approach. "Results," for instance, has a total weighted score of 22%. For this factor, the CMSE approach scored the highest score (14%) and would be ranked first based on this factor. In terms of laboratory testing, while all the other approaches have the same ranking based on equal scores (12%), the ME approach would be ranked last with a score of 6%. In terms of the overall scores (out of a total of 100%), the order of ranking is CMSE (75%), CM (73%), proposed MEPDG (69%), and ME (50%).

THE RECOMMENDED FATIGUE ANALYSIS APPROACH: THE CMSE APPROACH

Based on the value engineering assessment as shown in Table 10-3 and considering the materials and test conditions in this study, the CMSE fatigue analysis approach with the highest score (75%) was recommended for predicting HMAC mixture fatigue life. With the possibility of establishing an SE database in the future from various ongoing studies at TTI, the CMSE approach will become a reality both in terms further validation and practical implementation. Furthermore, a sensitivity analysis with more HMAC mixture characterization to streamline the CMSE analysis procedure will make the approach simple and practical to implement.

Based on the score ranking, the CM is recommended as the second alternative in lieu of the CMSE approach to be utilized particularly in the absence of SE data. Note, however, that the CM analysis models were modified in this study based on the CMSE results. Consequently, more independent HMAC mixtures need to be characterized for fatigue resistance to validate the correlation between the CMSE and CM approaches. With further validation through additional HMAC mixture characterization, the CM constitutes a potentially promising fatigue analysis approach over the CMSE in terms of analysis simplicity, practicality, and cost considerations, among other factors.

Effects of Binder Oxidative Aging

While some CMSE/CM aging shift factors (SF_{ag}) were developed in this study and produced promising results, validation of these concepts is still required through testing of additional binders and HMAC mixtures. In contrast to the simplicity adopted in these concepts, HMAC aging should possibly be modeled as a function of three processes: binder oxidation, binder hardening, and N_f reduction.

Additionally, the SF_{ag} should be able to account for mix-design characteristics, traffic loading, and environmental conditions. As pointed out in Chapter IX, field HMAC aging is a relatively complex process involving fluctuating traffic loading and environmental conditions, i.e., temperature variations. Note, however, that traffic (in terms of design ESALs) and environmental effects (in terms of temperature) are also taken into account by the SF_h (see Chapter V) in the CMSE approach. In addition, the rate of aging or response to binder oxidation and hardening and subsequent reduction in fatigue resistance may differ from mixture to mixture depending on the material type and mix-design characteristics. Most importantly, however, the SF_{ag} must be derived as a function of time so that N_f at any pavement age can be predicted. Once these SF_{ag} have been developed and validated for a group of similar HMAC mixtures, laboratory testing of aged HMAC mixtures may be unnecessary.

Surrogate Fatigue Tests and Analysis Protocol

The fatigue analysis approaches discussed in this report and the recommended CMSE approach incorporate stress-strain analysis that depends on both pavement structure and environmental location. This is because stress and/or strain are required as an input parameter in these N_f analyses. Unlike other distresses, such as rutting or permanent deformation, fatigue cracking in the HMAC layer depends on the entire pavement structure and its response to both traffic loading and the environment. Consequently, a surrogate fatigue test and N_f analysis protocol that is independent of the pavement structure and environment cannot be formulated based on the fatigue analysis approaches and results presented in this dissertation.

In the absence of a fatigue analysis model that is independent of stress and/or strain as input parameters, establishment of a database of a range of design stress and/or strain levels for typical TxDOT HMAC pavement structures and the Texas environment is recommended. Establishment of such a database to be used in conjunction with these fatigue analysis approaches will facilitate an easier and quicker way of characterizing the fatigue resistance of HMAC mixtures using some of the tests described in this dissertation as surrogate tests. This will also eliminate the need to conduct an extensive stress-strain analysis every time a HMAC mixture is to be characterized for fatigue resistance.

By contrast however, surrogate fatigue test protocols can be established for mix design and HMAC mixture screening to select fatigue-resistant mixtures based on the CMSE fatigue analysis approach. Limiting threshold values (i.e., σ_t, ε_f, E_1, m, and b) can be set to discriminate between adequate and inadequate fatigue-resistant HMAC mixtures based on TS, RM, and RDT testing, respectively, without having to predict N_f.

SUMMARY

Key points from a comparative evaluation of the fatigue analysis approaches and selection of the recommended approach are summarized as follows:

- The four fatigue analysis approaches (the ME, the CMSE, the CM, and the MEPDG) were comparatively evaluated in terms of the following factors: theoretical concepts, input data, laboratory testing, failure criteria, data analysis, results and variability, and associated costs.
- Selection and recommendation of the fatigue analysis approach was based on *Field* N_f results, costs, input data variability, analysis, laboratory testing, and incorporation of fundamental material properties consistent with the TxDOT level of significance of each parameter.
- Based on a value engineering assessment criteria and considering the materials and test conditions in this study, the CMSE fatigue analysis approach was selected and recommended for predicting HMAC mixture N_f.

- In comparison to other fatigue analysis approaches, the CMSE:
  - ⇒ Was conceptualized on the simple yet fundamental principle that energy must be expended to cause load-induced damage in the form of fatigue cracking and equally, energy must be expended to close up these fracture surfaces in a process called healing. The approach uses the continuum fracture-damage mechanics principles based on Schapery's work potential theory, the extended visco-elastic correspondence principle, and Paris' Law of fracture mechanics.
  - ⇒ Has a failure criterion that is based on a close simulation of a direct relationship between crack development and fatigue damage in an in situ HMAC pavement structure.
  - ⇒ Has fatigue analysis models based on data input obtained from simple routine laboratory material characteristics tests (tensile strength, relaxation modulus, repeated direct tension, and surface energy) instead of time-consuming fatigue tests such as the bending beam for the ME approach.
  - ⇒ Utilizes fundamental HMAC mixture properties to predict N_f and accounts for the fact that HMAC is a complex composite material that behaves in a non-linear visco-elastic manner, exhibits anisotropic behavior, ages with time, and heals during traffic loading rest periods.
  - ⇒ Has the potential to simultaneously model HMAC moisture sensitivity through the use of SE data under wet conditions.
  - ⇒ Exhibited comparatively lower statistical variability in the N_f predictions measured in terms of the COV of $Ln\ N_f$ and 95% PI range.

- By contrast:
  - ⇒ The ME approach is convenient as a less detailed analysis with fewer input data for HMAC pavement structures where the tensile strain at the bottom of the HMAC layer is critical to fatigue performance. The approach exhibited the highest statistical variability in the results and does not incorporate the significant aspect of aging that affects HMAC mixture fatigue performance. Additionally, its failure criterion does not provide a realistic simulation of actual fatigue damage accumulation in the field.
  - ⇒ The MEPDG incorporates aging effects in the analysis through the Global Aging model and provides comprehensive and realistic analysis models for both traffic loading and environmental effects. Furthermore, the approach has the potential to predict other HMAC pavement distresses including thermal cracking, rutting, and IRI. However, the approach does not account for binder healing nor anisotropic effects, and its failure criterion does not provide a realistic simulation of the actual fatigue damage accumulation in the field.

Although the CMSE fatigue analysis approach was selected and recommended in this study, it should be noted that any fatigue analysis approach can produce desired results provided it is well calibrated to the environmental and traffic loading conditions of interest and that all relevant factors affecting fatigue performance are appropriately taken into account.

CHAPTER XI
CONCLUSIONS AND RECOMMENDATIONS

Conclusions and recommendations from the data presented and analyzed in this dissertation are presented in this chapter.

CONCLUSIONS

The selected fatigue analysis approach, a comparison of mixture N_f results and the effects of binder oxidative aging, and other input variables on HMAC mixture fatigue resistance are summarized in this section.

Selected Fatigue Analysis Approach - CMSE

(1) Based on value engineering assessment criteria including laboratory testing, input data, statistical analysis, costs, and the analysis procedure of each approach, the CMSE fatigue analysis approach was recommended for predicting HMAC mixture fatigue life.

(2) In comparison to other approaches that were evaluated and for the materials and test conditions considered in this study, the CMSE approach exhibited better mixture field N_f prediction capability because:

- it utilizes fundamental mixture properties to estimate N_f and incorporates the continuum fracture-damage micromechanics and energy theories of fracture and healing in the fatigue analysis of HMAC mixtures;
- it exhibits greater flexibility and the potential to discretely account for most of the fundamental mixture properties that affect HMAC pavement fatigue performance, including fracture, binder aging effects, healing, visco-elasticity, anisotropy, crack initiation, and crack propagation;
- with the exception of SE measurements, the CMSE laboratory tests are routinely simple and less costly both in terms of billable time requirements and equipment. Laboratory testing for this approach utilizes gyratory compacted HMAC

specimens that are relatively easy to fabricate and handle compared to beam HMAC specimens for the ME approach;

- the failure criterion of a 7.5 mm microcrack initiation, growth, and propagation through the HMAC layer thickness closely correlates with actual fracture damage accumulation in an in situ HMAC pavement structure compared to the failure criteria of the other approaches (the MEPDG and the ME approach); and
- the CMSE mixture results exhibited relatively lower statistical variability measured in terms of the COV of $Ln\ N_f$ and 95% PI range.

(3) Although the SE measurements for the CMSE analysis are lengthy in terms of test time, the tests are performed only once for any binder or aggregate type from a particular source (as long as there are no major compositional changes). The SE data can then be utilized for numerous analysis applications including fatigue, permanent deformation, and moisture sensitivity modeling of HMAC mixtures. Thus SE measurements are actually efficient considering their repeated and widespread use for binder and aggregate materials that may be utilized in different mixture designs in different projects.

(4) In the absence of SE data, the CM approach is recommended to be utilized in lieu of the CMSE approach. The fundamental concepts, failure criteria, and analysis procedure are basically similar, except for the following:

- SE laboratory measurements (both for binders and aggregates) and RM tests in compression are not required in the CM approach, and
- SE input data for both the binder and aggregate are not required in the CM approach. Instead, the CM approach utilizes empirical relationships that were calibrated to the CMSE approach to compute SF_h and Paris' Law fracture coefficients that are dependent on RM (compression) and SE data in the CMSE approach.

Comparison of HMAC Mixture Fatigue Resistance

(1) The Yoakum mixture exhibited better fatigue resistance in terms of N_f magnitude compared to the Bryan mixture for all aging and environmental conditions and for all pavement structures considered in this study. This finding was observed in all the fatigue analysis approaches. Also, the Yoakum mixture exhibited less susceptibility to binder oxidative aging compared to the Bryan mixture. The Yoakum mixture's improved fatigue performance may be due to the following factors:

- The higher binder content for the Yoakum mixture (5.6% by weight of aggregate) probably increased its fatigue resistance compared to the Bryan mixture with 4.6% binder content by weight of aggregate.
- The effect of the SBS modifier and the 1% hydrated lime in the mixture could have possibly decreased the Yoakum mixture's susceptibility to oxidative age-hardening as well as improved its fatigue resistance. In their study, Wisneski et al. (1996) made similar observations that hydrated lime tended to improve the performance of asphalt mixtures. However, this phenomenon needs to be explored in greater depth.
- The binder-aggregate bond strength as exhibited by the SE results indicated a relatively better bond compatibility for the Yoakum mixture (PG 76-22 plus gravel aggregate) than for the Bryan mixture (PG 64-22 plus limestone aggregate).

(2) For the N_f results, the Yoakum mixture exhibited higher statistical variability in terms of the COV of Ln N_f and 95% PI range.

Effects of Binder Oxidative Aging and Other Variables on HMAC Mixture Fatigue Resistance

(1) Under strain-controlled laboratory testing, binder oxidative aging reduces HMAC mixture resistance to fracture and its ability to heal.

(2) Generally, all mixtures exhibited an exponentially declining N_f trend with aging and that the rate of N_f decline is mixture dependent.

(3) HMAC mixture fatigue resistance is both pavement structure and environmental condition dependent.

(4) The computed temperature shift factors (a_T) for the HMAC mixtures based on time-temperature superposition principles using the Arrhenius model exhibited a linear relationship with temperature. While these a_T showed some sensitivity to mixture type, they were by and large insensitive to binder oxidative aging effects.

(5) Within a ±15% error tolerance, mixture anisotropy as measured in terms of SF_a was observed to be insignificantly affected by binder oxidative aging, but it did vary considerably as a function of mixture type due to the differences in the aggregate gradations. This SF_a insensitivity to aging was theoretically attributed to the fact that mixture anisotropy is predominantly controlled by particle orientation due to compaction, which is insignificantly affected by aging exposure conditions.

(6) The CMSE/CM *SFag* developed in this study produced promising results and can be used as a basis for prediction of *Field* N_f at any pavement age without the need to test aged HMAC mixtures.

RECOMMENDATIONS

From the findings of this study, the following recommendations were made:

(1) More HMAC mixture laboratory fatigue characterization is recommended to:

- Provide confidence and validation in the selected CMSE approach. The CMSE laboratory test protocol, failure criteria, and analysis procedure should be reviewed and, if needed, modified accordingly. For instance the 7.5 mm microcrack threshold should be reviewed to establish its adequacy as representative of the fatigue cracking process and crack distribution in the entire HMAC pavement structure. The current CMSE version is based on the generalized hypothesis that the growth of one crack is representative of the field HAMC pavement crack size distribution. Consequently, more data are thus required to validate this hypothesis.
- Populate the *Field* N_f database of commonly used TxDOT HMAC mixtures

- Provide additional data to adequately model and incorporate the effects of binder oxidative aging.

(2) A numerical analysis software for the CMSE (and CM) fatigue analysis approach (es) should be developed based on the analysis procedure described in this study. Such a program will among others lead to the following benefits:
   - Simplify and reduce the time required for the CMSE/CM fatigue analysis process.
   - Minimize human errors resulting from manual calculations.
   - Facilitate a faster methodology of conducting a sensitivity analysis on the CMSE/CM approach so as to reduce/eliminate redundant variables in CMSE/CM analysis models.
   - Facilitate a quicker and convenient way to validate and, if need be, modify the CMSE/CM approach based on more laboratory HMAC mixture characterization.

(3) Because of the apparent importance of N_f decline with oxidative binder aging and subsequent stiffening, more work is needed to understand this phenomenon and the essential features of mix-design that impact this decline in N_f.

(4) For CMSE uniaxial laboratory testing, it is strongly recommended that the specimens always be properly aligned along the central axis of loading to minimize the induction of undesirable moments that can lead to erroneous results.

(5) Although the CMSE/CM SF_{ag} concept utilized in the study to account for binder oxidative aging effects based on CMAC's DSR_f produced promising results, more research is recommended to better quantify the N_f-aging relationship. This will inevitably allow for development of more representative SF_{ag} factors that will allow for realistic N_f predictions at any desired pavement age. Also the SF_{ag}-DSR_f concept itself need to be further validated through testing of additional binders and HMAC mixtures, possibly with longer laboratory aging periods that realistically simulate current HMAC pavement design practices

CLOSURE

The CMSE/CM approaches described in this study are relatively new analysis methodologies for fatigue characterization of HMAC mixtures and therefore still may be subject to review and/or modifications. Furthermore, because of the dependence of fatigue cracking in the HMAC layer on the entire pavement structure when subjected to traffic loading, this study does not, in the interim, recommend any surrogate fatigue test and N_f analysis protocol that is independent of the environment and HMAC pavement structure. The fatigue analysis approaches discussed in this report and the selected CMSE approach incorporate stress-strain analysis that is pavement structure and environment location dependent. This is because stress and/or strain are required as input parameters in these N_f analyses. Consequently, more research is recommended to formulate fatigue analysis models that are independent of stress-strain analysis. Otherwise, a database of a range of design stress and/or strain levels for typical TxDOT HMAC pavement structures and the Texas environment needs to be established to minimize the extensive and complex stress-strain analysis that is pavement structure and environmental location dependent.

However, a CMSE surrogate fatigue test protocol for mix design and HMAC mixture screening to select fatigue-resistant mixtures can be established that is independent of N_f analysis. Limiting threshold values (i.e., σ_t, ε_f, E_1, m, and b) can be set to discriminate between adequate and inadequate fatigue-resistant HMAC mixtures based on TS, RM, and RDT testing, respectively.

REFERENCES

AASHTO (2004*).* AASHTO 2002 pavement design guide. http://www.2002designguide.com, http://www.trb.org/mepdg, accessed November 2004.

AASHTO (2003). AASHTO designation: TP 62-03, Standard method of test for determining dynamic modulus of hot mix asphalt concrete mixtures. Washington, D.C.

AASHTO (2001). AASHTO designation: TP 62-03, Standard method of test for determining dynamic modulus of hot mix asphalt concrete mixtures. Washington D.C.

AASHTO (2000). *AASHTO provisional standards*, Interim Ed., American Association of State Highway and Transportation Officials. Washington, D.C.

AASHTO (1998). AASHTO designation: TP5-98, Standard test method for determining the rheological properties of asphalt binder using a dynamic shear rheometer. Washington, D.C.

AASHTO (1996a). AASHTO designation: TP8-94, Standard test method for determining the fatigue life of compacted hot-mix asphalt (HMAC) subjected to repeated flexural bending. Washington, D.C.

AASHTO (1996b). AASHTO designation: PP6-94, Standard practice for grading or verifying the performance grade of an asphalt binder. Washington, D.C.

AASHTO (1994). AASHTO designation: PP2, Standard practice for short and long term aging of hot mix asphalt, *AASHTO Provisional standards*. Washington, D.C. June Ed.

ABAQUS (1996). *ABAQUS users manual.* Hibbit, Karlsson and Sorenson, Inc., Pawtucket, Rhode Island.

Adu-Osei, A. (2000). "Characterization of unbound granular base" Ph.D. dissertation, Texas A&M University, College Station, Texas.

Ahlborn, G. (1969). "ELSYM5, computer program for determining stresses and deformations in five layer elastic system." University of California, Berkeley, California.

Ali, H. A., and Tayabji, S. D. (1998). "Evaluation of mechanistic-empirical performance prediction models for flexible pavements." *Transportation Research Record* 1629, 169-180.

Al-Qadi, I. L., and Nassar, W. N. (2003). "Fatigue shift factors to predict HMA performance", *The International Journal of Pavement Engineering*, 4(2), 69-76.

Aparicio Ramos, S I. (2003). "Study of the asphalt pavement damage through nondestructive testing on overweight truck routes", Master's thesis, Texas A&M University, College Station, Texas.

Anderson, T. L. (1995) "Fracture mechanics, fundamentals and applications." CRC Press LLC, Boca Raton, Florida .

Arramon, Y. P., Mehrabadi, M. M., Martin, D. W., and Cowin, S. C. (2000). "A multidimensional anisotropic strength criterion based on Kelvin modes." *International Journal of Solids and Structures*, 37, 2915-2935.

Adu-Osei, A. (2000). "Characterization of unbound granular base" Ph.D. dissertation, Texas A&M University, College Station, Texas.

Asphalt Institute (1991). *Thickness Design – Asphalt Pavements for Highways and Streets. Manual Series No. 1 (MS-1)*, Lexington, Kentucky.

Blab, R., and Litzka, J. (1995). "Measurements of the lateral distribution of heavy vehicles and its effects on the design of road pavements." *Proceedings of the International Symposium on Heavy Vehicle Weights and Dimensions*, Ontario, Canada, 389-395.

Bonnaure, F., Gravois, A., and Udron, J. (1980). "A new method for predicting the fatigue life of bituminous mixes," *Proceedings of the Association of Asphalt Paving Technologists*, AAPT, 49, 499-524.

Castell, M. A., and P. Pintado. (1999). "Sensitivity analysis for estimation of pavement fatigue life," *Journal of Transportation Engineering*, (125), 2, 114-122.

CastelloBlanco, A. (2004). "Probabilistic analysis of air void structure and its relationship to permeability and moisture damage of hot-mix asphalt." Master's thesis, Texas A&M University, College Station, Texas.

Cheng, D. (2002). "Surface free energy of asphalt-aggregate system and performance analysis of asphalt concrete based on surface energy," Ph.D. dissertation, Texas A&M University, College Station, Texas.

Christensen, R. M., and Anderson, D. A. (1992). "Interpretation of dynamic mechanical test data for paving grade asphalt cements." *Proceedings of the Association of Asphalt Paving Technologists,* AAPT, 61, 67-98.

Cleveland, G. S., Lytton, R. L., and Button, J. W. (2003). "Using pseudo-strain damage theory to characterize reinforcing benefits of geosynthetic materials in asphalt concrete overlays." *Journal of the Transportation Research Board 1849,* Washington D.C., 202-211.

Daniel, J. S., and Kim, Y. R (2002). "Development of a simplified fatigue test and analysis procedure using a viscoelastic, continuum damage model," *Paper presented at the annual meeting of the Association of Asphalt Paving Technologists*, March 18-20.

Deacon, J. A., Coplantz, J. S., Tayebali, A. A., and Monismith, C. L. (1994). "Temperature considerations in asphalt-aggregate mixture analysis and design," *Transportation Research Record* 1454, 97-112.

Doyle, P. C. (1958). "Cracking characteristics of asphalt cement," *Proceedings of the Association of Asphalt Paving Technologists*, AAPT, 27, 581-597.

Epps, A. L., Harvey, J. T., and Monismith, C. L. (1999). "Performance characteristics of mixes containing asphalt cements and crumb rubber modified binders," *Paper presented at the Symposium on Asphalt, Number One Thermoplastic Polymer as part of the 217th American Chemical Society Meeting*, Anaheim, California, March 23.

Francken, L. and Clauwaert, C. (1988). "Characterization and structural assessment of bound materials for flexible road structures," *Proceedings of the 6th International Conference on the Structural Design of Asphalt Pavements,* University of Michigan, Ann Arbor, 130-144.

Freeman, T. (2004). *Flexible pavement database.* Research Project 187-06, Texas Transportation Institute. College Station, Texas.

Ghuzlan , K.A., and Carpenter, S. H. (2002). Traditional fatigue analysis of asphalt concrete mixtures. Paper submitted for presentation and publication by TRB at January 2003 Annual Meeting, Washington, D.C.

Glover, C. J., Davison, R. R., Domke, C. H., Ruan, Y., Juristyarini, P., Knorr, D.B., and Jung, H.S. (2005). Development of a new method for assessing asphalt binder durability with field validation. Report FHWA/TX-03/1872-2, Texas Transportation Institute, College Station, Texas.

Good, R. J., and Van Oss, C. J. (1992). "The modern theory of contact angles and the hydrogen bond components of surface energies," *Modern Approaches to Wettability*, M. E. Schrader and G. Loeb, eds., Plenum Press, New York.

Halstead, W. J. (1984). *Relation of asphalt chemistry to physical properties and specifications*, Report FHWA/VA-84/85, Virginia Department of Highways and Transportation, Richmond, Virginia.

Harvey, J., Hoover, T., Nokes, W., Coetzee, N. F., and Rust, F. (1998). "CalTrans accelerated pavement test (CAL/APT) program - Test Results: 1994-1997." *Journal of the Association of Asphalt Paving Technologists*, AAPT, 67,644-689.

Hefer, A. W. (2004). "Adhesion in bitumen-aggregate systems and quantification of the effects of water on the adhesion bond." Ph.D. dissertation, Texas A&M University, College Station, Texas.

Hopman, P., and Nilsson, R. (2000). "COMPASS: To design functional mixes," *Proceedings of the 1st International World of Asphalt Pavements Conference*, Sydney, Australia, February 20-24, CD-ROM.

Huang, Y. H. (1993). Pavement Analysis and Design, Prentice Hall, New Jersey.

Ioannides, A. M. (1997). "Fracture mechanics in pavement engineering: The specimen-size effect." *Transportation Research Record* 1568, 10-16.

Jacobs, M. M. J., Hopman, P. C, and Molenaar, A. A. A. (1996). "Application of fracture mechanics principles to analyze cracking in asphalt concrete," *Journal of the Association of Asphalt Paving Technologists*, AAPT, 65, 1-39.

James Cox and Sons, Inc. (2004). *2004 price list*, Model CS7600 4-pt Bending Fixture, Colfax, California.

Jianlong, Z., and Francken, L. (1997). "A research on the dissipated energy density of bituminous mixtures and overlay," *Proceedings of the XIIIth World Meeting of the International Road Federation*, Toronto, Canada, June 16-20.

Juvinall, R. C., and Marshek., K. M. (2000). Fundamentals of machine component design. John Wiley & Sons Inc., New York.

Kallas. B. F. (1970). "Dynamic modulus of asphalt concrete in tension and tension-compression." *Journal of the Association of Asphalt Paving Technologists,* AAPT, 39, 1-20.

Khanal, P. P., and Mamlouk, M. (1995). "Tensile versus compressive moduli of asphalt concrete." *Transportation Research Record* 1482, Washington, D.C., 144-150.

Kim, S. H., Little, D. N., Masad, E., and Lytton, R. L. (2004). "Determination of anisotropic moduli considering aggregate particle shape and gradation in unbound granular layer." Paper Presented at the 83rd Annual Meeting of the TRB, Washington, D.C.

Kim, Y. R., Lee, H. J., and Little, D. N. (1997a). "Fatigue characterization of asphalt concrete using visco-elasticity and continuum damage theory." *Journal of the Association of Asphalt Paving Technologists*, AAPT, 66, 520-569.

Kim, Y. R., Lee, H. J, Kim, Y, and Little, D. N. (1997b). "Mechanistic evaluation of fatigue damage growth and healing of asphalt concrete: Laboratory and field experiments," *Proceedings of the 8th International Conference on Asphalt Pavements*, ISAP, Seattle, Washington, August 10-14, 1089-1107.

Kissam, Philip C. E. (1956). Surveying for Civil Engineers, McGraw-Hill, New York.

Knorr, D. B., Jr., Davison, R. R., and Glover, C. J. (2002). "The effect of various aging techniques on asphalt low-temperature properties," Paper presented at the *81st* Annual Meeting of the Transportation Research Board, Washington, D.C., January 13-17.

Lee, H. J., Daniel, J. S., and Kim, Y. R. (2000). "Continuum damage mechanics-based fatigue model of asphalt concrete." *Journal of Materials in Civil Engineering*, ASCE, 12 (2), 105-112.

Lee, H. J. (1996). "Uniaxial constitutive modeling of asphalt concrete using viscoelasicity and continuum damage theory." Ph.D. dissertation, North Carolina State University, Raleigh, North Carolina.

Lee, N. K., Morrison, G. R., and Hesp, S. A. M. (1995). "Low temperature fracture of polyethylene-modified asphalt binders and asphalt concrete mixes," *Journal of the Association of Asphalt Paving Technologists*, AAPT, 64, 534-574.

Liang, R. Y., and Zhou, J. (1997). "Prediction of fatigue life of asphalt concrete beams." *International Journal of Fatigue*, 19 (2), 117-124.

Little, D., Bhasin, A., Lytton, L. R., and Hefer, A. (2003). *Interim Report on Using Surface Energy Measurements to Select Materials for Asphalt Pavements*, NCHRP 9-37, National Cooperative Highway Research Program, Transportation Research Board, National Research Council, Washington, D.C.

Little, D., Lytton, R, Si, Z., Xin, D., and Kim, Y. R. (2000). *Crack phenomenology: Formation and healing - Task K findings, Interim Report*, Texas Transportation Institute, College Station, Texas.

Little, D., Lytton, R, Williams, D., Chen, C. W., Kim, Y. R., and Lee, H.J. (1998). *Fundamental properties of asphalts and modified asphalts: Task K - Microdamage Healing in asphalt and asphalt concrete, Final Report, Volume I: Microdamage and microdamage healing - Project summary report*, Federal Highway Administration, Washington, D.C.

Lundström, R. (2004). "On the rheological testing and modelling of asphalt mixtures with emphasis on fatigue characterization." Doctoral Dissertation, LTH Civil and Architectural Engineering, Stockholm, Sweden.

Lytton, R. L. (2004). Personal Communication. Texas Transportation Institute (TTI), College Station, Texas, May.

Lytton, R. L (2001). "CVEN 689, Special topics in micromechanics of civil engineering" graduate civil engineering course offered in Fall 2001, Texas A& M University, College Station, Texas.

Lytton, R. L. (2000). "Characterizing asphalt pavements for performance", *Transportation Research Record* 1723, 5-16.

Lytton, R. L., Uzan, J., Fernando, E.G, Roque, R., Hiltunen, D., and Stoffels, S. (1993). *Development and validation of performance prediction models and specifications for asphalt binders and paving mixes*, Report SHRP-A-357, Strategic Highway Research Program, National Research Council, Washington, D.C.

Mamlouk, M. S., and Khanal, P. P. (1997). "Bimodular analysis of asphalt pavements," *Proceedings of the 8th International Conference on Asphalt Pavements*, ICAP, Seattle, Washington, August 10-14, 707-723.

Marek, C. R., and Herrin, M. (1968). "Tensile behavior and failure characteristics of asphalt cements in thin films." *Proceedings of the Association of Asphalt Paving Technologists*, AAPT, Atlanta, February 26-28, 37, 386-421.

Matthews, J., Monismith, C. L., and Craus, J. (1993). "Investigation of laboratory fatigue testing procedures for asphalt aggregate mixtures," *Journal of Transportation Engineering*, 119, July/August, 634-654.

Maugis, D. (1999). *Contact, adhesion and rupture of elastic solids.* Springer, New York, 3-12.

Medani, T.O., Huurman, M., and Molenaar, A. A. A. (2004). "On the computation of master curves for bituminous mixes." *Proceedings of the 3rd EuroBitumen Congress*, Vienna, Austria, May 2004.

Miner, M.A. (1945). "Cumulative damage in fatigue," Transactions of ASME, 67, A159-A164.

Mirza, M.W. and Witczak, M.W. (1995). "Development of a global aging system short and long term aging of asphalt cements," *AAPT Journal,* 64, 393-430.

Mobasher, B., Mamlouk, M., and Lin, H. M. (1997). "Evaluation of crack propagation properties of asphalt mixtures," *Journal of Transportation Engineering*, 123 (5), 405-413.

Molenaar, A. A. A., and Medani, T. O. (2000). "Rational testing methods for performance based specifications," *Proceedings of the 1st International World of Asphalt Pavements Conference*, ICAP, Sydney, Australia, February 20-24, CD-ROM.

Monismith, C. L., Deacon, J. A., and Harvey, J. T. (2000). *WesTrack: Performance models for permanent deformation and fatigue*, Pavement Research Center, Institute of Transportation Studies, University of California, Berkeley, California.

Montgomery, D. C., and Runger, G.C. (2002). *Applied statistics and probability for engineers*. John Wiley & Sons, Inc. Third Ed., New York.

Montgomery, Elizabeth, A., Peck, and Geoffrey, G (2001). Introduction to linear regression analysis. John Wiley & Sons, Inc., New York.

Nishizawa, T., Shimeno, S., and Sekiguchi, M. (1997). "Fatigue analysis of asphalt pavements with thick asphalt mixture layer," *Proceedings of the 8th International Conference on Asphalt Pavements*, ISAP, Seattle, Washington, August 10-14, 969-976.

Oh Jeong-Ho. (2004). "Field monitoring and modeling of pavement response and service life consumption due to overweight truck traffics." Ph.D. Dissertation, Texas A&M University, College Station , Texas.

Paris, P., and Erdogan, F. (1963). "A critical analysis of crack propagation laws." *Journal of Basic Engineering*, 85, 528-534.

Park, D. W. (2004). "Characterization of permanent deformation in asphalt concrete using a laboratory prediction method and an elastic-viscoplastic model." Ph.D. dissertation, Texas A&M University, College Station, Texas.

Pellinen, T. K., and Witczak, M. W. (2002). "Stress dependent master curve construction for dynamic (complex) modulus." *Annual Meeting of Asphalt Paving Technologist*, AAPT, Colorado Springs, Colorado, March 18-20.

Roberts, F. L., Kandhal, P. S., Lee, D. Y., and Kennedy, T. W. (1996). Hot mix asphalt materials, mixture design, and construction. NAPA Research and Education Foundation, Lanham, Maryland, 187-189.

Roque, R., Birgisson, B., Kim, B., and Cui, Z. (2004). Use of binder rheology to predict the cracking performance of SBS modified mixtures, Volume 2: Guidelines for use of modifiers in superpave mixtures, *Final Report.* Florida Department of Transportation, Tallahassee, Florida.

Rowe, G. M., and Bouldin, M.G. (2000). "Improved techniques to evaluate the fatigue resistance of asphaltic mixtures". 2nd Euroaphalt and Eurobitumen Congress, Book 1, Barcelona, 754-763.

Rowe, G. M., and Brown, S. F (1997a). "Validation of the fatigue performance of asphalt mixtures with small scale wheel tracking experiments," *Journal of the Association of Asphalt Paving Technologists*, AAPT, Seattle, Washington, August 10-14, 66, 31-73.

Rowe, G. M., and Brown, S. F. (1997b). "Fatigue life prediction using visco-elastic analysis," *Proceedings of the 8th International Conference on Asphalt Pavements*, AAPT, Seattle, Washington, August 10-14, 1109-1122.

Schapery, R. A. (1984). "Correspondence principles and a generalized J-integral for large deformation and fracture analysis of viscoelastic media." *International Journal of Fracture*, 25, 195-223.

Schapery, R. A. A. (1973). Theory of crack growth in viscoelastic media, Technical Report No. 2, Mechanics & Materials Research Center, Texas A&M University, College Station, Texas.

Si, Z. (2001). "Characterization of microdamage and healing of asphalt concrete mixtures." Ph.D. Dissertation, Texas A&M University, College Station, Texas.

Simons, J. W., and Seaman, L. (2000). "Finite-element analysis of fatigue lifetime in pavements," *Transportation Research Record* 1709, 36-42.

Superpave Models Team (2000). *Simple performance test: Test results and Recommendations, Interim Task C Report*, NCHRP 9-19 Superpave Support and Performance Models Management, Project Deliverable Subtask C.3, Arizona State University, Tempe, Arizona.

Tashman, L., Masad, E., Zbib, H., Little, D., and Kaloush, K. (2005). "Microstructural viscoplastic continuum model for asphalt concrete." *Journal of Engineering Mechanics, ASCE*, 1 (131), 48-57.

Tayebali, A. A., Deacon, J. A., Coplantz, J. S., Harvey, J. T., and Monismith, C. L. (1992). Fatigue response of asphalt aggregate mixes. Report SHRP A-003, Washington, D.C.

Tsai, B.W., Harvey, J. T., and Monismith, C. C. L. (2004). "Calibration of pavement fatigue performance using recursive Miner's Law." *2nd International Conference on Accelerated Pavement Testing*, Minneapolis, Minnesota, September 25-29.

Tsai, B. W., Harvey, J. T., and Monismith, C. L. (2002). "Westrack fatigue performance prediction using Miner's Law." Paper presented at the 81st Annual Meeting of the Transportation Research Board, Washington, D.C., January 13-17.

Tseng, K. H., and Lytton, R. L. (1990). "Fatigue damage properties of asphaltic concrete pavements." *Transportation Research Record* 1022, National Research Council, Washington, D.C., 52-59.

TxDOT (2003a). "Condition of Texas Pavements. PMIS annual report, FY 2001 - 2003", TxDOT, Construction Division, Materials and Pavement Section, Austin, Texas.

TxDOT (2003b). *Pocket Facts*. TxDOT test specification manuals. http://manuals.dot.state.tx.us, accessed May, 2003.

TxDOT (2002). Texas Department of Transportation (TxDOT), Bryan District Laboratory. HMACP mixture design used on US 290 and SH 47, unpublished Internal Laboratory Test Report, Bryan, Texas.

TxDOT (1995). *Standard Specifications for Construction and Maintenance of Highways, Streets, and Bridges*. Austin, Texas.

Uzan, J. (1997). "Evaluation of fatigue cracking." *Transportation Research Record* 1570, 89-95.

Uzan, J. (1996). "Asphalt concrete characterization for pavement performance prediction." *Journal of the Association of Asphalt Paving Technologists*, 65, 573-607.

van de Ven, M., Smit, A. d. F., and Krans, R. (1997). "Possibilities of a semi-circular bending test." *Proceedings of the 8th International Conference on Asphalt Pavements*, ISAP, Seattle, Washington, D.C., August 10-14, 939-950.

Vassiliev, N.Y., Davison, R. R., and Glover, C. J. (2002). "Development of a stirred airflow test procedure for short-term aging of asphaltic materials." *Transportation Research Record* 1810, Washington D.C., 25-32.

Walubita, L. F., Epps Martin, A., Jung, H. S., Glover, C. J., Park, E. S., Chowdhury, A., and Lytton, R. L. (2005). Comparison of fatigue analysis approaches for two hot mix asphalt concrete (HMAC) mixtures. Draft TxDOT Technical Research Report FHWA/TX-05/0-4468-2, TTI, College Station, Texas.

Walubita, L. F., Hugo, F., and Epps, A. (2002). "Indirect tensile fatigue performance of asphalt concrete after MMLS3 MK3 trafficking under different environmental conditions." *Journal of the South African Institute of Civil Engineering (SAICE),* 44-3, 2-11.

Walubita, L.F, Hugo, F., and Epps, A. (2000). *Performance of rehabilitated lightweight aggregate asphalt concrete pavements under wet and heated model mobile load simulator trafficking: A comparative study with the TxMLS*, Center for Transportation Research Report #1814-3, The University of Texas at Austin, Austin, Texas.

Wen, H., and Kim, Y. R. (2002). "A Simple performance test for fatigue cracking of asphalt concrete based on viscoelastic analysis of indirect tensile testing and its validation using Westrack asphalt mixtures," Paper presented at the 81st Annual Meeting of the Transportation Research Board, Washington, D.C., January 13-17.

Wisneski, M. L., Chaffin, J. M., Davison, R. R., Bullin, J. A., and Glover, C.J. (1996). "Use of lime in recycling asphalt." *Transportation Research Record* 1535, Washington, D.C., 117-123.

Witczak, M. (2001). *Chapter 2: Material characterization*, Draft Report NCHRP 1-37A, Arizona State University, Tempe, Arizona.

Witczak, M., and Pellinen, T. (2002). "Use of stiffness of hot-mix asphalt as a simple performance test." *Transportation Research Record* 1789, Washington, D.C., 80-90.

Zhang, T., and Raad, L. (2001). "Numerical methodology in fatigue analysis: Applications." *Journal of Transportation Engineering*, 127 (1), 59-66.

Zhou, J., and Liang, R. Y. (1996). "Fatigue model of asphalt concrete." *Proceedings of the 11th Conference on Engineering Mechanics*, ASCE, Fort Lauderdale, Florida, May 19-22, 563-567.

APPENDIX A

EVALUATION FIELD SURVEY QUESTIONNAIRE

EVALUATION FIELD SURVEY QUESTIONNAIRE
(FOR GOVERNMENT AGENCIES AND THE INDUSTRY)

TxDOT PROJECT 0-4468

FATIGUE RESISTANT MIXES AND DESIGN METHODOLOGY SURVEY

This survey is conducted as part of the Texas Department of Transportation (TxDOT) Project 0-4468, Evaluation of the Fatigue Resistance of Rut Resistant Mixes, under the supervision of Gregory Cleveland (512-506-5830). The primary goal of this project is to develop and recommend the process for incorporating fatigue analysis and testing into TxDOT's pavement design and mixture design process. TxDOT already has the means to screen out mixtures that are susceptible to rutting; mixtures with stiffer binders greatly decrease the risk of premature failure due to rutting. However, there are concerns that some of the mixtures that are highly resistant to rutting may be more prone to fatigue failure. To identify, document, and compare several materials, mixtures, and pavement structures types in terms of fatigue resistance, we are sending out this survey to several government agencies and industry representatives in order to create a complete knowledge database.

We would appreciate your participation. If there are any questions concerning this survey or this project, please contact Dr. Amy Epps Martin (979-862-1750) of the Texas Transportation Institute. Once again we appreciate your time and assistance.

Agency Name: _____ **Contact Name:** _____

Phone: (____ ___) - _____ - _____ **Fax:** (_____) - _____ - _____

---

1. Do you utilize any methodology or approach to design and/or check for fatigue resistance?

   YES _____ [*please proceed to question 2*] **NO** _____ [*please stop*]

2. What mix design methodology (ies) or approach (es) do you follow? _____

3. List literature references you have found useful to approach fatigue resistance designs._____

4. List the laboratory tests, and corresponding standards, performed as part of the fatigue resistance approach (es) you use.

   _____

5. What type(s) of aggregate(s) and binder(s) grades do you use for fatigue resistant mixes?

Aggregate Type	Binder Type/Grade

What pavement structure(s) do you commonly use for fatigue-resistant pavement design?

Layer	Thickness	Elastic Modulus

7. What type and amount of resources (time, persons, equipment, etc.) do you require to perform a fatigue-resistant mix and pavement design?

[You may attach extra papers if the information does not fit on this page.]

Thank you for your time and effort in completing this survey. The results will aid us in identifying, document, and comparing several materials, mixtures, and pavement structure types in terms in fatigue resistance.

SUMMARY RESULTS OF EVALUATION FIELD SURVEY QUESTIONNAIRE
(FROM GOVERNMENT AGENCIES AND THE INDUSTRY)

TxDOT PROJECT 0-4468: FATIGUE-RESISTANT MIXES AND DESIGN METHODOLOGY SURVEY

Table A-1. Summary of Respondent Questionnaire Survey Details

No.	Agency	Fatigue Methodology	Laboratory Tests	Materials		Pavement Structures	Resources	Standards/ References
				Aggregate	Binder			
1	Advanced Asphalt Technologies, LLC 814-278 1991	Continuum damage analysis (NCHRP 9-25 and 9-31)	Uniaxial fatigue testing	9.5 -12 mm, dense gradation	X	X	-16 hrs -Compactor, ovens, molds, saw, coring rig, MTS system	AAPT papers on Continuum Damage modeling & analysis
2	Abatech 215 – 215 258	Superpave	Bending beam and SHRP IDT	X	X	X	≥ $40,000	Various paper publications
3	Louisiana DOTD 225-767 9109	Superpave	Modified T-283, Moisture sensitivity & retained ITS	Various	PG 76-22 modified	Use SN criteria, i.e. 0.44 to 0.48 for HMAC	No special design procedure for fatigue	Superpave
4	North Carolina State University 619-515 7758	Visco-elastic continuum damage model	Uniaxial tension & indirect tension	Granite	PG 64-22		MTS & graduate students	-
5	Minnesota DOT 651-779 5218	Superpave & MnPave	No fatigue tests	X	X	Mechanistic-empirically based	One researcher	Superpave
6	UCB, Berkeley 510-231-5746	Caltrans & Asphalt Institute	Bending beam, AASHTO TP-8	Crushed stone, dense graded	AR 4000 AR 8000	AC, 150 mm, 1000 – 8000 MPa	-2-3 wks -4 people -bending beam device (Cox & Sons)	-NCHRP 39 -Various publications

X – No data

APPENDIX B

TTI SURFACE ENERGY (SE) MEASUREMENTS

EXAMPLE OF SURFACE ENERGY (SE) RESULTS MEASURED AT TTI

Table B-1. Binder SE Components (Unaged)

No.	Asphalt	Source	Wetting (Healing) (ergs/cm^2)					Dewetting (Fracture) (ergs/cm^2)				
			Γ^+	Γ^-	Γ^{AB}	Γ^{LW}	Γ^{Total}	Γ^+	Γ^-	Γ^{AB}	Γ^{LW}	Γ^{Total}
1	PG 64-22	TX	1.83	4.43	8.87	4.28	13.16	4.06	7.05	10.58	20.01	30.60
2	PG 67-22	FL (Adhara)	0.05	4.05	0.9	21.68	22.58	0.23	11.28	3.22	42.01	45.23
3	PG 70-28	(Lytton)	0.19	3.09	1.63	18.23	19.85	18.38	28.76	45.98	7.34	53.31
4	PG 76-22	TX	1.15	2.28	4.23	13.63	17.15	4.48	9.42	5.98	76.92	17.15

EXAMPLE OF SURFACE ENERGY (SE) RESULTS MEASURED AT TTI

Table B-2. Aggregate SE Components (Unaged)

No.	Aggregate	Source	ergs/cm^2					m^2/gm
			G^+	G^-	G^{AB}	G^{LW}	G^{Total}	SSA
1	Granite	Ga (Adhara)	31.86	194.78	157.55	61.08	218.63	X
2	Granite	TX, Wichita Falls (Corey)	43.59	782.71	368.88	56.34	425.22	0.67
3	Gravel	TX (Victoria)	1.10	426.85	43.31	81.34	124.65	X
4	Gravel	TX, Atlanta (Corey)	1.25	286.03	37.06	59.49	96.59	0.80
5	Gravel	OH (Corey)	7.74	546.37	129.74	63.42	193.21	4.76
6	Limestone	TX (Caldwell)	1.62	362.71	48.51	79.89	128.40	X
7	Limestone	OH (Corey)	1.77	401.18	53.01	58.05	111.14	0.53
8	Limestone	FL (Adhara)	27.76	184.87	135.30	88.46	223.77	X
9	Limestone	MD (Amit)	0.08	373.17	11.23	71.02	82.25	X
10	Limestone	TX (Ding)	0.40	285.50	16.10	86.50	102.60	X
11	Limestone	CO (Ding)	0.10	206.50	7.30	79.90	87.30	X
12	Limestone Screenings	TX (Corey)	18.88	561.15	205.59	59.88	265.47	0.49
13	Granite	GA (DX)	24.10	96.00	73.30	133.20	206.50	X
14	Quartzite	TX, Atlanta (Corey)	8.86	545.04	139.22	60.81	200.13	1.35
15	Sandstone (Light)	TX, Atlanta (Corey)	2.03	222.67	42.55	62.43	105.05	0.83
16	Sandstone (Light)	TX, Atlanta (Corey)	8.52	316.92	103.93	63.96	167.88	1.00

Legend: X = No data

APPENDIX C

THE CMSE FATIGUE ANALYSIS APPROACH

BRIEF BACKGROUND: CMSE AND CONTINUUM FRACTURE-DAMAGE MECHANICS FATIGUE ANALYSIS APPROACHES

Over the past decades, a number of approaches for characterizing the fracture properties of hot-mix asphalt concrete (HMAC) mixtures have been developed and some have gained widespread usage in the industry. Continuum fracture-damage mechanics by far constitutes some of the most promising approaches for fundamentally characterizing the fracture properties of HMAC mixtures used in fatigue damage analysis. Unlike phenomenological-based approaches, their failure criterion is based on a direct relationship between crack development and fracture damage (Lundström 2004). Additionally, the fracture-damage mechanics models are based on data input obtained explicitly from simple routine laboratory material characteristic tests instead of time-consuming fatigue tests such as the bending beam.

Fundamental Concepts:

Schapery's Work Potential Theory and Paris' Law of Fracture Mechanics

Continuum fracture-damage mechanics approaches are conceptualized on the fundamental theory that HMAC is a complex composite material that behaves in a non-linear visco-elastic manner and requires energy to be expended to cause load-induced damage in the form of fracture or fatigue cracking. The approaches utilizes the visco-elastic correspondence principle, Paris' Law of fracture mechanics (Paris and Erdogan 1963), and Schapery's (1984) work potential theory (WPT) to remove the viscous effects and monitoring of accumulated fracture damage through changes in dissipated pseudo strain energy (DPSE) under simple repeated uniaxial tensile tests (Lytton et al. 1993, Si 2001).

According to Schapery's WPT based on continuum damage models for linear-elastic materials, the total work done during the damaging process is assumed to be path-independent, and therefore, the total fracture damage growth is considered to be solely dependent on the external loading. Based on this assumption, the damage process can simply be characterized by the changes in the internal material state variables such as the stress, strain, and strain energy density.

To account for non-linear visco-elastic materials like HMAC which are loading time-dependent, Schapery proposed the extended visco-elastic correspondence principle in which he introduced pseudo-elastic variables represented in the form of convolution integrals that exhibit time-independent boundary conditions. Under this extended visco-elastic correspondence principle, the primary variable of importance is the pseudo-strain energy function that is used to characterize the fracture damage process while at the same time correcting for the non-linearity and visco-elasticity behavior of the material. On this basis, the total work done or energy expended to cause fracture or fatigue damage can be expressed as a function of stress and strain as follows:

$$W_R = f(\sigma_m(t), \varepsilon_R(t)) \qquad \text{(C-1)}$$

where:

W_R	=	Represents the total work done in the form of dissipated pseudo strain energy (DPSE) (J/m^3)
$\sigma_m(t)$	=	Physically measured time-dependent stress (MPa)
$\varepsilon_R(t)$	=	Calculated pseudo strain (mm/mm).

Because of its ability to account for the material non-linearity and visco-elasticity under repeated tensile loading, DPSE constitutes a very significant variable for characterizing the fracture properties of HMAC mixtures used in fatigue damage analysis.

In the structural application of continuum fracture-damage analysis, the development of microcracks basically affects the stress-strain fields in a given media. Consequently, a stress intensity factor (K) is introduced to characterize the stress intensity and distribution in the vicinity of a microcrack tip under repeated loading and unloading cycles. According to Paris' Law of fracture mechanics, the crack growth rate per load cycle (dc/dN) can be modeled as a function of K using the fracture damage characterization model illustrated below:

$$\frac{dc}{dN} = A[K]^n \qquad \text{(C-2)}$$

where:

A, n	=	Paris' Law fracture coefficients
dc/dN	=	Crack growth rate per load cycle

According to Eq. (C-2), the rate of fracture crack growth per load cycle is quantitatively a function of the stress intensity and distribution in the vicinity of the microcrack tip under repeated loading and unloading cycles. Consequently, Paris' Law of fracture is utilized to model this relationship. The Paris' Law fracture coefficients (A and n) are experimentally determined parameters and often depend on material properties, temperature, loading mode and magnitude, stress state, and environmental conditions. A and n are significant parameters used for characterizing fracture crack growth in an assumed linear visco-elastic homogeneous media. Essentially, these fracture coefficients define the rate of crack growth and propagation during the fracturing process and generally exhibit an inverse proportional relationship with HMAC mixture fracture resistance. According to Schapery's (1973) visco-elastic fracture mechanics theory, these coefficients (A and n) can be determined from simple material characteristic tests such as creep compliance, relaxation modulus, tensile strength, and surface energy.

Analogous to K for linear elastic fracture mechanics (LEFM) analysis, the *J-integral* is often used in Eq. C-2 for non-linear fracture mechanics (NLFM) analysis of materials like HMAC mixtures. According to Anderson (1995), this *J-integral* can be used both as an energy parameter and stress intensity parameter, and is thus valid for both non-linear elastic and elastic-plastic materials, i.e., it is applicable to both LEFM and NLFM analyses (Lundström 2004). From Schapery's modified WPT and Paris' Law, the fundamental laws of fracture mechanics based on NLFM analysis for visco-elastic materials are governed by two principal models illustrated below and represented in Fig. C-1 (Lytton et al. 1993):

$$\Delta G_f = E_R\left[D(t_\alpha)\right]J_R \tag{C-3}$$

$$\frac{dc}{dN} = A\left[J_R(\max)\right]^n \tag{C-4}$$

Where:

ΔG_f = Bond strength or fracture surface energy (ergs/cm^2) which represents the work that is required to separate a unit area of a material to form two separate crack surface faces

E_R = Reference modulus used in determining the pseudo-strain energy that is available to extend the crack (MPa)

$D(t_\alpha)$ = Compliance of the material for the time that is required for the crack to travel the length of the fracture process zone ahead of the tip of the crack (MPa^{-1})

t_α = Length of time that is required for the crack to travel the length of the fracture process zone, α (s)

J_R = Pseudo J-integral representing the amount of pseudo strain energy that is released per unit of area of crack surface area

c	=	Crack length (mm),
N	=	Number of load repetitions.
A, n	=	Paris' Law fracture coefficients.

Fig. C-2 is a typical representation of a fracture crack growth as characterized by Paris' Law and illustrated by Eq. C-4**.**

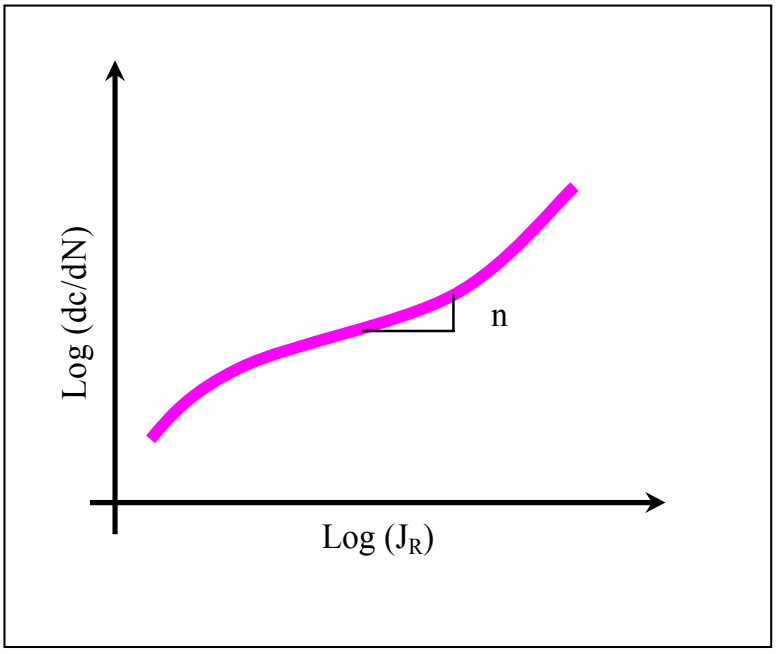

Fig. C-1. Typical Fracture Crack Growth

Note that when applied to LEFM analysis, the *J-integral* is related to the *K* in Eq. (C-2) as a function of the Poisson's ratio (υ) and the material elastic modulus (*E*) in MPa by the following expression:

$$J = K^2 \left[\frac{\left(1 - \upsilon^2\right)}{E} \right] \qquad \text{(C-5)}$$

Numerical Derivation of Paris' Law Fracture Coefficients, *A* and *n*

This section summarizes the numerical derivation of Paris' Law fracture coefficients *A* and *n* based on Eqs. (C-3) and (C-4), respectively. From Eq. (C-3), the material compliance $D(t_\alpha)$ is defined as follows:

$$\left[D(t_\alpha)\right] = D_0 + D_1\left(\frac{\alpha}{\dot{c}}\right)^m \tag{C-6}$$

Then,

$$\Delta G_f = E_R\left[D_0 + D_1\left(\frac{\alpha}{\dot{c}}\right)^m\right]J_R \tag{C-7}$$

From Eq. (C-7):

$$\dot{c} = \frac{dc}{dt} = \alpha\left[\frac{D_1 E_R J_R}{\Delta G_f - \left(D_0 E_R J_R\right)}\right]^{\left(\frac{1}{m}\right)} \tag{C-8}$$

But,

$$\alpha = k\left[\frac{J_R}{D_1 \sigma_t^2 I_1}\right], \text{ for stress-controlled loading} \tag{C-9}$$

And,

$$I_i = \frac{2}{\left(1 + n_{BD}\right)} \tag{C-10}$$

Therefore, Eq. (C-8) becomes:

$$\frac{dc}{dt} = k\left[\frac{D_1^{\left(\frac{1}{m}-1\right)} E_R^{\left(\frac{1}{m}\right)} J_R^{\left(1+\frac{1}{m}\right)}}{\left[\Delta G_f - \left(D_0 E_R J_R\right)\right]^{\left(\frac{1}{m}\right)}}\right]\left[\frac{1}{\sigma_t^2 I_1}\right] \tag{C-11}$$

Considering that

$$t = N\Delta t, \text{ i.e., } \frac{dt}{dN} = \Delta t \tag{C-12}$$

And,

$$\frac{dc}{dt} = \frac{dc}{dN}\frac{dN}{dt} = \frac{dc}{dN}\frac{1}{\Delta t} \tag{C-13}$$

Eq. (C-11) becomes;

$$\frac{dc}{dN} = k\left[\frac{D_1^{(1-m)} E_R}{\left[\Delta G_f - \left(D_0 E_R J_R\right)\right]}\right]^{\left(\frac{1}{m}\right)} \int_0^{\Delta t}\left[\frac{J_R^{\left(1+\frac{1}{m}\right)}(t)}{\sigma_t^2 I_i}\right] dt \tag{C-14a}$$

$$\frac{dc}{dN} = k\left[\frac{D_1^{(1-m)} E_R}{\left[\Delta G_f - \left(D_0 E_R J_R\right)\right]}\right]^{\left(\frac{1}{m}\right)} \int_0^{\Delta t}\left[\frac{\left(J_R\right)_{(\max)}^{\left(1+\frac{1}{m}\right)}\left[w(t)\right]^{\left(1+\frac{1}{m}\right)}}{\sigma_t^2 I_i}\right] dt \tag{C-14b}$$

$$\frac{dc}{dN} = \left| k\left[\frac{D_1^{(1-m)} E_R}{\left[\Delta G_f - \left(D_0 E_R J_R\right)\right]}\right]^{\left(\frac{1}{m}\right)} \int_0^{\Delta t}\left[\frac{\left[w(t)\right]^{\left(1+\frac{1}{m}\right)}}{\sigma_t^2 I_i}\right] dt \right| \left[J_R(\max)\right]^{\left(1+\frac{1}{m}\right)} \tag{C-15}$$

Assuming linear visco-elasticity for the HMAC material under constant stress- or strain-controlled uniaxial repeated direct-tension (RDT) testing and comparing Eq. (C-15) to (C-4), Paris' Law fracture coefficients A and n are derived as follows:

$$A = \left| k\left[\frac{D_1^{(1-m)} E_R}{\left[\Delta G_f - \left(D_0 E_R J_R\right)\right]} \right]^{\left(\frac{1}{m}\right)} \int_0^{\Delta t} \left[\frac{\left[w(t)\right]^{\left(1+\frac{1}{m}\right)}}{\sigma_t^2 I_i} \right] dt \right| \tag{C-16}$$

$$n = \left[1 + \frac{1}{m}\right], \text{ for stress-controlled RDT testing} \tag{C-17a}$$

$$n = \left[\frac{1}{m}\right], \text{ for strain-controlled RDT testing} \tag{C-17b}$$

with $\alpha = \left[\frac{k}{D_1 \sigma_t^2 I_1}\right]$ in Eq. (C-9)

For $D_0 \cong 0$, and introducing n_{BD} to account for HMAC brittle-ductility state, Eq. (C-16) becomes:

$$A = \left| \frac{k}{\sigma_t^2 I_i} \right| \left[\left(\frac{D_1^{(1-m)} E_1}{\Delta G_f} \right)^{\left(\frac{1}{m}\left[\frac{1}{1+n_{BD}}\right]\right)} \right] \left| \int_0^{\Delta t} w^n(t)\, dt \right| \tag{C-18}$$

Where;

$$I_i = \frac{2}{\left(1 + n_{BD}\right)} \tag{C-19}$$

$$D_1 = \left(\frac{1}{E_1}\right)\left(\frac{Sin[m\pi]}{m\pi}\right) \quad \text{(C-20a)}$$

That is,

$$D(t) = \left(\frac{1}{E(t)}\right)\left(\frac{Sin[m\pi]}{m\pi}\right) \quad \text{(C-20b)}$$

$$\int_0^{\Delta t} w^n(t)dt = \int_0^{\Delta t}\left(Sin^{2n}\left[\frac{\pi}{\Delta t}t\right]\right)dt \quad \text{(C-21)}$$

where:

$\dot{c}$	=	Rate of microcrack growth as a function of time
α	=	Length of the fracture process zone (mm)
m	=	Stress relaxation rate obtained from the relaxation modulus (RM) master-curve
D_1	=	Time-dependent tensile creep compliance at 1.0 s (MPa^{-1})
E_1	=	Relaxation elastic modulus ($E(t)$) from RM master-curve at 1.0 s (MPa)
k	=	Material coefficient
σ_t	=	Maximum mixture tensile strength at break (MPa)
I_i	=	Dimensionless elasticity stress-integral factor in the crack failure zone (ranging between 1 and 2)
n_{BD}	=	Dimensionless brittle-ductile factor (ranging between 0 and 1)
Δt	=	Repeated loading time duration (s) (~0.01 s)
$w(t)$	=	Load pulse shape factor (ranging between 0 and 1)
t	=	Total load cycle time (s).

Numerical Derivation of N_i (Microcrack Initiation)

In this section, the derivation of the number of repetitive load cycles to microcrack initiation (N_i) is illustrated. From Eq. (C-4), let J_R(max) be defined as the change in W_R (*i.e.,* ΔW_R) with respect to changes in the cracked surface area (CSA) (i.e., $\Delta[C.S.A]$) as follows:

$$\left[J_R(\max)\right] \cong J_R = \left[\frac{\left(\frac{dW_R}{dN}\right)}{\left(\frac{d(CSA)}{dN}\right)}\right] \qquad \text{(C-22)}$$

And from a logarithmic plot of DPSE versus load cycles N (Fig. C-2):

$$W_R = a + bLog(N) \qquad \text{(C-23)}$$

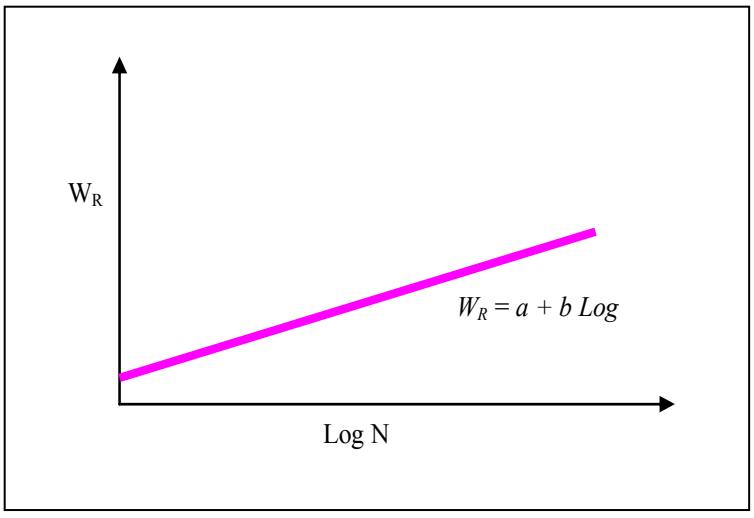

Fig. C-2. Example of a Plot of W_R – Log N

The rate of change of W_R (ΔW_R) with respect to the rate of change in N (ΔN) is simply:

$$\frac{dW_R}{dN} = \frac{b}{N} \tag{C-24}$$

And for a Cracked Surface Area (CSA) given by;

$$C.S.A = 2\pi\bar{c}^2 m = 2\pi A_c\left[\bar{c}^2\left(\frac{m_{crack}}{A_c}\right)\right] \tag{C-25}$$

$$\frac{d(CSA)}{dN} = \frac{d}{dN}\left[2\pi A_c\left(\bar{c}^2\,\frac{m_{crack}}{A_c}\right)\right] = 4\pi A_c\bar{c}\left(\frac{m_{crack}}{A_c}\right)\frac{d\bar{c}}{dN} \tag{C-26}$$

Letting

$$const = \bar{c}^2\left(\frac{m_{crack}}{A_c}\right) \tag{C-27}$$

Eq. C-26 becomes:

$$\frac{d(CSA)}{dN} = 4\pi A_c\,(const)\left(\frac{1}{\bar{c}}\right)\frac{d\bar{c}}{dN} \tag{C-28}$$

Therefore, Eq. (C-4) becomes:

$$\frac{dc}{dN} \cong \frac{d\bar{c}}{dN} = A\left[\frac{\dfrac{b}{N}}{4\pi A_c\,(const)\left(\dfrac{1}{\bar{c}}\right)\dfrac{d\bar{c}}{dN}}\right]^n \tag{C-29}$$

And simplifies to:

$$\left[\left(\frac{1}{\overline{c}}\right)^{\left(\frac{n}{1+n}\right)}\left(\frac{d\overline{c}}{dN}\right)\right]=\left[A\right]^{\left(\frac{1}{1+n}\right)}\left[\frac{\frac{b}{N}}{4\pi A_c\left(const\right)}\right]^{\left(\frac{n}{1+n}\right)} \tag{C-30a}$$

$$\left[\int_0^{\overline{c}_{\max}}\left(\overline{c}\right)^{\left(\frac{-n}{1+n}\right)}\,d\overline{c}\right]=\left|\left[A\right]^{\left(\frac{1}{1+n}\right)}\right|\left|\left[\frac{b}{4\pi A_c\left(const\right)}\right]^{\left(\frac{n}{1+n}\right)}\right|\left|\int_0^{N_i}\left(N\right)^{\left(\frac{-n}{1+n}\right)}dN\right| \tag{C-30b}$$

Within the set integral limits, Eq. (C-30[b]) integrates to;

$$\left|\left(1+n\right)\left[\overline{c}_{\max}\right]^{\left(\frac{1}{1+n}\right)}\right|=\left|\left[A\right]^{\left(\frac{1}{1+n}\right)}\right|\left|\left[\frac{b}{4\pi A_c\left(const\right)}\right]^{\left(\frac{n}{1+n}\right)}\right|\left|\left(1+n\right)\left[N_i\right]^{\left(\frac{1}{1+n}\right)}\right| \tag{C-30c}$$

And becomes:

$$N_i=\left[\overline{c}_{\max}\frac{1}{A_c}\right]\left[\frac{4\pi A_c\left(const\right)}{b}\right]^{(n)} \tag{C-30d}$$

At N_i,

$$const=\left(\overline{C}_{\max}\right)^2\left(\frac{m_{crack}}{A_c}\right) \tag{C-31}$$

And,

$$\left(\frac{m}{A_c}\right) = C_D \tag{C-32}$$

Therefore, the equation for N_i becomes:

$$N_i = \left[\frac{\left(\overline{C}_{\max}\right)^{(1+2n)}}{A_c}\right]\left[\frac{4\pi A_c}{b}\right]^{(n)}\left[C_D\right]^{(n)} \tag{C-33}$$

where:

$\overline{C}$	=	Crack length (mm)
$\overline{C}_{\max}$	=	Maximum microcrack length (mm)
A_c	=	HMAC specimen cross-sectional area (m^2)
b	=	Rate of accumulation of dissipation of pseudo strain energy (J/m^3) measured from RDT testing
C_D	=	Crack density (m/m^2)
m_{crack}	=	Total number of countable or measurable cracks on a given X-sectional area A_c

Numerical Derivation of N_p (Microcrack Propagation)

The numerical derivation of the number of repetitive load cycles to microcrack propagation (N_p) demonstrated in this section is based on the stress intensity force driving the crack growth through the HMAC layer of thickness (d). As repeated loading continues and the crack grows progressively, the crack ratio (C_R) will approach a value of 1.0, at which point complete failure occurs. Fig. C-3 is diagrammatic illustration of this relationship as a function of stress.

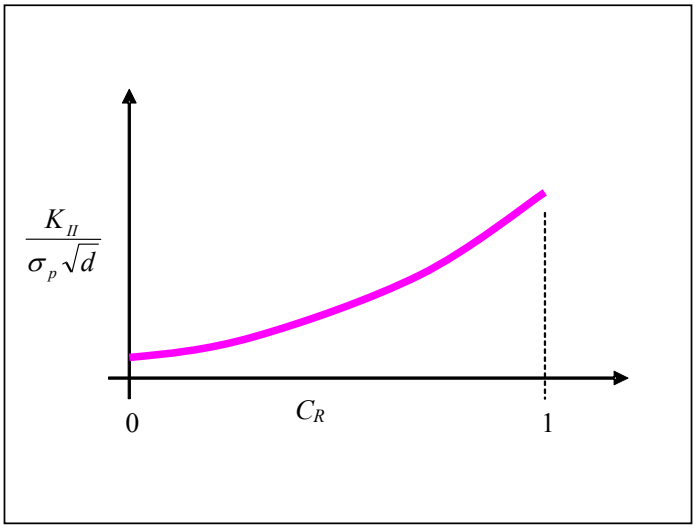

Fig. C-3. Relation between Stress and Crack Growth

Where:

$$C_R = \frac{\bar{c}}{d} \tag{C-34}$$

Based on this hypothesis as demonstrated in Fig. C-3, Eq. (C-2) is modified as follows:

$$\frac{dc}{dN} \cong \frac{d\bar{c}}{dN} = A\left[2K_{II}\right]^n \tag{C-35}$$

With

$$K_{II} = \left[\sigma_p \sqrt{d}\right]\left[r\left(\frac{\bar{c}}{d}\right)^q\right] \tag{C-36}$$

Eq. (C-35) becomes:

$$\frac{d\bar{c}}{dN} = A\left[2^n\right]\left[\bar{c}^{nq}\right]\left[\sigma_p r d^{\left(\frac{1}{2}-q\right)}\right]^n \tag{C-37}$$

Upon integration,

$$\int_0^{N_p} dN = \frac{1}{A\left[2^n\right]\left[\sigma_p r d^{\left(\frac{1}{2}-q\right)}\right]^n} \int_{\bar{c}_0}^{d} \bar{c}^{-nq} d\bar{c} \tag{C-38a}$$

$$N_p = \frac{\left[d^{(1-nq)} - \bar{c}_0^{\,(1-nq)}\right]}{A(1-nq)\left[(2r\sigma_p)^n\right]\left[d^{\left(\frac{n}{2}-nq\right)}\right]} \tag{C-38b}$$

Eq. (C-37) reduces to:

$$N_p = \frac{\left[d^{\left(1-\frac{n}{2}\right)}\left(1-\left(\frac{\bar{c}_0}{d}\right)^{(1-nq)}\right)\right]}{A(1-nq)\left[(2r)^n\right]\left[\sigma_p\right]^n} \tag{C-38c}$$

From elastic theory,

$$\sigma_{p(\max)} = S\tau_{\max} = SG\gamma_{\max} \tag{C-39}$$

Where:

$$S = \frac{1-\upsilon}{1-2\upsilon},\ G = \frac{E}{2(1+\upsilon)} \tag{C-40}$$

$$SG = \left|\frac{(1-\upsilon)}{(2(1-2\upsilon)(1+\upsilon))}\right| |E| \tag{C-41}$$

And $\overline{C}_0$ at the start of N_p is $\overline{C}_{\max}$ at N_i, therefore N_p, becomes:

$$N_p = \left[\frac{d^{\left(1-\frac{n}{2}\right)}}{A(1-nq)\left[(2r)^n\right]\left[SG\right]^n}\right]\left[1-\left(\frac{\overline{c}_{\max}}{d}\right)^{(1-nq)}\right]\left[\frac{1}{\gamma}\right]^{(n)} \tag{C-42}$$

If

$$k_1 = \left[\frac{d^{\left(1-\frac{n}{2}\right)}}{A(1-nq)\left[(2r)^n\right]\left[SG\right]^n}\right]\left[1-\left(\frac{\overline{c}_{\max}}{d}\right)^{(1-nq)}\right] \tag{C-43}$$

$$k_2 = n \tag{C-44}$$

Then N_p simplifies to:

$$N_p = k_1(\gamma)^{-k_2} \tag{C-45}$$

where:

C_R	=	Crack ratio
d	=	HMAC layer thickness (mm)
$\overline{C}_0$	=	Initial microcrack length (mm)
$\overline{C}$	=	Crack length (mm)
K_{II}	=	Stress intensity factor in the crack failure zone
r,q	=	Regression constants for K_{II}; σ_p is the applied tire pressure (kPa)
S	=	Shear stress coefficient
τ	=	Shear stress (MPa)
G	=	Shear modulus (MPa)
γ	=	Maximum design shear strain often computed at the edge of a loaded tire (mm/mm), and k_i are material constants

APPENDIX D

THE UNIVERSAL SORPTION DEVICE

THE UNIVERSAL SORPTION DEVICE

Table B-1. Summary of the Testing and Analysis Procedure for Determining the Surface Energy (SE) of Aggregates using the USD Method

Step	Action
1	Prepare the aggregate sample from the fraction passing the No.4 (4.75mm) sieve, retained on the No. 8 (2.36 mm) sieve. • Wet sieve approximately 150 g of each type of aggregate. • Wash the samples again using distilled water and dry in a 120 °C oven for at least 8 hr. • Move the samples into a vacuum desiccator at about 1 torr and 120 °C for at least 24 hr to de-gas. • Wash the aggregate sample holder with distilled water and acetone and then dry in a 120 °C oven for one hour.
2	Place the weighed aggregate in the container and proceed with chamber conditioning: • Connect the temperature control circulator with the high-pressure steel chamber. • Activate and calibrate the magnetic suspension balance. • Use the vacuum pump to evacuate the chamber to below 1 torr for one day while it is heated up to 60°C. • Reduce and maintain the chamber temperature at 25°C under the vacuum of below 1 torr for 8 hr.
3	Proceed with testing using the selected solvents: n-hexane (apolar), methyl-propyl-ketone (mono-polar), and water (bipolar): • Initiate the computer program to control testing and control data capturing, and enter 8 to 10 predetermined pressure steps based on the saturation vapor pressure of the solvents used. The following two steps are then controlled automatically and are included for completeness of process description. • Solvent vapor is injected into the system until the first predetermined value is reached by using the macro-adjustment valve. After the steady-state adsorption mass is reached and measured by the system, the pressure is changed to the next setting point. • The last step is repeated while the computer records the absorbed mass and vapor pressure until the saturated vapor pressure of the solvent is reached.
4	Use the specific amount of solvent adsorbed on the surface of the adsorbent and vapor pressure at the surface of the asphalt or aggregate to do surface energy calculations: • Calculate the specific surface area of the aggregate using the BET equation. • Calculate the spreading pressure at saturation vapor pressure for each solvent using the Gibbs adsorption equation. • Calculate the three unknown components of surface energy utilizing the equilibrium spreading pressure of adsorbed vapor on the solid surface and known surface energies of the a polar, mono-polar, and bipolar solvents.
5	Using SE results from step 4, calculate the total surface energy of the aggregate.

APPENDIX E

HMAC MIXTURE PROPERTY RESULTS

BENDING BEAM (BB) LABORATORY TEST DATA

Table E-1a. BB Test Data for 0, 3, and 6 Months Aging Conditions

Rows	Micro Strain	Nf Lab Bryan-0M	Nf Lab Bryan-3M	Nf Lab Yoakum-0M	Nf Lab Yoakum-3M	Nf Lab Yoakum-6M
1	374	131000	71400	246580	170000	76600
2	374	120000	90600	201000	191000	138000
3	374	130000	78560	.	155500	110000
4	468	55000	47000	95200	68200	40450
5	468	51000	32000	115500	90000	46000
6	468	46000	40500	.	100300	55000
7	157	.	.	.	.	.
8	278.96	.	.	.	.	.
9	273.21	.	.	.	.	.
10	289.47	.	.	.	.	.
11 (US 290)	98.97	.	.	.	.	.

Table E-1b. Example of ME Log-Transformation of Table E-1a Data

Rows	Log Micro Strain	Log Nf Lab Bryan-0M	Log Nf Lab Bryan-3M	Log Nf Lab Yoakum-0M	Log Nf Lab Yoakum-3M	Log Nf Lab Yoakum-6M
1	5.92	11.78	11.18	12.42	12.04	11.25
2	5.92	11.70	11.41	12.21	12.16	11.84
3	5.92	11.78	11.27	.	11.95	11.61
4	6.15	10.92	10.76	11.46	11.13	10.61
5	6.15	10.84	10.37	11.66	11.41	10.74
6	6.15	10.74	10.61	.	11.52	10.92
7	5.06	.	.	.	.	.
8	5.63	.	.	.	.	.
9	5.61	.	.	.	.	.
10	5.67	.	.	.	.	.
11 (US 290)	4.59	.	.	.	.	.

Table E-1c. Example of ME 95% Prediction Interval Estimates of Log N_f

(Bryan Mixture)

Rows	Log Micro Strain	Predicted Log Nf Bryan-0M (Yhat_B0)	Lower 95% prediction interval for Yhat_B0	Upper 95% prediction interval for Yhat_B0	Predicted Log Nf Bryan-3M (Yhat_B3)	Lower 95% prediction interval for Yhat_B3	Upper 95% prediction interval for Yhat_B3
1	5.92	11.75	11.52	11.98	11.29	10.77	11.80
2	5.92	11.75	11.52	11.98	11.29	10.77	11.80
3	5.92	11.75	11.52	11.98	11.29	10.77	11.80
4	6.15	10.83	10.60	11.06	10.58	10.06	11.10
5	6.15	10.83	10.60	11.06	10.58	10.06	11.10
6	6.15	10.83	10.60	11.06	10.58	10.06	11.10
7	*5.06*	*15.32*	*14.57*	*16.06*	*14.02*	*12.36*	*15.69*
8	*5.63*	*12.96*	*12.59*	*13.32*	*12.21*	*11.39*	*13.03*
9	*5.61*	*13.04*	*12.66*	*13.42*	*12.28*	*11.43*	*13.12*
10	*5.67*	*12.80*	*12.46*	*13.15*	*12.10*	*11.32*	*12.87*
11 (US 290)	4.59	17.21	16.14	18.28	15.48	13.08	17.88

Table E-1d. Example of ME 95% Prediction Interval Estimates of Log N_f (Yoakum Mixture)

Rows	Log Micro Strain	Predicted Log Nf Yoakum-0M (Yhat_Y0)	Lower 95% prediction interval for Yhat_Y0	Upper 95% prediction interval for Yhat_Y0	Predicted Log Nf Yoakum-3M (Yhat_Y3)	Lower 95% prediction interval for Yhat_Y3	Upper 95% prediction interval for Yhat_Y3
1	5.92	12.31	11.57	13.05	12.05	11.54	12.56
2	5.92	12.31	11.57	13.05	12.05	11.54	12.56
3	5.92	12.31	11.57	13.05	12.05	11.54	12.56
4	6.15	11.56	10.82	12.30	11.35	10.84	11.86
5	6.15	11.56	10.82	12.30	11.35	10.84	11.86
6	6.15	11.56	10.82	12.30	11.35	10.84	11.86
7	*5.06*	*15.23*	*12.50*	*17.96*	*14.77*	*13.13*	*16.41*
8	*5.63*	*13.30*	*12.01*	*14.58*	*12.97*	*12.17*	*13.77*
9	*5.61*	*13.37*	*12.03*	*14.70*	*13.04*	*12.20*	*13.87*
10	*5.67*	*13.17*	*11.97*	*14.38*	*12.85*	*12.10*	*13.61*

DYNAMIC MODULUS (DM) LABORATORY TEST DATA

Table E-2a. Summary of DM Values for Bryan Mixture:
Basic TxDOT Type C Mixture (PG 64-22 + Limestone]

Specimen #BDM0001, AV = 6.56%

Temperature		Dynamic Modulus, psi					
°C	°F	0.1 Hz	0.5 Hz	1.0 Hz	5.0 Hz	10 Hz	25 Hz
-10	14	2,833,936	3,359,219	3,512,016	3,959,646	4,093,719	4,340,675
4.4	40	1,362,920	1,742,570	1,922,417	2,313,526	2,529,980	2,753,048
21.1	70	471,605	680,590	808,919	1,125,797	1,300,089	1,599,810
37.8	100	152,623	247,913	297,864	490,257	622,778	878,987
54.4	130	68,023	92,476	106,168	175,264	230,189	366,307

Specimen #BDM0002, AV = 7.50%

Temperature		Dynamic Modulus, psi					
°C	°F	0.1 Hz	0.5 Hz	1.0 Hz	5.0 Hz	10 Hz	25 Hz
-10	14	2,120,104	2,497,956	2,645,111	3,008,257	3,159,546	3,359,538
4.4	40	1,109,930	1,483,373	1,657,332	2,085,121	2,303,968	2,614,421
21.1	70	418,492	630,972	753,195	1,080,343	1,276,608	1,604,175
37.8	100	172,696	266,202	311,860	531,505	659,501	948,953
54.4	130	52,025	74,158	84,804	138,163	188,041	283,114

Specimen #BDM0003, AV = 6.90%

Temperature		Dynamic Modulus, psi					
°C	°F	0.1 Hz	0.5 Hz	1.0 Hz	5.0 Hz	10 Hz	25 Hz
-10	14	2,316,644	2,778,531	2,950,198	3,420,947	3,601,258	3,895,873
4.4	40	1,269,660	1,634,343	1,813,320	2,221,456	2,431,326	2,738,008
21.1	70	445,048	655,781	781,057	1,103,070	1,288,348	1,601,993
37.8	100	125,313	193,466	226,085	369,658	478,044	645,244
54.4	130	72,983	95,478	104,862	165,952	215,831	338,576

Binder Content = 4.6% by weight of aggregate
VMA = 14% at maximum density

Table E-2b. Summary of DM Values for Yoakum Mixture:
Rut Resistant 12.5 mm Superpave Type D Mixture (PG 76-22 + Gravel]

Specimen # YDM0001, AV = 6.80%

Temperature		Dynamic Modulus, psi					
°C	°F	0.1 Hz	0.5 Hz	1.0 Hz	5.0 Hz	10 Hz	25 Hz
-10	14	1,823,472	2,389,410	2,612,666	3,241,115	3,485,344	3,899,108
4.4	40	1,124,434	1,558,590	1,759,177	2,291,190	2,525,325	2,890,051
21.1	70	269,944	504,934	638,616	1,011,870	1,223,640	1,607,120
37.8	100	71,852	124,239	152,333	283,839	388,353	641,603
54.4	130	32,996	46,862	52,547	95,116	135,030	251,495

Specimen # YDM0002, AV = 6.90%

Temperature		Dynamic Modulus, psi					
°C	°F	0.1 Hz	0.5 Hz	1.0 Hz	5.0 Hz	10 Hz	25 Hz
-10	14	1,102, 693	1,520,779	1,742,483	2,348,088	2,615,828	2,924,933
4.4	40	1,062,343	1,513,991	1,693,229	2,166,255	2,380,446	2,607,213
21.1	70	294,499	513,564	657,877	1,082,518	1,325,065	1,634,097
37.8	100	72,852	119,526	148,635	281,170	383,001	619,616
54.4	130	50,502	63,033	69,038	133,174	187,041	327,597

Specimen # YDM0003, AV = 7.30%

Temperature		Dynamic Modulus, psi					
°C	°F	0.1 Hz	0.5 Hz	1.0 Hz	5.0 Hz	10 Hz	25 Hz
-10	14	1,131,831	1,576,792	1,770,302	2,275,236	2,518,580	2,810,991
4.4	40	710,395	1,028,477	1,187,351	1,600,694	1,763,615	2,005,712
21.1	70	177,758	325,262	419,899	695,877	863,178	1,057,511
37.8	100	45,933	71,214	88,633	156,858	216,353	342,956
54.4	130	29,530	38,116	41,060	64,324	84,238	127,865

Binder Content = 5.6% by weight of aggregate
VMA = 15.9% at maximum density

APPENDIX F

HMAC MIXTURE *LAB* N_f RESULTS

THE ME APPROACH: 50% REDUCTION IN FLEXURAL STIFFNESS

Table F-1a. Example of ME Lab N_f Predictions for Bryan Mixture for Wet-Warm Environment

Pavement Structure (PS#)	0 Months			3 Months			6 Months		
	Lab N_f	95% Lab N_f Prediction Interval		Lab N_f	95% Lab N_f Prediction Interval		Lab N_f	95% Lab N_f Prediction Interval	
		Lower	Upper		Upper	Lower		Lower	Upper
1	4,483,670	2,124,669	9,461,849	1,232,934	232,469	6,539,046	755,762	13,829	31,095,112
2	423,048	293,301	610,190	201,184	88,761	456,001	123,017	19,976	757,585
3	460,826	315,567	672,950	214,843	92,205	500,598	130,707	19,828	861,609
4	363,435	257,421	513,108	179,035	82,856	386,855	110,460	20,190	604,323
5	29,828,466	10,197,087	87,254,077	5,284,069	480,383	58,123,166	2,512,795	9,467	66,694,421

Table F-1b Example of ME Lab N_f Predictions for Yoakum Mixture for Wet-Warm Environment

Pavement Structure (PS#)	0 Months			3 Months			6 Months		
	Lab N_f	95% Lab N_f Prediction Interval		Lab N_f	95% Lab N_f Prediction Interval		Lab N_f	95% Lab N_f Prediction Interval	
		Lower	Upper		Upper	Lower		Lower	Upper
1	4,105,724	267,604	62,992,098	2,592,589	502,685	13,371,222	2,420,257	208,917	28,038,084
2	595,841	164,629	2,156,527	429,285	192,011	959,764	303,309	91,221	1,008,496
3	639,003	168,256	2,426,800	458,188	199,448	1,052,585	327,014	94,442	1,132,320
4	526,257	158,105	1,751,663	382,383	179,264	815,650	265,371	85,614	822,545

Table F-1c. Example of Variance Estimates for Predicted *Log* N_f (Bryan Mixture, WW Conditions)

Micro Strain	Log (Micro Strain)	Var(Log(Log Nf))_Bryan-0M	Var(Log(Lab N_f))_Bryan-3M
157	5.06	0.27^2	0.60^2
278.96	5.63	0.13^2	0.29^2
273.21	5.61	0.14^2	0.30^2
289.47	5.67	0.12^2	0.28^2
98.97	4.59	0.39^2	0.86^2

Table F-1d. Example of Variance Estimates for Predicted *Log* ME N_f(Yoakum Mixture, WW Conditions)

Micro Strain	Log (Micro Strain)	Var(Log(Lab Nf))_Yaokum-0M	Var(Log(Log Nf))_Yaokum-3M	Var(Log(Log Nf))_Yaokum-6M
157	5.06	0.63^2	0.59^2	0.88^2
278.96	5.63	0.30^2	0.29^2	0.43^2
273.21	5.61	0.31^2	0.30^2	0.45^2
289.47	5.67	0.28^2	0.27^2	0.41^2
98.97	4.59	-	-	-

THE CMSE APPROACH: 7.5 mm MICROCRACK GROWTH HMAC LAYER

Table F-2a. Example of CMSE *Lab* N_f for Bryan Mixture (WW Environment)

PS#	0 Months			3 Months			6 Months		
	Lab N_f	95% Lab N_f Prediction Interval		Lab N_f	95% Lab N_f Prediction Interval		Lab N_f	95% Lab N_f Prediction Interval	
		Lower	Upper		Upper	Lower		Lower	Upper
1	6,310,031	5,891,450	7,896,612	2,419,856	2,175,875	3,181,037	940,447	820,866	1,258,028
2	4,310,723	4,008,142	4,613,304	2,311,781	1,809,200	2,814,362	1,001,560	798,979	1,204,141
3	4,425,803	4,120,250	4,728,412	2,428,810	1,926,329	2,931,491	1,211,403	1,008,822	1,413,984
4	3,960,542	3,955,200	4,005,620	2,189,413	1,686,832	2,691,994	1,309,518	1,106,937	1,512,099
5	11,123,548	9,820,967	13, 118,456	8,600,514	7,397,933	9,803,095	5,081,720	4,279,139	5,884,301

Table F-2b. Example of CMSE *Lab* N_f for Yoakum Mixture (WW Environment)

PS#	0 Months			3 Months			6 Months		
	Lab N_f	95% Lab N_f Prediction Interval		Lab N_f	95% Lab N_f Prediction Interval		Lab N_f	95% Lab N_f Prediction Interval	
		Lower	Upper		Upper	Lower		Lower	Upper
1	7,879,929	6,315,948	8,921,110	4,954,378	3,733,797	5,334,959	3,229,895	2,179,244	3,980,406
2	5,893,480	4,590,899	7,196,061	3,057,842	2,257,261	3,858,423	2,115,169	1,214,568	3,015,750
3	5,899,598	4,597,017	7,202,179	3,118,460	2,317,879	3,919,041	2,009,481	1,108,900	2,910,062
4	4,001,831	3,979,250	4,041,412	3,057,181	2,156,600	3,957,762	1,980,815	1,080,234	2,881,396

THE CM APPROACH: 7.5 mm MICROCRACK GROWTH HMAC LAYER

Table F-3a. Example of CM *Lab* N_f for Bryan Mixture (WW Environment)

PS#	0 Months			3 Months			6 Months		
	Lab N_f	95% Lab N_f Prediction Interval		Lab N_f	95% Lab N_f Prediction Interval		Lab N_f	95% Lab N_f Prediction Interval	
		Lower	Upper		Upper	Lower		Lower	Upper
1	6,290,861	5,825,280	7,626,442	2,313,584	1,651,003	3,452,165	914 ,861	612,480	1,413,442
2	4,811,422	3,910,841	5,712,003	2,011,781	2,011,781	2,912,362	989,795	589,214	1,390,376
3	4,181,312	3,980,731	4,381,893	2,611,912	2,611,912	3,512,493	1,009,215	808,634	1,209,796
4	3,980,182	3,959,601	4,000,763	2,204,315	2,204,315	3,104,896	995,850	895,264	1,096,431
5	10,891,433	9,690,852	12,092,014	8,401,515	8,401,515	9,902,096	4,890,253	3,889,672	5,890,834

Table F-3b. Example of CM *Lab* N_f for Yoakum Mixture (WW Environment)

PS#	0 Months			3 Months			6 Months		
	Lab N_f	95% Lab N_f Prediction Interval		Lab N_f	95% Lab N_f Prediction Interval		Lab N_f	95% Lab N_f Prediction Interval	
		Lower	Upper		Upper	Lower		Lower	Upper
1	7,281,594	6,121,013	7,922,175	5,169,851	3,960,670	5,761,832	3,132,561	2,633,980	3,335,142
2	4,989,845	4,089,264	5,890,420	3,000,221	2,699,640	3,300,802	2,542,506	2,161,925	2,923,087
3	5,600,125	5,0995,544	6,100,706	2,986,420	2,689,839	3,287,001	1,998,652	1,718,071	2,279,233
4	4,121,458	4,000,877	4,224,039	3,116,108	2,765,527	3,466,689	1,500,824	1,260,243	1,741,405

APPENDIX G

HMAC MIXTURE *FIELD* N_f RESULTS

THE ME APPROACH: 50% REDUCTION IN FLEXURAL STIFFNESS

Table G-1a. Example of ME Field N_f ($Field\ \ N_f = \frac{SF}{M \times TCF}\left[Lab\ N_f\right]$): Bryan Mixture, WW Environment

(PS#)	0 Months			3 Months			6 Months		
	Field N_f	95% Field N_f Prediction Interval		Field N_f	95% Field N_f Prediction Interval		Field N_f	95% Field N_f Prediction Interval	
		Lower	Upper		Upper	Lower		Lower	Upper
1	2.39E+07	1.13E+07	5.04E+07	6.56E+06	1.24E+06	3.48E+07	4.02E+06	7.36E+04	1.65E+08
2	2.25E+06	1.56E+06	3.25E+06	1.07E+06	4.72E+05	2.43E+06	6.55E+05	1.06E+05	4.03E+06
3	2.45E+06	1.68E+06	3.58E+06	1.14E+06	4.91E+05	2.66E+06	6.96E+05	1.06E+05	4.59E+06
4	1.93E+06	1.37E+06	2.73E+06	9.53E+05	4.41E+05	2.06E+06	5.88E+05	1.07E+05	3.22E+06
5	1.59E+07	5.43E+07	4.64E+08	2.81E+07	2.56E+06	3.09E+08	1.34E+07	5.04E+04	3.55E+08

Table G-1b. Example of ME Field N_f ($Field\ \ N_f = \frac{SF}{M \times TCF}\left[Lab\ N_f\right]$): Yoakum Mixture, WW Environment

Pavement Structure (PS#)	0 Months			3 Months			6 Months		
	Field N_f	95% Field N_f Prediction Interval		Field N_f	95% Field N_f Prediction Interval		Field N_f	95% Field N_f Prediction Interval	
		Lower	Upper		Upper	Lower		Lower	Upper
1	2.19E+07	1.42E+06	3.35E+08	1.38E+07	2.68E+06	7.12E+07	1.29E+07	1.11E+06	1.49E+08
2	3.17E+06	8.76E+05	1.15E+07	2.28E+06	1.02E+06	5.11E+06	1.61E+06	4.85E+05	5.37E+06
3	3.40E+06	8.96E+05	1.29E+07	2.44E+06	1.06E+06	5.60E+06	1.74E+06	5.03E+05	6.03E+06
4	2.80E+06	8.41E+05	9.32E+06	2.04E+06	9.54E+05	4.34E+06	1.41E+06	4.56E+05	4.38E+06

THE ME APPROACH: 50% REDUCTION IN FLEXURAL STIFFNESS

Table G-1c. ME Field N_f at Year 20 at 95% Reliability Level (WW Environment)

PS#	Bryan Mixture			Yoakum Mixture		
	Mean Field N_f	95% Field N_f PI		Mean Field N_f	95% Field N_f PI	
		Lower	Upper		Lower	Upper
1	1.03E+06	0.49E+06	2.17E+06	8.30E+06	5.41E+06	16.74E+06
2	0.26E+06	0.18E+06	0.37E+06	0.97E+06	0.27E+06	3.52E+06
3	0.25E+06	0.17E+06	0.36E+06	0.98E+06	0.26E+06	3.73E+06
4	0.28E+06	0.20E+06	0.39E+06	0.99E+06	2.96E+06	3.28E+06
5	1.62E+06	0.55E+06	4.74E+06	----------	----------	----------

Table G-1d. ME Field N_f at Year 20 at 95% Reliability Level (DC Environment)

PS#	Bryan Mixture			Yoakum Mixture		
	Mean Field N_f	95% Field N_f PI		Mean Field N_f	95% Field N_f PI	
		Lower	Upper		Lower	Upper
1	1.18E+06	5.64E+05	1.93E+07	9.59E+06	6.25E+06	1.93E+07
2	3.38E+05	2.34E+05	4.78E+05	1.28E+06	3.56E+05	4.65E+06
3	3.25E+05	2.21E+05	4.65E+05	1.27E+06	3.38E+05	4.85E+06
4	3.50E+05	2.50E+05	4.85E+05	1.27E+06	3.79E+06	4.20E+07
5	1.83E+06	6.22E+05	5.36E+06	----------	----------	----------

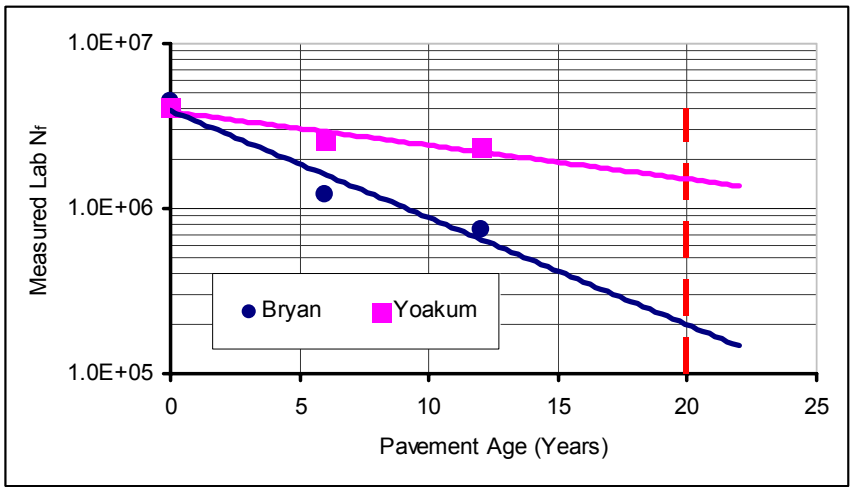

Fig. G-1. Example of Lab N_f Trend with Pavement Age
(0 months ≅ 0 Years, 3 months ≅ 6 Years, and 6 months ≅12 Years)

Approximate Lab N_f values at Year 20 based on extrapolations in Figure G-1 are about:

- Bryan mixture: Lab $N_f \cong$ 0.20 E+06
- Yoakum mixture: Lab $N_f \cong$ 1.56 E+06

Using the following ME equation (Chapter IV) with $SF = 19$, $M = 3.57$, and $TCF = 1$, the field N_f values at Year 20 are approximately predicted as follows:

$$FieldN_f = \frac{SF\left[k_i(\varepsilon_t)^{-k_2}\right]}{M \times TCF} = \frac{SF \times Lab\ N_f}{M \times TCF} \qquad \text{(G-1)}$$

- Bryan mixture: Field N_f = 19* 0.20E+06/(3.57*1) = 1.03 E+06
- Yoakum mixture: Field N_f = 19*1.56E+06/(3.57*1) = 8.30 E+06

Table G-2a. Example of CMSE Field N_f (*Field* $N_f = [SF_a \times SF_h] \times$ Lab N_f): Bryan Mixture, WW Environment

PS#	0 Months			3 Months			6 Months		
	Field N_f	95% Field N_f Prediction Interval		Field N_f	95% Field N_f Prediction Interval		Field N_f	95% Field N_f Prediction Interval	
		Lower	Upper		Upper	Lower		Lower	Upper
1	6.922E+07	6.463E+07	8.663E+07	1.893E+07	1.702E+07	2.488E+07	6.034E+06	5.267E+06	8.072E+06
2	4.729E+07	4.397E+07	5.061E+07	1.808E+07	1.415E+07	2.201E+07	6.426E+06	5.126E+06	7.726E+06
3	4.855E+07	4.520E+07	5.187E+07	1.900E+07	1.507E+07	2.293E+07	7.773E+06	6.473E+06	9.073E+06
4	4.345E+07	4.339E+07	4.394E+07	1.712E+07	1.319E+07	2.105E+07	8.402E+06	7.102E+06	9.702E+06
5	1.220E+08	1.077E+08	1.439E+08	6.726E+07	5.786E+07	7.667E+07	3.261E+07	2.746E+07	3.776E+07

Table G-2b. Example of CMSE Field N_f (*Field* $N_f = [SF_a \times SF_h] \times$ Lab N_f): Yoakum Mixture, WW Environment

PS#	0 Months			3 Months			6 Months		
	Field N_f	95% Field N_f Prediction Interval		Field N_f	95% Field N_f Prediction Interval		Field N_f	95% Field N_f Prediction Interval	
		Lower	Upper		Upper	Lower		Lower	Upper
1	1.201E+08	9.629E+07	1.360E+08	4.905E+07	3.697E+07	5.282E+07	2.953E+07	1.993E+07	3.640E+07
2	8.985E+07	6.999E+07	1.097E+08	3.028E+07	2.235E+07	3.820E+07	1.934E+07	1.111E+07	2.758E+07
3	8.995E+07	7.009E+07	1.098E+08	3.088E+07	2.295E+07	3.880E+07	1.837E+07	1.014E+07	2.661E+07
4	6.101E+07	6.067E+07	6.162E+07	3.027E+07	2.135E+07	3.919E+07	1.811E+07	9.878E+06	2.635E+07

Table G-2c. CMSE *Field* N_f at Year 20 at 95% Reliability Level (WW Environment)

PS#	Bryan Mixture			Yoakum Mixture		
	Mean Field N_f	95% Field N_f PI		Mean Field N_f	95% Field N_f PI	
		Lower	Upper		Lower	Upper
1	3.11E+06	3.08E+06	3.21E+06	8.40E+06	6.95E+06	9.82E+06
2	2.13E+06	1.98E+06	2.28E+06	6.56E+06	5.11E+06	8.01E+06
3	2.18E+06	2.03E+06	2.33E+06	6.57E+06	5.12E+06	8.02E+06
4	1.96E+06	1.95E+06	1.98E+06	4.45E+06	4.43E+06	4.50E+06
5	5.49E+06	4.85E+06	6.48E+06	X	X	X

Legend: X = No data

Table G-2d. CMSE *Field* N_f at Year 20 at 95% Reliability Level (DC Environment)

PS#	Bryan Mixture			Yoakum Mixture		
	Mean Field N_f	95% Field N_f PI		Mean Field N_f	95% Field N_f PI	
		Lower	Upper		Lower	Upper
1	3.60E+06	3.36E+06	4.50E+06	9.07E+06	7.27E+06	1.03E+07
2	2.46E+06	2.29E+06	2.63E+06	6.78E+06	5.28E+06	8.28E+06
3	2.52E+06	2.35E+06	2.70E+06	6.79E+06	5.29E+06	8.29E+06
4	2.26E+06	2.26E+06	2.28E+06	4.61E+06	4.58E+06	4.65E+06
5	6.34E+06	5.60E+06	7.48E+06	X	X	X

Legend: X = No data

Table G-2e. Example of CMSE Field N_f Prediction at Year 20 (PS# , WW Environment)

HMAC Mixture	**SF_{ag} @ Year 20**	**SF_a**	**SF_h**	**$[N_i + N_p]$**	**$N_f = [SF_{ag}] \times [SF_a \times SF_h] \times [N_i + N_p]$**
Bryan	0.045	1.63	6.73	6.31E+06	3.11E+06
Yoakum	0.070	2.10	7.26	7.88E+06	8.40E+06

THE CM APPROACH: 7.5 mm MICROCRACK GROWTH HMAC LAYER

Table G-3a. Example of CM Field N_f (*Field* N_f = [$SF_a \times SF_h$] × Lab N_f): Bryan Mixture, WW Environment

PS#	0 Months			3 Months			6 Months		
	Field N_f	95% Field N_f Prediction Interval		Field N_f	95% Field N_f Prediction Interval		Field N_f	95% Field N_f Prediction Interval	
		Lower	Upper		Upper	Lower		Lower	Upper
1	6.901E+07	6.390E+07	8.366E+07	1.809E+07	1.291E+07	2.700E+07	5.870E+06	3.930E+06	9.069E+06
2	5.278E+07	4.290E+07	6.266E+07	1.573E+07	1.573E+07	2.278E+07	6.351E+06	3.781E+06	8.921E+06
3	4.587E+07	4.367E+07	4.807E+07	2.043E+07	2.043E+07	2.747E+07	6.475E+06	5.188E+06	7.762E+06
4	4.366E+07	4.344E+07	4.389E+07	1.724E+07	1.724E+07	2.428E+07	6.390E+06	5.744E+06	7.035E+06
5	1.195E+08	1.063E+08	1.326E+08	6.571E+07	6.571E+07	7.744E+07	3.138E+07	2.496E+07	3.780E+07

Table G-3b. Example of CM Field N_f (*Field* N_f = [$SF_a \times SF_h$] × Lab N_f): Yoakum Mixture, WW Environment

PS#	0 Months			3 Months			6 Months		
	Field N_f	95% Field N_f Prediction Interval		Field N_f	95% Field N_f Prediction Interval		Field N_f	95% Field N_f Prediction Interval	
		Lower	Upper		Upper	Lower		Lower	Upper
1	1.110E+08	9.332E+07	1.208E+08	5.119E+07	3.921E+07	5.705E+07	2.864E+07	2.409E+07	3.050E+07
2	7.608E+07	6.234E+07	8.981E+07	2.970E+07	2.673E+07	3.268E+07	2.325E+07	1.977E+07	2.673E+07
3	8.538E+07	7.775E+08	9.301E+07	2.957E+07	2.663E+07	3.254E+07	1.828E+07	1.571E+07	2.084E+07
4	6.284E+07	6.100E+07	6.440E+07	3.085E+07	2.738E+07	3.432E+07	1.372E+07	1.152E+07	1.592E+07

THE CM APPROACH: 7.5 mm MICROCRACK GROWTH HMAC LAYER

Table G-3c. CM *Field* N_f at Year 20 at 95% Reliability Level (WW Environment)

PS#	Bryan Mixture			Yoakum Mixture		
	Mean Field N_f	95% Field N_f PI		Mean Field N_f	95% Field N_f PI	
		Lower	Upper		Lower	Upper
1	3.10E+06	2.98E+06	4.47E+06	7.77E+06	6.12E+06	8.08E+06
2	2.38E+06	1.93E+06	2.82E+06	5.55E+06	4.55E+06	6.56E+06
3	2.06E+06	1.97E+06	2.16E+06	6.23E+06	5.68E+07	6.79E+06
4	1.96E+06	1.95E+06	1.98E+06	4.59E+06	4.45E+06	4.70E+06
5	5.38E+06	4.78E+06	5.97E+06	X	X	X

Legend: X = No data

Table G-3d. CM *Field* N_f at Year 20 @ 95% Reliability Level (DC Environment)

PS#	Bryan Mixture			Yoakum Mixture		
	Mean Field N_f	95% Field N_f PI		Mean Field N_f	95% Field N_f PI	
		Lower	Upper		Lower	Upper
1	3.59E+06	3.32E+06	4.35E+06	8.46E+06	7.11E+06	9.20E+06
2	2.74E+06	2.23E+06	3.26E+06	5.80E+06	4.75E+06	6.84E+06
3	2.39E+06	2.27E+06	2.50E+06	6.51E+06	5.92E+07	7.09E+06
4	2.27E+06	2.26E+06	2.28E+06	4.79E+06	4.65E+06	4.91E+06
5	6.21E+06	5.53E+06	6.90E+06	X	X	X

Legend: X = No data

Table G-3e. Example of CM Field N_f Prediction at Year 20 (PS# 1, WW Environment)

HMAC Mixture	**SF_{ag} @ Year 20**	**SF_a**	**SF_h**	**$[N_i + N_p]$**	**$N_f = [SF_{ag}] \times [SF_a \times SF_h] \times [N_i + N_p]$**
Bryan	0.045	1.63	6.73	6.29E+06	3.10E+06
Yoakum	0.070	2.10	7.26	7.28E+06	7.77E+06

THE MEPDG: 50% WHEELPATH CRACKING

Table G4-a. Example of MEPDG Software Analysis
(Bryan Mixture, WW Environment)

PS#	HMAC Specimen	Traffic ESALs (Millions)	Percent Cracking in Wheelpath (Output from Software)
1	BDM0001	2.50	26.80
	BDM0002	2.50	38.3
	BDM0003	2.50	31.80
	BDM0001	5.00	45.60
	BDM0002	5.00	59.90
	BDM0003	5.00	51.60
2	BDM0001	2.50	21.9
	BDM0002	2.50	36.80
	BDM0003	2.50	28.60
	BDM0001	5.00	53.90
	BDM0002	5.00	71.50
	BDM0003	5.00	63.20
3	BDM0001	1.25	29.90
	BDM0002	1.25	40.10
	BDM0003	1.25	36.60
	BDM0001	2.50	61
	BDM0002	2.50	70.00
	BDM0003	2.50	67.20
	BDM0001	5.00	78.10
	BDM0002	5.00	89.80
	BDM0003	5.00	87.40
4	BDM0001	1.25	26.60
	BDM0002	1.25	43.80
	BDM0003	1.25	32.30
	BDM0001	2.50	58
	BDM0002	2.50	70.10
	BDM0003	2.50	64.30
	BDM0001	5.00	85.50
	BDM0002	5.00	96.25
	BDM0003	5.00	88.30
5	BDM0001	2.50	7.85
	BDM0002	2.50	13.51
	BDM0003	2.50	9.02
	BDM0001	5.00	15
	BDM0002	5.00	20.40
	BDM0003	5.00	18.10
	BDM0001	25	55.10
	BDM0002	25	70.40
	BDM0003	25	63.89

Table G-4b. Example of MEPDG Software Analysis
(Bryan Mixture, DC Environment)

PS	HMAC Specimen	Traffic ESALs (Millions)	Percent Cracking in Wheelpath (Output from Software)
2	BDM0001	2.50	18.40
	BDM0002	2.50	31.60
	BDM0003	2.50	23.70
	BDM0001	5.00	40.00
	BDM0002	5.00	53.90
	BDM0003	5.00	49.70
3	BDM0001	2.50	18.40
	BDM0002	2.50	27.90
	BDM0003	2.50	32.60
	BDM0001	5.00	48.50
	BDM0002	5.00	72.10
	BDM0003	5.00	57.6
4	BDM0001	2.50	30.50
	BDM0002	2.50	48.80
	BDM0003	2.50	36.50
	BDM0001	5.00	62.80
	BDM0002	5.00	73.00
	BDM0003	5.00	60.40

Table G-4c. *Field N_f* Results at Year 20 at 95% Reliability Level (WW Environment)

PS#	Bryan Mixture			Yoakum Mixture		
	Field N_f	95% Field N_f Prediction Interval		Field N_f	95% Field N_f Prediction Interval	
		Lower	Upper		Lower	Upper
1	4.705E+06	1.927E+06	9.737E+06	6.210E+06	2.037E+06	1.534E+07
2	4.047E+06	1.996E+06	6.354E+06	5.750E+06	2.348E+06	1.054E+07
3	1.932E+06	0.000E+00	3.737E+06	3.410E+06	1.345E+05	7.771E+06
4	2.018E+06	2.802E+05	3.563E+06	2.970E+06	3.491E+05	6.000E+06
5	1.929E+07	1.420E+07	2.483E+07	X	X	X

Legend: X = No data

Table G-4d. Example of *Field N_f* Results at Year 20 at 95% Reliability Level (DC Environment)

PS#	Bryan Mixture		
	Field N_f	95% Field N_f Prediction Interval	
		Lower	Upper
2	5.229E+06	2.948E+06	9.924E+06
3	4.290E+06	1.646E+06	7.836E+06
4	3.563E+06	2.639E+05	6.530E+06

APPENDIX H
RESOURCE REQUIREMENTS

Table H-1a. Typical Time (hr) Requirement to Produce at Least One Mixture N_f Result

Task	**MEPDG**	**ME**	**CMSE**	**CM**
Specimen fabrication	43.75 hr	45.5 hr	43.75 hr	43.75 hr
Specimen temperature conditioning	20 hr	4 hr	15 hr	11 hr
Lab testing (including set-up)	5 hr	30 hr	70 hr	5 hr
Data analysis	4.5 hr	3 hr	6 hr	5 hr
Total	72.25 hr	82.5 hr	134.75 hr	64.75 hr

Note: For the CMSE approach, about 65 hr lab testing is for surface energy SE measurements. SE values for asphalts and aggregates are required as CMSE input. Though the current SE test protocol for aggregates might require a test time of about 30 to 60 hours per aggregate, various alternate and time efficient SE measurement methods are being investigated in an ongoing research project. Despite the lengthy test time, SE measurements are only performed once for any asphalt or aggregate type from a particular source (as long as there are no major compositional changes). The SE data can then be utilized for numerous analysis applications including fatigue, permanent deformation, and moisture sensitivity modeling in HMAC pavements. Thus SE measurements are actually efficient considering their repeated and widespread use for asphalt and aggregate materials that may be utilized in different mixture designs.

Table H-1b. Typical Equipment Requirements

Task	MEPDG	ME	CMSE	CM
Binder-aggregate mixing	Electric mixer	Electric mixer	Electric mixer	Electric mixer
Compacting	SGC	Linear kneading	SGC	SGC
Testing	MTS LVDTs Control unit	MTS LVDT Control unit BB device	MTS LVDTs Control unit WP USD device	MTS LVDTs Control unit
Data acquisition	Automated computer system	Automated computer system	Automated computer system	Automated computer system
Temperature control unit	Thermocouples	Thermocouples	Thermocouples	Thermocouples
Other test accessories			Attachment plates	Attachment plates
Data analysis	2002 Design Guide software	Excel/manual	Excel/manual	Excel/manual

Table H-1c. Typical Time (hr) Requirements for a Single Specimen Fabrication

#	Task	ME (Beam Specimen)	CMSE, CM, & MEPDG, (Cylindrical Specimen)
1	Aggregate batching	0.5 hr	0.5 hr
2	Aggregate pre-heating (minimum ≅ 4 hr)	12 hr (overnight)	12 hr (overnight)
3	Binder liquefying (heating)	0.5 hr	0.5 hr
4	Binder aggregate mixing	0.25 hr	0.25 hr
5	PP2 Short-Term Oven Aging (STOA) @ 135 °C	4 hr	4 hr
6	Heating for compaction	0.5 hr	0.5 hr
7	Compaction	0.25 hr	0.25 hr
8	Specimen cooling	12 hr (overnight)	12 hr (overnight)
9	Sawing & coring (with water)	2 hr	0.5 hr
10	Drying after sawing/coring	12 hr (overnight)	12 hr (overnight)
11	AV measurements	0.75 hr	0.25 hr
12	Cleaning up	1 hr	1 hr
Total		45.75 hr	43.75 hr

Note that the time estimates in the above table are only representative of the author's laboratory experience in the course of this study. The actual time may vary from individual to individual and from machine to machine.

APPENDIX I

TxDOT EVALUATION SURVEY QUESTIONNAIRE

Table I-1a. Evaluation and Weighting of Factors for the Selection of Appropriate Fatigue Analysis Approach

Factor	**Rating: 1-10 (1 = least important, 10 = most important)**	**Sub-factor**	**Rating: 1-10 (1 = least important, 10 = most important)**
Laboratory testing		Simplicity	
		Equipment availability	
		Equipment versatility	
		Human resources	
Input variability		Traffic	
		Materials	
		Environment (temperature & moisture)	
Incorporation of material properties in analysis		Mixture volumetrics	
		Modulus/stiffness	
		Tensile strength	
		Aging	
		Healing	
		Fracture	
		Anisotropy	
Analysis		Simplicity	
		Versatility of inputs	
		Definition of failure criteria	
Results		N_f variability	
		Tie to field validation	
Cost		Lab testing (hrs)	
		Equipment ($)	
		Analysis (hrs) • Lab data reduction • N_f computation	
		Practicality of implementation	

Table I-2. Summary of Respondent Questionnaire Survey Details from TxDOT

Factor	**Rating: 1-10 (1 = least important,) 10 = most important)**	**Sub-factor**	**Rating: 1 – 10 (1 = least important, 10 = most important)**	**Weight**
Laboratory testing	5.1 *([5.1/34.4) = 14.83%*)	Simplicity	7.7	31.69%
		Equipment availability	7.0	28.81%
		Equipment versatility	5.3	21.81%
		Human resources	4.3	17.70%
		Total	23.4	100%
Input data	5.5 *([5.5/34.4] = 15.99%*)	Traffic	6.5	34.03%
		Materials	6.9	36.13%
		Environment (temperature & moisture)	5.7	29.84%
		Total	19.1	100%
Incorporation of material properties in analysis	4.8 *([4.8/34.4] = 13.95%*)	Mixture volumetrics	7.0	16.67%
		Modulus/stiffness	7.0	16.67%
		Tensile strength	6.3	15.00%
		Aging	6.0	14.29%
		Healing	5.0	11.90%
		Fracture	6.7	15.95%
		Anisotropy	4.0	9.52%
		Total	42.0	100%
Analysis	5.1 *([5.1/34.4] = 14.83%)*	Simplicity	6.7	35.83%
		Versatility of inputs	4.3	22.99%
		Definition of failure criteria	7.7	41.18%
		Total	18.7	100%
Results	7.6 *([7.6/34.4] = 22.09%)*	N_f variability	8.0	50.0%
		Tie to field validation	8.0	50.0%
		Total	16.0	100%
Cost	6.3 ([*6.3/34.4] = 18.31%)*	Lab testing (hr)	9.0	32.14%
		Equipment ($)	4.7	16.79%
		Analysis (hr) -Lab data reduction -N_f computation	5.3	18.92%
		Practicality of implementation	9.0	32.14%
		Total	28.0	100%
Total	10 *(100%)*			

APPENDIX J

RATING CRITERIA OF THE FATIGUE ANALYSIS APPROACHES

APPENDIX J

Table J. Rating Criteria of the Fatigue Analysis Approaches

CATEGORY	WEIGHT	ITEM	WEIGHT	ME		CMSE		CM		MEPDG		COMMENT
				SCORE	EVALUATION	SCORE	EVALUATION	SCORE	EVALUATION	SCORE	EVALUATION	
Results	*22%*	N_f variability	*50%*	3/10	3.30%	8/10	8.80%	7/10	7.70%	5/10	5.50%	
		Tie to field validation	*50%*	5/10	5.50%	5/10	5.50%	5/10	5.50%	5/10	5.50%	CMSE
			100%	**40%**		**65%**		**60%**		**50%**		
Cost	*18%*	Practicality	*32%*	6/10	3.46%	6/10	3%	6/10	3%	6/10	3%	
		Testing (hrs)	*32%*	4/10	2.30%	7/10	4%	8/10	5%	7/10	4%	
		Analysis (hrs)	*19%*	8/10	2.74%	6/10	3%	6/10	3%	6/10	3%	CM
		Equipment ($)	*17%*	6/10	1.84%	7/10	4%	8/10	5%	8/10	5%	
			100%	**57%**		**65%**		**70%**		**67%**		
Input variability	*16%*	Materials	*36%*	5/10	3%	8/10	5%	8/10	5%	6/10	3%	
		Traffic	*34%*	5/10	3%	5/10	3%	5/10	3%	7/10	4%	
		Environment	*29%*	5/10	2%	5/10	2%	5/10	2%	7/10	4%	MEPDG
			100%	**50%**		**60%**		**60%**		**66%**		
Analysis	*15%*	Failure criteria	*41%*	5/10	3%	8/10	5%	7/10	4%	5/10	3%	
		Simplicity	*36%*	8/10	4%	5/10	3%	6/10	3%	6/10	3%	
		Versatility of inputs	*23%*	4/10	1%	10	3%	8/10	3%	7/10	2%	CMSE
			100%	**59%**		**74%**		**69%**		**59%**		
Lab testing	*15%*	Simplicity	*32%*	5/10	3.1%	8/10	3.84%	9/10	4.32%	9/10	4.32%	
		Equipment availability	*29%*	3/10	1.6%	7/10	3.05%	7/10	3.05%	7/10	3.05%	
		Equipment versatility	*22%*	0/10	0.0%	10/10	3.30%	7/10	1.64%	8/10	2.64%	CMSE
		Human resources	*18%*	5/10	1.7%	8/10	2.16%	8/10	2.16%	8/10	2.16%	
			100%	**34%**		**82%**		**81%**		**81%**		
Incorporation of Material Properties	*14%*	Mixture volumetrics	*17%*	6/10	1.4%	9/10	2.1%	9/10	2.1%	10/10	2.4%	
		Modulus/stiffness	*17%*	8/10	1.9%	9/10	2.1%	9/10	2.1%	10/10	2.4%	
		Fracture	*16%*	5/10	1.1%	10/10	2.2%	9/10	2.0%	5/10	1.1%	
		Tensile strength	*15%*	5/10	1.1%	10/10	2.1%	1/100	2.1%	5/10	1.1%	CMSE
		Aging	*14%*	5/10	1.0%	9/10	1.8%	9/10	1.8%	9/10	1.8%	
		Healing	*12%*	5/10	0.8%	9/10	1.5%	8/10	1.3%	5/10	0.8%	
		Anisotropy	*9%*	5/10	0.6%	8/10	1.0%	8/10	1.0%	5/10	0.6%	
			100%	**48%**		**82%**		**79%**		**62%**		
Total	***100%***				**50%**		**75%**		**73%**		**69%**	**CMSE**

VITA

Lubinda F. Walubita was born in Mongu, Zambia. He received his Bachelor of Engineering degree (B.Eng.) in Civil Engineering from the University of Zambia (UNZA) in May 1996. Upon completion of his B.Eng. degree from UNZA, he worked as a graduate roads engineer with ASCO (Z) Ltd Consulting Engineers until he moved to the University of Stellenbosch (South Africa) in January 1998 to pursue his master's degree. He received his Master of Science in Engineering degree (M.S.) in pavement technology in December 2000. During his M.S. academic program at Stellenbosch, he was attached as an exchange research scholar to The University of Texas (UT) at Austin in 1999, where he worked for the Center for Transportation Research (CTR) as a research engineer/scientist associate. Upon completion of his M.S. degree in December 2000, he again worked for ASCO (Z) Ltd as a roads and materials engineer, and briefly in Pretoria (South Africa) with Letaba Consulting Engineers Ltd. before joining Texas A&M University in August 2001. While at Texas A&M University, he was also concurrently working as a research assistant for Texas Transportation Institute (TTI) in the materials and pavement engineering division. Lubinda received his Ph.D. degree in May 2006. His permanent address is as follows:

C/o: UNZA
Department of Civil Engineering
School of Engineering
P.O. Box 32379
Lusaka 10101
Zambia